Proceedings of International Conference
Applications of Structural Fire Engineering
Prague, 19-20 February 2009

Session 5

Steel Structures

INVESTIGATION INTO METHODS FOR PREDICTING CONNECTION TEMPERATURES

Kate Anderson [a], Martin Gillie [a]

[a] University of Edinburgh, School of Engineering and Electronics, Edinburgh, United Kingdom

INTRODUCTION

Structural fire design is, to a large extent, based on single member tests. Due to the nature of these tests, the behaviour of the connections is neglected suggesting that they do not play a critical role in fire. In support of this theory, connections generally have a lower temperature than the surrounding structure during fires and are usually protected. This assumption of cooler connections is valid but this does not justify ignoring them in fire design. During both heating and cooling, connections will be subject to conditions, for example large moments and shear forces, which they will not typically have been designed for [1]. The response of connections to these conditions is complex and is largely based on the material strength degradation and the interactions between the various components of the connection. To predict how the behaviour of connections affects global performance in fire, temperature profiles must initially be established in order to evaluate the material strength degradation over time.

This paper examines two current methods available for predicting connection temperatures as defined in Eurocode 3 [2]. The first of these methods suggests that connection temperatures can be defined as a percentage of the adjacent beam temperature and a second is based on the lumped mass of material at the connection. A 3D finite element model is also created to predict connection temperatures using the commercial software package Abaqus[3]. Abaqus uses heat transfer theory to predict connection temperatures over time. These methods are all compared to experimental data and the validity and accuracy of each is evaluated and its limitations explored.

1 THEORY

1.1 Eurocode Percentages Method

Eurocode 3 details two methods for predicting connection temperatures. The first assumes that connection temperatures follow the same general trend as local beam temperatures but are a percentage lower. This method simplifies connections into 2 categories based on whether the connecting beam is less than or equal to 400mm deep or greater than that. In the first case, where the top of the connection is adjacent to the concrete slab, connection temperatures are approximated at 88% of the beam lower flange mid-span temperature at the bottom of the connection, 75% at mid-height and 62% at the top. Between these points the temperature is assumed to vary linearly. Where the connecting beam is more than 400mm deep, temperatures are calculated as 88% of the beam temperature at the bottom and mid-height of the connection, tapering to 70% at the top.

Connections are cooler at the top for two main reasons. The largest contributor to heating is radiation from hot surfaces such as compartment or furnace walls. Where there is no direct line of sight between these walls and the member, in this case the connection, the radiative heating will decrease. This phenomenon is known as shadowing and causes the top of the

connection to be cooler than the rest. The provision of a heat sink in the form of a concrete slab will also reduce connection temperatures.

1.2 Lumped Capacitance

Connection temperatures can also be predicted using the ratio of material volume to exposed surface area. An average connection temperature or the that of a specific connection component, such as a bolt or end plate, can be calculated, assuming the gas temperature-time curve is known.

The lumped capacitance method [4] calculates the uniform temperature rise in an unprotected steel member using a series of finite time steps Δt as given in *Eq (1)*.

$$\Delta T_s = \frac{h}{C_s\,(W/D)}\,(T_f - T_s)\,\Delta t \qquad (1)$$

where h heat transfer co-efficient,
T_f gas temperature,
T_s steel temperature,
C_s steel specific heat,
D heated perimeter
W steel volume per meter length

When applied to connections, this method must take into consideration the large volume of steel at the connection therefore the equation has been modified to use the ratio of volume of steel, V, to heated surface area, A, as shown in *Eq (2)*.

$$\Delta T_s = \frac{h}{C_s\,(V/A)}\,(T_f - T_s)\,\Delta t \qquad (2)$$

This method does not account for the concrete slab above the connection and as the effect of the slab on connection temperatures has not been well researched, the validity of applying this method to connections is uncertain.

1.3 Finite Element Modelling

An alternative means of predicting structural temperatures is to carry out a finite-element heat transfer analysis. Detailed temperature profiles can be created and this information can be used as direct input for a structural model. In principle, this method is highly accurate, however obtaining correct values for the all input parameters is very challenging. The modelling process is outlined below.

For the purpose of this paper, the gas temperature-time curve to which a connection is exposed is assumed to be known, therefore the modelling will be limited to the convective and radiative heat transfer between the gas and solid, and to the conduction between the connection components. Perfect conduction is assumed between the various connection components such as bolts and bolt holes and through the welds.

Convective heat transfer is heating by movement of the hot gases where the heat flux due to convection, q_c" and is given by:

$$q_c" = h\,(T_f - T_{su}) \qquad (3)$$

where T_{su} is the surface temperature.

The heat transfer coefficient varies with temperature and depends on the hot gas velocity. Its value for structural steel is given in Eurocode 3 as 25W/m^2.K [2]. At the connections, the convective heating will be less due to lower gas velocities in these areas, however, no practical methods exist for accurately calculating heat transfer coefficient at connections. This

paper has therefore used the Eurocode recommended value. This assumption was verified with a sensitivity study.
Radiative heat transfer is heating directly between one item and another or between the fire source and a structural element or between one structural element and other. Emissivity is used to describe the radiative power of an object and can be defined as the ratio of the radiative power of the object to the radiative power of a black body where a black body is a perfect emitter and emissivity can never be greater than 1.
Emissivity varies with temperature and in large building fires is usually the dominant mode of heating. There are a huge number of factors which affect radiative heating, for example the make up of the air in the room: if the air contains soot particles the radiation between objects will be lower than in clear air or if an element becomes charred or sooty its emissive power will reduce, i.e. less heat will be absorbed by the element. Due to the many variables affecting emissivity, predicting radiative heating is extremely difficult: for one structural member, there will be variations not only with temperature but also with factors such as location in the building, fuel type and ventilation conditions.
The heat flux due to radiative heating, or total emissive power of an object is given in *Eq (4)*.

$$q_e'' = \varepsilon \sigma T_{su}^4 \quad (4)$$

where ε emissivity and
σ Stefan Boltzmann constant
The emissivity at a connection will be lower than that of the local beams and columns due to the shadow effect, as discussed in section 1.1. Eurocode 3 suggests that for 'shadowed' areas a reduction factor for unprotected steel temperatures can be defined as shown in *Eq (5)*.

$$k_{sh} = [A_m/V]_b/[A_m/V] \quad (5)$$

where $[A_m/V]_b$ box section factor
$[A_m/V]$ section factor
A_m surface area of the member per unit length
This method is suggested for beams but has not yet been validated for connections. Further research is required to validate this assumption.

2 RESULTS

Two sets of experimental data have been used to investigate the accuracy of these methods for predicting connection temperatures. These are briefly summarised here.

- Manchester University furnace tests carried out in 2008 [5-6] consisting of 4 beams spanning from one column with a concrete slab on top. The steel members were all unprotected. This whole assembly was tested in a furnace where the gas temperatures followed a 60 minute standard fire. Connection temperatures were recorded at several locations. Cooling was not considered. 4 connection types were used: flush and flexible end plate, fin plate and web cleats. The flush end plate and fin plate have been used for validation in this paper.
- Cardington full scale tests from January 2003 [7]. This was a compartment fire test on the 4th storey of an 8 storey building where one of the main objectives was to monitor the connection behaviour including temperature evolution during the heating and cooling phases. The interior beam to column connections were flexible end plates. The columns were protected to the underside of the beams whilst the connection remained unprotected.

2.1 Eurocode Percentages Method

The Eurocode percentages method was used to predict the temperatures of two connections, a flush end plate from the Manchester University tests and a flexible end plate from the Cardington tests. The results of these are shown in Figs 1 and 2.

Figure 1 shows the predicted temperatures at 3 locations on the connection, bottom, mid-height and top, in comparison to the recorded temperatures at the same locations. For the first 15 minutes the predicted temperatures are of reasonable accuracy but after this point predicted temperatures are much higher than experimental ones. After 50 minutes the predicted temperature of the bottom of the connection is 900°C whereas the measured temperature was 250°C lower at 650°C; there is a similar error margin for the mid-height temperature. The peak temperature of the connection is estimated to be at around 50 minutes, coinciding with the peak beam temperature. Connections, however, can continue to heat after the surrounding structure has started cooling and experimental results show that this connection does not start cooling until 15 minutes later. During the cooling stage the connection temperatures are under-predicted by between 150°C and 250°C for the 60 minute cooling period at all locations.

The results for the flush end plate, Fig. 2, shows that the temperatures at three locations on the connection are initially over conservative by up to 200°C but are equally under conservative after about 25 minutes until the conclusion of the test. The trend of connection temperatures relative to one another is also not shown: The experimental test shows connection temperatures varying by around 75°C from top to bottom whereas the Eurocode method shows a variation of close to 200°C.

This method provides a very simple means of estimating connection temperatures where the only information required is the beam mid-span temperature and depth. However, results show it to be unreliable in both heating and, to a larger extent, in cooling. The implication of this is that using this method is inappropriate except for very crude calculations.

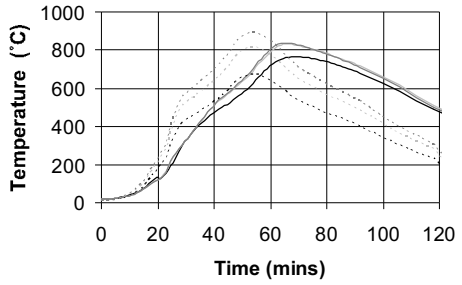

Fig. 1. EC % Method: Flexible End Plate

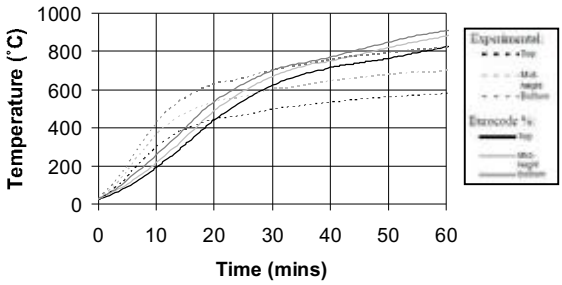

Fig. 2. EC % Method: Flush End Plate

2.2 Lumped Capacitance

The lumped capacitance method has been used to predict the average temperature of a fin-plate connection from the Manchester University tests and of the flexible end plate used in the Cardington tests. The results are shown in Fig. 3 and compared to the recorded average connection temperature.

For fin-plate, the average temperature is predicted well. However it is noteworthy that this experiment was carried out in a highly controlled environment. The same lumped capacitance method is then used to calculate the average temperature for the flexible end plate. The temperatures predicted are consistently higher than the experimental results by between 30°C

and 90°C and are therefore conservative however there is a good correlation between the predicted and experimental trend.
More input data is required for this method than for the percentages method: connection geometry and gas temperature-time curve. Despite calculations being basic, results show that good average temperatures are predicted. There are, however, many factors that could affect the results such how much of the beam or column is considered to be part of the connection and what effect the concrete slab has on the heating rate. As the effect of the slab on connection temperatures has not been well researched, this assumption may be invalid. Also, temperature gradients are present over connections and mechanical response may vary notably between a connection with one average temperature to that with a temperature profile therefore an average temperature may not be adequate for detailed calculation purposes.

2.3 Finite Element Modelling

A model of the flexible end plate created in Abaqus for the 200 minute fire which includes a 140 minute cooling phase. In creating the finite element model there were three main areas for consideration: radiative heating, convective heating and the inclusion of a concrete slab.
A sensitivity study was carried out to look at these three parameters and examine their effect on results. It was found that varying the heat transfer coefficient, and therefore the level of convective heating, at the connection had a negligible affect on results. When the concrete slab was included in the model the temperatures of the upper flanges of the beams were affected but other temperature predictions remained unchanged. Based on these results the concrete slab was excluded from further modelling.
The value of emissivity affected results and therefore the area near to the connection was assigned a lower emissivity that the rest of the structure. This is based on the shadow effect in this location as discussed in section 1.1.

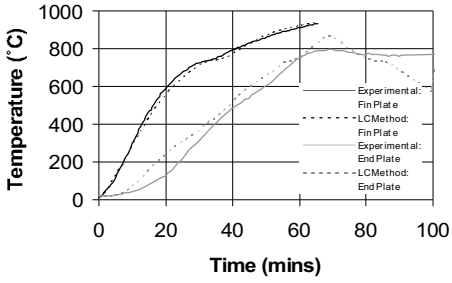

Fig. 3. Lumped Capacitance Method for Fin Plate and Flexible End Plate

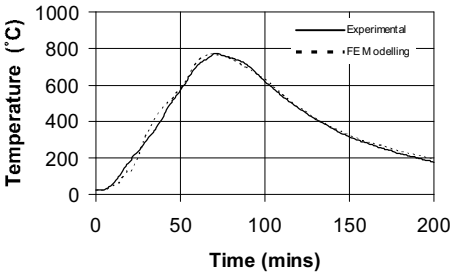

Fig. 4. Finite Element for Flexible End Plate: Top of Connection

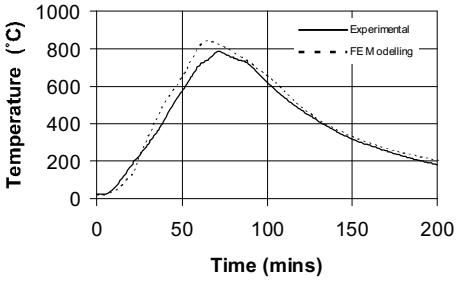

Fig. 5. Finite Element for Flexible End Plate: Bottom of Connection

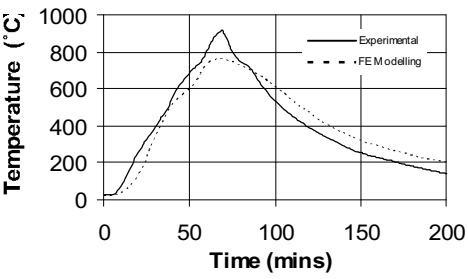

Fig. 6. Finite Element for Flexible End Plate: Top Flange of Beam

The known gas temperature over time was input to the model and heating assumed on all faces apart from the upper flanges of the beams and top of the column where there was contact with the concrete slab.
Results from the finite element modelling are shown in Figs. 4 and 5 and all show close correlation with experimental data. Figure 6 shows that the biggest difference between predicted and experimental temperatures is on the underside of the beam upper flange. This is due to the concrete being excluded from the analysis.
For detailed calculations where the exact connection geometry is known, this method provides accurate results. It can be used for all connection types where a detailed knowledge of its response in fire is required. This method, however, is time consuming both in model creation and simulation run time therefore it could not be a day to day modelling approach.

3. CONCLUSIONS

This paper has investigated three methods for predicting connection temperatures. The Eurocode suggests connection temperatures can be calculated as percentages of the mid-span beam flange temperature. However, results show this method to be unreliable and should therefore be used with caution.
The lumped capacitance method, based on the heated surface area of the connection and its volume, showed good correlation with average connection temperatures. More work should be done to look at predicting temperatures of individual connection elements and to definite what volume of the connection beams and columns should be included in calculations.
The Abaqus modelling also showed good correlation with experimental results. This method can therefore be recommended if a detailed temperature profile is needed for mechanical analysis. During the modelling it was found that the inclusion of the concrete slab did not affect the predicted temperatures of the connection therefore it in need not be included allowing for much quicker computational times.
A detailed yet simple method for predicting connection temperatures is still unavailable and therefore more work is required in this field.

4. ACKNOWLDGEMENT

The authors wish to thank Arup Fire and EPSRC for funding this research. They also thank Dr. Y. Wang and Dr. X. Dai of the University of Manchester for allowing access to experimental results in advance of publication.

REFERENCES

[1] Bailey, CG, Lennon, T and Moore, DB, “The behaviour of full-scale steel framed buildings subjected to compartment fires”, The Structural Engineer, pp. 15-21, April 1999
[2] CEN, EC 3: Design of Steel Structures part 1.2: General rules - Structural Fire Design, BS EN 1993-1-2:2005, Brussels: CEN, European Committee for Standardisation, 2006b
[3] ABAQUS User’s Manual, version 6.6, Providence, RI, USA
[4] Incropea, FP, DeWitt, DP, Bergman, TL and Lavine, AS, ‘Fundamentals of Heat and Mass Transfer’ John Wiley & Sons, Hoboken, USA, Sixth Edition , 2005
[5] Dai, XH, Wang, YC & Bailey, CG, ‘Temperature distributions in unprotected steel connections in fire’ Proc. Steel & Composite Structures, Manchester, UK , pp. 535-540, 2007
[6] Dai, XH, Wang YC & Bailey CG, ‘Effects of partial fire protection on temperatures developments in steel joints protected by intumescent coating’ Fire Safety J., pp. 16-32, Jan. 2009
[7] Lennon, T. and Moore, DB, ‘Results and observations from full-scale fire test at BRE Cardington, 16 January 2003’ BRE, Watford, UK, 2004

STRUCTURAL FIRE ENGINEERING ASSESSMENTS OF THE FRACOF AND MOKRSKO FIRE TESTS
An Engineering Prediction

Anthony K. Abu [a], Florian M. Block [a], Neal A. Butterworth [a] and Ian W. Burgess [b]

[a] Buro Happold Ltd., FEDRA, Leeds, United Kingdom
[b] University of Sheffield, Department of Civil and Strructral Engineering, Sheffield, United Kingdom

INTRODUCTION

The fire engineering of steel and composite frame buildings has become more and more standard practice in the UK in recent years. Simplified design methods allow structural engineers to omit fire protection from large numbers of composite beams. However, there are always buildings which fall outside the relatively tight boundaries of the simplified methods, and more advanced analysis approaches, normally implying the use of general or specialist finite element programs, are used. Although, these programs have been extensively validated during their development against available test data, the way in which a model is created and its results interpreted is extremely important. This was seen during the "Round Robin" CFD modelling of the Dalmarnock fire test [1]. Acknowledging that modelling of the dynamics of a fire is inherently less deterministic than that of the structural response of a building in fire, a similar lesson should be learned, as the effects of possible "modelling" mistakes could lead to catastrophic consequences.

As mentioned above, the FEM programs used to predict the structural response to fire have been validated against available test data. However, the bulk of the available test data comes from a series of just seven fire tests on a single building constructed in an old airship hanger in Bedfordshire, UK. The Cardington test building was designed as a typical composite frame building of the early 1990s, using standard UK building practice and details, which limits the available validation cases for the FEM programs to one particular type of construction. None of the tests led to the collapse of the building. The fact that the building techniques have developed further, and that finite element analyses of buildings in fire are conducted all over the world, means that programs are likely to be used outside the boundaries of the validations conducted. It is therefore even more important that parametric studies are carried out and that special care is given to the "modelling" assumptions and interpretation during the design process in order to give robust answers.

The year 2008, provided the opportunity for more diverse validation cases, with two full scale fire tests on parts of composite steel frame buildings. The first was the FRACOF fire test in Metz, France, in which a single slab panel with two unprotected secondary beams was tested under exposure to a 120-minute ISO834 Standard Fire. The second was the Mokrsko fire test, south of Prague in the Czech Republic, which exposed a purpose-built single-storey building to a natural fire. Buro Happold Ltd and the University of Sheffield used these opportunities to predict the structural behaviour prior to the tests, using the specialist finite element program *Vulcan*. During the assessments a number of parameters were varied within the normal range expected on site. For the FRACOF test two models were analysed before the test, with a more detailed follow-up in its aftermath. For the Mokrsko test the majority of the analyses were initiated before the test. The analyses were treated no differently from those for normal structural fire engineering projects, and it was expected to see conservative results. The results of the FRACOF assessment will be shown first, followed by the Mokrsko predictions.

1 THE FRACOF FIRE TEST

The FRACOF test was designed to demonstrate the benefits of incorporating tensile membrane action into the design of steel-framed composite floor systems in the European Community, and to assist in preparation of design guidance for its implementation. The test was therefore to investigate the performance of slab panels, as documented in the SCI document P-288 [2], and the effects of different construction details on their fire resistance.

1.1 Test description

The test was set up as an 8.74m x 6.66m composite slab panel, representative of a corner compartment. It included four equally-spaced IPE 300 downstand secondary beams spanning in the longer direction, with IPE 400 primary beams. The floor arrangement was supported by HEB 260 steel columns, using simple connections. The slab was 155mm deep, on COFRAPLUS 60 decking, acting compositely with the steel beams. Beams and columns at the edge of the structure were wrapped in 50mm of Cerablanket protection (density = 128kg/m^3; specific heat capacity = 1130J/kgK; thermal conductivity = 0.06 – 0.2W/mK). Continuity across the two adjacent "internal" edges was simulated by welding the anti-crack mesh (7mm diameter bars at 150mm centres, placed 50mm below the top of the slab) to the flanges of horizontally-aligned HEB 200 sections before the concrete slab was cast. A gravity load of 3.87kN/m^2 was placed on the slab to simulate live loading at the fire limit state. The base of the structural assembly was exposed to the Standard Fire for 120min. Details of the test setup and results can be found in Reference [3].

1.2 Test predictions

Five finite element test predictions are reported here; the first two were made before the test, with the subsequent three conducted afterwards, to correct differences in assumptions between the test design brief and the models. An overall slab thickness of 160mm had been specified in the brief, with no specific data on concrete strength. The applied load was given as 3.75kN/m^2, and it was assumed that the intended slab continuity would be achieved along the two adjacent "internal" edges. Based on the design brief and an assumed concrete cube strength of 40N/mm^2 the first predictions were made with protected beam and column temperatures following Eurocode 3: Part 1.2 [4] calculations, making a conservative assumption of Cerablanket thermal conductivity of 0.2W/mK. One-dimensional heat transfer was assumed for the concrete slab. The structural response predictions were made using *Vulcan* [5].

The first model considered the 8.74m x 6.66m slab as an isolated slab panel, supported vertically at its corners, with protected beams providing the necessary vertical support along the slab edges. The model used no axial restraints along its edges, but rotational restraints along two adjacent edges to simulate slab continuity across those boundaries. For conservatism, the 102mm thick continuous concrete layer above the decking troughs was modelled as a flat slab. The second *Vulcan* assessment used a full model of the test setup. It included the columns at the corners of the panel and the two horizontally-aligned HEB 200 sections along the "internal" adjacent edges for continuity. The orthotropic nature of the slab was accounted for by the using the *Vulcan* effective stiffness representation, developed by Huang *et al.* [6]. In this approach the full depth of the composite slab is modelled as a flat slab with different bending stiffnesses in the two orthogonal directions to account for the contribution of the ribs. The two models are shown in *Fig. 1*.

Test observations showed that the continuity condition was only practically achieved across the shorter edge. It was also observed that the protected beams and columns were not entirely within the furnace, and so did not attain appreciable temperatures or deformations.

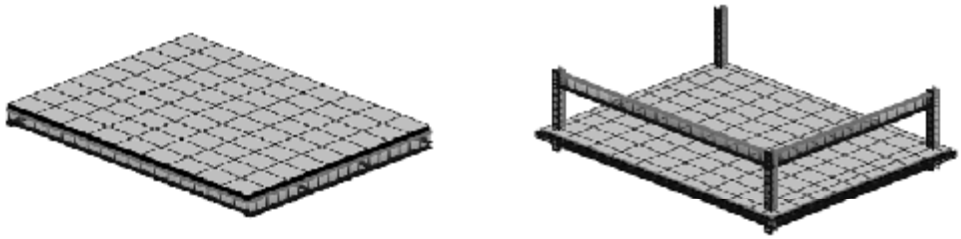

(a) *Vulcan* slab panel (b) Full *Vulcan* test setup

Fig.1. Vulcan models

This kept the slab panel boundaries supported vertically throughout the test. At 105mins however, fracture of a welded lap joint in the mesh caused an integrity failure of the central region of the slab. The *Vulcan* analyses are described in *Table 1*, and the central slab panel displacements predicted are plotted in *Figs. 2* and *3* together with the central vertical displacement from the test.

Table 1. Modified parameters in the *Vulcan* analyses

Parameter	V1	V2	V3	V4	V5
Concrete strength [N/mm^2]	40	40	37	37	37
Overall Slab thickness [mm]	160	160	155	155	155
Applied load [kN/m2]	3.75	3.75	3.87	3.87	3.87
Thermal conductivity [W/mK]	0.2	0.2	0.06	0.06	0.06
Protected beam temperature distribution	Uniform	Uniform	Uniform	Non-uniform	Non-uniform
Edge continuity condition	2 edges	2 edges	1 edge	1 edge	1 edge
Slab modelling approach	Thin continuous concrete	Effective stiffness	Effective stiffness	Effective stiffness	Average slab depth

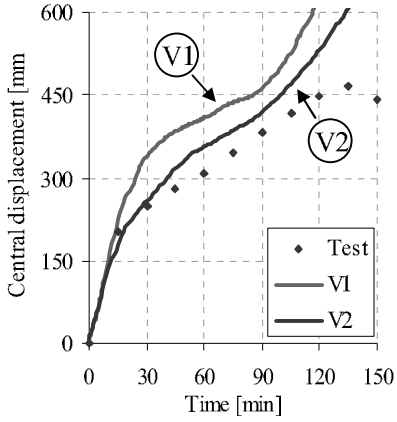

Fig. 2. Vulcan pre-test predictions

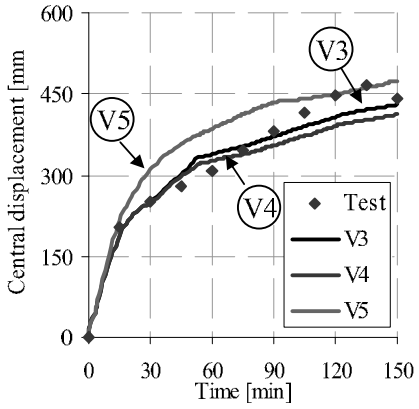

Fig. 3. Vulcan post-test predictions

It is observed that the initial predictions (*Fig. 2*) conservatively estimated the test deflection, although exact structural detail was not available. The subsequent analyses however showed better predictions (*Fig. 3*) using more realistic protected beam temperatures, non-uniform temperature distributions and the average slab depth approach. It is noticeable that the software's estimate of deflection worsened as the integrity failure point was approached.

2 THE MOKRSKO FIRE TEST

This fire test was conducted on the 18 September 2008 at Mokrsko, Czech Republic, by the Department of Steel and Timber Structures of the Czech Technical University of Prague.
The structure represented one floor of a steel and concrete composite office building consisting of four bays with a size of 9m x 6m each, and tested three different floor systems, namely "Angelina" composite beams developed by Arcelor-Mittal with elongated web openings, beams with corrugated webs made from thin steel plate, and precast hollow-core panels. The steel beams supported a composite slab with a total thickness of 120mm supported on CF46 metal decking. The slab was reinforced with a smooth mesh, providing a steel area of 196mm^2/m in each direction, situated 20mm from the top of the slab as well as 12mm bars in each rib. The connections of the Angelina beams were by specially designed endplates which only connected the top flange and a small part of the web of each beam. The bases of the columns were constructed as pinned. The imposed load of 3.0kN/m^2 on the slab was generated by sand bags, and the self-weight of the floor system was 2.6kN/m^2. Timber cribs generated a total fire load of about 620MJ/m^2, and two 2.5m x 4m openings at the front provided ventilation to the fire. Steelwork fire protection was omitted from all Angelina beams, as well as the beams with corrugated webs. The rest of the steelwork was fire-protected using fire-board. This protection arrangement generated a 9m x 12m bay of unprotected Angelina beams, and a 9m x 6m bay of beams with corrugated webs, surrounded by protected beams. However, it left one edge column restrained in only one direction by fire-protected beams.
The fire burned a little cooler than expected, but after about 61 minutes three quarters of the structure collapsed; this is the only large-scale structural fire experiment which has generated a structural collapse. The corrugated web beams developed shear buckles near their ends, but their overall vertical deflections were relatively small; this can be explained by their greater depths and flange thicknesses compared with the Angelina beams. The Angelina beams showed severe Vierendeel bending across their first two openings, and after about 50 minutes the bottom flanges of some of the Angelina beams deformed laterally, folding the beams along their longitudinal axes. More details are given by Wald and Kallerová [7].

3.2 *Vulcan* modelling of the Mokrsko fire test

Before the test, the experiment was modelled using *Vulcan,* using only the fairly limited data available at the time. For simplification only the 3 bays with the composite slab were modelled, and the Angelina beams and the corrugated-web beams were represented using an effective web thickness approach which calculates a reduced web thickness based on the net cross section. This approach usually gives good overall results for beams with web openings but cannot adequately represent local effects around the openings.

Fig. 4. Fire test set-up

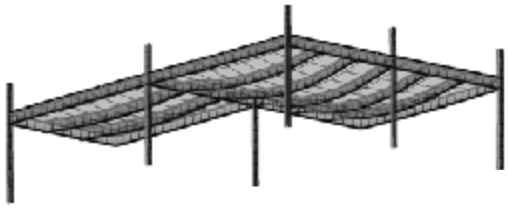

Fig. 5. Deformed Vulcan model

As with a normal structural fire engineering project a number of parameters were varied in order to test the robustness of the solution. Firstly, the fire was altered to produce a short-hot fire and a cooler-longer fire. The position of the reinforcement in the slab was then varied by

± 15mm to account for normal construction tolerances. The beam connections were modelled as rigid, which tends to be acceptable for normal composite connections designed to UK design rules in braced frames. Because of space restrictions here, only the results for the different fire curves are shown below.

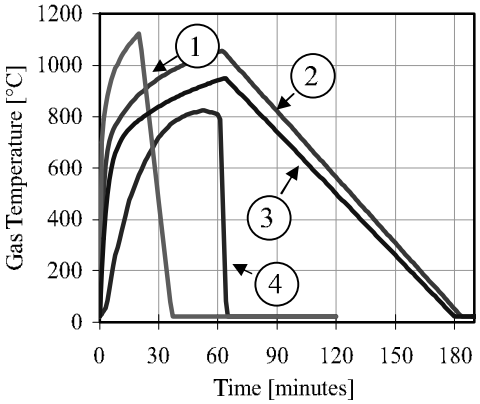

Fig. 6. Fire curves

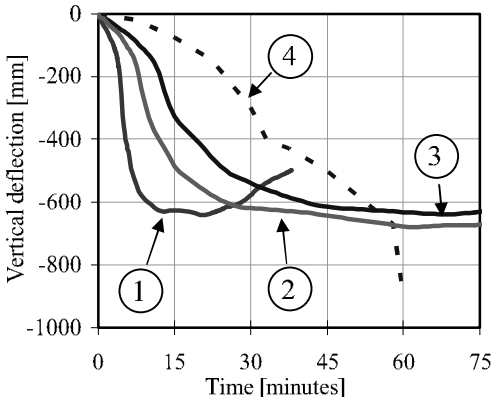

Fig. 7. Vulcan deflection prediction

It can be seen from *Fig. 6* that the real fire (4) in the experiment burned significantly cooler than the predicted fire (2). *Fig. 7* shows the resulting vertical deflections from the test and the three different design fires at the middle of the large bay of Angelina beams (V3).
The predictions show a much earlier increase in deflections than the experimental results. This is because the parametric fire curves represent post-flashover fires, and should therefore be moved by about 15minutes to give a realistic representation of the fire. This greatly improves the estimation of the fire test deflections. The models continued beyond the failure point of the test at about 61minutes, and do not show any indication of collapse, however the vertical deflections of the slab are in excess of span/15, which would normally result in an increase of reinforcement to limit the vertical deflections. Furthermore, all beams framing into columns would be protected in a robust design for fire.

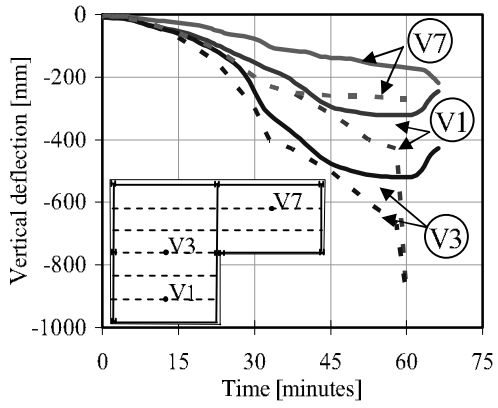

Fig. 8. Prediction using the average test temp.

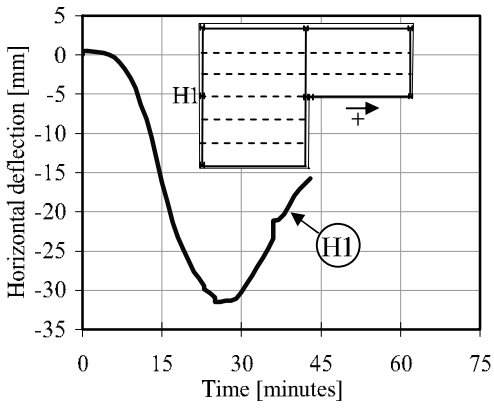

Fig. 9. Deflection of column head

After the test results were released, the actual temperature data was used as more accurate input data to the *Vulcan* model. *Fig. 8* shows that when the real temperature data is used the vertical deflections are represented relatively accurately up to about 44 minutes. The small vertical differences are due to the edge beam deflections, which are lower than those seen in the test, as well as to the use of average compartment gas temperatures to heat all elements.

The difference between prediction and reality for the beams with corrugated webs (V7) can be explained by the observed shear buckling of the thin webs, which cannot be represented by the chosen way of modelling the beams.
Due to the very flexible beam connections, another set of analyses were conducted in which the connections were modelled as pinned. In these cases the *Vulcan* models predict failure at around 43 minutes using the experimental fire temperature data. From *Fig. 8* it can be seen that this is the point at which the *Vulcan* and test results diverge. *Fig. 9* shows the horizontal displacement at the top of the edge column connected to an unprotected Angelina beam. It can be seen that, after an initial outwards movement due to thermal expansion of the structure, the column moves inwards due to pull-in by the vertically-deflecting Angelina beams. This observation may prompt speculation about a possible cause of the test failure, but due to the lack of test data and further in-depth analyses at this time, this is not investigated further here.

4 CONCLUSION

In this paper, it is again confirmed that it is possible to make conservative overall predictions of the response of composite structures to fire using sophisticated finite element programs and that modelling can be accurate with accurate data. However, in both test cases it was not possible to predict the exact failure mode or time prior to the tests. With the accurate data given by the tests a fairly accurate representation of the structural behaviour can be made, and this implies that conservative assumptions will produce conservative predictions.
The integrity failure in the FRACOF test was undoubtedly related to the lap-welding of the mesh, but it will be necessary in future to develop programmable criteria for this local slab fracture. The unexpected collapse in the Mokrsko test is at present unexplained, but probably relates to construction details (pinned column bases, connections with limited tying capacity, columns connected to unprotected beams, poor connection between slabs and edge beams) which lack robustness. It is essential that robust construction details are developed and specified if fire protection is to be omitted from structural elements. If finite element analyses are used to justify the behaviour of non-standard forms of construction, which are most likely to lie outside the bounds of software validation, great care should be taken when modelling these problems, using detailed parametric studies and possibly even physical fire testing.

REFERENCES

[1] G Rein, JL Torero, W Jahn, J Stern-Gottfried, NL Ryder, S Desanghere, M Lázaro, F Mowrer, A Coles, D Joyeux, D Alvear, JA Capote, A Jowsey, C Abecassis-Empis, P Reszka, *Round-Robin Study of a priori Modelling Predictions of The Dalmarnock Fire Test One*, Fire Safety Journal (in press), 2009.

[2] Newman, G. M., Robinson, J. T. and Bailey, C. G., *Fire Safe Design: A New Approach to Multi-Storey Steel-Framed Buildings*, Second Edition, SCI Publication P288, The Steel Construction Institute, UK, 2006

[3] Zhao, B., Roosefid, M. and Vassart, O., *Full scale test of a steel and concrete composite floor exposed to ISO fire*, Proceedings of the 5th Structures in Fire Workshop SiF'08, Singapore City, Singapore, 2008, 539-550.

[4] European Committee for Standardization, *Eurocode 3: Design of Steel Structures – Part 1.2: General Rules – Structural Fire Design.*

[5] Vulcan Solutions Limited: *http://www.vulcan-solutions.com*

[6] Huang, Z., Burgess, I.W. and Plank, R.J., *Effective Stiffness Modelling of Composite Concrete Slabs in Fire*, Engineering Structures 22 (9), 2000, 1133-1144

[7] Wald, F. and Kallerová, P., *Description of Fire Test on Experimental Structure in Mokrsko,* http://fire.fsv.cvut.cz/firetest_Mokrsko/pdf/Test_report.pdf

A NEW DESIGN METHOD FOR INDUSTRIAL PORTAL FRAMES IN FIRE

Yuanyuan Song [a], Zhaohui Huang [b], Ian Burgess [c], Roger Plank [d]

[a] Safe Consulting Limited, Manchester, UK
[b,c] Department of Civil and Structural Engineering, University of Sheffield, UK
[d] School of Architectural Studies, University of Sheffield, UK

INTRODUCTION

For single-storey steel portal frames in fire, especially when situated close to a site perimeter, it is imperative that the boundary walls stay close to vertical, so that fires which occur are not allowed to spread to adjacent properties. A current UK fire design guide [1] requires either that the whole frame be protected as a single element, or that the rafter can be left unprotected but the column bases and foundations should be designed to resist the forces and moments necessary to prevent collapse of rafter, in order to ensure the lateral stability of the boundary walls. Some arbitrary assumptions regarding the behaviour of the frame in fire, which are used to simplify this current design model, can lead to very uneconomical foundation design and base-plate detailing. Further understanding of the behaviour of portal frames in fire is required, to provide other design options so that over-design of column bases and foundations can be avoided, and a more reasonable prediction of real critical temperatures can be made.

On the basis of fire tests, a simplified method to estimate the critical temperatures of portal frames in fire was developed by Wong in 2001 [2] for single-span portal frames with simple base connections. It was shown by numerical modelling that this method could predict the temperature at which the rafters initially lose stability in fire. A recently developed quasi-static analysis [3], implemented in the program *Vulcan*, using a combination of static and dynamic solvers, has also shown that the strong base connections recommended by the current design method may not always lead to a conservative design. A second-phase failure mechanism observed in numerical modelling corresponds with the failure mode shown in one of the previous fire tests. The critical temperature at which run-away collapse occurs may be higher than that at which the roof initially loses its stability, because of re-stabilisation.

In this paper, a new method for estimating critical temperatures of single-span frames in fire, using these two failure mechanisms, is presented. Numerical tests on typical industrial frames are used to calibrate this new method against the current design method.

1 BEHAVIOUR OF SINGLE-STOREY PORTAL FRAMES IN FIRE

As early as 1979 the behaviour of steel portal frames in accidental fires was described in the report of a study [4] of fires in a number of portal frames in the UK. A typical variation of the overturning moment at the column base with time, after a fire is ignited in a pitched-roof portal frame is described in the CONSTRADO design guide [5]. It was believed that the stability of the column was mainly determined by the resistance provided by the column base connections. However, the fire test on a scaled pitched-roof portal frame performed in 1999 [2] showed that the steel columns, connected to their foundations by a fairly flexible connection, could stand almost upright throughout the fire while the rafters snapped-through to a inverted

shape. This indicates that strong column bases are not always essential to the stability of an industrial frame under fire conditions.

It has been postulated by O'Meagher *et al.* [6] that unaffected parts of a building can act as anchorage for the fire-affected zone, provided that the forces developed in the purlins are reasonably small and that they have sufficient capacity at high temperatures, so that cold frames will also deform in an acceptable mode. The results of a series of parametric studies [2] using the two- and three-dimensional modelling showed that that the initial collapse of a portal frame with semi-rigid bases initially loses stability in a combined mechanism, which differs from the assumption used in the current design method. Further deformation could not be simulated because of the limitations of the static solver.

In a previous paper the behaviour of single-span pitched portal frames was simulated using the recently-developed quasi-static solver [3] in *Vulcan*. This showed that collapse of the frame happens in two phases [7]. It was also found that initial collapse of the rafter is always caused by a plastic hinge mechanism which is based on the frame's initial configuration. If the frame can re-stabilize when the roof is substantially inverted, a second plastic mechanism based on the re-stabilized configuration leads to eventual failure of the whole frame.

2 NEW DESIGN METHOD

A single-span portal frame fails either in the first-phase mechanism when it initially loses stability, or may re-stabilise for a while before collapsing in the second-phase mechanism. The simple method developed by Wong [2] is based on the initial configuration of the frame. Hence, it is capable of explaining the reason why frames initially lose stability in fire, but is not valid for frame collapse in the second mechanism, in which the deformation of the frame is significant. The estimation of the critical temperatures for a two-phase failure mechanism should be based on different initial configurations for each of the two phases.

2.1 Estimation of First-Phase Failure

When the roof of the frame starts to deform downward under the loading and fire temperature, the columns are pushed outward due to the change of geometry and to thermal expansion of the rafters. For a portal frame with frictionless pinned base connections, high rotations can be generated at these bases, caused by either elastic or plastic deformation. These rotations, together with the fire hinges formed at the apex and eaves, can generate a "combined" plastic mechanism. Wong's simple model, as shown in *Fig. 1*, uses this mechanism, whose kinematics is referred to the initial configuration of the portal frame. This method can only apply to the frame's initial loss of stability at relatively low deflections. According to plastic theory, for the mechanism shown in *Fig. 1*, the fire hinge moments at corners 1 and 2 can be calculated. The ratio of the fire hinge moment to the normal moment capacity is given by the strength reduction factor at the critical temperature, so the critical temperature of this frame can be interpolated from stress-strain curves defined in Eurocode 3 Part 1. 2 [8].

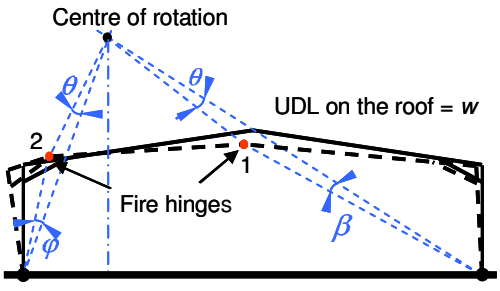

Fig. 1. The model of Wong's simple design method.

2.2 Estimation of Second-Phase Failure

The initial collapse of the roof frame may initiate a "combined" mechanism leading to

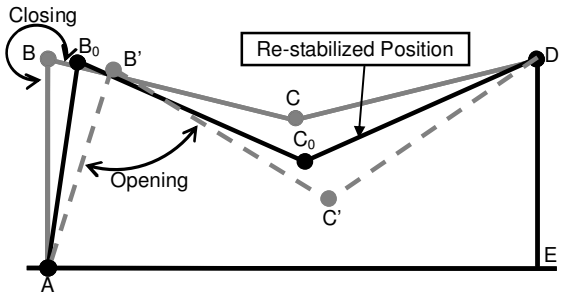

Fig. 2. Illustration of the second phase mechanism.

collapse of the whole frame, or the columns may be pulled back towards the upright position (see shape ABCDE in *Fig. 2*) due to the collapse of the rafters.

In the latter case the change of direction of the column's rotation causes elastic unloading of the base moments of the columns, so that the plastic hinges developed at the bases are effectively locked. When the pitched roof deflects further than the position BCD, column AB is pulled inward, so that the base moments of the columns increase again. When the rotation of the column AB is faster than the rotation of the adjacent rafter, the moment on one eave (corner B) starts to reverse, leading to locking of the adjacent plastic hinge. This causes the frame to re-stabilise at this position (Shape AB_0C_0DE in *Fig. 2*), at which the internal angle (AB_0C_0) between column AB_0 and the connected rafter BC_0 stops closing and starts opening. With further increase of the pulling force at the column top caused by catenary action of the inverted roof, the fire hinges at the eave and column base can be mobilised again (shape AB'C'DE in *Fig. 2*), and a new mechanism, referred to as the second-phase failure mechanism, is established which leads to complete collapse of the frame.

The new design method developed here focuses mainly on collapse caused by the second-phase mechanism in fire, and aims to predict the critical temperatures which initiate formation of the second-phase failure mechanism. The method is based on calculating the strength reduction factor of the fire hinge moment according to the work balance within the frame.

Because of the significant deformation of the roof frame before the start of the second failure mechanism, this new model has to identify the re-stabilised position of the frame and its critical position at the start point of the second-phase mechanism. Both the thermal elongation of rafters and degradation of fire hinge moments at elevated temperatures are considered under some temperature assumption. Moreover, because a plastic hinge at one column base is essential to generate a second-phase mechanism, the strength of the column bases is also included in this new method.

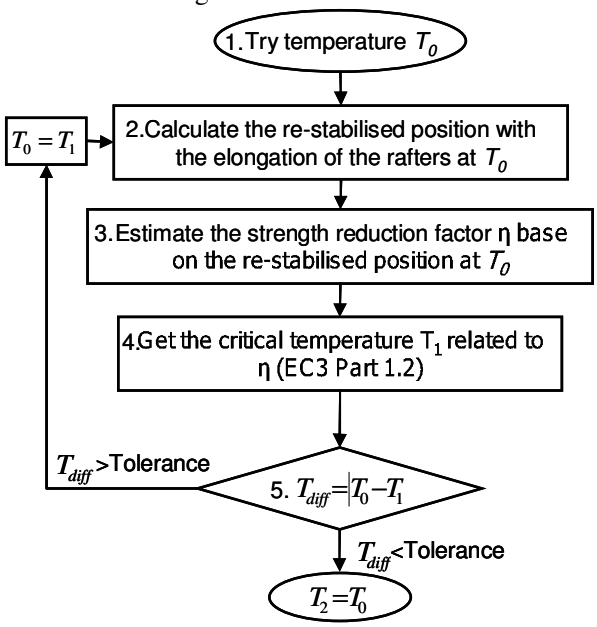

Fig. 3. The procedure for estimating the critical temperature of second phase failure.

When the second-phase mechanism of the frame is established, the elongation of the rafters is significant. This should not be ignored when the work balance is calculated within this system. Estimation of the critical temperature for the second-phase mechanism of the frame is also based on the reduced moment capacity of

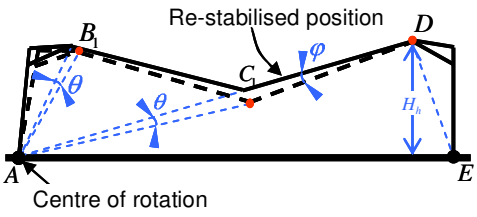

Fig. 4. The model of the second-phase failure

the rafters. Because the strength reduction factor and the steel elongation at the critical temperature are both unknown, an iterative solution procedure, illustrated by the flow chart in *Fig. 3,* is required.

At the beginning of the second-phase calculation, an initial temperature T_0 is assumed, so the re-stabilised position can be estimated on the basis of the geometry of the frame, including the elongation of the rafter, at temperature T_0. The fire hinge moment can also be calculated on the basis of the configuration of the frame at the re-stabilised position (as shown in *Fig. 4*) and the work balance based on plastic theory. The critical temperature T_1 can be obtained from the strength reduction factor given by dividing the fire hinge moment by the moment capacity of the rafter section, and relating this to the corresponding temperature, as defined in Eurocode 3 Part 1.2 [8]. If the difference between T_0 and T_1 is larger than the tolerance required, Steps 2 to 5 as defined in *Fig. 3* are repeated, using the elongated lengths of the rafters at T_1, until T_{diff} is smaller than the tolerance required. The temperature T_1 estimated from the final iteration is the critical temperature of the frame at the beginning of the second-phase mechanism.

3 VALIDATIONS AGAINST NUMERICAL TESTS

In order to validate the new design method a series of comparison between critical failure temperatures predicted using the new design method and those obtained from previous numerical tests [9], have been conducted. Because the two-phase mechanisms are included in this method, critical temperatures for the creation of both the first- and the second-phase mechanisms are compared.

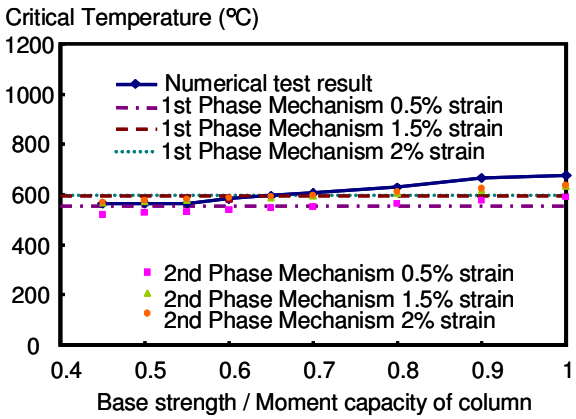

Fig. 5. Portal frames without haunches.

Figs. 5 and *6* compare the critical temperatures predicted by the new design method and numerical analysis results for two typical portal frames. The results presented in *Fig. 5* are for the portal frame designed without haunches but with varying base strength. Results for the other portal frame, which is designed with typical-sized haunches and modelled with different base strengths, are shown in *Fig. 6.*

The first re-stabilised position of the frame is reached when the rafter is deformed into the inverted position and the vertical displacement of the apex is around 5m. The prediction of the new design method is 5m. This confirms that re-stabilisation during the collapse of the portal frame is caused by locking of the plastic hinge near to an eave, which disables the first-phase mechanism. Once the opening of the locked angle exceeds the elastic rotation limit, the frame loses its stability again.

For the frame with haunches, the re-stabilised position predicted by the new design method is about 0.4m lower than for the numerical results. This is because, in the new design method, a re-stabilised position is assumed to occur when, in the first-phase mechanism, the rafter ceases to rotate relative to the column at hinge B (*Fig. 4*) and this hinge consequently locks itself. When the hinge finally begins to rotate again, in the opposite sense to its original rotation, the second-phase mechanism is created and failure occurs. Locking of the plastic hinges developed at one of the column bases could also be encountered when the column is pulled inward and passes its original position, so collapse is arrested until the plastic hinge at the base A is unlocked. When this hinge is mobilised, the frame is capable of continuing to collapse until the fire hinge near the end of the haunch locks itself. This explains the difference between the re-stabilised positions predicted by numerical tests and this new design method. It is worth noting that the main purpose for estimating the re-stabilised position is to determine the critical configuration of the frame on the basis of the principle of work balance. Therefore the final equilibrium position of the frame before it collapses again should be adopted in order to estimate the critical temperature.

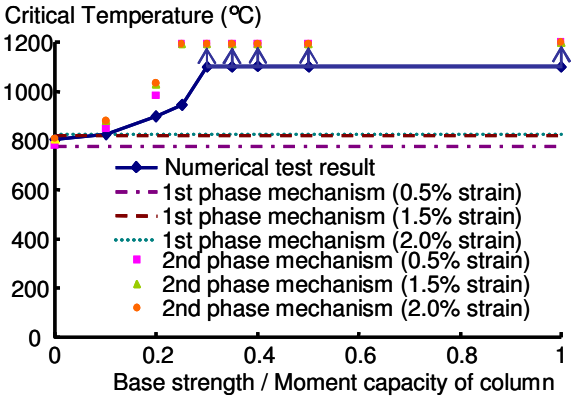

Fig. 6. Portal frames with haunches

From the previous numerical studies, the portal frame would fail in its first-phase mechanism when the ratio between the base strength and moment capacity of the column is lower than 0.55 for the unhaunched case and 0.1 for the haunched case. The reduced "yield stress" at 0.5% steel strain leads to a better prediction of the critical temperature of the frame without haunches in the new design method. As shown in *Fig. 5* the critical temperatures predicted by the new method for the second-phase mechanism according to the strength reduction factors at 1.5% and 2.0% strain show a similar trend to the numerical results.

From *Fig. 6* it is evident that, for a haunched frame with base strength equal to 10% of the moment capacity of the column section, the critical temperatures predicted by the new design method for the first-phase mechanism are very close to the numerical results. However, the numerical analyses give higher limiting temperatures for cases with base strength greater than 20% of the moment capacity of the column.

In the new design method the strength reduction factor obtained from equilibrium on the basis of the second-phase mechanism, becomes negative when the base strength is higher than 30% of the moment capacity of column. This means that the work done by the plastic hinges developed at the bases exceeds the work done by the external forces, and hence the second-phase mechanism can not happen, and the frame will stand in its re-stabilised position under further temperature increases.

4 CONCLUSION

A new design method, extended from Wong's model is presented in this paper. In this method, instead of relying on a single failure mechanism, the two most common failure mechanisms for pitched portal frames under fire conditions are considered to predict the critical temperatures of the frame. The critical temperatures predicted by the new design method on the basis of the first-phase failure mechanism show very good agreement with the numerical results at which a typical frame initially loses stability in fire. Very reasonable

predictions about the re-stabilised position and the final collapse temperatures of the frames were achieved using this new design method. It is evident from this study that the initial collapse of the frame due to the first failure mechanism is often a temporary instability, and that after this the frame can experience a second-phase mechanism with a higher critical temperature, which depends on the base strength and the loading conditions of the frame.
When the frame collapses at the beginning of the first-phase mechanism, the inclination of the columns may be relatively small, so this could be a lower bound for the design of portal frames in a fire boundary condition. The re-stabilisation after the initial loss of stability of the frame can be estimated from the critical temperature predicted on the basis of the second-phase mechanism. In this new design method, when the strength reduction factor, calculated from work equilibrium for the second-phase mechanism of the frame, becomes negative it is possible that the portal frame could remain in its re-stabilised state after snap-through of the pitched roof, and may not collapse until a very high temperature is achieved.

REFERENCES

[1] Simms, W. I. and Newman, G. M., SCI Publication P313: Single Storey Steel Framed Buildings in Fire Boundary Conditions (2002 edn.), *The Steel Construction Institute*, 2002.

[2] Wong, S. Y., The Structural Response of Industrial Portal Frame Structures in Fire, *PhD Thesis, University of Sheffield*, 2001

[3] Song, Y., Huang, Z., Burgess, I. W. and Plank, R. J., The Behaviour of Single-Storey Industrial Steel Frames in Fire. *Acc. Advanced Steel Construction: an International Journal*, 2008.

[4] CONSTRADO, The Study of the Behaviour of Portal Frames in Fire When Subject to Boundary Conditions, *The Constructional Steel Research and Development Organisation*, 1979.

[5] CONSTRADO, Fire and Steel Construction: The Behaviour of Steel Portal Frames in Boundary Conditions, *The Constructional Steel Research and Development Organisation*, 1980.

[6] O'Meagher, A. J., Bennetts I. D., Daywansa, P. H., Thomas, I. R. and BHP Research, Melbourne Laboratories, Design of Single Storey Industrial Buildings for Fire Resistance. *Journal of Australian Institute of Steel Construction, Vol. 26, No.2*, 1992.

[7] Song, Y., Huang, Z., Burgess, I. W. and Plank, R. J., A New Design Method for Industrial Portal Frames in Fire, *Proc. Structures in Fire Workshop, pp302-312*, 2008.

[8] CEN, BS EN 1993-1-8:2005: Eurocode 3: Design of Steel Structures: Part 1.2: General Rules-Structural Fire Design, *European Committee for Standardization*, 2005.

[9] Song, Y., Analysis of Industrial Steel Portal Frames under Fire Conditions, *PhD Thesis, University of Sheffield,* 2009.

AN EXPERIMENTAL STUDY OF STRUCTURAL BEHAVIOUR OF JOINTS IN RESTRAINED STEEL FRAMES IN FIRES

X. H. Dai, Y.C. Wang and C. G. Bailey

School of Mechanical, Aerospace and Civil Engineering, University of Manchester, UK

INTRODUCTION

Joints are important members in steel framed structures and play a critical role in controlling progressive collapse of the structure under accidental fire attacks. Although previous research studies on steel-framed structures in fire have resulted in the development of fire engineering design methods (Wang 2002) that are now being widely adopted in practical steel structural fire resistant design, gaps still exist in understanding joint performance in fires. In order to understand joint performance in fire and develop feasible methods to quantify joint behaviour under complex loading conditions, a research project at the University of Manchester, in collaboration with the University of Sheffield, has been carried out to investigate the robustness of steel joints in fires. This collaborative research programme includes determination of temperatures in connection components with different fire protection schemes, bolt tests, elevated temperature tests on isolated joint assemblies and steel framed structures, development of component based methods etc. This paper only presents experimental results of the fire tests on structural assemblies. The results have revealed different possible failure modes of joint components and effects of column size and different joint types on structural fire behaviour of the connected beams. These tests have also demonstrated catenary action in restrained steel frames (Yin and Wang 2004, 2005a,b), which may be used to control progressive collapse of steel framed structures under exceptional fire attacks.

1 DESCRIPTION OF FIRE TESTS

In total ten fire tests were carried out in the fire testing laboratory at the University of Manchester. Each test used a fresh specimen specially designed in the form of "rugby-goalpost". UB 178 x 102 x 19 was used as the beam in all ten tests. The two column sections were Grade S355 UC 254 x 254 x 73 (for Tests 1 - Test 5) and Grade S275 UC 152 x 152 x 23 (for Test 6 –Test 10). All the bolts and nuts were M20 Grade 8.8 except for the bolts in Test 5 (using extended endplate connection and large column section) which used M20 Grade G10.9 bolts and nuts to prevent premature failure of the bolts and nuts due to thread stripping. All connection components (including fin plates, end plates and web cleats) were grade S275 steel. *Table 1* summarises the beam size, the column size, the joint type and the main joint component size for all the ten tests.

All specimens were tested in the fire testing furnace which had internal dimensions of 3000mm x1600mm x 900mm. *Fig.1* presents the elevation view of the test set up. The internal faces of the furnace were lined with ceramic fibre wool materials of thickness 200mm which could efficiently transfer heat to the test specimen. The furnace temperatures were recorded by using six conventional bead thermocouples whose average temperature was intended to follow the standard fire condition in ISO 834 (1975) in all tests.

In order to simulate the heat-sink effect of the concrete slab on beam top, the top flange of the steel beam was wrapped with a layer of 15 mm thick ceramic fibre blanket. A specially designed steel truss was bolted to the beam top flange to account for the lateral restraining effect of the concrete slab. Except for the top flange of the beam and the additional truss, all other members of the test specimen were unprotected. As shown in *Fig.1*, the columns were restrained from lateral movement at both ends and were only free to move in the longitudinal direction at the top end where a 25mm gap between the column top and the reaction frame to allow the column to develop free axial movement. To ensure that the loading jacks remained attached to the test beam, the hydraulic loading jacks were attached to the test beam using a special pin bracket system.

The target load of 40kN was applied to the steel beam in each hydraulic loading jack at ambient temperature, followed by fire exposure until the end of the test. This target load corresponds to a nominal load ratio of 0.5 in the beam, calculated as the ratio of the theoretical maximum bending moment in the simply supported beam to the plastic bending moment capacity of the beam at ambient temperature using a nominal steel yield stress of 275 N/mm^2. It was recognised that the presence of a compressive load in the column would affect the performance of the system. However, due to limitations in the laboratory, the columns were unloaded in all tests.

Table 1: Summary of specimen dimensions

Test ID	Joint type	Connection component dimension (mm)	Column section	Beam section
Test-1	fin plate	150x130x10	UC 254x254x73	UB 178x102x19
Test-2	flexible endplate	150x130x8		
Test-3	flush endplate	150x200x8		
Test-4	web cleat	90x150x10 (depth: 130)		
Test-5	extended endplate	150x250x8		
Test-6	fin plate	150x130x10	UC152x152x23	
Test-7	flexible endplate	150x130x8		
Test-8	flush endplate	150x200x8		
Test-9	web cleat	90x150x10 (depth: 130)		
Test-10	extended endplate	150x250x8		

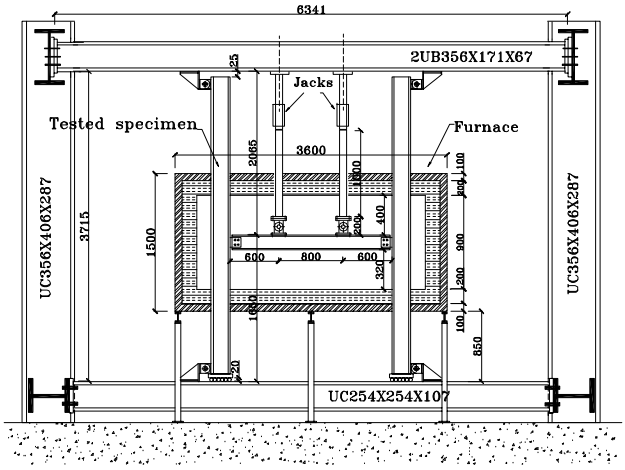

Fig.1: Elevation view of the test set up

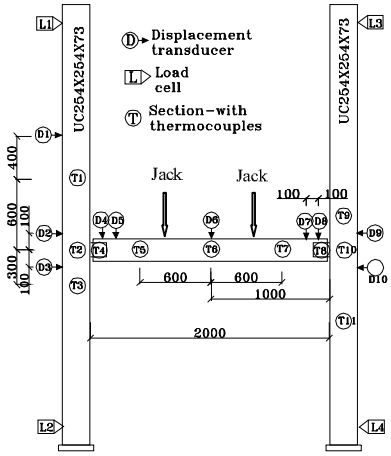

Fig.2: Arrangement of measurement devices on a specimen

To capture the temperature distribution in the tested specimen, numerous thermocouples were installed in the beam, columns and joint components. *Fig.2* shows the thermocouple stations. Since this paper will only concentrate on the structural behaviour, detailed temperature information will not be presented here. *Fig.2* also shows the displacement transducers (D1-D10) placed on the beam, the columns and around the joint zone to measure the beam deflections and column deformations. In order to obtain the axial load in the test beam, the horizontal reaction force at each column end was measured by a pin load cell (L1-L4) as shown in *Fig.2*.

2 TEST OBSERVATIONS AND FAILURE MODES OF JOINTS

The "failure" definition adopted here is to reflect the main objective of this study: to provide an insight into joint behaviour in terms of its contribution to preventing progressive collapse of the steel structure in fire. Therefore, as long as the structure is not physically detached from each other (fracture), it is assumed that the structure is still functioning or has not failed. Based on this

definition, *Table 2* summarised the main observations and failure modes (if observed) in each test. *Fig.3* shows possible connection failure modes. The following conclusions may be drawn based on the test observations: (1) With axial restraint to the steel beam, there will be axial force in the steel beam in fire. However, there was no failure in the structure when axial compression was developed in the beam. Failure was a result of the development of tension in the beam. (2) Failure occurred in the connections, not in the beams. When failure occurred, it was due to inadequate shear resistance of the beam web (Test-2) or weld fracture or bolt thread stripping due to a combination of the tensile forces from catenary action and hogging bending moment in the connection. (3) Although no quantitative analysis has been undertaken, it is possible to suggest that the web cleat connection would appear to be the most robust connection. Its good bending flexibility reduced the concentration of tensile axial force which reduced the extent of any tensile failure. Flush end plate and extended end plate connection could also provide sufficient connection robustness, but high strength bolts should be used to avoid thread stripping. Fin plate and flexible end plate connections performed poorly. (4) Catenary action is often relied on to ensure robustness of steel framed structures in fire. Although it is necessary for the joint to possess sufficient axial stiffness in order to develop catenary action in the steel beam, too large an axial restraint stiffness could attract a great catenary force to fracture the connection components.

Table 2: Summary of specimen observations and failure modes

Test ID	Joint type	Main observations	Failure mode
Test-1	fin plate	Beam flange bearing against column flange, little column deformation	Weld fracture
Test-2	flexible endplate	Beam web fractured mainly in shear, complete detachment of beam from column, little column deformation	Beam web fracture & detachment
Test-3	flush endplate	Thread-stripping of bolts and nuts, complete detachment of beam from column, little column deformation	Bolt thread stripping & detachment
Test-4	web cleat	Web cleat large deformation, thread-stripping of bolts and nuts of top bolts but connection not detached, little column deformation	Some bolt thread stripping
Test-5	extended endplate	Classical end plate ductile deformation, compressive buckling in beam lower flange, little column deformation	-
Test-6	fin plate	Beam flange bearing against column flange, plastic hinges in column	Weld fracture
Test-7	flexible endplate	Large flexible end plate and column flange deformations	Slight weld fracture
Test-8	flush endplate	Large column flange deformations, moderate end plate deformation	-
Test-9	web cleat	Large web cleat and column flange deformations	-
Test-10	extended endplate	Moderate end plate deformation, large column flange deformations, plastic hinges in column flanges	-

(a) Test-1 (b) Test-2 (c) Test-3 (d) Test-4

Fig. 3: Failure modes of joint components

3 EFFECTS OF COLUMN SIZE AND JOINT TYPES ON STRUCTURAL FIRE BEHAVIOUR

The qualitative behaviour of an axially restrained beam is now well established (Wang 2002) and confirmed by a theoretical study by Yin and Wang (2004, 2005a, 2005b). Generally, the temperature at which the axial force of an axially restrained steel beam returns to zero is the same as the limiting temperature of the same beam without axial restraint. However, when the beam enters catenary stage, its ability to survive high temperature will depend on the connection's ability to resist the tension force due to catenary action and hogging bending moment. There are many factors may influence the connection's ability, such as joint types, structural member size, structural material, fire characteristics etc. The paper will only focus on effects of the two factors considered in this study: column size and connection types.

3.1 Effects of column sizes on structural fire behaviour

As a demonstration, *Fig.4(a)* compares beam mid-span deflections between frames using flush endplate connection with the two column section sizes. It can be seen that the beam experienced rapid increase in deflections within a very narrow temperature range. *Fig.4(b)* compares the corresponding beam axial forces. It can be seen that the temperature at which the beam experienced rapid increase in deflection is the same temperature at which the beam's axial force returns to zero, or changing from compression to tension. As expected, the beam temperature at which the beam started to experience large deflections (beam running away) in the frame using the larger columns was higher than that in the frame using the smaller columns. This means specimen that used the larger column size allowed the connections to develop higher bending moment capacities than the specimen that used the smaller column size. For the tested frames with other joint types (fin plate, web cleat, flexible endplate and extended endplate), similar observations have been obtained (figures are not presented here due to space limitation). Nevertheless, the temperature differences between these two sets (using different column sizes) of results are small as shown in *Fig. 4(b)*. *Fig. 4(b)* shows that the compressive axial forces in the test beams using the two different column sizes were drastically different with the large columns providing much greater axial restraint during the thermal expansion stage. However, if using the conventional limiting temperature, which is the temperature at which the beam's axial force is zero, and whose values are given in *Table 3*, the maximum difference between these two sets of results is 28 C. Therefore, it appears that changing the steel column size is an unlikely source of improving the beam's fire resistance if adopting the conventional limiting temperature approach. According to the theoretical studies of Yin and Wang (2004,2005a,b), the catenary force will reach a peak and then decrease at increasing beam temperatures due to increasing beam deflection as well as decreasing mechanical properties of steel. However, due to connection failure in some tests (see *Table 2*) and limitations in the test setup it was not possible to observe this stage of beam behaviour.

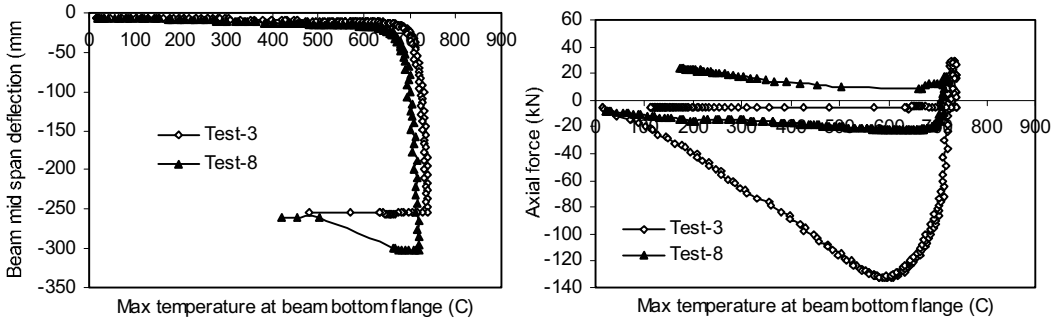

(a) Beam deflection (b) Beam end axial force

Fig.4: Comparisons of beam mid span deflection and axial forces to show the effects of different column sizes (flush end plate connection)

Table 3: Summary of beam limiting temperatures (with axial force=0)

Test ID	Test-1	Test-2	Test-3	Test-4	Test-5	Max temp difference by connection type (C)
Temperature (C)	748	728	728	750	753	25
Test ID	Test-6	Test-7	Test-8	Test-9	Test-10	
Temperature (C)	733	700	710	725	745	45
Max temp difference by column sizes (C)	15	28	18	25	8	

3.2 Effects of joint types on structural fire behaviour

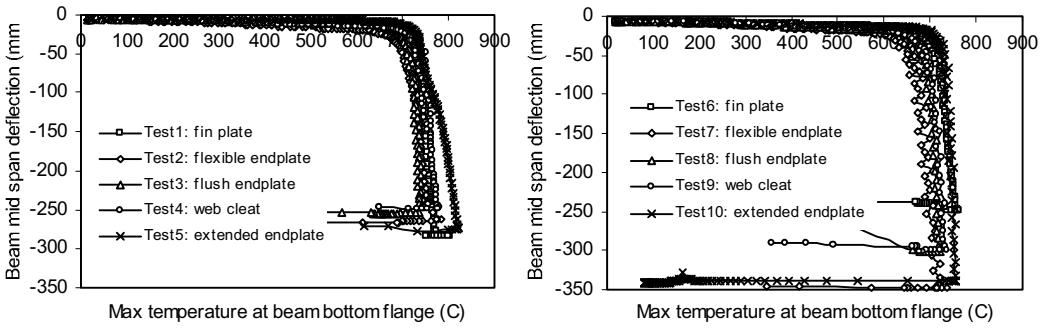

(a) Column size: UC254x254x73 (b) Column size: UC152x152x23

Fig. 5: Comparisons of beam deflections for different joint types

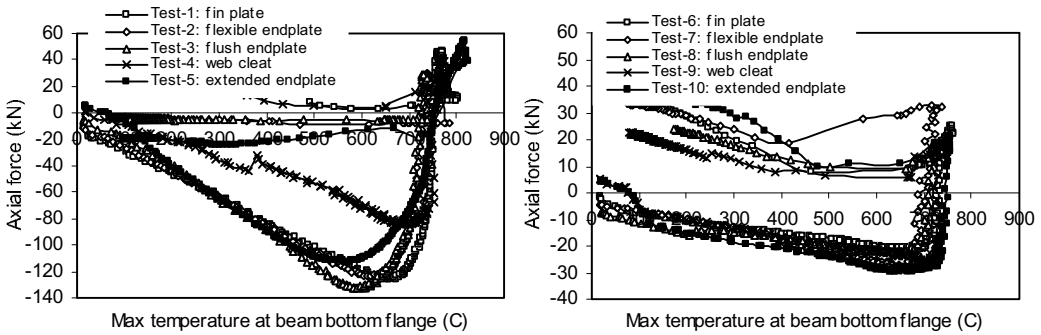

(a) Column size: UC254x254x73 (b) Column size: UC152x152x23

Fig. 6: Comparisons of beam axial forces for different joint types

Fig. 5 compares the beam mid-span deflections for using different joint types. It can be seen the difference is relatively small comparing to the large difference in joint types, ranging from nominal pin joints (fin plate, flexible endplate) to the relatively rigid extended end plate joints. Due to bearing between the beam lower flange and the column flange when using the fin plate connection, the nominally pinned fin plate connection resulted in a much more rigid behaviour. The poor behaviour of flush end plate in Test-3 is a result of severe asymmetrical heating in the testing furnace. *Fig. 6* compares the beam axial forces for the five different connection types. It is very clear that during the compression phase, the joint type had little effect on the axial force development except for the specimen using web cleat when the large columns were used. This is clearly an indication that due to the small joint zone, the joint may be considered to possess almost infinite axial restraint stiffness to the beam compared to the column size. This may be used to considerably simplify the whole frame analysis model when using springs to represent the effects of the joints. Again, if using the temperature at which the beam's axial force returns from compression to zero as its limiting temperature, the beam's limiting temperatures from the different tests are very

similar, the maximum difference being 45 C as given in *Table 3*. Considering the large range in connection bending behaviour (from nominally pinned to almost full strength), this indicates that it is not worthy using stiffer and stronger joints to increase the limiting temperature of the connected beam, if the beam's limiting temperature is based on its bending moment resistance.

4. CONCLUSIONS

This paper presents some results on test observations, connection failure modes and effects of different column sizes and joint types on the behaviour of the joints and the connected beams. Although due to limitations of the test set up, the structural behaviour during the entire phase of beam catenary action has not been fully captured, it is still possible to achieve some tangible conclusions with regard to robust joint design and fire resistant design of steel framed structures. The main conclusions are:

- The fire tests have revealed a number of joint failure modes, including weld tearing, beam web fracture and bolt thread stripping. The test data will provide valuable insight in detailed understanding of joint behaviour and failure.
- The test beams were able to experience very large deflections (span/8~span/6) without fracture.
- If beam limiting temperature is calculated based on its bending moment resistance, the effect of using different joints (ranging from nominally pinned to almost full strength) has very little effect, with the changing in beam limiting temperature being less than 50°C. The effect of column size is even smaller, less than 30°C.
- Using different joint types had very little effect on the beam's axial force in compression. But using different column sizes had great effect. However, irrespective of the great effect of using different column sizes, the structure was able to sustain the applied load throughout the beam-in-compression phase.
- If catenary action in the beam is considered in fire resistant design (e.g. to consider structural robustness), the effects of different columns and different joints should be considered.
- If using the ability of a joint to allow the connected beam to develop catenary action without joint failure as criterion to assess joint robustness, the flexible end plate connection performed the poorest, then followed by flush end plate connection, fin plate connections, web cleat and extended end plate connections.

5. ACKNOWLEDGEMENTS

This research reported in this paper is funded by a research grant from the UK's Engineering and Physical Science Research Council (EP/C003004/1). The fire tests were conducted at the University of Manchester's Fire Test Laboratory, with technical assistance from Mr. Jim Gorst, Mr. Jim Gee, Mr. Martin Cruikshank and help from a number of PhD students including Jifeng Yuan, Pinyu Yan, Henry He, Penjun Wang in the authors' research group.

REFERENCES

[1] International Organization for Standardization (ISO 834 1975): Fire Resistance Tests, Elements of Building Construction, Geneva: International Organization for Standardization.

[2] Wang Y.C. (2002), Steel and composite structures, behaviour and design for fire safety. London: Spon Press; 2002.

[3] Yin, Y.Z. and Wang, Y.C. (2004), "A numerical study of large deflection behaviour of restrained steel beams at elevated temperatures". Journal of Constructional Steel Research 60(2004) 1029-1047. 2004.

[4] Yin, Y.Z. and Wang, Y.C. (2005a), "Analysis of catenary action in steel beams using a simplified hand calculation method, Part 1: theory and validation for uniform temperature distribution". Journal of Constructional Steel Research 61(2005) 183-211. 2005.

[5] Yin, Y.Z. and Wang, Y.C. (2005b), "Analysis of catenary action in steel beams using a simplified hand calculation method, Part 2: validation for non-uniform temperature distribution". Journal of Constructional Steel Research 61(2005) 213-234. 2005.

EFFECTS OF FLAME RADIATION ON TEMPERATURE ELEVATION

of Steel Members in Large Space Building Fire

Du Yong [a]， Li Guo-qiang [b]

[a] Nanjing University of Technology, School of Architecture and Urban Planning, Nanjing, China

[b] Tongji University, School of Civil Engineering, Shanghai, China

INTRODUCTION

A significant amount of research work shows that in small compartments the temperature conditions at a given time are considered to be uniform and can be approximate as the flame temperature. However, temperature fields are non-uniform in large space building fires and lower than small compartment fires generally[1]. Then the histories of temperature of steel members unprotected are difference under various temperature fields in fires.

For *Ref.2* propose, in the large space building fires if the distance from the flame to the surface of steel members is far enough, heat transfer between the flame and the steel member may be disregarded. Otherwise the radiant heat transfer from the flame to steel members must be considered in the heat equilibrium equation based on the lumped differential formulation. The incremental rise in temperature of an uniformly heated unprotected steel section in time interval Δt due to heat transfer from hot smoke and flame radiant is given by

$$\frac{\Delta T_{sf}}{\Delta t}=\frac{\varepsilon_r\varepsilon_s c_0 F\left[(T_g+273)^4-(T_{sf}(t)+273)^4\right]+\varepsilon_f\varepsilon_s\varphi_{sf}\xi F(1-\varepsilon_g)c_0\left[(T_f+273)^4-(T_{sf}(t)+273)^4\right]+F\varepsilon_c(T_g-T_{sf}(t))}{V\rho_s c_s} \quad (1)$$

where c_s , ρ_s specific heat of steel [J/ (kg ·℃)] and the density of steel [7850kg/m^3] respectively

Δt time interval (recommended Δt is not more than 5 seconds)

ε_r resultant emissivity representing the radiation transmitted between the hot smoke and the steel member surface [$\varepsilon_r=0.5$]

ε_s , ε_f emissivity of steel members and flames respectively [$\varepsilon_c=0.8$, $\varepsilon_f=0.7$]

ε_c convective heat transfer coefficient [25W/(m^2·℃)]

c_0 Stefan-Boltzmann constant [5.67×10^{-8} W/m^2 ·K^4]

F surface area of the unprotected steel member per unit length [m^2/m]

V volume of the unprotected steel member per unit length [m^3/m]

$T_{sf}(t)$ temperature of the unprotected steel member, which is due to heat transfer by convection and radiant from hot smoke and by flame radiant

T_f average temperature of flame [℃]

φ_{sf} configuration factor in the particular case of two parallel surfaces

ξ ratio of the surface area of the unprotected steel member exposed to flame radiation given by

$$\xi=F_{sr}/F$$

where F_{sr} surface area of the unprotected steel member exposed to flame radiation

$T_g(t)$ temperature of hot smoke in the large space building fire at a particular time given by

$$T_g(t)-T_g(0)=T_g^{\max}\left[1-0.8e^{(-\beta t)}-0.2e^{(-0.1\beta t)}\right]\cdot\left[\eta+(1-\eta)e^{\left(\frac{b-x}{\mu}\right)}\right] \quad (2)$$

where $T_g(0)$ ambient temperature [℃]

$T_g^{\max}$ maximum temperature of smoke depended on the fire load and the dimension of compartment [℃]

B, η, μ temperature gradient factors relevant to the growth rate and the heat release rate of design fires, given by CECS200:2006 (the Technical code for fire safety of steel structures in buildings of China)

b distance from the centre to the edge of the fire source [m]

Eq.(2) is a regression formula[3], which is solved statistically over the set of data from the computer program FDS based on field model and adopted by CECS200:2006[4].

With step-by-step method, solution of the incremental *Eq.(1)* formulates the time history of temperature of steel members $T_{sf}(t)$. If the second term at the right side of *Eq.(1)* is neglected, the temperature of steel members generated by the hot smoke could be solved by the same method. This traditional method does not lend to rapid calculation of the temperature rise in steel members for fire resistance design, so an alternative simplified approach for temperature calculation is developed in this paper.

1 PROPOSED SIMPLIFIED FORMULA

Eq.(3) is defined to describe the effect of flame radiation on the elevated temperature in steel members. The typical temperature history based on *Eq.(3)* is shown in *Fig.1*

$$T_{sf}' = T_{sf}(t)-T_s(t) \quad (3)$$

where T_{sf}' temperature of the steel member generated by the flame radiation alone

$T_s(t)$ temperature of the steel member generated by the hot smoke

The simple expression for typical temperature course of T_{sf}' shown in *Fig.1* is gotten by

$$T_{sf}' = T_m\left(k_1 e^{-k_2 \lg^2(t/t_m)}+k_3 e^{-k_4 \lg^2(t/t_m)}\right) \quad (4)$$

where T_m maximum temperature generated by the flame radiation lonely

t_m time at maximum temperature

k_i shape coefficient for i=1,2,3,4

lg logarithm as base to 10

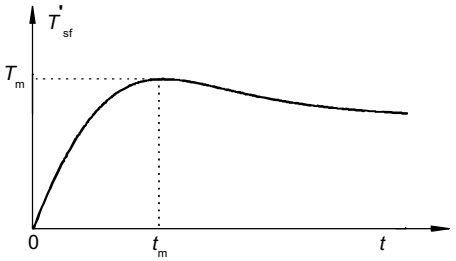

Fig. 1. Typical temperature course of steel members

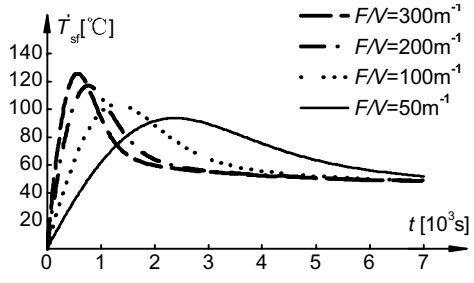

Fig. 2. Relationship of time with temperature of steel members for factor *F*/*V*

2 KEY PARAMETERS DUE TO FLAME RADIANT ALONE

A large number of curves for temperature elevated in steel members formed from *Eq.(1)* to

Eq.(3), which are provided for analysis the key parameters affecting temperature histories of steel members generated by flame radiation alone in large space building fire are discussed further as follows.

2.1 Effects of the section factor *F/V*

Fig.2 shows the temperature history T_{sf}' with a range of F/V between 300m^{-1} and 50m^{-1}. Here the other factors are given as $\varphi_{sf}=0.9$, $\xi=0.7$, $\beta=0.003$, $T_g^{max}=500$ ℃. A series of temperature course shows that the maximum temperature T_m is increase and the time at the maximum temperature t_m is early with the developed F/V for given other factors.

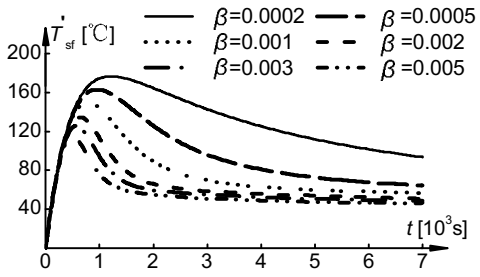

Fig. 3. Relationship of time with the temperature T_{sf}' for factor β

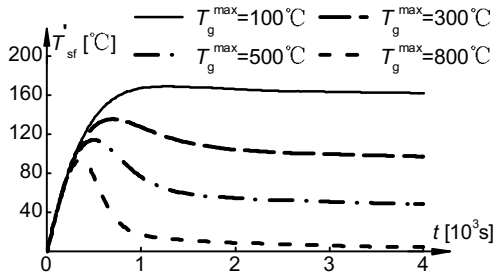

Fig. 4. Relationship of time with the temperature T_{sf}' for factor T_g^{max}

2.2 Effects of the temperature gradient factor of the smoke *β*

Fig.3 shows the temperature history T_{sf}' with a range of β between 0.0002 and 0.005. Here the other factors are given as $\varphi_{sf}=0.9$, $\xi=0.7$, $F/V=300\text{m}^{-1}$, $T_g^{max}=500$ ℃. A series of temperature course shows that the maximum temperature T_m is decrease and the time at the maximum temperature t_m is early with the developed β for given other factors.

2.2 Effects of the maximum temperature of smoke T_g^{max}

Fig.4 shows the temperature history T_{sf}' with a range of T_g^{max} between 100℃ and 800℃. Here the other factors are given as $\varphi_{sf}=0.9$, $\xi=0.7$, $F/V=300\text{m}^{-1}$, $\beta=0.003$. A series of temperature course shows that the maximum temperature T_m is decrease and the time at the maximum temperature t_m is early with the developed T_g^{max} for given other factors.

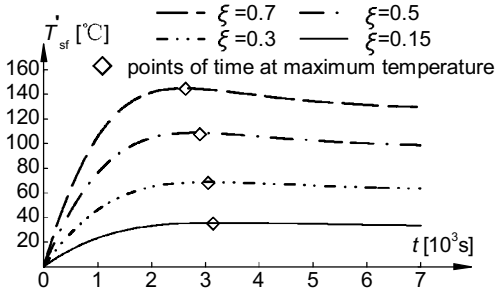

Fig.5. Relationship of time with temperature of steel members for factor ξ

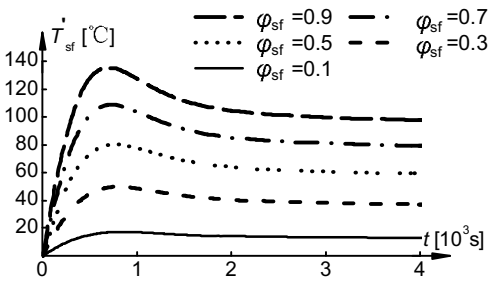

Fig.6. Relationship of time with temperature of steel members for factor φ_{sf}

2.4 Effects of the rate of the surface area under flame radiant ξ

Fig.5 shows the temperature history T_{sf}' with a range of ξ between 0.15 and 0.70. Here the other factors are given as $\varphi_{sf}=0.9$, $F/V=100\text{m}^{-1}$, $T_g^{max}=200\,℃$, $\beta=0.003$. A series of temperature course shows that the maximum temperature T_m is increase and the time at the maximum temperature t_m is late with the developed ξ for given other factors.

2.5 Effects of the configuration factor φ_{sf}

Fig.6 shows the temperature history T_{sf}' with a range of φ_{sf} between 0.1 and 0.9. Here the other factors are given as $T_g^{max}=300\,℃$, $\xi=0.7$, $F/V=300\text{m}^{-1}$, $\beta=0.003$. A series of temperature course shows that the maximum temperature T_m is increase and the time at the maximum temperature t_m is the same with the developed φ_{sf} for given other factors.

3 REGRESSION COEFFICIENTS FOR DESIGN PROPOSES

3.1 Determine the shape coefficient k_i

Fig.1 shows the curve shape is deference between growth and decay phase. The shape coefficient with *Eq.4* can be gotten by fitting the curves shown in *Fig.2* for given T_m and t_m. Although the curves in *Fig.2* differ in T_m and t_m, all the shape coefficients k_i mentioned above are approximate with each other. Then two rows of average value for k_i are given in *table 1* to describe the curve shape through growth and decay phase respectively.

Table 1. Values of shape coefficients

Curve shape	k_1	k_2	k_3	k_4
Growth phase（$t \le t_m$）	0.624	1.253	0.364	0.134
Decay phase（$t > t_m$）	0.430	0.075	0.576	0.116

3.2 Determine maximum temperature T_m and the time at maximum temperature t_m

With the step-by-step method, a series of temperature histories of steel members due to flames radiant alone could be calculated from *Eq.(1)* to *Eq.(3)* for various key parameters ,which are similar to curves discussed in *chapter 2*. The T_m and t_m can easily be obtained from each temperature history curve to form the curves shown in *Fig.7* to *Fig.9*.

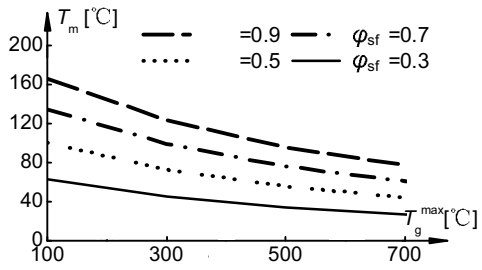

Fig.7. Relation of T_g^{max} between T_m for a rang of φ_{sf}

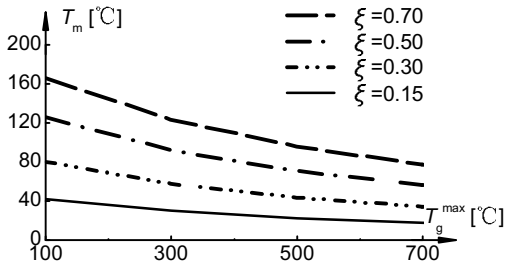

Fig.8. Relation of T_g^{max} between T_m for a rang of ξ

Shown in *Fig.4* to *Fig.6* the maximum temperature T_m is depend on, ξ and T_g^{max} for given factors F/V and φ_{sf}, in the meantime the time at maximum temperature t_m is determined by T_g^{max} and ξ mainly. Shown in *Fig.7* to *Fig.9* curves for various factor φ_{sf} and ξ follow

the same form as an exponential function of T_g^{max} with *Eq.(5)* and *Eq.(6)* respectively.

$$T_m = A + Be^{-T_g^{max}/C} \quad (5)$$

$$t_m = A' + B'e^{-T_g^{max}/C'} \quad (6)$$

Where A, B, C and A', B', C' are functions of the parameter ξ and φ_{sf} given by *Eq.(7)* and *Eq.(8)* respectively

$$\begin{cases} A = a_1 + a_2\xi^2 + (a_3 + a_4\xi)\varphi_{sf} \\ B = b_1 + b_2\xi^2 + (b_3 + b_4\xi)\varphi_{sf} \\ C = c_1 + c_2\xi^2 + (c_3 + c_4\xi)\varphi_{sf} \end{cases} \quad (7);$$

$$\begin{cases} A' = a_1' - a_2'\xi \\ B' = b_1' - b_2'\xi \\ C' = c_1' - c_2'\xi \end{cases} \quad (8)$$

Where a_i, b_i and c_i (i=1~4) regression coefficients given in *Table 2*

a_i', b_i' and c_i' (i=1~2) regression coefficients given in *Table 3*

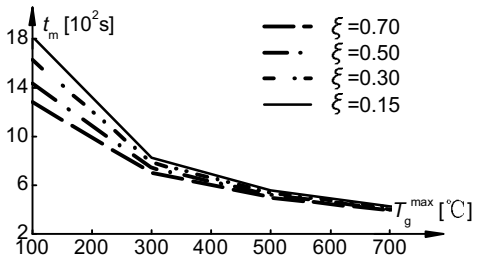

Fig.9. Relation t_m between T_g^{max} for a range of parameter ξ

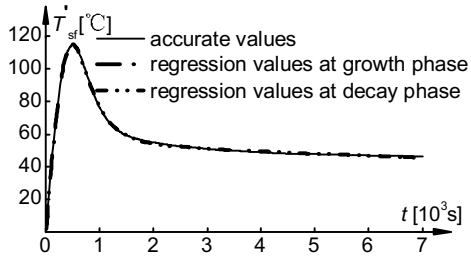

Fig.10. Comparison between the accurate value and the application result

4 APPLICATION

It is important to estimate the temperature in steel members conveniently for engineer to assess fire resistance. A simple approximate formula is presented as

$$T_{sf}(t) = T_m\left(k_1 e^{-k_2 \lg^2(t/t_m)} + k_3 e^{-k_4 \lg^2(t/t_m)}\right) + T_s(t) \quad (9)$$

where $T_s(t)$ is provided by CECS200:2006 as

$$T_s(t) = T_g(t) - \left[T_g(t) - T_g(0)\right] \cdot \left[-a + (1+a)\cdot e^{(-b\times 10^{-4}t)}\right] \quad (10)$$

Where *a, b* regression coefficients given by CECS200:2006 for T_g^{max}, β and F/V

It has been proved that the *Eq.(10)* is precise enough to estimate the temperature in unprotected steel members due to hot smoke heat entering by *Ref.5* .To verify the accuracy of *Eq.(4)* a common fire scenario is designed as $T_g^{max} = 500$ ℃, $\xi = 0.7$, $F/V = 300\text{m}^{-1}$, $\beta = 0.005$ and $\varphi_{sf} = 0.9$. The regression coefficients list in *Table 2.* and *Table 3* for given F/V and β are induced into *Eq.(7)* or *Eq.(8)* to calculate T_m and t_m, and the shape coefficients k_i are given in *Table 1.* Then the temperature history derived from *Eq.(4)* is shown in *Fig.10* as regression values. Referring to *Fig.10* the exact solution with *Eq.(1)* and *Eq.(3)* for temperature T_{sf}' and the approximate solution from empirical formula *Eq.(4)* almost merge into one another. The compare shown that *Eq.(9)* can give a very good prediction of unprotected steel member temperatures caused by both hot smoke and flame heat entering and provide a simple calculation method for engineers concerned with structural fire safety.

Table 2. Values of regression coefficients for the maximum temperature

β	F/V [m^{-1}]	A				B				C			
		a_1	a_2	a_3	a_4	b_1	b_2	b_3	b_4	c_1	c_2	c_3	c_4
0.005	300	-0.027	3.024	2.429	108.6	0.356	16.330	21.399	153.7	402.3	-5.84	15.56	160.1
	200				90.6				172.1	397.3	-5.69	15.48	155.4
	100				57.1				203.6	405.1	-1.77	17.34	162.4
	50				35.7				245.3	444.9	0.00	18.00	157.5
	⩽30	-0.026	2.951	1.728	34.9	0.348	15.957	20.910	239.7	444.9	0.00	18.00	157.5
0.001	300	-0.049	5.334	4.033	176.1	0.233	16.170	17.760	85.0	552.6	-57.71	6.09	208.7
	200				159.7				100.0	494.9	-21.41	-12.77	152.3
	100				130.7				131.8	425.0	-5.72	22.67	149.9
	50				86.7				168.0	465.1	0.00	35.96	139.2
	⩽30	-0.045	4.897	3.703	79.6	0.214	14.845	16.304	154.2	465.1	0.0	35.96	139.2
0.0002	300	-0.040	8.305	6.627	229.5	0.037	12.409	11.525	45.0	878.5	-251.84	-26.93	406.2
	200				218.2			13.020	56.5	771.0	-167.74	-11.13	311.5
	100				195.4			15.180	75.6	634.3	-89.57	-0.13	239.3
	50				155.0			21.421	90.1	651.2	0.00	18.99	235.3
	⩽30	-0.037	7.667	6.118	143.1	0.035	11.459	19.772	83.2	651.2	0.00	18.99	235.3

Table 3. Values of regression coefficients for the time at maximum temperature

β	F/V [m^{-1}]	a_1' [10^3]	a_2'	b_1' [10^3]	b_2' [10^3]	c_1'	c_2'
0.005	300	0.382	71.4	3.427	2.321	167.1	73.3
	200	0.487	89.6	5.419	3.618	165.6	69.8
	100	0.860	247.1	11.815	8.150	152.5	84.0
	50	0.828	182.5	13.597	6.849	255.6	74.5
	⩽30	1.252	338.2	23.687	12.200	244.0	80.0
0.001	300	0.684	124.8	2.248	1.311	233.3	49.8
	200	0.887	174.8	3.620	2.179	210.9	69.8
	100	1.454	317.7	9.043	6.068	166.5	80.8
	50	1.646	268.2	12.050	6.342	263.9	80.3
	⩽30	2.203	361.7	17.623	6.304	267.2	51.0
0.0002	300	1.213	322.5	2.114	1.198	292.3	20.1
	200	1.592	401.3	3.177	1.803	277.0	37.0
	100	2.527	561.8	6.385	3.657	245.4	47.9
	50	3.171	515.2	9.801	4.932	355.6	76.0
	⩽30	4.459	724.4	13.780	6.934	355.6	76.0

REFERENCES

[1] Guo-qiang Li, Yong Du, Analyses the parameters of fire temperature elevation at the top of large space buildings, *Fire Science and Technology* (in chinese)2005; Vol.24 No.1:19-21

[2] Yong Du, Guo-qiang Li, Fire radiation effect on steel member at elevated temperature in large space fire, *Fire Safety Science* (in chinese) 2006; Vol.15 No.4:189-199

[3] Yong Du, Guo-qiang Li, Utility temperature elevation empirical formula in large space fire, *Fire Science and Technology* (in chinese)2005; Vol.24 No.3:283-287

[4] National Institute of Standards for Engineering, *Technical code for fire safety of steel structures in buildings, CECS 200：2006 China*

[5] Yong Du, Guo-qiang Li, Simplified algorithm of steel members at elevated temperature in large space fire based on field model, *Fire Science and Technology* (in chinese)2006; Vol.25 No.3:299-303

APPLICATION OF STRUCTURAL FIRE DESIGN TO STEEL BUILDINGS
New Zealand Experience 1986 to 2008

Martin Feeney [a] and G Charles Clifton [b]

[a] Senior Fire Engineer and Principal, Holmes Fire & Safety, Auckland, New Zealand.
[b] Associate Professor of Civil Engineering, Department of Civil and Environmental Engineering, University of Auckland, Auckland, New Zealand.

INTRODUCTION

This paper outlines the application of structural fire design to apartment buildings, hotels, shopping centres, grandstands, offices and parking buildings in New Zealand since the introduction of a performance based Building Control System in 1992, through a series of case studies illustrating the various design approaches and bases for regulatory approval.

New Zealand's long-standing requirements for seismic design and detailing, which require steel structures to withstand inelastic demand without failure, mean that these structures have a dependable ability to redistribute load when heated during a severe fire. This ability has been exploited in the development of structural fire engineering solutions for steel framed buildings. This has been supplemented more recently by design procedures developed from research focussed specifically on experimental testing of structures exposed to fire.

The processes for regulatory approval are also covered in the case studies. This aspect of the process has highlighted the importance of education for the authority having jurisdiction. Comments on this part of the process are also included in the paper.

1. HISTORY OF BUILDING REGULATORY CONTROLS AFFECTING FIRE SAFETY

Prior to the introduction of the performance-based building control system in 1992, building fire safety in New Zealand was controlled by a prescriptive Model Building Bylaw NZS1900 Chapter 5 [1]. The Standard prescribed a specific and simplistic solution that took no account of performance of structures or materials in fire. This regulatory approach was used in most parts of the world at the time, as there were no accepted calculation methods available.

In 1992, the Model Building Bylaws were all replaced with a fully performance based Building Control System (BCS) as regulated by the 1992 (since revised in 2004) Building Act and the current national Building Code [2]. The NZ Building Code specifies mandatory functional requirements and performance criteria, but these may be achieved by any means. A prescriptive fire safety Compliance Document is available, produced by the Department of Building and Housing (the relevant Government department). This provides designers with one option for a solution which is deemed to comply with the Building Code, but is non-mandatory. Alternative solutions using other performance verification methods can be used. Routine fire safety design for most buildings is undertaken in accordance with the Compliance Document.

2. DEVELOPMENT OF ANALYSIS AND DESIGN METHODS FOR STRUCTURAL FIRE ENGINEERING

A consequence of the lack of flexibility characterised in the traditional prescriptive approach to structural fire design was a two stage design process: structure design and then subsequently ensuring adequate fire resistance were carried out as two separate activities. Structures were analysed and

designed to withstand all other environmental loads and effects, using whatever materials and methods considered appropriate for each specific case, but for structural fire safety the only solutions available were construction in concrete, or applied insulative fire protection of the structure. For example, the Standard [1] prescribed that "internal columns and main beams supporting concrete floors…shall be of concrete or masonry..(or)..other materials when the equivalent fire resistance rating is provided by the use of protective material".

The 1992 performance based Building Control System offered the option of quantifying the expected fire severity (fire threat) on an individual building basis, subject to knowing the building use (hence fire load energy density) and characteristics such as firecell geometry and features of the external walls. Although some calculations can be carried out, the most common simplified design approach is still semi-prescriptive, as the method itself and the range of values used as input parameters are tightly constrained. The assessment of structure performance is also most commonly done with reference to individual structural element/member fire resistance as measured by the standard fire test eg. ISO 834 [3]. Structure fire safety solutions derived in this way almost always use externally applied fire protection to achieve the calculated fire resistance rating.

Since 1996, more advanced analyses have based fire exposure on natural fires (not the time-temperature curve used in the Standard Fire test) eg. the parametric fire curve described in Eurocode ENV 1991-2-2 [4]. While the fire time-temperature equations are a function of many of the same variables as simpler methods, such as firecell geometry, fire load, external ventilation area, etc. the fire curve includes a cooling phase. Maximum steel temperatures in fire depend on duration of the heating phase. For some steel structures, in which the fire load is low and ventilation conditions good, or the building is sprinkler protected, adequate performance is achieved without externally applied fire protection as the fire temperature does not increase indefinitely (as it does in the standard fire test). Assessment of limiting temperature hence period of structural adequacy takes into account the reduced likelihood of maximum effect from other loads occurring during a fire [5]. Although performance is assessed on an individual structural element basis, in some cases a nominal level of inelastic structure behaviour has been included in the assessment of member capacity eg. partial moment capacity from simple (pinned) end connections.

Building on work by Bailey [6], Lim [7] and others, the HERA Slab Panel Method [8] (based on the tensile membrane model of Bailey [6]) was released in 2006. This HERA method is the result of New Zealand experimental and theoretical research programme as well as overseas research and testing. It applies to steel framed buildings with composite concrete floors and for structural members which may be subjected to high temperatures, considerable inelastic demand and large deformation of the floor system. A dependable proportion of the additional reserve of strength available from the structure when the floor system undergoes large deformation is included in the structure assessment. This consideration of three dimensional structure behaviour goes beyond an assessment which considers only individual structural elements basis and strength contribution from one material (steel) and provides a much better understanding of overall behaviour of steel structures in fire. In special circumstances, 3D finite element modelling of structure sub-assemblages with partial fire protection has been carried out [9].

3. CASE STUDIES

Open-sided steel carpark buildings, which have low fire load and are well ventilated, in effect being a firecell (the car) within a firecell, have been constructed without passive fire protection since 1986. Approval under the earlier prescriptive Building Code requirements was achieved with detailed submissions to the approving authority referring to results of full scale experimental tests and citing

overseas design recommendations. Since 1992, under the performance based Building Control System, enclosed sprinklered carparks have also been designed with unprotected steel structure. Studies of sprinkler reliability and more recent full scale experimental test results have been referenced to support the design basis. Quantitative analysis methods include calculation of fire effects using measured car fire heat release rates and assessment of steel structure stability using limiting temperature concepts.

Apartment and hotel buildings in New Zealand are characterised by low fire load, a high degree of internal compartmentation, relatively small firecell area and moderate to high levels of external glazing. Accordingly, the structural fire severity in these types of buildings is usually very low and with the high compartment into multiple firecells on each floor, the extent of structure influenced by a fully developed fire in one firecell is limited to only part of a floor.

Most of these multi-storey accommodation buildings are sprinklered, because of trade-offs permitted by the fire safety compliance document for non-structural aspects of fire safety. A natural fire concept has been applied to a number of steel framed buildings (since 1996, [10]) in conjunction with an analysis of the limiting steel temperatures for steel beams, to determine which structural elements remain stable with no passive fire protection and those which need applied fire protection. Beam design is based on assessment of the period of structural adequacy of individual members in the standard fire test, in accordance with the current Steel Structures Standard, NZS 3404 [11]. Steel columns are almost invariably concealed with fire protection materials.

In some apartment and hotel buildings where a plasterboard ceiling is required for Building Code compliance for non-fire safety reasons (eg. acoustic separation between floors), the effectiveness of the ceiling as a radiation shield has been included in the analyses. Performance of the ceiling in fire conditions has been determined from a series of natural fire tests [12] and further supported by observations of performance of the same types of ceiling assembly in standard furnace tests.

Another category of building types that have been the subject of performance based structural fire engineering are large, low rise, public assembly buildings in which the occupants are awake, alert, and predominantly ambulant and in many cases familiar with their immediate environment. Examples include shopping centres, conference facilities, grandstands, stadia and low rise office buildings. Where there is no requirement for structure to remain stable to protect other property, structure performance criteria relate to safety of occupants while escaping and protection of fire fighters. Fire design for life safety usually requires high capacity escape routes for short evacuation time, or else the building covers a large plan area so that performance of structure impacts only a small area of the building. These buildings are also usually sprinklered because of their large firecell area and high occupant load, and to take advantage of trade-offs that benefit occupant safety. Structure design for these buildings has applied a natural fire concept to compare on a time line the ‘real time’ at which fire conditions threaten structure stability (assuming sprinklers do not operate) with the time required for safe egress. A conservative safety margin has been applied to account for uncertainty in predicting fire effects. In most cases the regulators have also requested an assessment of ‘equivalent time’ fire resistance ratings to benchmark against more familiar prescriptive requirements. This approach is similar to that proposed in Australia [13, 14]. Performance based structure design has been applied in New Zealand to these types of buildings since 1998.

High rise office buildings present a more complex challenge for structural fire engineering. These buildings are characterised by medium level fire load energy density, firecell area ranging from small to large, firecell ventilation ranging from minimal to highly ventilated and occupant egress times that are often in the range 30 to 60 minutes after an emergency is declared. Understanding actual structure performance in fire is important because of the potentially disastrous consequences of overall structure

instability, even when full compliance is achieved for Building Code approval with a deemed to comply prescriptive solution. The actual duration of exposure to severe fire is often long when compared with fire resistance ratings based on exposure to the standard fire test. Also, modes of structure failure that are not apparent from individual element furnace tests have an influence on overall structure behaviour.

Because of the magnitude and variability of fire severity for this type of occupancy, assessment of the impact of a natural fire on structure stability based on performance of individual members in the standard fire test is neither sufficiently conservative nor accurate to assess whole structure performance with partial fire protection. For these buildings, the design approach considers 3D structure performance when exposed to elevated temperatures. The HERA Slab Panel Method has been used to assess performance in fire with partial structure protection (some beams not protected; all columns protected at office levels) for at least three recent high rise office buildings in Auckland. For one of these buildings 3D finite element analysis was used to model non-typical parts of the structure (slender cellular beams and large capacity seismic dominated frames) which did not fit within typical structure parameters assumed for the Slab Panel Method. Time-temperature relationships for these finite element analyses considered equivalent time fire resistance (the standard fire test) as prescribed by the non-mandatory Compliance Document and also natural fire time-temperature profiles.

Most of the new office buildings assessed to date have had extensive area of external walls with curtain wall glazing, providing a high floor area to ventilation area ratio and lower fire severity. Sensitivity analyses have been undertaken varying the ventilation area from 50% to 100% of the actual glazed area to gauge the effect this would have on structure performance when subjected to natural fires. The prescriptive solution assumes 100% of glazed wall area contributes to effective fire ventilation.

A consequence of this more complex design optimisation approach to assess the extent where fire protection provides no real benefit to structure performance is a requirement for more thorough on-site inspection of applied fire protection. The building constructor and fire protection applicator need greater quality control to ensure that the specification for structure fire protection is correctly interpreted and implemented. Not all contractors are prepared for this increased demand on their on-site resources.

For existing buildings, the NZ Building Control System allows for compliance with the Building Code performance requirements to be ‘the same as a new building as nearly as is reasonably practicable’. This allows the particular circumstances for each building to be taken into account when assessing the extent of compliance. A first-principles approach concentrating on the objectives and functional requirements of the Building Code has provided more flexibility in design approach.

For example, where asbestos-based fire protection material needs to be removed for public health reasons or where the structure of an historic building cannot be easily insulated with fire protection in the usual way, then other factors have been considered to compensate for the constraints associated with the existing construction. For office buildings this has included a comparison with performance outcomes from experimental testing [15] where structure and firecell details are similar. In other cases, where existing unsprinklered buildings have had sprinkler systems installed to improve occupant life safety, an improvement in the reliability of the sprinkler system (which reduces the likelihood of the fire threatening structure stability) has been accepted as compensation for not being able to provide formal certification of fire resistance rating of existing fire protection materials. By necessity these judgements of compliance for existing buildings are frequently qualitative.

4. STRUCTURE REQUIRING SPECIAL CONSIDERATION

Special structural elements such as load transfer beams, transfer trusses, slender columns or any other part of structure whose deformation or collapse during a fire would result in a disproportionate extent of damage or collapse are designed with greater caution, and usually receive insulative fire protection, even if the strength of the member is sufficient without it. This applies particularly to structural elements which could endanger fire fighters located in other firecells during fire fighting operations (eg. columns supporting large areas of roof in buildings without open plan internal layout).

The more sophisticated 3D modelling of structure behaviour in fire has highlighted the importance of structure robustness, rather than strength at elevated temperature, which is likely to be the dominant feature characterising adequate performance. While adequate strength at elevated temperature is necessary, in design it is unwise to assume that it is sufficient. To date, excessive reliance is still placed on a semi-prescriptive calculation of equivalent fire rating (required fire resistance). But in natural fires, as our understanding of modes of failure in fire improves, the cooling phase arguably becomes more important to more accurately determine where and how structural failure might occur. Careful structural detailing to accommodate inelastic demand assumes greater importance than an analysis concentrating on performance of a structure 'heated' to failure.

5. EXPERIENCE WITH REGULATORY REVIEW AND APPROVAL

The change to performance based Building Codes and advances in structural fire engineering analysis that have occurred over the last 15 years now provide different solutions in many to those that have become familiar from prescriptive approaches. The knowledge gap between building control officials more familiar with historical designs and structural fire engineers proposing the new methods is wider than ever. The necessary level of expertise is not available within the authorities with jurisdiction for building approvals. It is no longer sufficient just to understand the impact of fire effects, or simple elemental response to standard fire tests. The assessment of adequacy of structural fire designs requires greater reliance on independent peer review. This has been the experience in New Zealand. However, even the level of understanding within the regulatory organisations that is necessary to identify the need for peer review varies widely across the country.

Accordingly where there is a lack of full understanding there is greater suspicion of the adequacy of the outcome – especially where a solution is different to that produced by historical approaches. Confusion also arises between the meaning of 'equivalent time' such as the period of structural adequacy (measured with reference to performance in the standard fire test) and 'real' time relating to fire development or occupant evacuation time or Fire Service response time. The difference between fire protection (usually applied insulative coatings or concealment) and fire resistance – a measure of a structure or member's ability to resist fire effects is still a common misunderstanding.

Misconceptions about performance of various structural materials in fire (steel, concrete and timber) are still widespread. Structures provided with traditional solutions for insulative fire protection are usually assumed by regulators to be immune from the effects of fire, and structures without such protection are therefore regarded as highly vulnerable. It is of interest to note that 3D finite element analyses for natural fire exposure which compared the performance of partially protected structure with fully protected structure [9] showed better performance with partial fire protection. The structure with full fire protection exhibited a much less desirable potential failure mode for the same fire exposure.

6. IMPLEMENTATION INTO THE STEEL STRUCTURES STANDARD

The current Steel Structures Standard [11] provides only a simplistic and element based approach to the design for fire, as this material was written for application under the previous prescriptive based system. This is one reason for the problems with the regulatory approval process described in the previous section.

A complete revision of this standard commenced late in 2008 and the design provisions for fire are to be presented in an expanded new stand-alone part, which will incorporate the steel based fire engineering design methods described above directly into the Standard as an Approved Document means of compliance with the NZ Building Code [2]. An outline of this amended part has been produced and it is expected to be released for public comment towards the end of 2009.

REFERENCES

[1] NZS 1900 Chapter 5 Model Building Bylaw: Fire, Standards New Zealand, Wellington, NZ

[2] New Zealand Building Code, 1992, Department of Building and Housing, Wellington, NZ

[3] ISO 834, (1975), Fire resistance tests – elements of building construction, International Organisation for Standardisation, Geneva, Switzerland

[4] ENV 1991-2-2:1995, (1995), Eurocode 1: Basis of Design and Actions on Structures, Part 2.2 Actions on Structures Exposed to Fire, British Standards Institution, London, England.

[5] NZS 4203, (1992), Code of Practice for General Structural Design and Design Loadings for Buildings, Standards New Zealand, Wellington, New Zealand.

[6] Bailey, C. G. (2000). Design of steel members with composite slabs at the fire limit state, Building Research Establishment, United Kingdom

[7] Lim, L. (2003). Membrane Action in Fire Exposed Concrete Floor Systems, Fire Engineering Research Report 03/02. Dept of Civil Engineering, University of Canterbury, Christchurch, New Zealand

[8] Clifton, G.C., (2006), Slab Panel Method – Design of composite steel floor systems for severe fires, 3rd Edition, HERA Report R4-131, Heavy Engineering Research Association, Manukau City, New Zealand.

[9] Feeney, M.J., Clifton, G.C. and Mago, N., (2008), Dependable Performance of Steel Structures in Fire – The Britomart East Office Building, *Structures in Fire Conference 08*, Singapore.

[10] Feeney, M.J., (1998), Design of Steel Framed Apartment and Hotel Buildings for Fire, Proceedings 1998 *Australasian Structural Engineering Conference, Auckland*, Vol. 2, pp 563-570, New Zealand Structural Engineering Society, Auckland, New Zealand

[11] NZS 3404:1997 Steel Structures Standard, incorporating Amendment No 1:2001 and No 2:2007, Standards New Zealand, Wellington, New Zealand

[12] Brown, N.C., (2005), Steelwork Partially Protected from Post-Flashover Fires in Gib®Board Lined Compartments: Research Proposal for ME (Fire) Thesis, Dept of Civil Engineering, University of Canterbury, Christchurch, New Zealand.

[13] Bennetts, I.D., Poh, K.W., Poon, S.L., Thomas, I.R., Lee, A.C., Beever, P.F., Ramsay, G.C. and Timms, G.R., (1998), Fire Safety In Shopping Centres, Final Research Report Project 6, Fire Code Reform Centre Ltd, Sydney, Australia

[14] Bennetts, I.D., Goh, C. C., Thomas, I.R. and Poh, K.W. (2000), Low Rise Office Construction - A Guide to Fire Safety, One Steel Market Mills, Newcastle, Australia

[15] Thomas, I.R., Bennetts, I.D., Poon, S.L., and Sims, J.A, (1992), *The Effect of Fire in the Building at 140 William Street*, BHPR/ENG/R/92/044/SG2C, BHP Research, Melbourne, Australia

INFLUENCE OF FIRE ON STEEL BRIDGE
Over Vistula River In Puławy

Grzegorz Głuch [a]

[a] Wrocław University of Technology, Institute of Civil Engineering, Wrocław, Poland

INTRODUCTION

The conclusion form the traffic studies shows that the probability of fire in the area of bridge is relatively low. However, the importance of bridge structures, as a parts of road and transportation systems, for local economy and industry is significant. Damaged bridges are usually hard to detour and affect traffic quality in the region. It seems to be reasonable to consider the fire danger of bridges during design process, especially for structures along main roads and highways.

Although bridges are usually made of flame resist materials, traffic accidents can lead to fire develop, Fig 2.. High temperatures occurring during fires, cause additional stresses and thermal strains in structure [1, 2]. Steel is one of the most popular materials in civil engineering, the world's biggest bridges are made of steel. Unfortunately it is very sensitive to high temperatures, it's loads capacity is decreasing in fire's conditions. It can result in damage of bridge elements or, in case of large fires, the structure may even collapse, Fig. 1.

In extreme cases the bridge equipment, as a plastic cover of suspension system or paint on the steel elements, may begin to burn. The bridge fires cause usually no human casualties but the costs of bridge repair or road close due to fire damage are significant and highly disturb traffic in the area.

Fig. 1. Bridge collapsed after fire [12]

Fig. 2. Fire on the Big Four Bridge [13]

Fires are uneasy to modelling due to the complexity of the phenomena, the number of physical and chemical processes involved in combustion and the size of structure subjected to fire. In case of buildings and industry facilities fire engineering is well developed [7, 8, 9]. Unfortunately fires in open space, as on the bridges, are more difficult to simulate and analyse because of atmospheric and terrain influence on model.

The paper presents the algorithm for estimation the temperature of the suspended bridge when fire appears on deck. As an example the new build steel arch bridge over Vistula river in Puławy was analysed. The main span of bridge is 212m long, deck is suspended to two steel arches by the 28 hangers. The arch is a box in cross section. Each hanger is build from 4 steel bars, 82 mm in diameter. The deck is composed with concrete slab and steel grill. It was assumed the temperature, caused by the fire, affects only elements above deck as arch elements and suspension cables. The other issues are fires under bridges, especially in case of girders bridges, where main structure elements ale located below the deck.

FIRE SIMULATIONS ON THE BRIDGE

There are many mathematical models describing fires in civil engineering structures. Most of them are prepared for fires in closed area of rooms in buildings [7, 8, 9]. Only several models can be used in open space [10, 11] for example to simulate bridge's fires. Complex geometry of bridge and the surrounding terrain can be modelled with use of CFD, the algorithm based on fluid dynamics. The computation space is divided in to finite volumes and for each volume algorithm solves system of differential equations of mass, momentum, energy conservation and the equation of state (1) [8]:

$$\begin{gathered}\frac{\partial \rho}{\partial t}+\nabla \rho u=0 \\ \frac{\partial}{\partial t}(\rho u)+\nabla \rho u u+\nabla p=\rho f+\nabla \tau_{ij} \\ \frac{\partial}{\partial t}(\rho h)+\nabla \rho h u+\nabla p=\frac{D p}{D t}+q'''-\nabla q+\Phi \\ p=\frac{\rho R T}{M}\end{gathered} \tag{1}$$

where unknowns are: ρ – fluid density, $\boldsymbol{u}$ – fluid velocity vector , T – temperature, p – pressure. All functions depend on space coordinates and time. As the result of simulations various information can be received, including the temperature of elements contained in computation domain. The received temperatures of the bridge elements can be written as:

$$t_i=\left\{T_d^i, T_z^i, T_g^i, T_w^i\right\} \tag{2}$$

where t_i – temperature of element i exposed to fire,

T_d, T_z, T_g, T_w – temperatures in element's cross section, as in Fig. 3

When the fire affects more then one bridge element, temperature can be presented as a vector:

$$T=col\{t_1,...,t_i,...t_k\} \tag{3}$$

where k – number of elements exposed to high temperature.

The temperature t_i, as in (2), can be transformed into thermal loads for structure (4). Transformation rules are placed in [4].

$$d_i=\left\{\Delta t_i, \delta t_z^i, \delta t_y^i\right\} \tag{4}$$

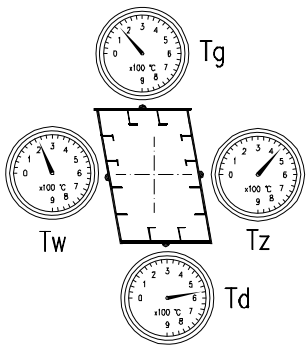

Fig. 3. Temperature of bridge element

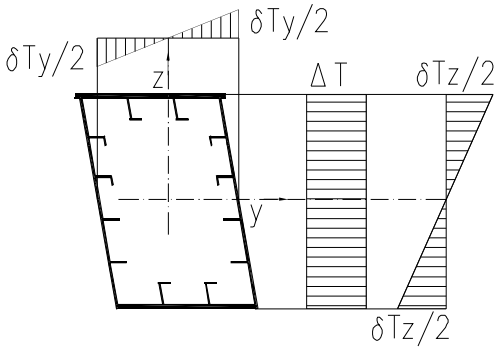

Fig. 4. Thermal loads

Forces, as shown in Fig 8 and in equations (5), cause deformation of whole bridge structure, also the element *e*, which deformed shape is presented in Fig 9. Displacement on direction of any force, as in Fig. 9 is equivalent to stresses in element *E* as in (6), it is the direct result form definition of influence function.

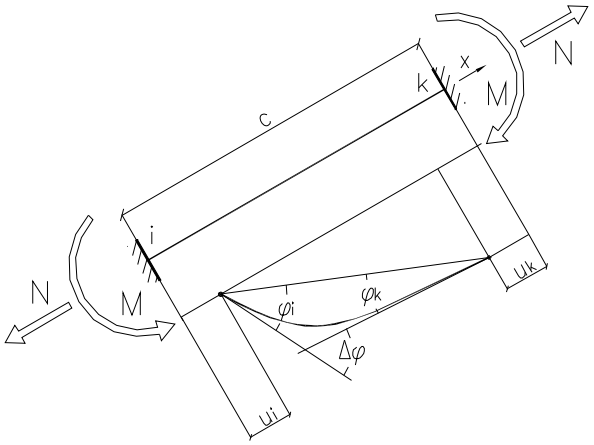

Fig. 9. Deformed bridge element

$$S_u = \frac{EA}{a} \cdot \frac{1}{A} = \frac{E}{A}$$
$$S_\varphi = \frac{EJ}{a} \cdot \frac{v}{J} = \frac{Ev}{a} \tag{5}$$

where
a – length of element E,
A – cross section of element E,
E – elasticity modulus,
J – moment of interia,
v – half of cross section height.

$$\sigma_u = N \cdot \Delta c_{ik}$$
$$\sigma_\varphi = M \cdot \Delta\varphi \tag{6}$$

The length change Δc_{ik} of element e (7) corresponds with the normal stress in element E generated by axial force N, as in Fig. 9. The angle between tangents $\Delta\varphi$ (7) corresponds with the normal stress in element E generated by bending moments M, as in Fig. 9.

$$\Delta c_{ik} = u_i - u_k$$
$$\Delta\varphi = \varphi_i + \varphi_k \tag{7}$$

where
u_i, u_k – displacement of nodes i, k of element e in x direction,
φ_i, φ_k – rotations of nodes i, k of element e.
The element's e length change Δc_{ik} can be caused by axial force N or by temperature change Δt:

$$\Delta c(\Delta t)_{ik} = \alpha \cdot \Delta t \cdot c_{ik}$$
$$\Delta c(N)_{ik} = \frac{N}{EA_{ik}} \cdot c_{ik} \tag{8}$$
$$\Delta c(\Delta t)_{ik} = \Delta c(N)_{ik} \Rightarrow N = \alpha \cdot EA_{ik} \cdot \Delta t$$

Analyses were carried out for new build steel arch bridge over Vistula river in Puławy [3]. The truck fire on the bridge deck was assumed as a heat source. During simulations truck was stopped. Different fire powers were considered. HRR curve shape was assumed according to [5]. The influence of high temperature on construction elements below deck was neglect, because of high thermal capacity of concrete slab. Fires were placed in 30 locations on the deck and temperature were calculated in 76 points on the steel arch. Example results are presented below. Figure 5 shows the temperature of suspension cable versus time and distance from the fire. The highest value of temperature *T=470 °C* is significant for the bridge safety. Figure 6 shows temperature of arch element versus time. The influence of fire on the different sides of box cross section is various. Temperature of top and inner side reaches value of 250 °C, and other sides are practically in ambient temperature. The inequality of temperatures on bottom, outer, top and inner sides of arch cross section generates bending moments.

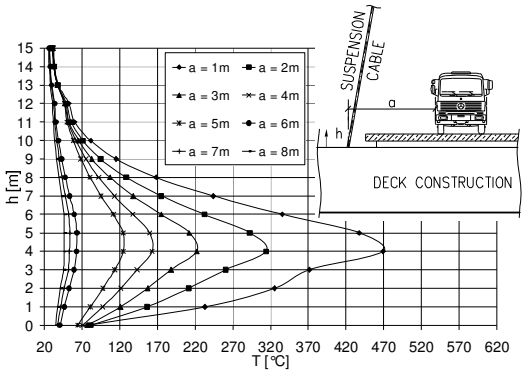

Fig. 5. Hanger temperature

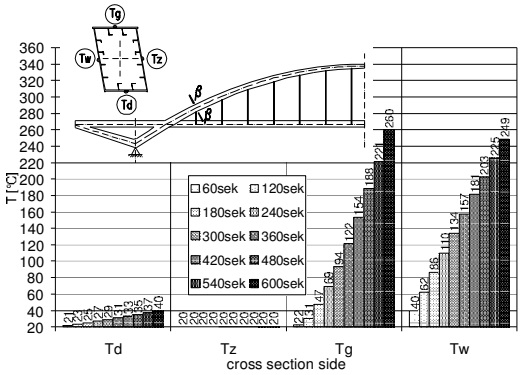

Fig. 6. Temperature of arch's cross section

THERMAL INFLUENCE FUNCTIONS

The scheme of analysed bridge and the example locations of elements *E* and *e* are shown in Fig. 7. Stresses are analysed in element *E*, heat is acting on element *e*. Bridge's elements *e*, exposed to fire influence, are subjected to high temperatures and are being heated. The differences of the temperature of structure generate thermal stresses in element *E*. However size of fire is usually smaller than the bridges and it can be located in various places on bridge deck. When the most dangerous location of fire, for the stresses in element *E*, is known, it makes the analyses faster and easier because the only one location of fire could be simulated. To find such a location the influence function and kinematical excitations for stresses [6], as in (5) and in Fig 8**,** can be used.

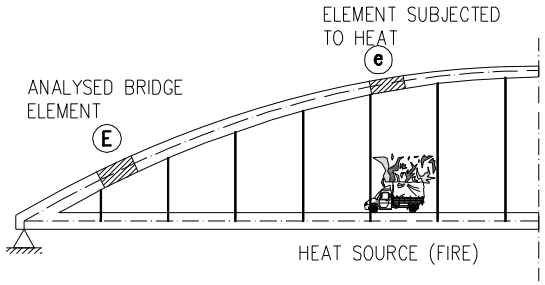

Fig. 7. Fire on the bridge scheme

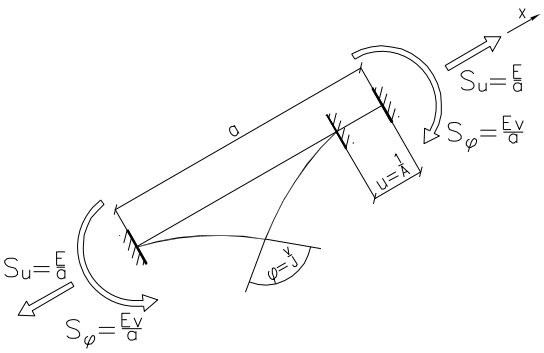

Fig. 8. Kinematical stress excitation

Finally the stresses in element E (6) generated by temperature change Δt can be written as:

$$\sigma_u = \alpha \cdot EA_{ik} \cdot \Delta c_{ik} \cdot \Delta t \tag{9}$$

The angle between tangents $\Delta\varphi$ can be caused by bending moments M or by temperature δt:

$$\begin{aligned} \Delta\varphi(\delta t)_{ik} &= \frac{\alpha \cdot \delta t \cdot c_{ik}}{h_{ik}} \\ \Delta\varphi(M)_{ik} &= \frac{M}{EJ_{ik}} \cdot c_{ik} \\ \Delta\varphi(\delta t)_{ik} = \Delta\varphi(M)_{ik} &\Rightarrow M = \frac{\alpha \cdot EJ_{ik}}{h_{ik}} \cdot \delta t \end{aligned} \tag{10}$$

Eventually the stresses in element E (6) generated by temperature δt can be written as:

$$\sigma_\varphi = \frac{\Delta\varphi_{ik} \cdot \alpha \cdot EJ_{ik}}{h_{ik}} \cdot \delta t \tag{11}$$

If the temperatures Δt and δt work in element e simultaneously the stress in element E is the sum of components generated by Δt and δt:

$$\begin{aligned} \sigma &= \sigma_u + \sigma_\varphi \\ \sigma &= \alpha EA\Delta c_{ik} \cdot \Delta t + \frac{\Delta\varphi_{ik}\alpha EJ_{ik}}{h_{ik}} \cdot \delta t \end{aligned} \tag{12}$$

When more than one element E is analysed and temperature acts on more than one element e, the equation in (12) becomes a matrix equation:

$$\mathbf{s} = \mathbf{l}_\Delta \cdot \Delta\mathbf{t} + \mathbf{l}_\delta \cdot \delta\mathbf{t} \tag{13}$$

Vectors $\mathbf{l}_\Delta$ and $\mathbf{l}_\delta$ in (13) are the thermal influence vectors and can be used to locate most dangerous fires location for stresses in analysed bridge element E. Influence vectors are shown below, the β cross section of arch was chosen as an example:

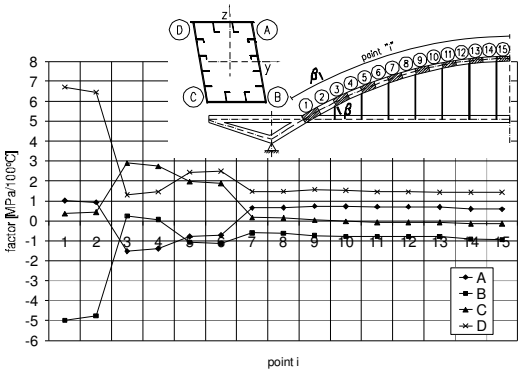

Fig. 10. Thermal influence vector $\mathbf{l}_\Delta$

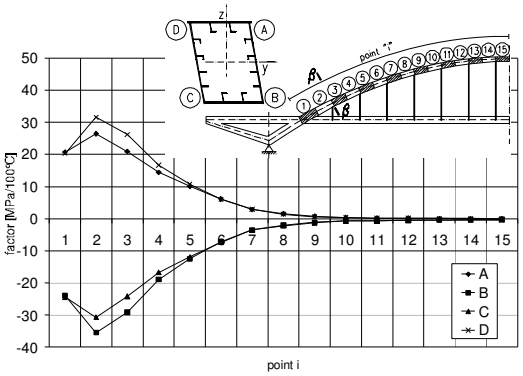

Fig. 11. Thermal influence vector $\mathbf{l}_\delta$

BRIDGE SAFETY ESTIMATION

To estimate bridge safety the μ coefficient (14) was proposed. This parameter compares thermal stresses with the stresses generated by the live loads in analysed element E. Live loads match the class A loads form polish design code for bridges.

$$\mu = \frac{\sigma(T)}{\sigma(P)} \tag{14}$$

If $\mu<1$ safety of the bridge is preserved, values of thermal stresses are lower than live loads stresses. If $\mu>1$ the thermal stresses in arch elements exceed stresses generated by live loads. If $\mu>1$ thermal stresses can lead to bridge's elements or equipment damage. For example, if $\mu=3,03$ the thermal stress is tree times greater then live loads stress. As shown in *Table 1*, fires with 30 MW peak HRR are not hazardous for analysed bridge. However 120 MW peak HRR fire generate dangerous thermal stresses in bridge structure.

Table 1. Values of μ coefficient

distance from deck edge to fire [m]	Peak HRR							
	30 MW				120 MW			
	cross section				cross section			
	β	γ	δ	ε	β	γ	δ	ε
2,40	3,03	0,51	0,34	0,44	7,31	3,28	3,26	4,41
5,70	1,23	0,46	0,31	0,40	2,80	2,08	1,96	2,75
9,00	0,67	0,31	0,17	0,17	1,81	1,43	1,10	1,13

Presented algorithm shows the bridge's structure stresses dependence on high temperature generated by fires on the deck. The temperatures during fire reach significant value for bridge safety and should be considered. Use of thermal stress influence functions simplifies the simulations and analyses.

REFERENCES

[1] Głuch G., Efekty oddziaływania wysokiej temperatury na dźwigary mostowe, *Zeszyty Naukowe Politechniki Śląskiej. Seria „Budownictwo", z. 104*, Gliwice 2005.

[2] Głuch G., Ocena zagrożenia pożarowego mostu łukowego w Puławach, *Wrocławskie Dni Mostowe*, Wrocław 2008.

[3] Bąk J., Grej K., Oleksiak C., Sałach W., Nowy most przez rzekę Wisłę w Puławach. Wybrane zagadnienia projektowe, *Wrocławskie Dni Mostowe,* Wrocław 2008.

[4] Biliszczuk J., Machelski Cz., Głuch G., Modelowanie pożaru na moście łukowym w Puławach, *Instytut Inżynierii Lądowej Politechniki Wrocławskiej Raport serii SPR 10/2008*, Wrocław, marzec 2008.

[5] Schleich J. B., Cajo L. G., Pierre M., Brasseur M., Development of Design Rules for Steel Structures Subjected to Natural Fires in Closed Car Parks, *European Commission,* Luxembourg 1999.

[6] Machelski Cz., Zastosowanie macierzy wpływu do projektowania kładki podwieszonej, *Inżynieria i Budownictwo, nr 3-4/2002.*

[7] Mangs J., On the fire dynamics of vehicles and electrical equipment, *VTT Building and Transport Department of Physical Sciences Faculty of Science*, University of Helsinki 2004.

[8] McGrattan K., Klein B., Hostikka S., Floyd J., Fire Dynamics Simulator (Version 5) User's Guide NIST Special Publication 1019-5 U.S., *Department of Commerce National Institute of Standards and Technology.*

[9] Yuguang L., Assessment of Vehicle Fires in New Zealand Parking Buildings, *Fire Engineering Research Report 04/2 May 2004*, Department of Civil Engineering University of Canterbury.

[10] Zobel H., Golubińska A., Symulacja pożaru mostu podwieszonego, *Drogownictwo, nr 4/2002.*

[11] Zobel H., Golubińska A., Pożary mostów, *Prace IBDiM,* Warszawa 2000.

[12] www.vermontbridges.com

[13] www.google.com

Application of Structural Fire Design, 19-20 February 2009, Prague, Czech Republic

DESIGN METHOD FOR RESTRAINED STEEL COLUMNS IN FIRE

Guo-Qiang Li[a,b], Peijun Wang[b], Yong-Chang Wang[c]

[a] State Key Laboratory for Disaster Reduction in Civil Engineering, No.1239 Siping Road, Shanghai, 200092, China

[b] College of Civil Engineering, Tongji University, Shanghai, 200092, China

[c] School of Mechanical, Aerospace and Civil Engineering, the University of Manchester, PO Box 88, Manchester, M60 1QD, UK

INTRODUCTION

Present fire resistance design codes [1, 2] are mainly based on isolated structural members, only adopt the design procedure at ambient temperature by using the reduced strength and stiffness of steel at elevated temperatures in fire. In fire situation, design method should consider the interactions among structural members.

Wang [3] presented an advanced design method for axially restrained column under axial load in fire. Huang et al. [4], Neves [5], Valente and Neves [6], and Li et al. [7] proposed different procedures to produce the axial force-temperature curve of a restrained column in fire. All the procedures have similar precision in predicting the failure temperature of restrained columns. The advanced design method is simple compared to the Finite Element Method (FEM). However, for design purpose, it may be necessary to further simplify the problem because the main target of design calculation is to find the buckling and failure temperatures of the restrained column.

Among the efforts that have been made in order to present analytical design formulae for restrained columns in fire, the early contribution presented by CTICM [8] should be highlighted. However, the design method of CTICM [8] did not include the post-buckling phase. Based on a limited numerical study, Franssen [9] found that if the axial restraint ratio was higher than a certain value the failure temperature of a restrained column could not reduce any more with the increase in the axial restraint stiffness ratio. Wang [10] presented a design proposal to consider the effect of structural continuity on behaviours of steel columns in fire. He proposed that there is no need to explicitly consider the effect of axial restraint and rotational restraint to the column in fire. Neves et al. [11] presented a simple method to calculated failure temperatures of restrained steel columns under axial load.

Despite many research results on the design of restrained columns in fire, a method is still necessary for axially and rotationally restrained columns under combined axial load and bending moment.

1. DESIGN METHODS FOR RESTRAINED COLUMNS

1.1 Equivalent bending moment factor

When a column is loaded by end bending moments, the maximum bending moment may not occur at the mid-height of the column when the two end bending moments are not the same. On the other hand, for design purpose, the value of the maximum bending moment is more important than its position on the column. The equivalent moment factor, β_{mx}, is used to calculate the maximum bending moment in a simplified way. At ambient temperature, β_{mx} is calculated by [12]:

$$\beta_{mx} = 0.65 - 0.35\alpha_M \tag{1}$$

Fig.1 shows the maximum bending moments in the restrained column at failure temperature with different end bending moment ratio. It can be seen that the end bending moment ratio has little

effects on the maximum bending moments in the column at failure temperatures.

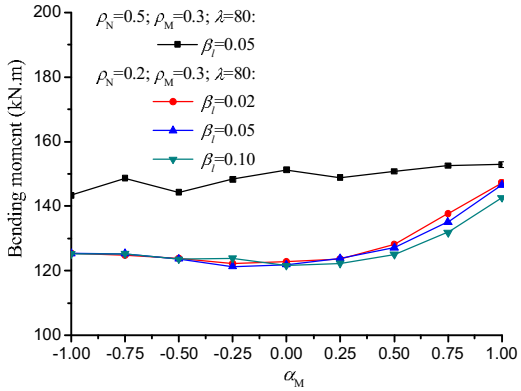

Fig. 1. Maximum bending moments at failure temperature

1.2 Structural behaviours of the restrained column

ABAQUS simulations on restrained columns under combined axial load and bending moment were carried out for the following cases: (1) slenderness ratio is 80; (2) axial restraint stiffness ratiois 0.02; (3) bending moment load ratio is 0.3; (4) end moment ratio is -1.0; and (5) axial load ratios are 0.1, 0.2, 0.3, 0.4, 0.5, 0.6, 0.7, 0.8, and 0.9.

The simulation results are shown in *Fig.2*. As shown in *Fig.2(a)* and *Fig.2(b)*, before the restrained column buckles, the axial force in the restrained column increases linearly and the bending moment changes little. Hence, for determining the buckling temperature of the retrained column, the design equations for the unrestrained column can be used, but with increased column axial load due to restraint thermal expansion. After buckling, the axial force in the restrained column drops, and the bending moment increases. Again, as shown in *Fig.1(c)* and *Fig.1(d)*, at the column failure the $N/N_{cr,T}+M/M_{p,T}$ value is greater than 1.0, but the value $N/N_{u,T}+M/M_{p,T}$ is close to 1.0.

1.3 Design method for the buckling temperature

(1) Design Equations

Before the restrained column buckles, the axial force increases linearly and the bending moment changes little. The design equation is

$$\frac{N}{N_{cr,T}}+\frac{\beta_{mx}M_x}{\gamma_x W_{1x}\left(1.0-0.8\frac{N}{N'_{EX}}\right)}=1.0 \tag{2}$$

$$N=P_0+k_l u_l \tag{3}$$

where, γ_x is the plastic factor of the section. W_{1x} is the elastic modulus of the cross-section; and u_l is the displacement of the axial restraint and it is calculated by

$$u_l=\frac{k_c}{k_c+k_l}\left(\varepsilon_{th}l-\frac{P_0}{k_c}+\frac{P_0}{k_{c,0}}\right) \tag{4}$$

The buckling temperature of the restrained column should not be higher than the failure temperature of the unrestrained column.

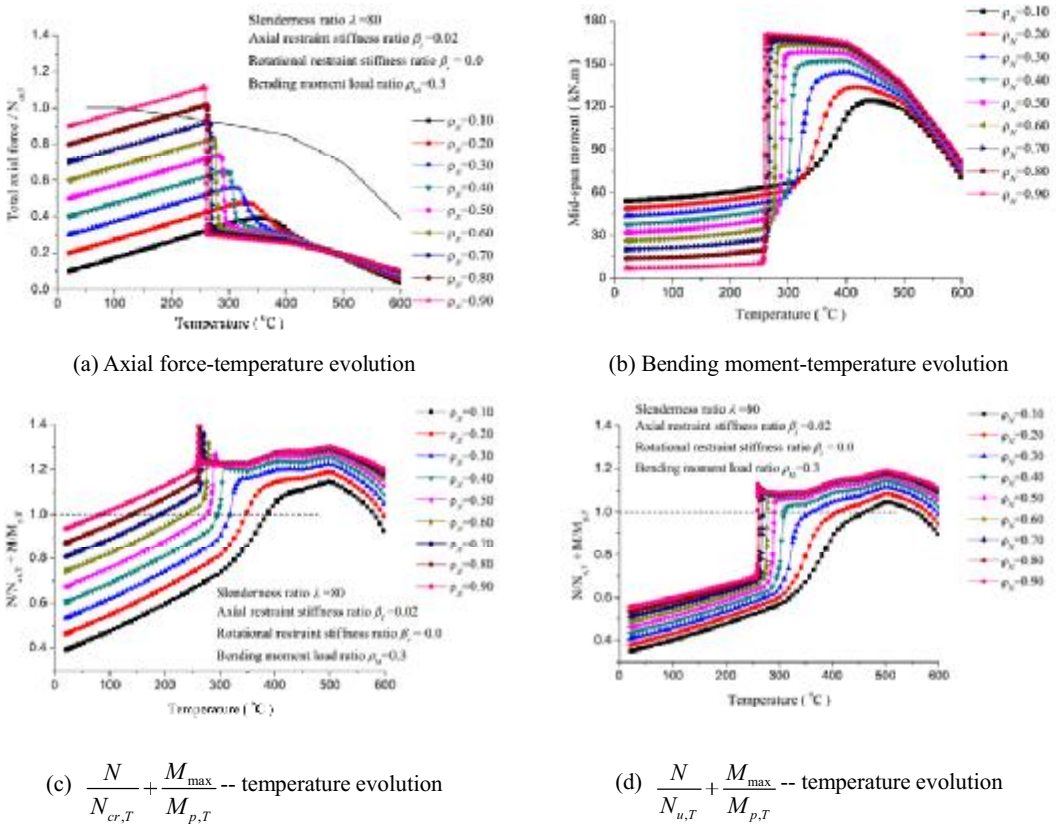

(a) Axial force-temperature evolution

(b) Bending moment-temperature evolution

(c) $\frac{N}{N_{cr,T}}+\frac{M_{\max}}{M_{p,T}}$ -- temperature evolution

(d) $\frac{N}{N_{u,T}}+\frac{M_{\max}}{M_{p,T}}$ -- temperature evolution

Fig. 2 Behaviours of restrained columns

(2) Verification of the buckling temperature equation

To check the accuracy of the proposed method, ABAQUS simulations have been run. The simulation results are shown in *Fig.3*. From *Fig.3(a)*, it can be seen that, for columns with axial restraint stiffness ratio less than 0.05, the buckling temperature predicted by the proposed method is greater than that of ABAQUS by about 80°C. However, for columns with axial restraint stiffness ratio greater than 0.1, the buckling temperature predicted by the proposed method is less than that of ABAQUS by about 50°C. The difference between buckling temperature predicted by ABAQUS and the simplified method becomes greater for columns with bigger bending moment ratio, as shown in *Fig.3(a)* and *Fig.3(b)*. Again the difference is primarily due to the difference between ABAQUS simulation results and CECS200 calculations of column buckling resistance at high temperature. Fortunately, in practice the initial axial load ratio rarely exceeds 0.6.

1.4 Design method for the failure temperature

(1) Design equations

The design equation for failure temperature of the restrained column is

$$\frac{N}{N_{u,T}}+\frac{N\cdot w+\beta_{mx}M_x}{M_{p,T}}=1.0 \tag{5}$$

here

$$N=P_0 \tag{6}$$

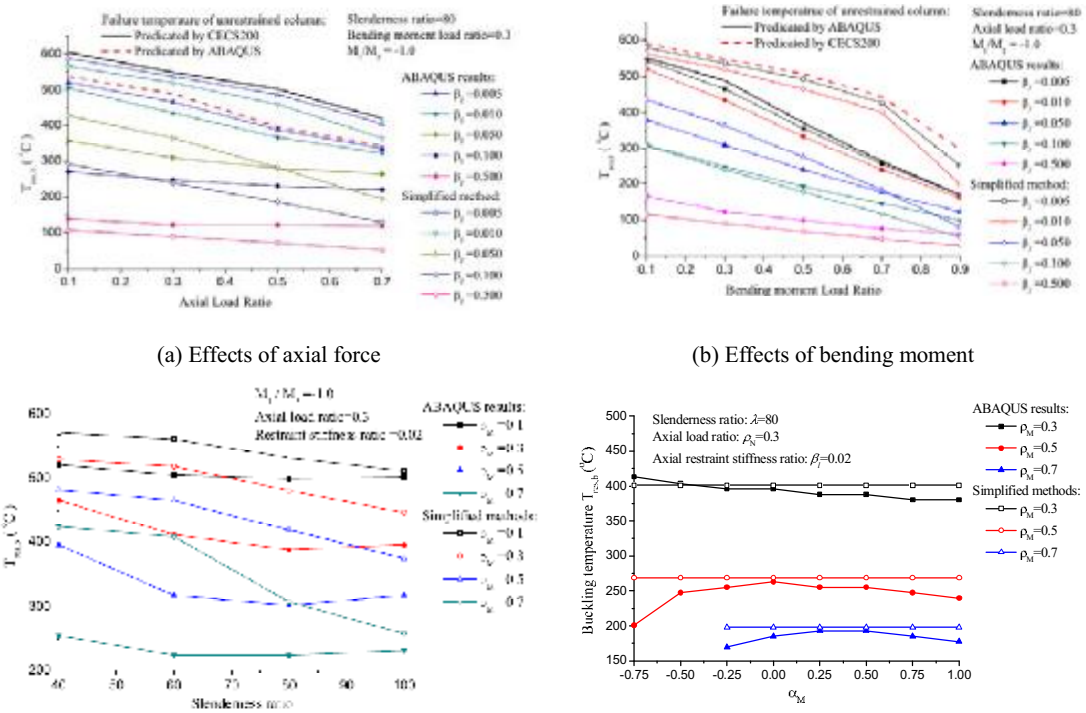

(a) Effects of axial force

(b) Effects of bending moment

(c) Effects of slenderness

(d) Effects of end moment ratio

Fig.3 Verification of the buckling temperature equation

The maximum column lateral deflection can be related to the axial restraint displacement u_l in the following way:

$$w = \sqrt{\frac{u_l \cdot l}{\alpha}} \tag{7}$$

where u_l is calculated using *Eq.(7)*; α is a function of slenderness ratio (λ), the axial restraint stiffness ratio (β_l), the axial load ratio (ρ_N), the bending moment load ratio (ρ_M) and the end moment ratio (α_M)

$$\alpha = (\rho_N, \rho_M, \lambda, \beta_l, \alpha_M) \tag{8}$$

Here the expression of α is obtained by curve fitting ABAQUS results. The following equations are obtained:

$$\begin{aligned} \alpha &= c_{\rho_N} c_{\rho_M} c_{\beta_l} c_\lambda \geq 2.5 \\ c_{\rho_N} &= 1.10\rho_N + 0.06 \\ c_{\rho_M} &= -1.60\rho_N + 2.10 \\ c_{\beta_l} &= 4.72e^{-\frac{\beta_l}{0.002}} + 205.35e^{-\frac{\beta_l}{136.81}} - 203.32 \\ c_\lambda &= 10.87e^{-\frac{\beta_l}{406.80}} - 7.70 \end{aligned} \tag{9}$$

(2) Verification of the failure temperature equation

To check accuracy of the proposed method, ABAQUS simulations have been carried out. *Fig.4* compares the column failure temperatures obtained by the proposed method and from ABAQUS

simulations.

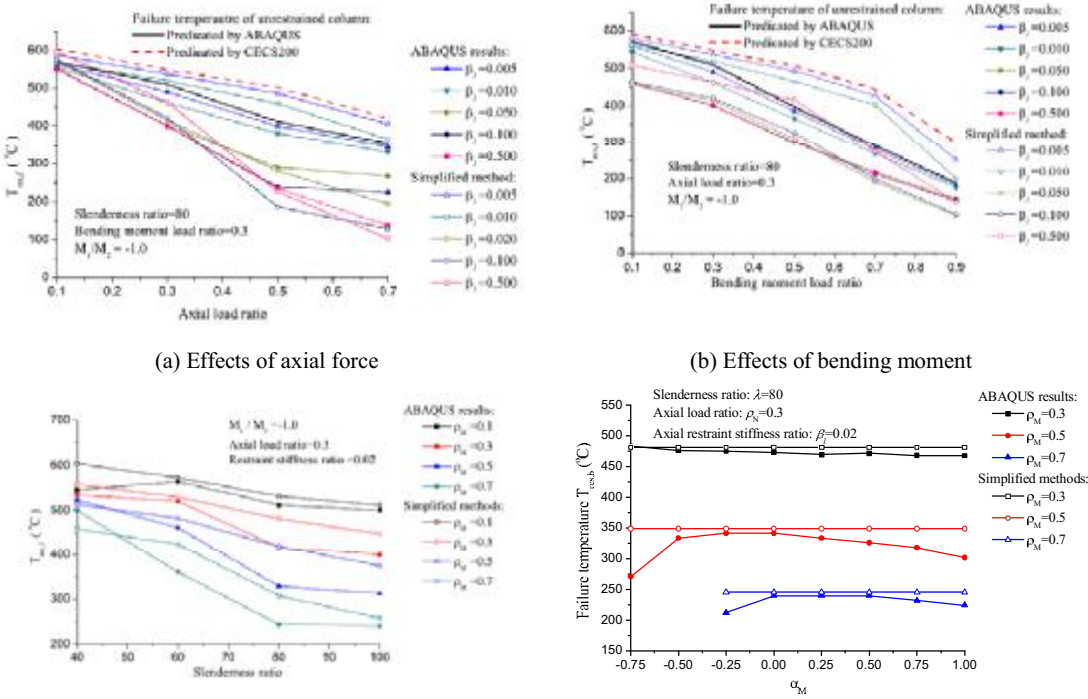

(a) Effects of axial force

(b) Effects of bending moment

(c) Effects of slenderness ratio

(d) Effects of end moments ratio

Fig. 4 Verification of the failure temperature equation

For columns with axial restraint stiffness lower than 0.02, the failure temperature predicted by the proposed method is greater than the prediction of ABAQUS. At increasing load ratio, the difference between the failure temperature obtained by the two methods increases, as shown in *Fig.4(a)* and *Fig.4(b)*. For columns with great axial restraint stiffness, the failure temperatures predicted by the proposed method is slightly lower than those by ABAQUS. For columns with different slenderness ratio, the failure temperatures predicted by the proposed method are greater than that by ABAQUS by about 80°C, as shown in *Fig.4(c)*. Except for α_M=-0.75, the failure temperature predicted by the proposed method is not affected by the end moment ratio, as shown in *Fig.4(d)*. The simplified method gives a slightly higher failure temperature.

3. CONCLUSIONS

This paper has studied the behaviour and developed a new method for calculating the buckling and failure temperatures of restrained columns under axial load or combined axial load and bending moment in fire. Results from the proposed calculation methods are compared with ABAQUS simulations for different cases. The main works and conclusions of this paper are:

1. simplified methods to calculate the buckling and failure temperature of restrained columns under combined axial load and bending moment are proposed.
2. by including the additional axial force due to restrained thermal elongation, the design equation for unrestrained column is used to predict the buckling temperature of restrained columns. For calculating the failure temperature, the yield axial strength-plastic bending moment interaction curve is adopted. The failure criterion is defined as the temperature at which the axial force returns to its initial value.

3. For the restrained column with realistic parameters, the buckling and failure temperatures predicted by the proposed method agree well with those of ABAQUS.

ACKNOWLEDGEMENT

The work reported hereinabove was financially supported by the National Natural Science Foundation of China under contracts 50621062, 50738005 and 50728805. The support is gratefully acknowledged.

REFERENCES:

[1] EN1993-1-2. Eurocode 3: Design of steel structures, Part 1-2: General rules--structural fire design. European committee for standardization, 2005.

[2] CECS200. Technical Code for fire safety of steel structural in buildings (CECS200:2006). China Planning Press, Beijing, 2006.

[3] Y. C. Wang. Post-buckling behaviour of axially restrained and axially loaded steel columns under fire conditions. Journal of Structural Engineering, 130(3):371--380, 2004.

[4] Z. F. Huang, K. H. Tan. Structural response of restrained steel columns at elevated temperatures. Part 2: Fe simulation with focus on experimental secondary effects. Engineering Structures, 29(9):2036--2047, 2007.

[5] I. C. Neves. The failure temperature of steel columns with restrained thermal elongation. Fire Safety Journal, 24(3):211--227, 1995.

[6] J. C. Valente, I. C. Neves. Fire resistance of steel columns with elastically restrained axial elongation and bending. Journal of Constructional Steel Research, 52(3):319--331, 1999.

[7] G. Q. Li, P. J. Wang, H. T. Hou. Behaviour of axially restrained steel columns incorporating strain reversal effects of steel at elevated temperatures in fire. Steel & Composite Structures, In Press.

[8] CTICM. Měthode de prěvision par le calcul du comportement au feu des structures an acier. Doucument Technique Unifiě, Construction Mětallique, 3, 1982.

[9] J. M. Franssen. Failure temperature of a system comprising a restrained column submitted to fire. Fire Safety Journal, 34(2):191--207, 2000.

[10] Y. C. Wang. Effects of structural continuity on fire resistant design of steel columns in non-sway multi-storey frames. Fire Safety Journal, 28(2):101--116, 1997.

[11] I. C. Neves, J. C. Valente, J. P. C. Rodrigues. Thermal restraint and fire resistance of columns. Fire Safety Journal, 37(8):753--771, 2002.

[12] GB50017. Design of Steel Structure (GB50017-2003). China Building Industry Press, Beijing, 2003.

INTEGRATED FIRE ENGINEERING OF STEEL SKELETON

USING WELL ESTABLISHED FIRE SOURCES

Heinisuo M.[a], Hietaniemi J.[b]., Kaitila O.[c], Laasonen M.[a], Outinen J.[d]

[a] Tampere University of Technology, Department of Civil Engineering, Tampere, Finland
[b] Technical Research Centre of Finland, Espoo, Finland
[c] Finnish Constructional Steelwork Association, Helsinki, Finland
[d] Rautaruukki Oyj, Vantaa, Finland

INTRODUCTION

Representation of all the information needed to describe buildings throughout the whole life cycle has long been an objective for those applying information technology to building construction. One discipline involving a considerable amount of computing effort in building projects has so far been missing both from the commonly used product modelling softwares and from the product model standards. This topic is fire engineering. Considerable efforts have been put to enhance this discipline during the last 20 years.

The natural fire safety concept [1] has now been accepted in many countries as a valid method to perform the structural design in fire. To do this, some level of fire simulation has to be done for the building in order to obtain the temperatures and other quantities in fire.

The basic question is how to integrate fire engineering to the product model? The basic idea of this paper (see also [2], [3] and [4]) is that all the information needed in the fire simulation is derived from the physical model of the building. This means that we use a single program to model both the geometrical and material entities of the building and all the data needed in the fire simulation and then map this data to the separate fire simulation program using special interface softwares.

The product model software used in this study is Tekla Structures (TS). The fire simulation program is FDS, Version 5 [5]. FDS includes both the fire fluid dynamics and the evacuation module. Only the fire dynamics module is applied in this study. Virtual thermometers are modelled in the fire simulation input file. The locations of these are determined on the basis of the structural analysis model. In this study, the thermometers are located at the centre points of each steel member. It is worth noting that typically the steel skeleton is so slender that its inclusion in the fire simulation model is not necessary [3], [6]. If desired, however, the steel skeleton can be included in the fire simulation. Difficulties when modeling the steel skeleton to the fire simulations have been considered in [2]. If there are important changes in steel skeleton layout during the design, the fire simulation should be done again, if it is modeled to the fire simulations, which can cause extra work.

After fire simulations the temperatures of the virtual thermometers are transferred into the structural analysis program and the resistance of the steel skeleton is checked using these temperatures. In this study the linear analysis resistance checks of the steel members were done using the program SCIA Engineering and its fire engineering module. Some cases have been checked using the program ABAQUS Standard in order to verify the analyses and obtain information on the geometrically and materially non-linear 3D behaviour of the building. Joint resistances are not dealt in this study.

The essential features when running the fire simulations are the applied fire sources. In this study, well established fire sources, called fuel packages [7], based on experimental and

theoretical bases are proposed for the cases under consideration, and fulfilling the safety level of the Eurocodes.
The developed tool has been applied in this paper to a typical warehouse steel skeleton for a heavy-good vehicle fire and for other fire scenarios. The resistance times for the unprotected steel skeleton have been defined using the simple engineering tool, i.e. checking of members individually, and comparisons on the results of the non-linear analysis are carried out.
The goal is to demonstrate how to enhance the fire design of steel structures by the integration of different disciplines applying product modelling techniques.

1 DEVELOPED INTEGRATED FIRE ENGINEERING TOOL

This project is an industrial project financed by the Finnish steel company Rautaruukki Oyj and the Finnish Funding Agency for Technology and Innovation (Tekes). The main goal of the project was to integrate fire engineering to the practises and softwares presently used in the company without the need to introduce new softwares to the end user. Figure 1 illustrates the integration completed in this study.

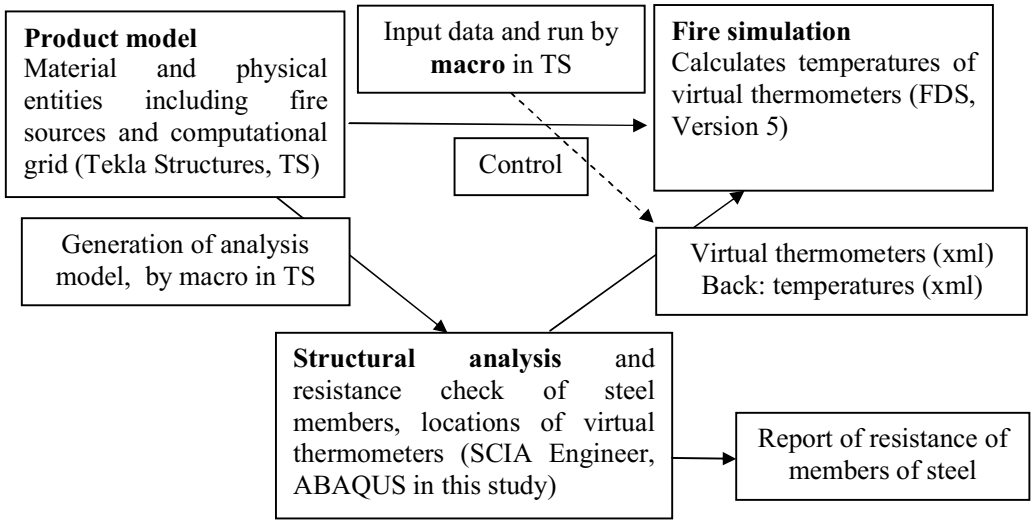

Fig. 1. Fire engineering in product modelling

Constant values for the convection coefficient (h = 25 W/(mK)) and emissivity (ε = 0.7) at the steel surfaces were used in this study. The specific heat of the steel members varied according to the steel temperature according to EN 1993-1-2. The increment time 30 seconds was found to be suitable for all calculations.

2 FUEL PACKAGES

VTT has developed a fuel-package-based approach [7] to characterise fire scenarios in buildings with different end uses such as car parks, offices, shops and warehouses. The basic problem is the assessment of the heat release rate (HRR). The fuel-package-based approach employs two ways to assess the heat release rate in fires.

1. Analysis and synthesis of experimental data.
2. Modelling and fire simulation.

The approach 1 is the primary way so that whenever there is reliable and relevant data available, it should be used. There is abundantly of experimental data available but in general, the larger fires one has consider, the less there is relevant data.
The approach 2 can be used where *no directly relevant* HRR data is found. It is also based on experimental data, but now the data is used so that first, the fire load is broken down to its basic constituents and then, using small-scale experiments on HRR per unit area, heat of combustion, ignition delays, thermal properties, etc., the HRR model is constructed using appropriate mass, volume and area weighted properties; and *before use validated against some experimental results*.
In this study, the following fire scenarios for typical warehouses were considered

- ISO fire,
- heavy-good-vehicle (HGV) fire,
- local and global wood fire,
- local and global plastic fire.

The local fire describes the fire in the building with sprinklers, but with the worst scenario: the sprinkler just above the fire ignition location is not working. It is believed that the above three cases include the most severe fire scenarios, which may be occur in typical warehouses.
As an example the next figure illustrates the estimate for HGV fire corresponding to 95% fractiles of the maximum HRR (50 MW) and the fire load (245 GJ).

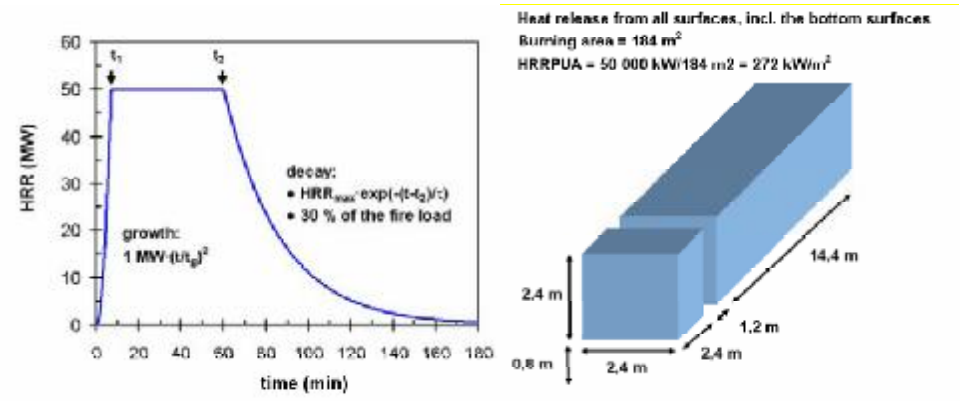

Figure 2. HGV fire source

2 EXAMPLES

Consider the steel skeleton shown in the next figures. Here it is used for the demonstrations of the developed tool. The building is 24 m wide and 41 m long. The height at the eaves is about 6.5 m and at the top about 8.8 m.

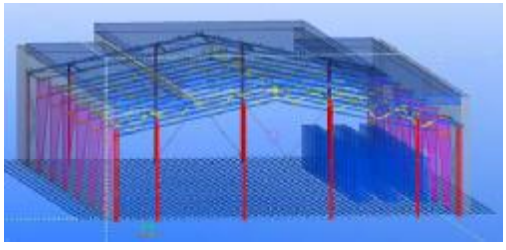

Fig. 3. View of product model

Fig. 4. View of analysis model

The main frame is a two hinge frame with hinges at the base bolt joints. The top chord and the bottom chord of the frame are connected (hinges) to the tapered columns. The steel skeleton is stiffened at the roof level, at the ends of the building and at the long outer wall lines with X-braces, as shown in the figure. The floor, walls and the roof were modeled using INERT coding of FDS, meaning non-combustible material. In the wall near the fire ignition location are two openings 6×3 m^2 portraying open doors. In the roof just above the fire ignition location is an opening 2×5 m^2.
The entire steel skeleton with all the members was modelled. The X-braces and roof purlins were modelled as tubular members, which are not as in the real building. The main columns were modeled using the uniform IPE500 profiles, not as welded tapered members, as in the real building. All the other members were modeled as they are in the real building. All the members but the columns are rectangular steel tubes and the columns are I-profiles. The detailed data for the building is available from Rautaruukki Oyj.
The mechanical load combination used in all structural analyses was the dead load (28 kg/m^2 applied to the whole roof area) plus 40 % of the uniform characteristic snow load on the entire roof (100 kg/m^2). All the loads are acting on the roof; purlins and mid points at top chords between purlins.
The following fire scenarios were applied:

- ISO fire all around the building,
- HGV fire so that the vehicle is just below one frame as shown in the figure 5,
- Local and global wood fire starting from the local fire source as shown in the figure 6,
- Local and global plastic fire starting from the local fire source as shown in the figure 7.

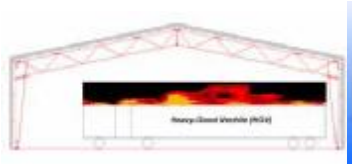

Fig. 5. Heavy-good vehicle fire

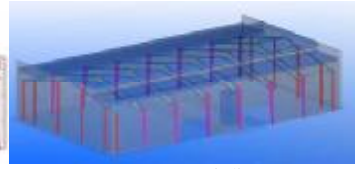

Fig. 6. Local fire

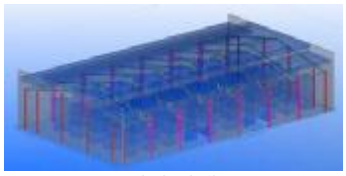

Fig. 7. Global fire

The global fires start from one ignite fire source (same as in the local fire) and then spread following the given ignition temperatures to other fire sources modelled as rectangular boxes in the figure 6. The size of one fire source in the local and global fire is 2×2×5 m^3 and the c/c distances between the sources in the global fire is 2 m. The size of the HGV fire source is as given in figure 2 representing the real vehicle. The heat release rates were given using the coding HRRPUA to the FDS program and the ramps described in [7].
In the ISO fire case the resistance of the steel skeleton was about 12-14 minutes in both SCIA Engineer and ABAQUS analyses. The resistance time in the ABAQUS calculations was defined as the time when vertical displacement rates of critical points were radically increasing.
The simplified analysis using the program SCIA Engineer showed that the entire steel skeleton could resist the HGV fire 2 hours, but for the second brace of the truss from the outer wall. Its resistance was 19.5 minutes and the temperatures of that member are shown in the next figure. The second largest utility ratio during the entire fire (2 hours) was at the top chord member nearest the ridge of the skeleton and it was 0.7, meaning that it can resist the fire.

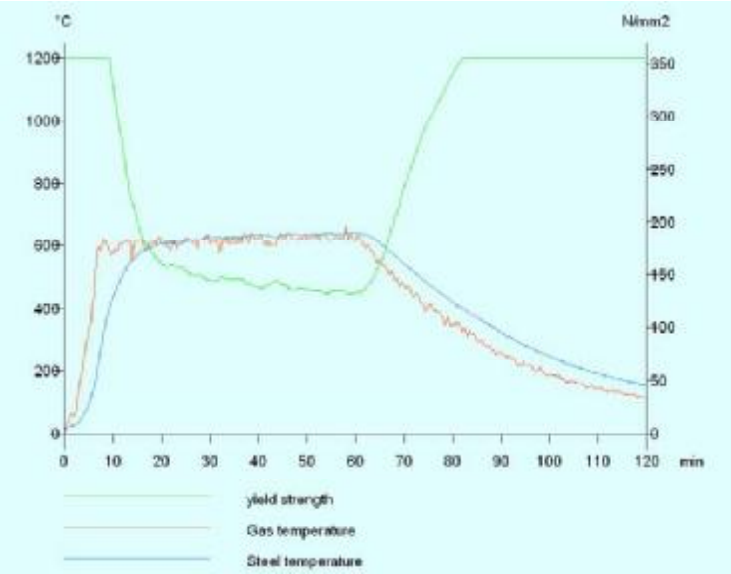

Fig. 8. Temperatures of the critical steel member in HGV fire

This means, that by changing the second braces of the trusses to the rectangular hollow sections with a little bit larger wall thicknesses (from 4 mm to 6 mm), the whole skeleton can resist the HGV fire for 2 hours. The reason for this is that the heat release rate for the area of the vehicle is just 272 kW/m^2 and the vehicle is rather low, so that the hot gases do not reach the roof structures. The total heat release rate was 50 MW for the vehicle. After one hour the fire starts to decrease. This case was not analysed using ABAQUS.

The global wood and plastic fires are quite different from each other both in the time scale (one plastic fire source lasts longer) and in the intensity (one wood source: 35 MW, one plastic source: 62 MW). Moreover, the start ramp was quicker in both fires compared to the ISO fire. The global wood fire firstly increases and then descends near the doors.

The global plastic fire did not descend during the simulation times up to 4700 seconds (78 minutes) but after about 2000 seconds it was rather constant and reaching the entire simulation space.

In both global fires the resistance of the steel skeleton is very low without applied fire protection. Due to the rapid temperature increase in the global fires, the fire resistance times are lower than in the ISO fire. The resistance times using the program SCIA Engineer and ABAQUS were about 10 minutes for the global wood fire. The global plastic fire is more severe and it was calculated only using the program SCIA Engineer.

In the local wood fire case the resistance of the steel skeleton was about 10 minutes for the most critical member using the program SCIA Engineer. However, in this case the resistance duration of the steel skeleton using the program ABAQUS is infinite! Practically the calculations were stopped at 2400 s when the fire was already practically over. This considerable difference in analysis results is explained by the use of non-linear analysis techniques in ABAQUS, which allow for the redistribution of actions during the analysis.

3 CONCLUSIONS

The developed tool worked well in the cases considered and it is considered by the authors that the developed tool enhances the fire design of steel structures considerably. However, the

joint behaviour and the resistance checks of joints should be included in the analyses in the future.
The local wood fire analysis case was based on a realistic fire scenario in an industrial hall or a warehouse equipped with sprinklers. In order to provide a more severe approach, the sprinkler device closest to fire ignition was assumed to be out of order. The analysis showed that the structure survives this type of fire safely due to three-dimensional structural behaviour and the redistribution of loads and stresses during the fire. The catenary actions in the purlins play an important role in providing support for the most severely affected frame. No structural failure was observed during the whole analysis that included the decreasing phase of the fire.
However, in an actual design case special consideration should be paid on the strength of connections between structural members, which are of primary importance when considering the 3D-behaviour of a complete structure and the catenary actions present in the fire situation. The effects of connections have not been considered in this study.
The results of the cases considered showed that

- The skeleton can resist the HGV fire with a slight structural modification without applied fire protection,
- The skeleton can resist without applied fire protection a typical cellulose based fire with sprinklers and by taking into account the worst scenario: the sprinkler just above the fire ignition is considered to be out of order during the fire (local wood fire). This is due to the catenary action and the three dimensional behaviour of the skeleton during the fire, meaning that these should be taken into account when seeking good solutions for steel skeletons in fire.

In order to get reliable results from the fire simulations, the used fire sources should be well defined and based on experimental and theoretical data. Obviously, the user of tools of this type should have both fire engineering and structural engineering skills and access to detailed information on all factors considered.

REFERENCES

[1] Natural fire safety concept – Valorisation project, Dissemination of Structural Fire Safety Engineering Knowledge – DIFISEK, RFS-C2-03048, 2005.

[2] Heinisuo M., Laasonen M., Product modeling, part of the fire safety concept in the future for metal structures?, Advanced Research Workshop, Fire Computer Modeling, Santander 18-20 October, Universidad de Cantabria, 2007, pp. 261-272.

[3] Heinisuo M., Laasonen M., Hyvärinen T., Berg T., Product modeling in fire safety concept, effects of grid sizes and obstacles to steel temperatures, Proceedings of IABSE Conference on Information and Communication Technology (ICT) for Bridges, Buildings and Construction Practice, Helsinki, Finland, June 4-6, 2008.

[4] Heinisuo M., Laasonen M., Hyvärinen T., Product modeling in fire safety concept, calculation of steel temperatures, Proceedings of 15th Workshop of the European Group of Intelligent Computing in Engineering (EG-ICE), Plymouth, July 2-4, 2008, pp. 460-469.

[5] McGrattan, K., Hostikka, S., Floyd, J., Baum, H. and Rehm,. R., Fire Dynamics Simulator (Version 5), Technical Reference Guide (Draft: may 30, 2007), NIST Special Publication 1018-5, 2007.

[6] Prasad, K. and Baum, H.R., Coupled Fire Dynamics and Thermal Response of Complex Building Structures, Proceedings of the Combustion Institute 30, 2005, pp. 2255-2262.

[7] Hietaniemi J., Fuel Packages for Structural Fire Safety Design, To be published in the VTT Working Papers Series, Espoo, 2009.

BUCKLING BEHAVIOUR OF STEEL COLUMNS IN FIRE CONDITIONS AND COMPARISON WITH EUROCODE 3

Tomaž Hozjan[a,b], Luka Kurnjek[a], Igor Planinc[a], Miran Saje[a], Stanislav Srpčič[a]

[a] University of Ljubljana, Faculty of Civil and Geodetic Engineering, Ljubljana, Slovenia
[b] Trimo d.d., Prijateljeva cesta 12, 8210 Trebnje, Slovenia

INTRODUCTION

Steel columns are efficient structural elements both in terms of construction time and load bearing capacity. Steel is vulnerable to fire, however, and steel structures, potentially exposed to fire, require a particularly careful design. This especially holds true for steel columns as they are loaded in compression and are thus prone to buckling. With an increase of temperature, strength of steel and the stiffness of columns decrease leading to buckling at an even much lower level of external loading than at room temperature. We can find numerous results of experiments on steel columns in fire. Yet extensive parametric studies of behaviour of steel columns in fire can only be performed with numerical programs previously validated with the results of experiments. These programs are rather complex and not appropriate for a routine engineering usage. Therefore engineers will rather use simplified, practical methods such as those given in building codes, e.g. Eurocode 3 [3], and BS5950 [1]. These codes offer methods for the fire analysis for isolated columns, which, however, may not result in sufficiently reliable quantitative predictions of the fire bearing capacity of a column.

A deeper insight into the thermo-mechanical behaviour of a column during fire can be achieved by the use of sophisticated mathematical models and modern numerical tools. These formulations make it possible to consider and analyse various material models, fire load scenarios, boundary conditions, restraints and geometric imperfections. Such models have been applied to steel columns subjected to elevated temperatures [2, 4, 10, 15]. Although they have been performed only for simple boundary conditions their results have shown that the critical temperature depends on slenderness of the column and on material model of steel at elevated temperatures.

Analytical solutions are much more difficult to obtain and are only limited to the determination of fire resistance. The majority of analytical solutions revolves around the Merchant-Rankine equation and the second-order theory of beams. Skowronski [13] derived an analytical formula for the fire resistance of a simple steel column. Tang et al. [14] improved their formulae by taking into account the effects of an initial crookedness, residual stresses, material models and the load eccentricity. Huang et al. [6] significantly improved their results by additionally considering axial restraints.

The present article presents a systematic analytical procedure for the determination of the critical temperature of a straight, geometrically perfect and axially loaded steel column exposed to fire. A series of standard simplifications and assumptions need to be introduced, however, to enable the analytical solution to be derived. In particular, we assume that a steel column can be realistically modelled by a kinematically exact planar beam model of Reissner [12] neglecting the effect of shear strain. Next, we assume a non-linear, temperature dependent material law, which accounts for both viscous and plastic strains. The mathematical expressions for the stress-strain law of steel at high temperatures are taken from EC 3 [3] along with the explicit expressions for temperature-dependent material parameters. As the walls of the steel sections are thin, we further assume that the temperature field in the column is uniform, but somewhat delayed with regard to temperature of the surrounding gas. After the thermo-mechanical equations are set up, the fundamental equilibrium solution of the column is obtained and the set of linearized equations at the fundamental equilibrium state is

derived. The condition for the existence of the non-trivial solution of the linearized equations supplies us with the value of the critical temperature.
The basic equations for the derivation of determination of the critical temperature for steel columns in fire conditions are presented in Sec. 1. The parametric analyses and the comparisons with the results of the European standard EC 3 [3] are given in Sec. 2.

1 FIRE ANALYSIS OF RESTRAINED STEEL COLUMNS

1.1 Preliminaries

We consider a straight steel column of initial, undeformed length L and a constant I-shaped cross-section. The column is centrically loaded with an axial force F while simultaneously being exposed to fire (*Fig*. 1). The plane of deformation of the column is the plane (x, z) of the Cartesian coordinate system (x, y, z). The reference axis of the column is assumed to coincide with its centroidal axis.

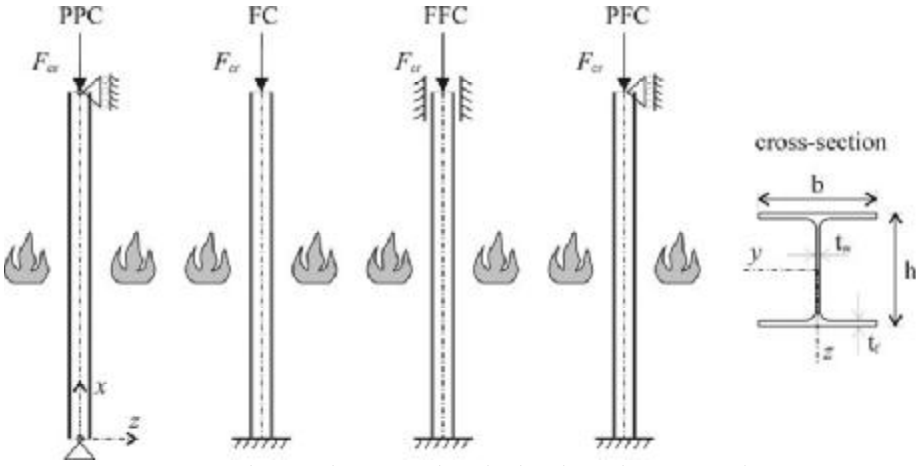

Fig 1. Euler's columns and typical I-shaped cross-section

In modelling the interaction between fire and a structure, we assume two independent analysis steps, the first one being the determination of the temperature field in the column and the second one consisting of the determination of the stress and strain field due to a combined effect of mechanical and temperature loads.

1.2 The temperature field

The development of gas temperature in the fire compartment depends on many parameters and is therefore both a complex task to do and unreliable. That is why convenient, yet very much simplified parametric temperature-time curves are introduced for the engineering design practice, which uniquely define explicit relationships between gas temperature in the compartment and time for a number of typical situations, including the amount of fire load and the thermo-dynamical and geometrical properties of the compartment [9]. Once the variation of gas temperature in the compartment has been obtained, we can determine the temperature distribution within the structure by integrating the differential equation of heat conduction. For a typical I-shaped steel cross-section uniformly heated over all surfaces, it is appropriate to assume an instantaneously uniform temperature distribution over the cross-section. One such simplified solution, which is also used in this article, is proposed by the EC 3 standard [3]. *Fig*. 2a shows some typical parametric temperature-time curves, while on *Fig*. 2b displays the development of temperature with time in the typical steel cross-sections for standard fire curve ISO 834 [7].

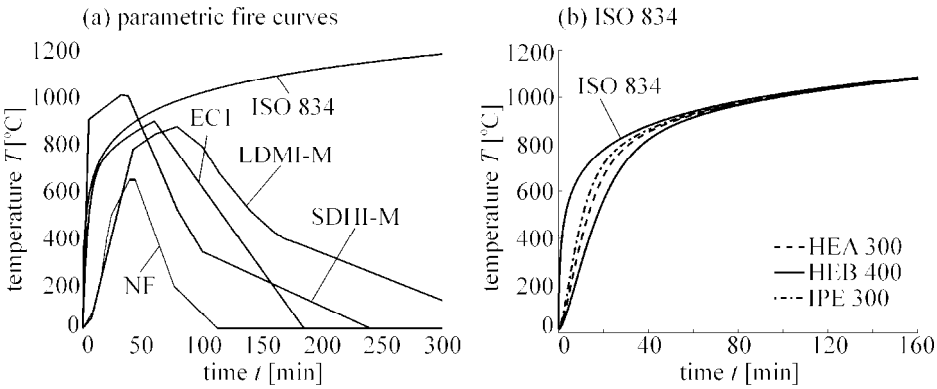

Fig 2. (a) Parametric fire curves. (b) Temperature-time curves for different steel profiles for fire curve ISO 834

1.3 The stress-strain field

Once the temperature variation in time has been obtained, we may start the mechanical analysis of the structure. We find the solution in an incremental way. We divide the time of the duration of fire into time intervals $[t^{i-1}, t^i]$ ($i = 1,2,3,\ldots$) and determine iteratively the stress and strain state at each time t^i . The column is modelled by Reissner's geometrically exact beam theory [12], but with the effect of shear deformations being neglected. The corresponding governing equations of such a beam model are:

$$1+u^{i\prime}-(1+\varepsilon^i)\cos\varphi^i=0, \tag{1}$$

$$w^{i\prime}+(1+\varepsilon^i)\sin\varphi^i=0, \tag{2}$$

$$\varphi^{i\prime}-\kappa^i=0, \tag{3}$$

$$\mathcal{H}^{i\prime}=0, \tag{4}$$

$$\mathcal{V}^{i\prime}=0, \tag{5}$$

$$\mathcal{M}^{i\prime}-(1+\varepsilon^i)\mathcal{Q}^i=0, \tag{6}$$

$$\mathcal{N}^i=\mathcal{H}^i\cos\varphi^i-\mathcal{V}^i\sin\varphi^i=0, \tag{7}$$

$$\mathcal{Q}^i=\mathcal{H}^i\sin\varphi^i+\mathcal{V}^i\cos\varphi^i=0, \tag{8}$$

$$\mathcal{N}^i=\int_{\mathcal{A}}\sigma^i\,\mathrm{d}A, \tag{9}$$

$$\mathcal{M}^i=\int_{\mathcal{A}}z\sigma^i\,\mathrm{d}A, \tag{10}$$

where $(\bullet)'$ denotes the derivative with respect to x; u^i and w^i are the components of the displacement vector of the centroidal axis of the column in x and z directions, φ^i is the cross-sectional rotation around y. Deformations ε^i and κ^i are the extensional strain of the centroidal axis and its bending strain (also termed the 'pseudocurvature'). $\mathcal{N}^i$ and $\mathcal{Q}^i$ are the axial and the shear force and $\mathcal{M}^i$ is the bending moment. $\mathcal{H}^i$ and $\mathcal{V}^i$ are the components of the resulting cross-sectional force with respect to spatial axes x and z, respectively.

Based on the given stress and strain state at time t^{i-1} and temperature at t^i, we can determine the strain D^i at time t^i of any point of the column by the equation

$$D^i=D^{i-1}+\Delta D^i, \tag{11}$$

where ΔD^i is the increment of the total strain (also termed the 'geometrical deformation') in time interval i. Considering the principle of additivity of strains and the material model of steel at elevated temperatures according to EC 3 [3], we propose that the strain increment ΔD^i is the sum of the strain increments due to temperature, ΔD^i_{th}, and stress, ΔD^i_{σ}:

$$\Delta D^i(T^i) = \Delta D^i_{\text{th}}(T^i) + \Delta D^i_{\sigma}(T^i). \tag{12}$$

In this material model, viscous strains are assumed to be included in ΔD^i_{σ} and are thus not treated separately. The temperature strain increment, ΔD^i_{th}, is calculated from the EC 3 formula [3], where the total temperature strain, D_{th}, is given with a formal expression $D_{\text{th}} = f(T^i)$; thus, $\Delta D^i_{\text{th}} = f(T^i) - f(T^{i-1})$. The stress-dependent strain increment, $\Delta D^i_{\sigma}(T^i)$, also termed the 'mechanical strain increment', is assumed to be equal to the sum of elastic and plastic strains, $\Delta D^i_{\sigma}(T^i) = \Delta D^i_{\text{e}}(T^i) + \Delta D^i_{\text{p}}(T^i)$. Here we use the stress-strain law for steel at high temperatures according to EC 3; for full description of the model, see [3].

1.4 Linearized buckling analysis

We wish to find the buckling load or critical temperature of a column with the help of the linear theory of stability [8]. By the linearization of the governing equations, Eqs. (1)–(10), around the fundamental solution, which is characterized by the condition $\varphi^i = 0$, we get a system of 10 algebraic-differential equations. For the complete derivation of the equations, see [5]. After a systematic elimination of the unknowns is made, we end up with the system of two linear differential equations with constant coefficients

$$\delta u^{i\prime\prime} = 0, \tag{13}$$

$$\delta w^{i\prime\prime\prime\prime} + k^{i^2}\delta w^{i\prime\prime} = 0, \tag{14}$$

in which the buckling load parameter k^i is introduced as

$$k^{i^2} = \frac{\left(1+\varepsilon^i\right)\left|\mathcal{N}^i\right|}{E^i_{\text{t}} J} \geq 0. \tag{15}$$

In Eq. (15) E^i_{t} is the tangent modulus of steel at time t^i and temperature T^i and J is the momentum of inertia of the cross-section. The general solutions of Eqs. (13) and (14) are

$$\delta u^i(x) = \mathcal{K}^i_1 x + \mathcal{K}^i_2, \tag{16}$$

$$\delta w^i(x) = C^i_1 \cos k^i x + C^i_2 \sin k^i x + C^i_3 x + C^i_4. \tag{17}$$

The unknown integration constants, $\mathcal{K}^i_1, \mathcal{K}^i_2, C^i_1, C^i_2, C^i_3$ and C^i_4, are obtained with the help of boundary conditions. the implementation of the boundary conditions into Eqs. (16) and (17) results in the homogeneous system of six linear algebraic equations for the unknown constants. It is well known that the non-trivial solution of the homogeneous system of linear algebraic equations is possible only if the determinant of the system matrix is zero [11]

$$\det \boldsymbol{L}^i_T = \det \boldsymbol{H}^i_T \det \boldsymbol{K}^i_T = 0. \tag{18}$$

Matrix $\boldsymbol{H}^i_T$ depends solely on $\mathcal{K}^i_1, \mathcal{K}^i_2$, while matrix $\boldsymbol{K}^i_T$ only on C^i_1, C^i_2, C^i_3 and C^i_4. It is easy to show that $\det \boldsymbol{H}^i_T \neq 0$ for any $\mathcal{K}^i_1$ and $\mathcal{K}^i_2$ thus requiring condition (18) to imply $\det \boldsymbol{K}^i_T = 0$. Finally, to determine the buckling load, the following set of non-linear algebraic equations for the three unknowns, critical axial force $\mathcal{N}_{\text{cr}}$, critical axial strain ε_{cr} and critical temperature T_{cr}, has to be solved

$$\mathcal{N}_{\text{cr}} + F_{\text{cr}} + \mu_H \varepsilon_{\text{cr}} L = 0, \tag{19}$$

$$\mathcal{N}_{\text{cr}} - \sigma_{\text{cr}} A = 0, \tag{20}$$

$$\det \boldsymbol{K}_T = 0. \tag{21}$$

Eqs. (19)–(21) are solved with the Newton iterative solution method for three critical values, $\mathcal{N}_{\text{cr}}$, ε_{cr} and T_{cr}. Once critical temperature T_{cr} is known, we determine the critical time t_{cr} directly from the known temperature field of steel column [7], which is possible only because the time-independent material model of steel at elevated temperatures has been employed.

2 NUMERICAL EXAMPLE

We analyze the effect of the adopted material model on the buckling resistanceof Euller's columns (*Fig*. 1). The columns are made of section HEA 300 and steel S 235. In *Fig 3* the critical stress ratio, $\sigma_{cr}/\sigma_{y,20}$ vs the column slenderness, λ, is depicted for the range of temperatures from $20\,^{\circ}\mathrm{C}$ to $800\,^{\circ}\mathrm{C}$. Results for our model are presented with full lines, while the dotted lines present the results of the simplified method proposed by EC 3 [3]. For a full description of the simplified method, see EC 3 [3], section 4.2.3.2.

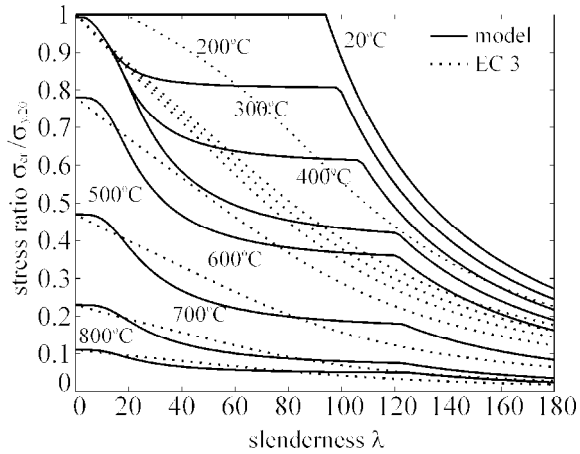

Fig 3. Euler's columns. Relationships between the critical stress ratio, $\sigma_{cr}/\sigma_{y,20}$, and the slenderness, λ, at different temperatures

The results (*Fig*. 3) show that the drop of the critical stress ratio with temperature is significant. For instance, the buckling resistance of a column with slenderness λ=60 at T=500°C is about 40% and at T=800°C only about 5% of the related resistance at room temperature. The point, separating elastic and plastic buckling regimes, also notably varies with the slenderness. Somewhat unexpected is the position of the point separating the loss of stability by buckling and by the material failure of the column. At room temperature, the slenderness as high as 93 triggers buckling, while at temperatures higher than 200°C, the slenderness of about 2 is already sufficient for buckling. Hence, in practice buckling will appear to be the only mode of fracture of columns due to fire.

Fig. 3 further shows the difference between the critical stress, obtained by the present model and the one determined by simplified method from EC 3. The behaviour of columns with slenderness up to 20 at room temperature is similar for the two models. For the slendernesses $\lambda < 20$ and $\lambda > 90$ the EC 3 method gives lower values of the critical stress. This difference is probably due to neglecting imperfections in the present model. By contrast for slendernesses $20 < \lambda < 90$, the EC 3 gives bigger critical stress than the one determined by the present procedure. The largest difference is about 20% at $T = 500\,^{\circ}\mathrm{C}$. This may be due to the fact that present model accounts for the dependence of tangent modulus E_t on deformation. Namely, once deformation is in the non-elastic range, the tangent modulus significantly decreases. Because the critical temperature depends on the tangent modulus, it also decreases when the tangent modulus decreases. By contrast, in simplified method EC 3, the tangent modulus does not depend on deformation and hence remains constant if the temperature is constant. As a results the EC 3 method is proved to be not conservative in this case.

3 CONCLUSIONS

We presented an analytical procedure for the determination of the critical temperature of an axially loaded, axially restrained, geometrically perfect steel column, if exposed to a temperature increase, which is characteristic for the standard or natural fire. Within the assumption that steel at high temperature behaves in accordance with the material model proposed by European standard EC 3 [3], the critical temperature is determined exactly. From numerical example we can conclude that the critical temperature highly depends on both the slenderness of a column and the material model of steel at elevated temperatures. We could also see that the simplified method proposed by EC 3 can be unsafe for moderate slendernesses.

4 ACKNOWLEDGMENT

The work of T. Hozjan was financially supported by the Ministry of Education, Science and Sport and by the Ministry of the Economy of the Republic of Slovenia under contract 3311-04-831816. The support is gratefully acknowledged.

REFERENCES

[1] BS5950-8. Structural Use of Steelwork in Building - Part 8: Code of Practice for Fire Resistant Design. *London*: *British Standard Institution*; 2003

[2] Burgess IW, Olawale AO, Plank RJ. Failure of steel columns in fire. *Fire Safety J*, 1992;18:183–201

[3] Eurocode 3. Design of Steel Structures, Part 1.2: Structural fire design (draft). *European Committee for Standardization* 2003

[4] Franssen JM, Dotreppe JC. Fire resistance of columns in steel frames. *Fire Safety J*, 1992;19:159–175

[5] Hozjan T, Planinc I, Saje M, Srpčič S. Buckling of an axially restrained steel column under fire loading. *Fire Safety J*, 2007, submitted for publication

[6] Huang ZF, Tan KH. Analytical fire resistance of axially restrained steel columns. *J Struct Eng ASCE*, 2003;129(11):1531–1537

[7] ISO 834 Fire resistance tests – elements of building constructions. *International Standard ISO 834*; 1975

[8] Keller HB. Nonlinear bifurcation. *J Diff Eq*, 1970;7:417–434

[9] Ma ZC, Mäkeläinen P. Parametric temperature–time curves of medium compartment fires for structural design, *Fire Safety J*, 2000;34:361–375

[10] Oda H, Usami T. Stability design of steel plane frames by second-order elastic analysis. *Eng Struct*, 1997;19:617–627

[11] Planinc I, Saje M. A quadratically convergent algorithm for the computation of stability points: the application of the determinant of the tangent stiffness matrix. *Comp Meth Appl Mech Eng*, 1999;169:89–105

[12] Reissner E. On one-dimensional finite-strain beam theory: The plane problem. *J Appl Math Phys (ZAMP)*, 1972;23:795–804

[13] Skowronski W. Buckling fire endurance of steel columns in fire. *J Struct Eng ASCE*, 1993;119(6):1712–1732

[14] Tang CY, Tan KH, Ting SK. Basis and application of a simple interaction formula for steel columns under fire conditions. *J Struct Eng ASCE.* 2001;127(10):1206–1213

[15] Vila Real PMM, Hopes N, da Silva S, Piloto P, Franssen JM, Numerical modelling of steel beam-columns in case of fire–comparison with Eurocode 3. *Fire Safety J*, 2004;39:23–39

BEHAVIOUR OF HIGH STRENGTH GRADE 10.9 BOLTS UNDER FIRE CONDITIONS

Dipl.-Ing. Fernando González [a], Prof. Dr.-Ing. Jörg Lange [b]

[a ;b] Technische Universität Darmstadt, Department of Civil Engineering and Geodesy, Darmstadt, Germany

INTRODUCTION

In the last decades structural fire design has changed essentially. In the past the structural integrity of single elements was mostly proven by load tables which were based on fire tests. The introduction of the "hot" Eurocodes (Parts 1-2) offers the possibility to assess the resistance even of complex structural systems under fire conditions. For this purpose a calculation can be made according to the Eurocodes taking into account the relevant material behaviour which is mainly known for structural steel and concrete elements. The material behaviour is defined in the ECs by stress – strain curves, depending on the affecting temperature. Even for connections design rules are given in the Eurocodes. The resistance of bolts and welding seams under fire conditions can easily be calculated using global reduction factors which depend on the element temperature. The global reduction factors for bolts are currently valid for all grades. The experience shows that either differing alloying materials or varying treatment methods can lead to a relevant change in the stress – strain curve. These two points have an important influence on the production process of high strength grade 10.9 bolts. Due to this tension tests on specimens and bolt assemblies have been carried out in order to evaluate the behaviour under fire conditions. The results will give on one hand the possibility to verify the reduction factors for grade 10.9 bolts given in the Eurocode and on the other hand give a more precise understanding of high strength bolt behaviour under fire conditions.

The paper will describe the state of the art, the elaborated tests in more depth and present first results.

1. STATE OF THE ART

The joint behaviour under fire exposure has currently moved into the focus of researchers. The global aim of forecasting the behaviour of complete structures under fire conditions can only be achieved by merging the knowledge of all single structural elements. The behaviour of the joint area is very complex and still not fully predictable in the hot stage. On that background various publications have been published in recent years dealing with the behaviour of bolted connections like fin plate or endplate connections ([1], [2]). Research concerning the behaviour of pure bolt assemblies is rare. In [3] and [4] series of tests are presented using grade 8.8 bolts, analysing the pure material and the bolt assembly behaviour. Experiences respectively test series for grade 10.9 bolts are not existent. The reason for this is, that from the international point of view the grade 10.9 bolts are rarely used and therefore not in the focus of investigations. In Germany and France by contrast grade 10.9 bolt assemblies are very common for endplate connections. Globally very little knowledge exists in this area. In [5] high-strength fire resistant (FR) bolts have been tested, showing similar properties at room temperature compared to grade 10.9 bolts. But due to some differences concerning the alloy and fabrication the test results at high temperatures are not fully comparable.

Eurocode 3 Part 1-2 Annex D [6] proposes for the connection area a design concept providing strength reduction factors for bolts and welding seams. The factors depend on the local temperature of the connection area and are valid for all bolt grades. The local temperature at the connection can be estimated using a method given in Annex D. It has to be stated that the handling is not transparent and leads at least to very rough solutions.

2. HIGH TEMPERATURE TESTS OF SPECIMENS AND GRADE 10.9 BOLT ASSEMBLIES

2.1 General Procedure

Due to the obvious lack of knowledge concerning the behaviour of grade 10.9 bolt assemblies under fire conditions a large test series was planed to be executed in order to fill up this gap. Some of the tests are already completed, others are outstanding or still in course. Due to this the paper will show the pure material and the first 10.9 bolt assembly tension test results. The specimens used have been milled of grade 10.9 bolts.

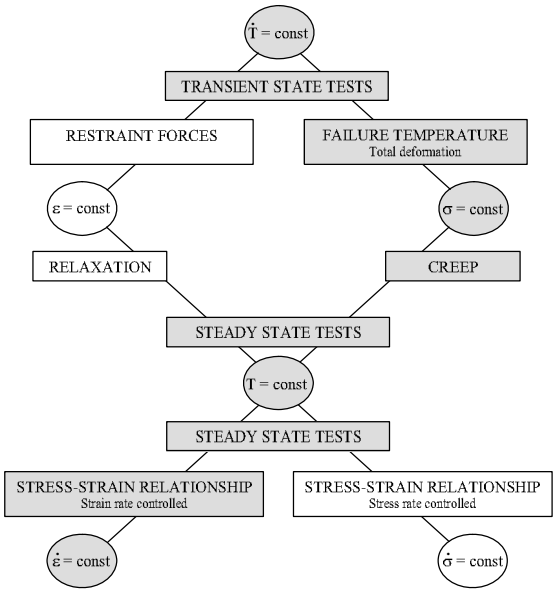

Fig. 1. Different testing methods according to [8]

As described in numerous publications, the high temperature test procedure itself has an enormous impact on the outcome and can lead to clearly differing results. Therefore the specification of the test procedure is fundamental for the outcome. In [8] different high temperature test methods are listed and described. *Figure 1* shows the different test methods. During a fire the material is normally subjected to a transient process which is directly depending on the applied temperature sequence. Therefore the transient test will normally lead to more realistic results, but it has to be noted that the temperature curve is not exactly defined and correlates with various factors like ventilation, thermal conductivity of the elements etc. The steady state test on the other hand is strain rate controlled and the results depend severely on this parameter. Due to the great sensitivity of the results concerning the heating velocity as well as the strain rate, it was decided to perform both steady state tests and transient state tests in order to be able to compare and to verify the results. At first glance a direct comparison of the two tension test results is not possible. The strain of the transient state test is composed of the thermal strain, the stress related strain and the creep strain, where thermal strain can easily be eliminated measuring the thermal elongation of an unstressed specimen. In comparison to the steady state test the strain is mainly composed by the stress related strain. The creep effects are negligible because of the short duration of the test. In order to make the results comparable additional creep tests have been performed. The grey shaded boxes in *Figure 1* show the specimen tests realized by now. The bolt assemblies have only been tested under steady state conditions in order to determine the maximum failure load at the hot stage. For the bolt assemblies a much higher testing load (app. 270 kN at room temperature) was necessary to reach the failure, than in comparison to

the milled specimens (app. 18 kN at room temperature). This made the realization of the tests quite difficult. A measurement of the strain was not possible and even not useful due to the varying diameter along the bolt length. As it will be shown further on the creep effect has in a certain margin no significant influence on the ultimate strength of the material, so it can be stated, that the test procedure used gives a realistic failure load for the bolt assemblies.

2.2 Test Arrangement and Test Method

The round milled test specimens were made from high strength grade 10.9 bolts with a diameter of 16 mm. The bolts were manufactured by cold forging followed by a quench and temper heat treatment in order to achieve the required minimum mechanical properties as shown in *Table 1*. The chemical composition of the bolt material complies with the DIN EN ISO 898-1 [10].

Table 1: Mechanical properties of grade 10.9 bolts

Steel grade	minimum tensile strength	minimum strength at strain of 0,2%	minimum expansion	minimum lateral contraction	Vickers hardness, HN; F ≥ 98 N
10.9 bolt	1040 N/mm²	940 N/mm²	9 %	48 %	320 - 380

The dimensions of the specimens used for the different tests are in accordance with DIN EN 10002 Part 5 [9] and are shown in *Figure 3*. The gauge length was 30 mm. The extensometer which was fixed on the specimen was able to measure a maximum extension of 3 mm. The furnace in which the specimen was situated during the tests is equipped with three separate controlled resistor elements and three thermocouples (*Figure 2*). For the steady state test the specimens were heated to a given temperature and held for approximately half an hour. During this time the thermal expansion was permanently controlled due to the fact that this indicates the completion of the warming phase of the specimen. If no further thermal expansion occurs, the warming is completed. The tension test was performed at a strain rate of 0,001/min to provide proof stress values up to 2 %, after that the strain rate was raised to 0,025/min and maintained until rupture. The chosen strain rates correspond to the values given in [9]. The results of this testing method can be shown in a stress strain curve. Three specimens were tested under steady state conditions at each temperature.

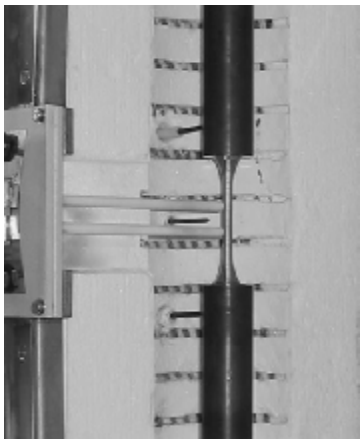

Fig. 2: Testing device specimen

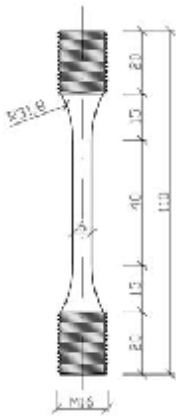

Fig. 3: Dimensions of specimen in mm

For the transient test the specimens were located accordingly in the testing device and stressed with a constant load. The steel temperature was additionally measured by a K-Type thermocouple which was directly fixed on the surface of the specimen. The test was performed using a constant heating rate of 10 K/min. The results can be shown in a temperature strain curve. It has to be kept in mind that under these testing conditions the thermal expansion is included in the results which can be eliminated easily as explained before. For the transient tests two specimens were tested at different stress levels. The additionally performed creep tests require a constant loading and a constant temperature. Due to this the specimens were heated up to a certain temperature and loaded subsequently. After applying the load the occurring strain was recorded constantly.

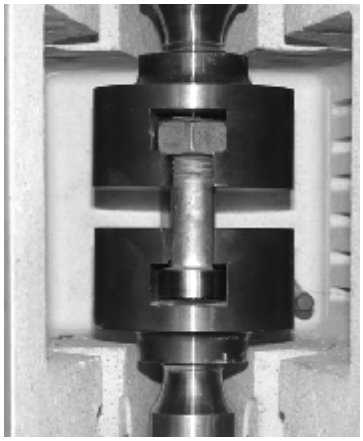

Fig. 4: Testing device bolt

Fig. 5: Fitting

The bolt assemblies have been tested in a different device with a maximum traction load of 1000 kN. The load transfer into the bolt assemblies was realized by a bracket made of Nimonic 80A which has been designed to fit with all the constraints like furnace and bolt dimensions. The bracket is shown in F*igure 4*. First tension tests showed that the opening on the front of the bracket, which is necessary to put the bolt in place, has a big impact on the outcome. Due to this an additional fitting was produced to realize a rotation symmetric load transfer to the bolt (*Figure 5)*. The bolt temperature was constantly measured by two K-type thermocouples which were fixed on the nut and on the shank of the bolt. Due to the big mass of the brackets the heating phase was very long and a small temperature gradient between shank and nut was not avoidable. Even though, the temperature gradient during the tension tests was smaller than 5°C. After reaching the target temperature it has been maintained constant about half an hour. The tension test of the bolts was performed using a constant strain rate of 0,001/min which was held constant until the end of the test. A code for tension tests of bolt assemblies is not existent and therefore the test procedure follows closely DIN EN 10002 Part 5 [9].

2.3 Test Results

The results of the high temperature tests on the round milled specimens are shown in F*igure 6.* The indicated curves describe the stress-strain relation up to a strain of 2% and are based on the steady state tests. From 300°C onwards the strength reduction is significant and clearly visible, see also *Fig. 7.* At 700°C respectively 800°C the strength is only about 5% in comparison to the strength at room temperature. As indicated before the strain rate was increased after an extension of 2% in order to obtain the tensile strength. The strain rate

acceleration occurs relatively early and leads to a considerably hardening of the material. Comparing the 2% strain stress ratio at 600°C with the tensile strength ratio at the same temperature a hardening of about 70% occurs (*Fig. 7*). This effect is very interesting comparing it with the results in [3]. There the strain rate was held constant until an expansion of 5% was reached. The maximum strength was obtained within this range, so that a significant hardening effect after 5% was not noticeable. During a transient test this effect will not occur, due to this the tensile strength ratios shown in *Figure 7* have to be used very carefully. But on the other hand it is interesting to see, that the tensile strength ratios are fitting with the reduction factors given in the Eurocode 3 Part 1-2 Annex D. Comparing the stress ratio curve at 2% of extension with the Eurocode curve a significant difference can be noticed. The tension tests on bolt assemblies show in comparison to the Eurocode reduction factor curve up to 450°C a similar behaviour, but from that point on the bolt assemblies behave more like the strength ratio curve at 2% strain. From 550°C onwards the 10.9 bolt strength ratio behaves a bit stronger than expected due to the pure material tests. First tests on bolts of a different manufacturer show a similar behaviour. Nevertheless the 10.9 bolt strength ratio runs significantly underneath the Eurocode reduction factor curve given in Annex D. In *Figure 6* some additional values resulting from the transient tests are indicated by dots. The values belonging to a temperature of 200°C (Transient test Tr.t. 200°C) are following quite well the curve obtained by a steady state test. This is understandable comparing it with the results of the creep tests. At low temperatures none or just negligible creep deformation occur, so that the transient test results fully correspond with the results of the steady state tests. For higher temperatures the transient test values are quite beneath the corresponding steady state results, due to the fact that from 300°C upwards a creep effect is visible and not further negligible. The horizontal distance in *Figure 6* between the transient test values and the steady state curve is approximately the creep deformation tested in the corresponding tests.

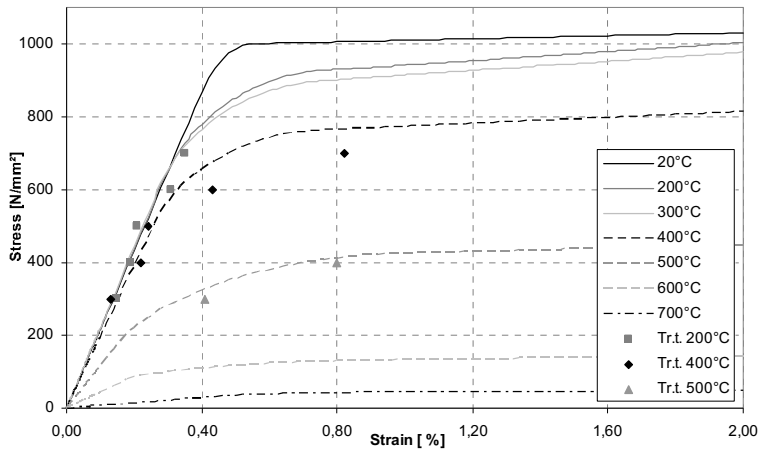

Fig. 6: Stress-Strain Curve

3 SUMMARY AND OUTLOOK

The performed tension tests show that high temperatures have a strong effect on the grade 10.9 bolt material behaviour. Comparable tests for this material are nearly not existent. Further examinations will be performed using more bolt assemblies for tension and shear tests.

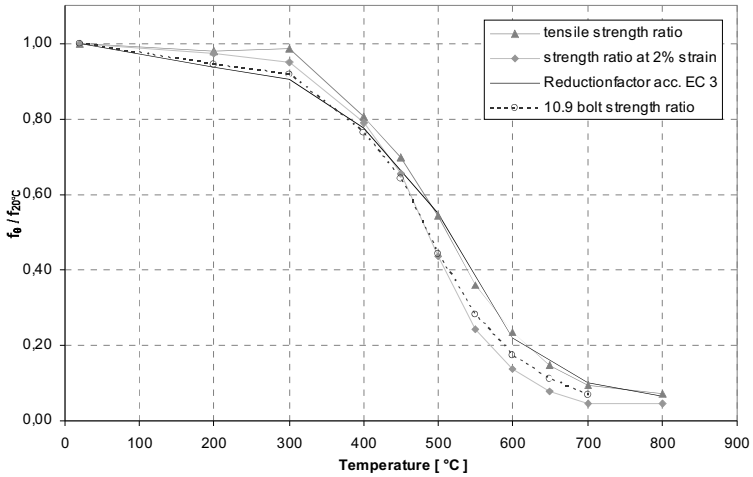

Fig. 7: Reduction factors

REFERENCES

[1] Heddrich, Rolf, „Untersuchungen zum Trag- und Verformungsverhalten von Schrauben-verbindungen bei feuerwiderstandsfähigen Verbundprofil-Konstruktionen unter Brandeinwirkung“, Doctoral thesis D17, *Konstruktiver Ingenieurbau der Technischen Universität Darmstadt*, 1990

[2] Hongxia Yu, I.W. Burgess & J.B. Davison, “Experimental investigation of the behaviour of fin plate connections in fire”, Proceedings of the 3rd International Conference on Steel and Composite Structures (ICSCS07) Manchester, *Taylor and Francis*, 2007

[3] Kirby, B.R., “The behaviour of high-strength grade 8.8 bolts in fire”, J. Construct. Steel Research 33, *Elsevier Science Limited*, 1995

[4] Hu Y, J.B. Davison & I.W. Burgess, “Comparative study of the behaviour of BS 4190 and BS EN ISO 4014 bolts in fire”, Proceedings of the 3rd international conference on steel and composite structures (ICSCS07) Manchester, *Taylor and Francis*, 2007

[5] Sakumoto Y., “Test of fire resistant bolts and joints”, Journal of Structural Engineering Vol. 119 No. 11, *ASCE Publication*, 1993

[6] DIN EN 1993-1-2, “Eurocode 3: Bemessung und Konstruktion von Stahlbauten, Teil 1-2 Allgemeine Regeln – Tragwerksbemessung für den Brandfall”, *Beuth Verlag*, 2006

[7] BS 5950-8, “British Standard: Structural use of steel work in building – Part 8: Code of practice for fire resistant design”, *British Standards Institution*, 2003

[8] Anderberg, Yngve, “Modelling Steel Behaviour”, Report LUTCDG/(TVBB-3028), *Lund Institute of Technology*, 1986

[9] DIN EN 10002-5, “Metallische Werkstoffe Zugversuch Teil 5: Prüfverfahren bei erhöhter Temperatur”, *Beuth Verlag*, 1992

[10] DIN EN ISO 898-1, “Mechanische Eigenschaften von Verbindungselementen aus Kohlenstoffstahl und legiertem Stahl- Teil 1: Schrauben”, *Beuth Verlag*, 2007

STAINLESS STEEL BEAM-COLUMNS INTERACTION CURVES IN CASE OF FIRE WITH AND WITHOUT LATERAL TORSIONAL BUCKLING

Nuno Lopes [a], Paulo Vila Real [a], Luís Simões da Silva [b], J.-M. Franssen [c]

[a] University of Aveiro, LABEST-Department of Civil Engineering, Aveiro, Portugal
[b] University of Coimbra, ISISE-Department of Civil Engineering, Coimbra, Portugal
[c] University of Liege, Structural Engineering, Belgium

INTRODUCTION

The use of stainless steel in construction is increasing [1]. However, it is still necessary to develop the knowledge of its structural behaviour. Stainless steels are known by their non-linear stress-strain relationships with low proportional stress and extensive hardening phase.
The EN 1993-1-4 "Supplementary rules for stainless steels" [2] gives design rules for stainless steel structural elements at room temperature, and only makes mention to its fire resistance by referring to the fire part of the Eurocode 3 (EC3), EN 1993-1-2 [3], stating that stainless steel structural members subjected to high temperatures must be designed with the same formulae as those used for carbon steel members. However, as these two materials have different constitutive laws, it can be expected that different formulae for the calculation of member stability should be used for fire design.
In previous papers, [4] and [5], new proposals for the flexural buckling of stainless steel columns and LTB of stainless steel beams were made.
It is the purpose of this paper to evaluate the accuracy and safety of the currently prescribed design rules in EC3: Part 1.2 for the evaluation of the resistance of stainless steel beam-columns with and without lateral-torsional buckling (LTB). In this evaluation the new carbon steel beam-column formulae at room temperature were also tested [6, 7, 8], after being adapted to deal with stainless steel in fire situation.
A parametric study of the behaviour of the several stainless steel grades (austenitics, austenitic-ferritic and ferritics grades) beam-columns subjected to fire are presented, and new proposals for the design of these structural elements are made.
This evaluation is carried out by performing numerical simulations on Class1 and Class 2 stainless steel H-columns subjected to compression plus uni-axial bending. It is considered buckling in the two main cross-section axes and different bending moments diagrams ($\psi = 1; \psi = 0$ and $\psi = -1$), with and without lateral-torsional buckling. The stainless steel mechanical and thermal properties at high temperatures used in this paper can be found in Part 1.2 of EC3 [3]. The following welded cross-sections were used: HEA200, HEB280 and HEB200. The types of stainless steel grade used were: 1.4301, 1.4003 and 1.4462. An average of 5 beam lengths and 8 bending moment / axial load ratios were analysed for each case. A uniform temperature distribution of 600ºC in the cross-section was used.
In the numerical simulations, a sinusoidal lateral geometric imperfection was considered [4]. The adopted residual stresses follows the typical pattern for carbon steel welded sections [4, 9, 10], considered constant across the thickness of the web and flanges.
The program SAFIR [11], a geometrical and material non linear finite element code, which has been adapted according to the material properties defined in EN 1993-1-4 [2] and EN 1993-1-2 [3], to model the behaviour of stainless steel structures, was used in the numerical simulations.

It is shown an evaluation of the performance of the interaction curves obtained with part 1.2 of EC3 [10], concluding that these interaction curves don't provide a good approximation to the numerical results obtained with SAFIR. Therefore it was necessary to find other curves that could fit better these numerical results, testing the new formulae from part 1.1 of EC3 [6] and finally proposing new formulae.

1 BEAM-COLUMN WITHOUT LTB

1.1 EC3 proposals for fire situation

The EC3 states that the safety evaluation should be made with the same expressions as those used in carbon steel elements, which are

$$\frac{N_{fi,Ed}}{\chi_{i,fi} A k_{y,\theta} \frac{f_{y,\theta}}{\gamma_{M,fi}}} + k_i \frac{M_{i,fi,Ed}}{W_{pl,i} \frac{f_{y,\theta}}{\gamma_{M,fi}}} \leq 1 \tag{1}$$

where, $i = y$ or z, and

$$k_i = 1 - \frac{\mu_{i\theta} N_{fi,Ed}}{\chi_{i,fi} A k_{y,\theta} \frac{f_y}{\gamma_{M,fi}}} \leq 3 \tag{2}$$

with, according to [12],

$$\mu_{y,\theta} = (2\beta_{M,y} - 5)\overline{\lambda}_{y,\theta} + 0.44\beta_{M,y} + 0.29 \leq 0.8 \text{ with } \overline{\lambda}_{y,20^oC} \leq 1.1 \tag{3}$$

$$\mu_{z,\theta} = (1.2\beta_{M,z} - 3)\overline{\lambda}_{z,\theta} + 0.71\beta_{M,z} - 0.29 \leq 0.8 \tag{4}$$

The equivalent uniform moment factor $\beta_{M,y}$ and $\beta_{M,z}$ is determined according to the expression (5), in function of the bending diagram shape.

$$\beta_{M,i} = 1.8 - 0.7\psi_i \tag{5}$$

The curves obtained with these formulae are denoted "EN 1993-1-2" in Figure 2, while the curve "EN 1993-1-2 mod" was obtained together with the new proposal for columns [4].
From figure 2 it can be concluded that the interaction curves from part 1.2 of Eurocode 3 together with the new proposal for columns [4], is closer to the numerical results but still can be improved.

1.2 Formulation of a new proposal

Based in the procedure adopted by Talamona [13] for the determination of the carbon steel interaction curves at high temperatures, new formulae for the stainless steel beam-columns safety evaluation were developed and are here presented.
Comparing with EC3 [3, 14] the main changes appear in the determination of the interactions factors $K_{i,fi}$ ($K_{y,fi}$ or $K_{z,fi}$).

$$K_{i,fi} = 1 - \frac{\mu_{i,\theta} N_{fi,Ed}}{\chi_{i,fi} A k_{y,\theta} \frac{f_y}{\gamma_{M,fi}}} \quad \text{with} \quad K_{i,fi} \leq 0.8\overline{\lambda}_{i,\theta} + 0.9 \tag{6}$$

Now the limits for $K_{i,fi}$ are dependent of the Slenderness. Figure 1 shows the influence in the interaction curves due to those limits.
The interaction curve given by (1) can be written in the following schematic way.

$$N^* + M^* - \mu N^* M^* = 1 \tag{7}$$

Figure 1 shows the shape of the interaction curves for different values of the coefficient μ. It is concave for positive values of μ (meaning that higher resistance is available) and turns convex with negative values of μ (meaning that lower resistance is available). The linear branch near the N* axis comes from the limitations of $k_i = 1 - \mu N^*$ in equations (2) and (6).

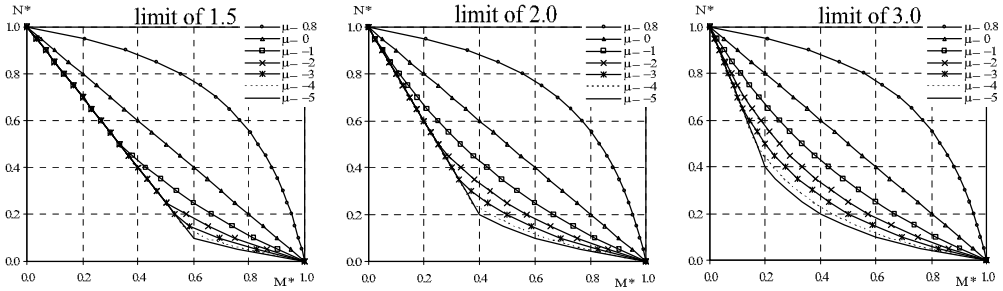

Fig. 1. Interaction curve shape for different interaction factor limits.

To determine the values of $\mu_{y,\theta}$ and $\mu_{z,\theta}$ the following equations should be used for the stainless steel grades 1.4301 and 1.4003:

$$\mu_{y,\theta} = \left(4.33\beta_{M,y} - 8.56\right)\overline{\lambda}_{y,\theta} + 0.33\beta_{M,y} + 0.11 \le 0.7 \tag{8}$$

$$\mu_{z,\theta} = \left(3.03\beta_{M,z} - 6.33\right)\overline{\lambda}_{z,\theta} + 1.93\beta_{M,z} - 2.45 \le 0.7 \tag{9}$$

It was found that for the duplex grade, the changes introduced in the flexural buckling curves [15], when compared to the other grades, were not enough to approximate satisfactory the beam-columns numerical results. Therefore, for the duplex stainless steel grade 1.4462 different formulae should be adopted.

$$\mu_{y,\theta} = \left(1.27\beta_{M,y} - 2.63\right)\overline{\lambda}_{y,\theta} + 0.66\beta_{M,y} - 0.49 \le 0.8 \tag{10}$$

$$\mu_{z,\theta} = \left(1.53\beta_{M,z} - 3.20\right)\overline{\lambda}_{z,\theta} + 0.41\beta_{M,z} + 0.24 \le 0.9 \tag{11}$$

The equations from (8) to (11) were developed to approximate the numerical results being on the safe side when compared to them, as shown in the next section.

1.3 Accuracy of the proposals

Numerical validation

Due to space limitations only few results of the parametric study are shown.
The graphics from Figure 2 were obtained for beam-columns with welded cross-sections equivalent to an HEA200 at 600ºC of the stainless steel grade 1.4301, for the buckling modes about the y and z axis, with uniaxial bending in the strong and weak axis respectively. Here, the length of 7m corresponds to $\overline{\lambda}_{y,\theta} = 0.84$ and was used $\overline{\lambda}_{z,\theta} = 1.39$.
The four interaction curves in the graphics from Figure 2 are obtained from: a) part 1-2 of EC3 "EN 1993-1-2"; b) part 1-2 of EC3 with the new proposal for columns [4] "EN 1993-1-2 mod"; c) part 1-1 of EC3 for carbon steel beam-columns with the new proposal for columns

[4] “Method 1”and “Method 2” [6, 7, 8]; and d) the formulated interaction curves presented in the previous section “New proposal”.

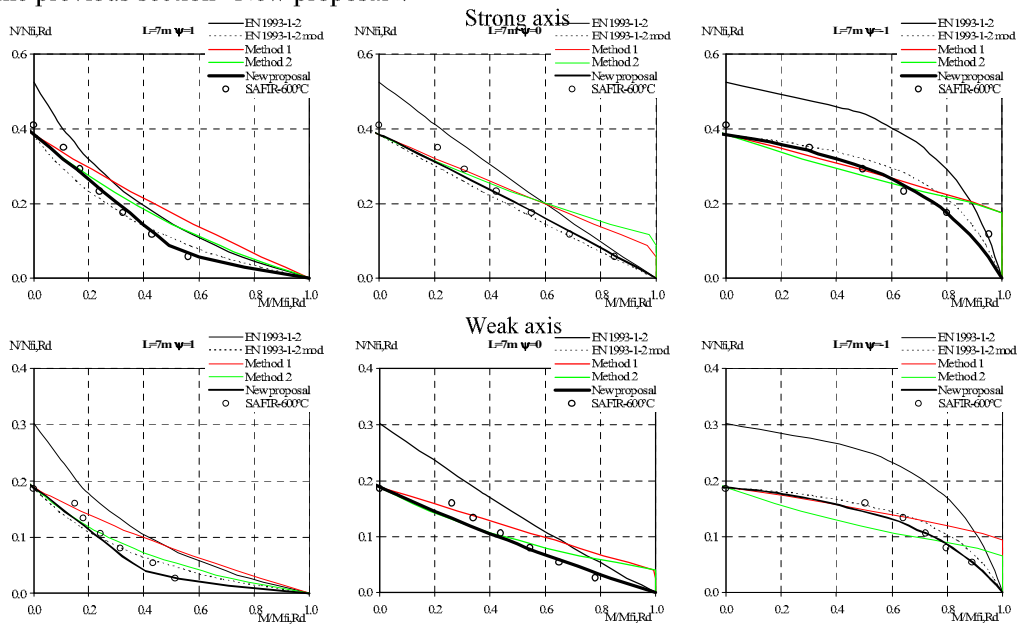

Fig. 2. Comparison between different interaction curves for welded HEA200 beam-columns of the stainless steel grade 1.4301.

The method that is the best approximation of the numerical results from SAFIR is the method “New proposal”. As it can be seen in Figure 2 the other methods present unsafe approximations compared with numerical results.
It can be also observed that the new proposal for columns [4] introduces a significant improvement in the interaction curves.

Statistical evaluation

All the obtained results, with the several proposals for the interaction curves (“EN 1993-1-2”, “EN 1993-1-2mod”, “Method 1”, “Method 2” and “New proposal”), are shown in Figure 3.
Table 1 presents the average and standard deviation obtained with the different methods for determining the austenitic and the ferritic stainless steel beam columns interaction curves at high temperatures.

Table 1. Statistical results of beam-columns without LTB at high temperatures.

		EN 1993-1-2	EN 1993-1-2 mod	Method 1	Method 2	New proposal
Strong axis	Average value	1.355	1.017	1.185	1.122	0.961
	Standard deviation	0.312	0.218	0.320	0.272	0.162
Weak axis	Average value	1.342	0.973	1.188	0.951	0.903
	Standard deviation	0.281	0.195	0.270	0.261	0.154

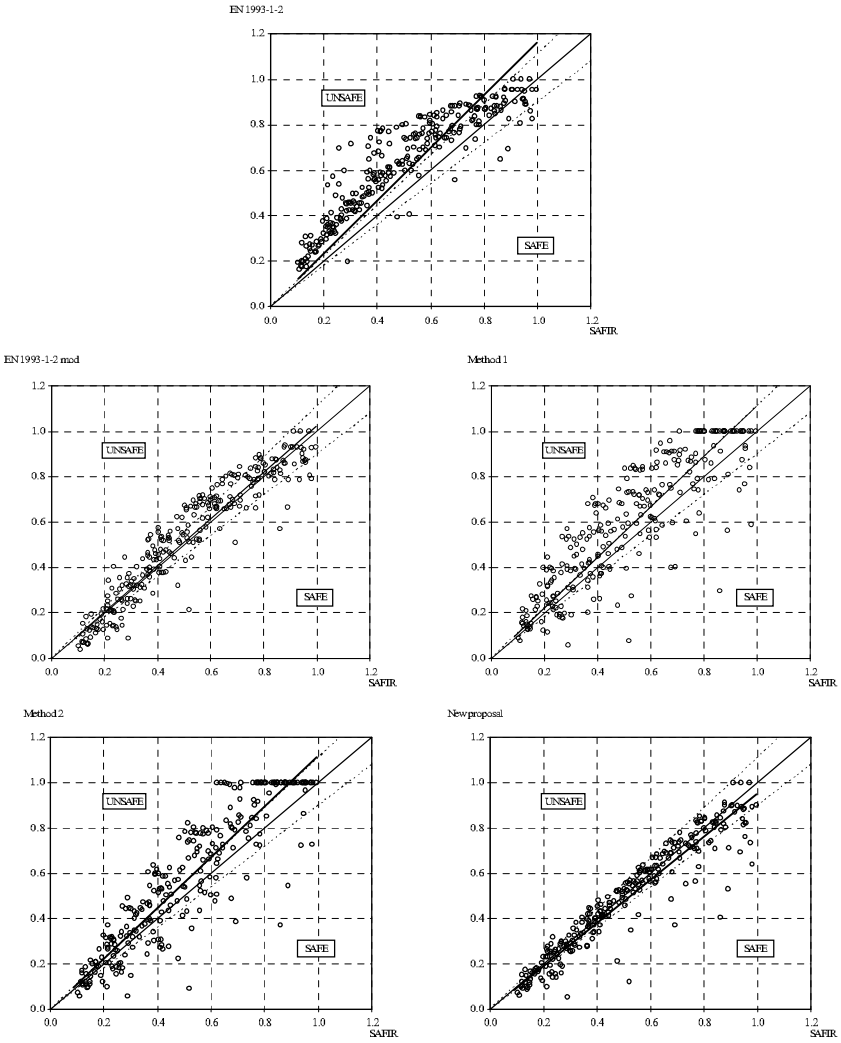

Fig. 3. Comparison with the numerical results for the strong axis for steel grade 1.4301 and 1.4003.

Table 2 presents the average and standard deviation obtained with the different methods for determining the duplex stainless steel beam columns interaction curves at high temperatures.

Table 2. Statistical results of duplex beam-columns without LTB at high temperatures.

		EN 1993-1-2	EN 1993-1-2 mod	Method 1	Method 2	New proposal
Strong axis	Average value	1.004	0.860	1.065	0.993	0.956
	Standard deviation	0.153	0.173	0.230	0.246	0.122
Weak axis	Average value	1.004	0.753	0.912	0.711	0.896
	Standard deviation	0.132	0.181	0.223	0.236	0.178

It can be observed that, although having a few unsafe results, the new proposal presents the best agreement with the numerical results for all the stainless steel grades. It is also clear that specific interaction formulae are needed for the 1.4462 stainless steel grade.

2 BEAM-COLUMN WITH LTB

2.1 EC3 proposals for fire situation

The EC3 states that the safety evaluation should be made with the same expressions as those used in carbon steel elements, which are

$$\frac{N_{fi,Ed}}{\chi_{z,fi} A \frac{k_{y,\theta} f_y}{\gamma_{M,fi}}} + K_{LT,fi} \frac{M_{y,fi,Ed}}{\chi_{LT} W_{pl,y} \frac{k_{y,\theta} f_y}{\gamma_{M,fi}}} \leq 1 \tag{12}$$

where,

$$K_{LT,fi} = 1 - \frac{\mu_{LT,\theta} N_{fi,Ed}}{\chi_{z,fi} A k_{y,\theta} \frac{f_y}{\gamma_{M,fi}}} \quad \text{with} \quad K_{LT,fi} \leq 1 \tag{13}$$

with,

$$\mu_{LT,\theta} = 0.15 \overline{\lambda}_{z,\theta} \beta_{M,LT} - 0.15 \leq 0.9 \tag{14}$$

The equivalent uniform moment factor $\beta_{M,LT}$ is determined according to the expression (5), in function of the bending diagram shape in the strong axis.

2.2 Formulation of a new proposal

It is proposed that the safety evaluation of elements subjected to bending and axial compression with LTB should satisfy expression (12), using the new proposal for LTB presented in [5], and a new $\mu_{LT,\theta}$ given by

$$\mu_{LT,\theta} = \left(-0.14 \beta_{M,LT} + 0.11\right) \overline{\lambda}_{z,\theta} + 0.50 \beta_{M,LT} - 0.09 \leq 0.8 \tag{15}$$

The equation (15) was developed to be a good approximation to the numerical results. In this case it was not necessary to differentiate the duplex 1.4462 stainless steel grade, because of the high values obtained for μ.

2.3 Accuracy of the proposals

The graphics from Figure 4 were obtained for beam-columns with welded cross-sections equivalent to an HEA200 of the stainless steel grade 1.4301, with the possibility of LTB, with bending in the strong axis. Here, the length of 7m corresponds to $\overline{\lambda}_{z,\theta} = 1.39$. The non-dimensional slenderness values for the LTB phenomena are 0.89 for $\psi = 1$, 0.67 for $\psi = 0$, and 0.55 for $\psi = -1$. Again, due to space limitations only few results, of the parametric study, are shown here.

The interaction curves named “EN 1993-1-2 mod” in the graphics from Figure 4 were obtained from part 1-2 of EC3 with the new proposal for columns presented in [4] and with the new proposal for LTB presented in [5], as for the other methods studied (“Method 1”, “Method 2” and “New proposal”).

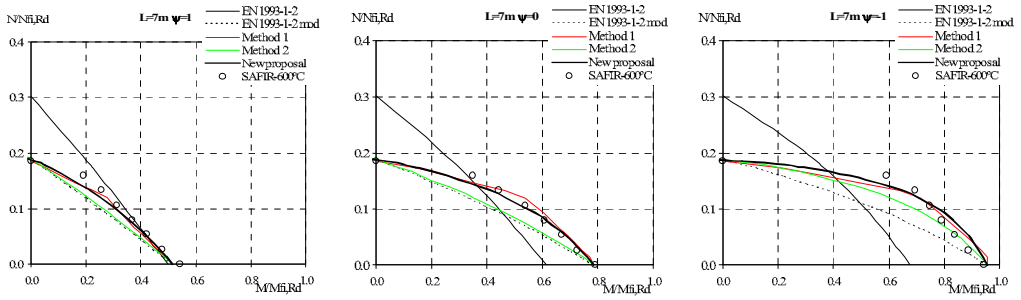

Fig. 4. Comparison between different interaction curves for welded HEA200 beam-columns of the stainless steel grade 1.4301, for beam-columns with LTB.

Figure 4 shows that the best approximation to the numerical results is given by the "New proposal".
The "Method 1" and "Method 2" [6, 7] also present good approximations. From these two methods, the one that has a better behaviour is the "Method 1".
It can be also observed that the new proposals, for columns [4] and for LTB of beams [5], introduce significant improvements in the models.
In Figure 5 all the obtained results with the different proposals for the interaction curves (EC3, "Method 1", "Method 2" and "New proposal"), are shown

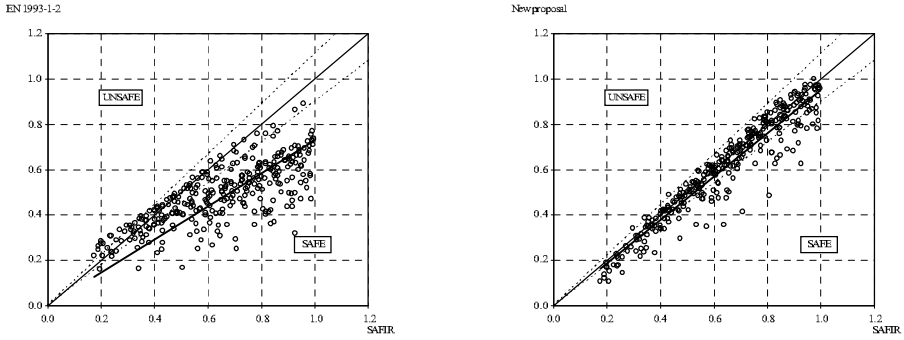

Fig. 5. Comparison with the numerical results for all steel grades, for beam-columns with LTB.

It can be observed that the new proposal presents the best agreement with the numerical results, providing at the same time safety.

3 CONCLUSIONS

In this paper, new approaches for evaluating the safety of stainless steel elements subjected to axial compression and bending in the fire situation were presented. These approaches address the influence of global buckling phenomena (flexural buckling and LTB).
The studies on stainless steel beam-columns concluded that the direct adaptation of the new carbon steel interaction curves to stainless steel in case of fire didn't give good results. As a consequence, new interaction curves for the design of stainless steel beam-columns with and without LTB, and at high temperatures, were proposed, providing safe and economic approximations to the obtained numerical results.

The studies presented in this paper were made in different stainless steel grades. Due to the fact that they have different stress-strain relationships at high temperatures, it was necessary to account for this influence, mainly in the ferritic and duplex grades.

REFERENCES

[1] Euro Inox and Steel Construction Institute, "Design Manual for Structural Stainless Steel", 3rd edition, 2006.

[2] CEN, EN 1993-1-4, Eurocode 3: Design of steel Structures – Part 1-4: General rules – Supplementary Rules for Stainless steels, Belgium, 2006.

[3] CEN, EN 1993-1-2, Eurocode 3, Design of Steel Structures – Part 1-2: General rules – Structural fire design, Belgium, 2005.

[4] Lopes, N., Vila Real, P., Silva, L., Franssen, J.-M., Mirambell, E., Numerical modelling of axially loaded stainless steel members under fire conditions, proceedings of the *International Colloquium SDSS'06*, Lisboa, Portugal, 2006.

[5] Vila Real, P., Lopes, N., Simões da Silva, L., Franssen, J.-M., Lateral-torsional buckling of Stainless steel I-beams in case of fire, *Journal of Constructional Steel Research*, ELSEVIER, 2008.

[6] CEN, "EN 1993-1-1, Eurocode 3, Design of Steel Structures – Part 1-1: General rules and rules for buildings", Belgium, 2005.

[7] Boissonnade, N., Greiner, R., Jaspart, J. P., Rules for Member Stability in EN1993-1-1 Background documentation and design guidelines, *ECCS Technical Committee 8 – Stability*, 2006.

[8] Lopes, N., Vila Real, P., Simões da Silva, L., Franssen, J.-M., Stainless steel beam-columns in case of fire, proceedings of the *ICSAS'07*, Oxford, United Kingdom, 2007.

[9] Chen, W. F. and Lui, E. M., Stability design of steel frames, CRC Press, 1991.

[10] Gardner, L., Nethercot, D., Numerical Modelling of Stainless Steel Structural Components - A consistent Approach, *Journal of Constr. Engineering*, ASCE, 2004.

[11] Franssen, J.-M., SAFIR. A Thermal/Structural Program Modelling Structures under Fire, E*ngineering Journal*, A.I.S.C., 2005.

[12] Talamona, D., Franssen, J.-M., Schleich, J.-B., Kruppa, J., Stability of Steel Columns in Case of Fire: Numerical Modeling, *Journal of Structural Engineering*, 1997.

[13] Talamona, D., Flambement de poteaux métalliques sous charge excentrée, à haute température, (in french); *Ph.D. thesis*, Université Blaise Pascal Ecole Doctorale Sciences pour l'Ingenieur de Clermont-Ferrand, 1995.

[14] Talamona, D.; Castagne, S.; Lopes, N.; Vila Real, P.; Franssen, J.-M. "Comparative study of analytical formulae for the fire resistance of steel beam-columns", proceedings of the 5th International Conference on Structures in Fire SiF'08, pp. 101 a 112, ISBN 978-981-08-0767-2, Singapore, Singapore, 28 to 30 of May of 2008.

[15] Lopes, N., Vila Real, P., Simões da Silva, L., Franssen, J.-M., duplex stainless steel columns and beam-columns in case of fire, proceedings of the *SiF'08*, Singapore, 2008.

FIRE PROTECTION OF STEEL STRUCTURES USING SPRINKLER SYSTEMS

Jyri Outinen [a], Jouko Kansa [b]

[a] Rautaruukki Oyj, Ruukki Construction, Vantaa, Finland
[b] Rautaruukki Oyj, Ruukki Construction, Seinäjoki, Finland

INTRODUCTION

An experimental research program has been carried out in Finland in order to study the cooling effect of two different sprinkler systems in fire situation to steel structures. The aim was to study how the temperatures of the load-bearing structures develop in fire situation, when there's a sprinkler system present. The aim is to have the possibility to use unprotected steel trusses, beams and columns within certain limits when a specified sprinkler network is installed.
The research was based on experimental fire tests [1,2] carried out in a small building built from steel structures in Finland year 2007. The building was constructed only for this research's purposes. The study consists of two kind of different sprinkler systems. One is a traditional sprinkler system and the other is a hi-fog sprinkler system using a lot less water than the previous one. The temperature inside the building was tried to follow the standard fire curve and the temperatures from the surrounding structures were studied.

1 BACKGROUND

It is very common to have a 1 hour fire resistance requirement to load-bearing structures in typical buildings in Finland and also in other European countries. To fulfil this requirement using steel structures needs normally passive fire protection, e.g. intumescent coating, gypsum or other boards to cover and protect the structure. These are naturally simple ways of achieving the fire resistance, but there are also some problems with these.
The aim of this research was to study whether the cooling effect of normal and also the hi-fog sprinkler systems is enough to ensure the temperatures of steel structures to be so low that there is no need for passive fire protection. It is known that automatic water suppression also keeps the fire local in most cases when functioning properly[4].
The fire protection is always expensive whether it is done by passive or active measures. That is why there's also a financial benefit when either of these can be totally or partly left out. The sprinkler system is more important when talking about protecting the people, which of course is more essential than the building itself. Naturally in some cases the passive protection is more reasonable than using active measures.
When the automatic water suppression is required to the building for common fire safety reasons, the use of it also as structural fire protection can be very cost-effective, still not risking the life safety of the occupants or users of the building. When the fire sprinkler system is designed, installed and maintained properly, the risk that it won't work is very little [4]. As it is known the sprinkler systems are required in certain types of buildings with certain criteria. This differs from country to another, even within EU countries.
In some countries the structural fire resistance can be lowered when the fire sprinklers are present. Almost in every country some other benefits in fire safety design can be gained, e.g.

bigger fire-compartments, compromises in smoke extraction etc. This is also the case in Finland and especially the fire-compartment size is a normal compensation.
The Authorities can then decide whether the water suppression system can also be used to lower e.g. the structural fire resistance requirements. These differences in various countries and different building types can be seen from the next Table taken from the European Sprinkler Organisations's homepages [3]. This is just a clip of the original table, which covers more countries and building types. As can be seen e.g. in Germany the Fire rating can be lowered 60 minutes, which is actually one aim of this study also.

Table 1. Summary of Legislative Incentives for Fire Sprinklers. Part of the original Table [3].

Summary of Legislative Incentives for Fire Sprinklers
Construction Alternatives are in red

	Major airports sprinklered?	Places of assembly	Shopping Centres	Industry	Warehouses
Austria	No			Larger compartments	Depends on height and g goods but generally req sprinklers > 1800m²
Belgium	Yes		>2,000m²		
Czech Republic	No	Exhibition halls with compartment > 5,000m²	>1 000m²	>20m³ of flammable liquids	Postal stores >800m² >80m³ of flammable liquids
Denmark	Yes		>1,000m² multi-floor >2,000m² one floor	>2,000m² high fire load >5 000m² other fire load Can increase compartment from 1 000m² to 10,000m²	>2 000m² high fire loa >5,000m² other fire loa Can increase compartm from 1,000m² to 10,000
Finland	Yes	Unlimited compartment or halve fire rating and 25% smoke extraction	Unlimited compartment or halve fire rating and 25% smoke extraction	Unlimited compartment or halve fire rating and 25% smoke extraction	Unlimited compartme or halve fire rating an 25% smoke extractio
France	No		>3 000m² or with restaurant or >10,000kg paint Can increase storage of dangerous goods from 1,000m² to 2,000m²		>2000m² and less than 6 >5000m² with risk assess and approval from Fire
Germany	Yes	>3,800m²* or >22m high or below ground	>3000m² or underground floors >500m² 60 minutes less fire resistance for walls and ceilings; no need for smoke extraction; can increase travel distance by 30m	fire load >15kWh/m² and >400m² fire load >45kWh/m² and <400m² Width >40m & structure not rated Halve fire service water needs Increase compartment area 3-10 times depending on fire resistance Increase first basement floor from 1,000m² to 2,500m²; lower floors from 500m² to 1,200m² Can increase travel distances by 15m <5m high; 30m <10m high Need less smoke extraction	>1,200m² Storage > 7.5m high fire load >15kWh/m² & >4 fire load >45kWh/m² & <4
Hungary			>9,000m² >13,95m height		Double compartment s

2 TESTING FACILITIES

2.1 Tested building

The fire tests were conducted in Finland in the summer of 2007. A 8mx8mx8m sized steel framed hall was constructed, the sprinkler system was installed to the ceiling and the studied steel trusses, beams and columns and other parts of the building were equipped with temperature detectors. The outer walls were left enough open from the bottom so that there

would be enough oxygen for the fire. In Figures 1 and 2 the basic geometry and the sprinkler locations of the tested system are presented. The outer walls were constructed from sandwich panels and the roof was built from load-bearing corrugated steel sheets with insulations above it. Temperatures were measured also from the corrugated steel sheeting.

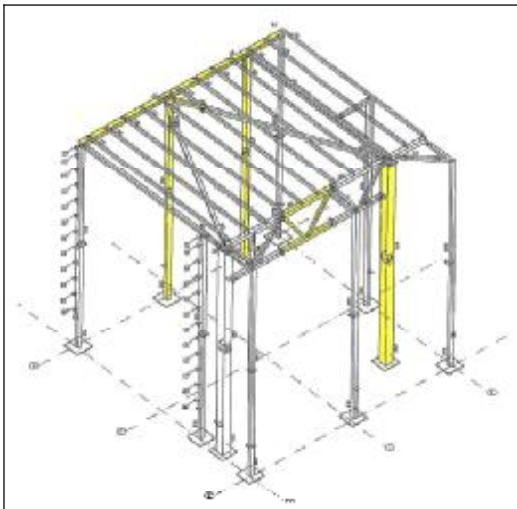

Fig. 1. Skeleton of the structures

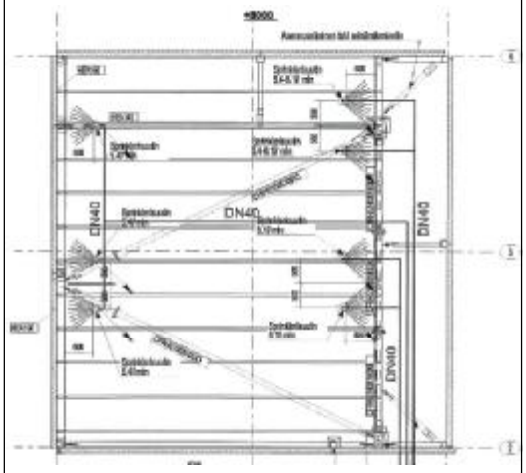

Fig 2. Sprinkler nozzles in one test

2.2 Fire scenario

The system was to be tested against standard ISO-fire. The fire load was produced by heptan-spray burner, which was situated centrally under the studied structures spreading the fire with three nozzles. The aim was to run the test over 1 hour to get the needed data for the product approval of the system.

2.3 Tested structures

The temperatures were measured from tubular steel trusses , beams and columns. Also the temperatures from the connections, bracing and steel sheeting were measured. The height of the steel truss was about 1,5m and it was built from different sized cross-sections. The temperatures were measured from different parts of the truss. The other structures were also selected so that they represented the smaller sized structures normally used, in order to widen the use of the results to bigger sections.

2.4 Fire sprinkler systems

Two kinds of sprinkler systems were used in the tests, a traditional water sprinkler system and hi-fog sprinkler system. The nozzles were installed with 3mx3m distances. The water flow of the normal fire sprinkler system was put to very low level in order to define the minimum water flow to the structures that would be needed for the cooling in this kind of a system.
In the hi-fog system the sprinklers produce water mist that fulfils the space and with that keeps the fire and the structures cooled during the fire. This system has previously mainly

been used in cruise ships, tunnels and e.g. historic buildings [5] and the aim is to begin to use this system also in wider range of buildings.

3. RESULTS

The standard fire exposure was set by using heptan-spray burners underneath the structure system. Temperatures from the installed structures were measured during the test. For the defined set of cross-sections, the temperatures of the steel structures did not raise above critical level in standard fire exposure [1,2].
In figure 3 the temperatures from the steel trusses top chord in one test and in figure 4 the temperatures of the steel sheeting temperatures in another test with hi-fog sprinklers are presented.

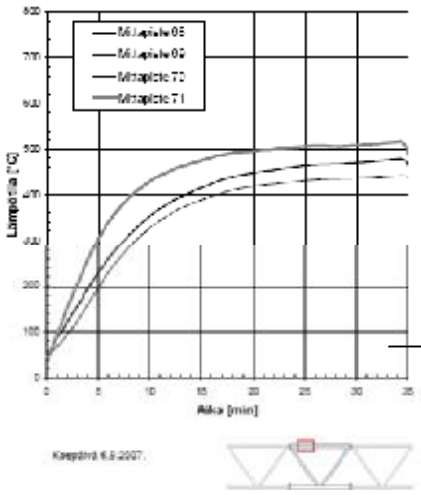

Fig 3. Temperatures of the steel structures during the test.

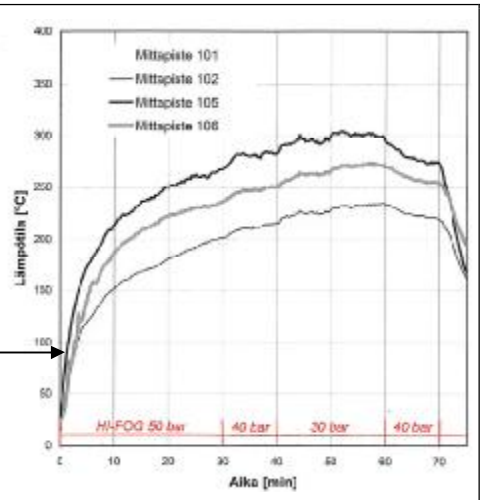

Fig. 4. Temperatures of the steel sheeting during the test.

All in all the temperatures of the structures stayed at adequate level. On the basis of these tests product approvals for 1 hour fire rating were got to the systems. The tests went well and the measurements were carried out successfully.

On the basis of the tests a short design guide for structural design and also for the design of the water sprinkler system was introduced. In these instructions the limitations to the structures, cross-sections, structure dimensions are set. For the water sprinklers the design principles concerning the water flow, number and location of the sprinkler nozzles are instructed.

Some of the tested steel structures and sprinkler system are presented in the next figure 5.

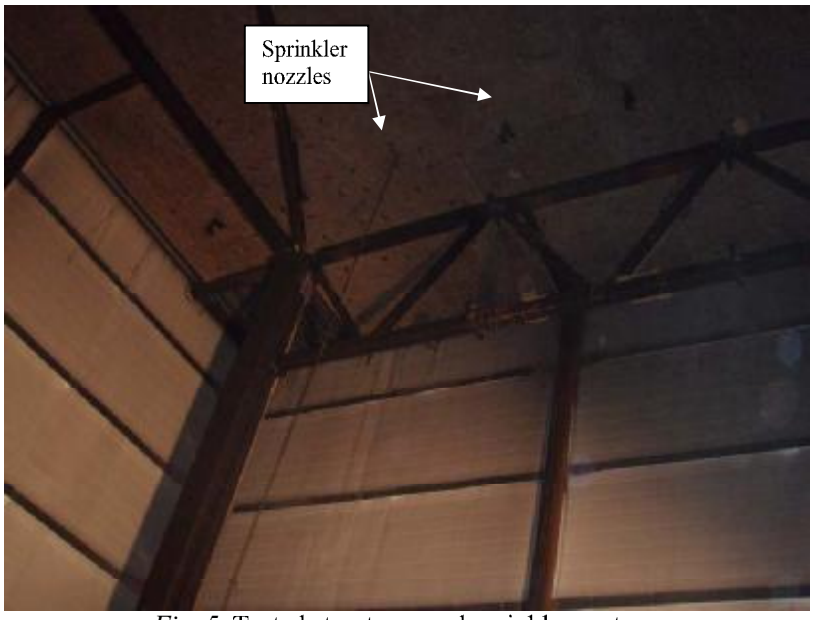

Fig. 5. Tested structures and sprinkler system.

4 SUMMARY AND ACKNOWLEDGMENT

A small experimental study concerning the fire protection of steel structures in standard fire exposure was carried out in Finland. Structural fire protection of steel structures was studied using fire sprinkler systems. Two different sprinkler types were used to study the temperatures in selected steel structures.

The aim was to get fire resistance rating of 1 hour to the system and this was accomplished. The temperatures of the steel structures stayed at very low level so that there is no need for additional fire protection in this kind of case.

As a result the systems got product approvals of 1 hour fire resistance [6]. These systems will be used typically in 1-2 storey building at the moment, but the field of application will be widened in the future.

The writers want to acknowledge the Marioff Corporation, Tampere University of Technology and also Finnish Constructional Steelwork Association for a good co-operation.

REFERENCES

[1] Tampere University of Technology, Fire protection of steel structures with water sprinklers, Report 404/2007/463, Tampere, Finland, 2007

[2] Tampere University of Technology, Fire protection of steel structures with hi-fog sprinklers, Report Palo 1645/2008, Tampere, Finland, 2008

[3] European sprinkler organisation homepage, www.eurosprinkler.org

[4] Hietaniemi, J., Cajot, L.-G., Pierre, M., Fraser-Mitchell, J. Joyeux, D. & Papaioannou, K. Risk-Based Fire Resistance Requirements. Final Report. Luxembourg: *Office for Official Publications of the European Communities 2005.*

[5] Marioff Corporation, www.marioff.com

[6] Finnish Constructional Steelwork Association, FCSA, www.fcsa.fi

FSE ANALYSIS OF A 19th CENTURY CAST-IRON BRIDGE STRUCTURE
A performance based analysis of a solution that combines water suppression and ventilation to avoid passive protection.

Ramón Ugartetxe [a], Fernando Morente [a], Jon Aurtenetxe [a], Christian Pérez [a]
Jesús De la Quintana [b]

[a] Labein-sai. Derio, Spain
[b] Head of Labein-sai. Derio, Spain.

1. INTRODUCTION AND GENERAL APPROACH

A cast-iron massive structure enters Bilbao city centre from one of it's iconic bridges to an underground level underneath an English-style park. This underground space has been silent for decades, but new access demands in the city were asking for the shelter that this unexpected "cast-iron tunnel" was giving them.

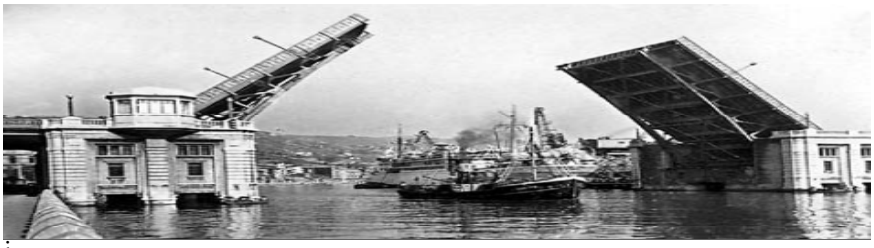

Fig.: Deusto Bridge. Circa 1950

This volume is also giving road path and access to three different buildings, an underground parking, a commercial centre, and the headquarters of an important electrical company. This mean that several hundreds of cars and some small trucks and vans will move in and out through it, and can even collapse it in rush-hours, creating a potentially harmful scenario for people involved there, and for the rest of inhabitants in the surroundings.

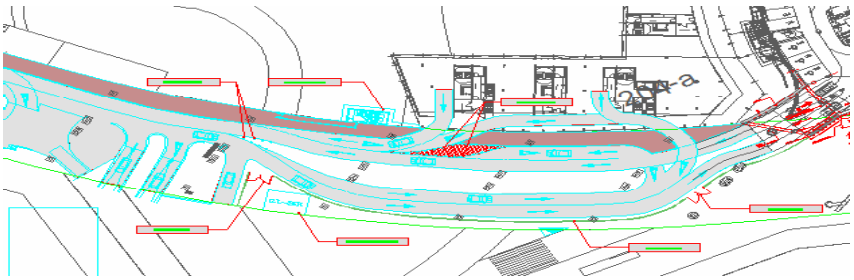

Fig.: General view of the "tunnel" case study.

The mayor problem that arises was that the new function of this structure was exponentially increasing the fire load under it, others than cars, small trucks must be

taken into account reaching a 30Mw value, and thus turning a beautiful bridge into a dangerous tunnel.

Then, last but not least, this nineteenth century cast-iron riveted structure, was in the way to disappear under a thick sturdy layer of intumescent protection required for a one hundred and twenty minutes resistance to ISO fire according to regulatory prescriptions.

Fig.: Structure details.

Bilbao town council architects implore heaven (and technicians) for an alternative safe solution which might fulfil regulatory requirements without destroying structural harmony.

Labein was asked to do a complete "research-meets-practice" work identifying, defining and validating an integrated solution based on a combined fire suppression and ventilation systems. A zone-detection-activation-sprinkler system was proposed together with mechanical ventilation for smoke evacuation.

2. FIRE SCENARIOS

Firstly, a risk analysis of the whole infrastructure was made, in which five fire design scenarios were identified as the most extremely dangerous because of their high impact on the structural stability and people's safety.

It has to be commented that the objective for this fire safety engineering analysis, was holistic in the sense that not only the structural stability has to be assessed, but the final safety of people attending to tenability conditions during escape, and last but not least, safe operation of Fire Brigades were key aspects to be demonstrated.

So fires that block the openings of the tunnel, or the escape routes of people were considered, together with critical fires attending to their position regarding structural elements.

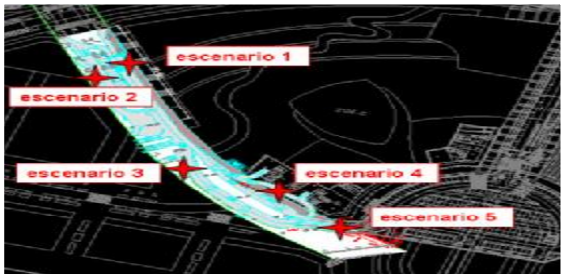

Fig.: Fire scenarios

2.1.Fire load and R.H.R. curve

A medium sized van loaded with wood pallets has been considered as the most critical fire load expected, experimental data was obtained to define R.H.R.curve

Fig.: fire load

The R.H.R. (Rate of Heat Release) curve represents the evolution of the fire, for this case the addition of the previous two loads, give the R.H.R. that is shown in the next figure.

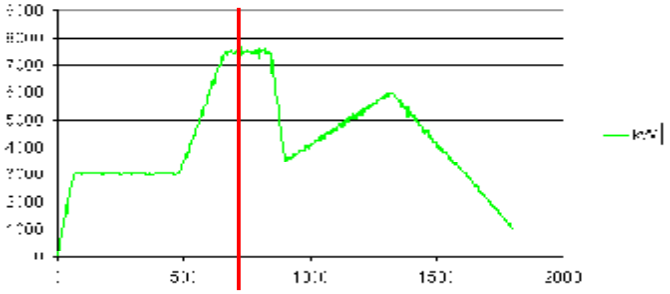

Fig.: Rate of heat release curve.

3. ALTERNATIVE SOLUTION

The solution proposed for this case was to turn from a passive protection to an active one including detection, ventilation and fire suppression through sprinklers. Thus early detection and activation of sprinklers will drastically limit the fire to an extent compatible with the structure performance. A performance based analysis is needed to demonstrate that an equal safety level is reached with this solution.

4. CFD ANALYSIS

A numerical model of the case study has been prepared in order to calculate the evolution of the fire in the defined scenarios, considering also the interaction of the active systems that need to be assessed.

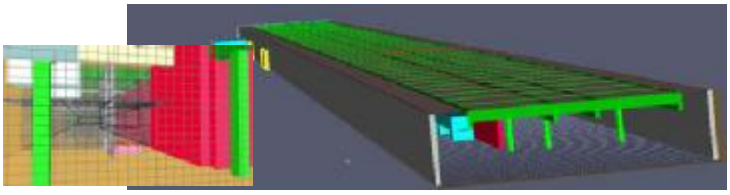

Fig.: Numerical model of the “tunnel”

Thermal and non-thermal effects are obtained. The heat flux over the structure is the key data to establish the thermal actions in the structural analysis and from them to calculate the thermal and thus the mechanical response. Other effects are the visibility, and toxicity of the smoke, so the smoke movement is analysed in detail.

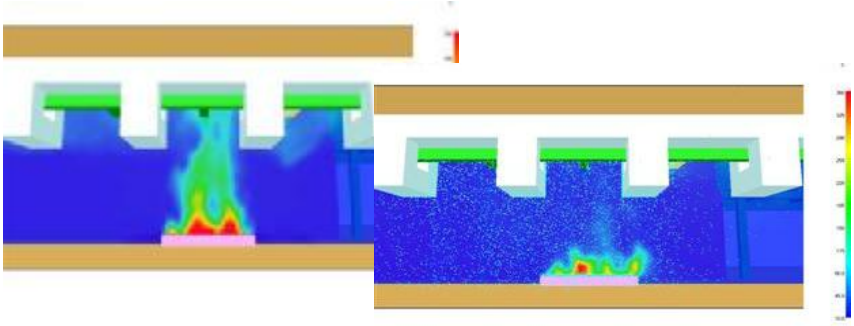

Fig.: Analysis of the fire suppression system performance

5. ADVANCED EVACUATION ANALYSIS

This kind of analysis allows the designer to consider how the environmental conditions modified by fire are endangering the escape of people, and how their behaviour is also being modified towards the objective of a safe escape.

A population design is considered including physical and psychological characteristics, and the time changing conditions are inputs from the CFD analysis including both thermal and non-thermal effects.

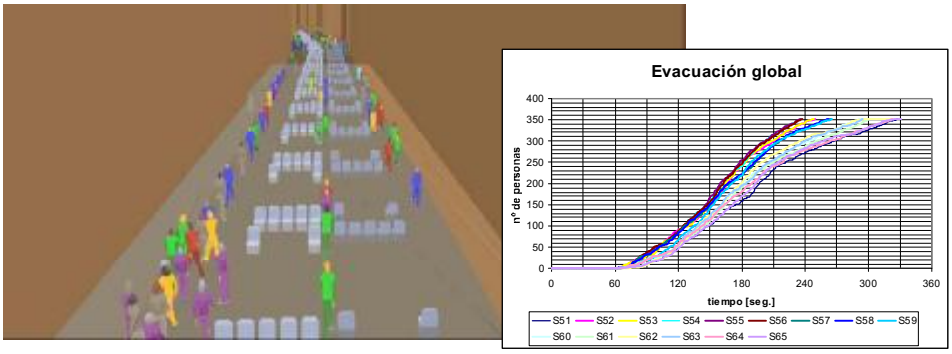

Fig.: Evacuation model and results: Persons / time

6. STRUCTURAL ANALYSIS

The structural analysis started with the construction of the structural global model, that include the search of the original drawings, dated 1930, and several topographic studies, and material analysis to determine the state and properties of the iron, elements, and rivets.

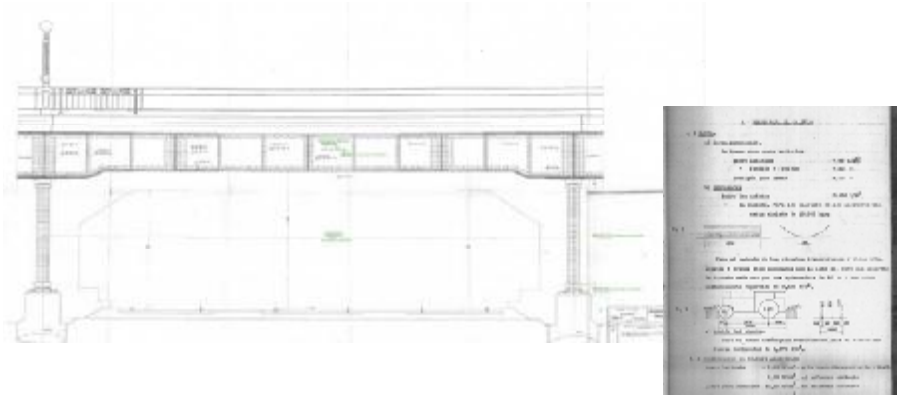

Fig.: Original drawings and calculations. Dated 1930

A global structural model was needed to take the maximum advantage of the interaction of all elements in a combined working performance, as it happens in reality.

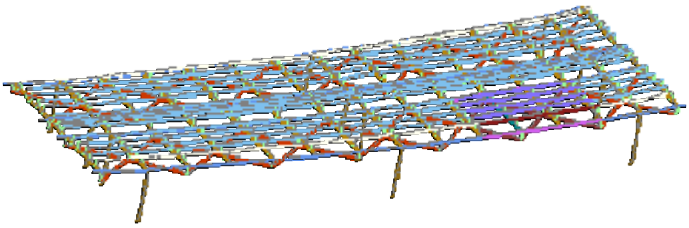

Fig.: Numerical model F.E.M. (beam elements)

Natural Fire Safety Concept was considered according to fire scenarios, but also ISO fire analysis was performed to determine failure modes.

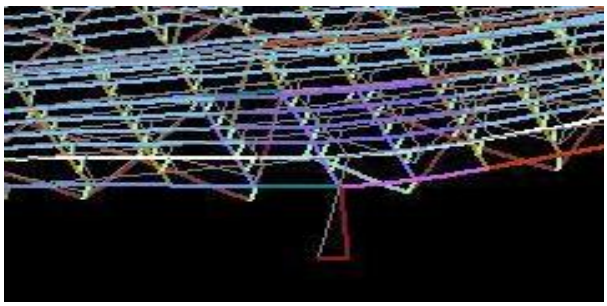

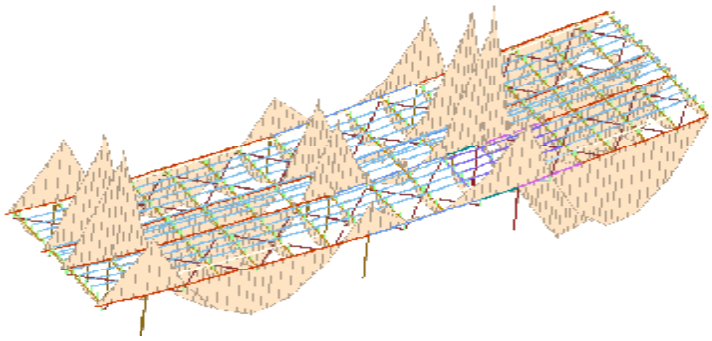

Fig.: Structural results: Thermal response and mechanical response.

7. CONCLUSION

No passive protection of the structure was required. A performance based analysis of an alternative solution has allowed to assess structural behaviour and people safety demonstrating that heritage can survive to fire without jeopardizing its beauty and splendour.

Acknowledgements:

Labein wants to thank Bilbao Ria 2000, for entrusting us in this interesting work with the aim of a safer environment for people using the most advanced technologies for a performance based design .

EXPERIMENTAL RESEARCH ON THE FIRE BEHAVIOUR OF STEEL COLUMNS EMBEDDED ON WALLS

António J. P. Moura Correia[a], João Paulo C. Rodrigues[b] & Valdir Pignatta e Silva[c]

[a]Faculty of Sciences and Technology of University of Coimbra & Superior School of Technology and Management of Oliveira of the Hospital. Portugal.
[b]Faculty of Sciences and Technology of University of Coimbra. Portugal.
[c]Polytechnic School of University of S. Paulo, Brazil.

INTRODUCTION

The fire resistance of a steel column is strongly influenced by the conditions in which it is inserted in the building. Beyond other parameters the contact of the column with the building walls has a great influence on its behaviour in fire. The walls, on one hand, have a favourable influence on the fire resistance of the steel columns because they protect a large part of its lateral surface from heating, but on the other hand, they will have an unfavourable influence because they lead to differential heating of the cross-section. The design methods considered in Eurocode 3 part 1.2 do not take into account this fact and the fire resistance is determined as if the heating was uniform [1].

In this paper, the results of fire resistance tests in steel columns embedded on walls, carried out at the Laboratory of Testing Materials and Structures of the University of Coimbra, are presented. The evolution of temperatures registered in the experimental models are compared with the ones obtained in numerical simulations performed with the FEM program SUPERTEMPCALC (STC), developed by Y. Anderberg of Fire Safety Design, Lund, Sweden [2]. SUPERTEMPCALC is a thermal finite element program that solves two-dimensional, non-linear, transient, heat transfer differential equation, incorporating thermal properties which vary with temperature. This program allows the use of rectangular or triangular finite elements, in cylindrical or rectangular co-ordinates. Heat transfer by convection and radiation at the boundaries can be modelled as a function of time.

1. EXPERIMENTAL PROGRAM

The aim of this study was to analyse the thermal behaviour of steel columns embedded in walls. Fire resistance tests with two different column cross-sections, two orientations of the inertia axis in relation to the fire and two thicknesses of the building walls, were tested [3].

The columns had cross-sections of HEA160 and HEA200, steel class S355 and the walls different thicknesses and were made of bricks (fig. 3). The bricks were placed by ordinary cement mortar.

The columns in the test were placed on the center of a 3D restraining frame (fig. 2 a). This frame was composed by columns HEB200 of 3m high and beams HEB200 of 6m spam, steel class S355. Two brick walls were then built, one of each side of the column (fig. 2b).

The specimens were instrumented with thermocouples type k (cromo-alumel) in different positions of the cross-section of the columns and on the walls (fig.1).

The thermal action was applied only on one side of the element, in such a way as to permit the analysis of the thermal gradient produced through the wall and across the cross section of the column. The evolution of temperatures in the furnace followed the ISO 834 standard fire curve. The temperatures inside the furnace were measured by shielded probe thermocouples type K in the first 4 four tests (cases 1 to 4 in fig. 3) and were later exchanged for plate thermometers in the last 4 tests (cases 5 to 8 in fig. 3). This change was due to the fact that a small delay in the heating of the furnace was observed in the first 4 tests and so the decision to change the thermocouples that controlled the furnace had to be taken.

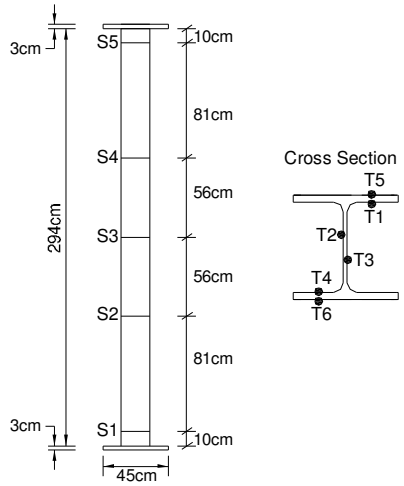

Figure 1 – Specimen and position of thermocouples

a) **b)** **c)**

Figure 2 – a) Construction of the test model, b) Column embedded on the wall, c) Instrumentation of the specimen.

2. NUMERICAL MODELLING

The computational modelling was performed using the computer code SUPERTEMPCALC (STC) – Temperature Calculation and Design v.5, developed by ANDERBERG [2] for thermal two-dimensional analysis of sections exposed to heat of any elements.

The thermal properties of the materials, adopted in this work for the numerical analysis, were the ones presented in Eurocode 3 [1] for steel and Eurocode 2 [4] for concrete parts 1.2. For the mortar covering the bricks the same properties for the concrete recommended by the Eurocode 2 were adopted.

The thermal properties adopted for the masonry were the same as the values adopted in the computer program Ozone developed in the University of Liège, which are: thermal conductivity = 0,7 W/m°C, specific heat = 840 J/kg°C; specific weight = 1600 kg/m3; specific heat x specific mass = 1344000 J/m3°C.

The emissivity was $\varepsilon = 0.7$, for the steel profile, as well as for the masonry and the mortar.

The coefficient of heat transmission by convection in the face exposed to the fire was $\alpha_c = 25$ W/m2°C. For the non-exposed face, the values recommended by Eurocode 1 [5] were used: $\alpha c = 4$ W/m2°C and $\varepsilon = 0.7$.

The models were meshed in finite rectangular elements of 4 mm or 5 mm of side. The computer code STC can draw isothermals, temperature fields, for each instant of time, and, punctually, give the value of the temperature in function of the time.

The cases studied are summarized in figure 3.

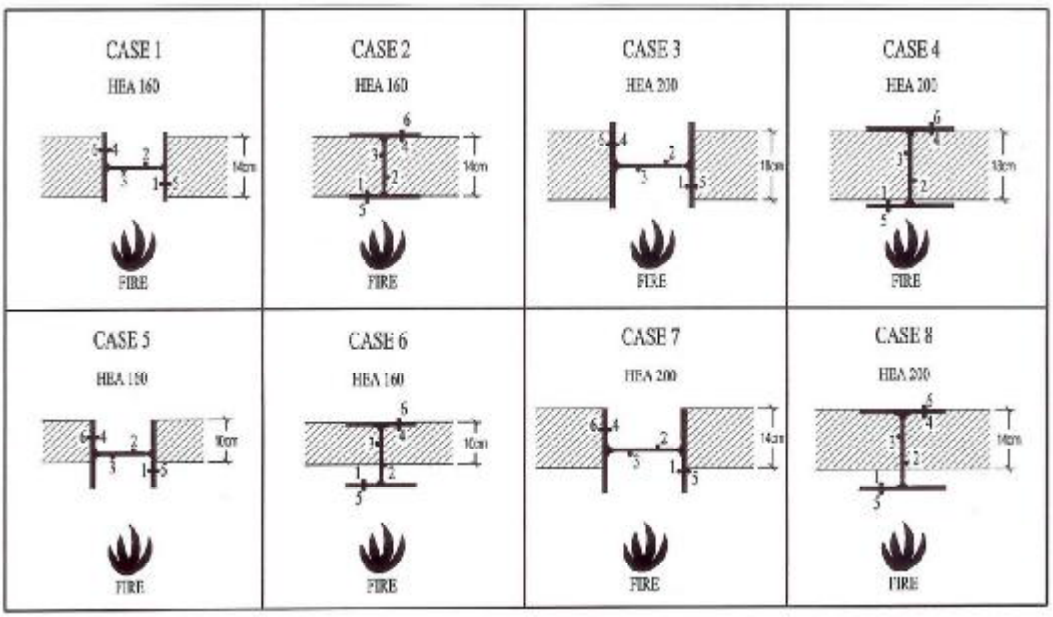

Figure 3 – Cases studied

3. COMPARISONS EXPERIMENTAL vs NUMERICAL ANALYSIS

3.1. Furnace temperatures

The temperatures inside the furnace were very uniform in both series of tests (cases 1 to 4 and 5 to 8) however a small delay to the ISO 834 fire curve is observed in the first series of four tests (cases 1 to 4) (fig. 4). As already explained, this delay is maybe related to the type of thermocouples used in the furnace on the first series of tests.

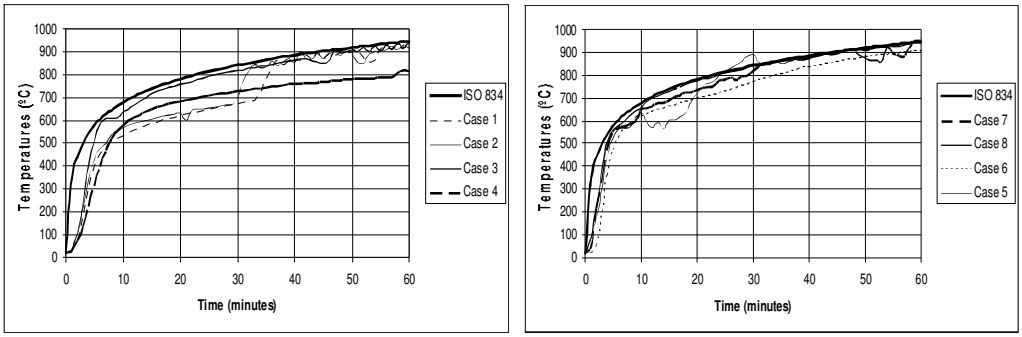

a) b)

Figure 4 – Furnace curves a) cases 1 to 4 b) cases 5 to 8

3.2. Thermal gradients in the cross-sections

Figure 5 shows the isothermals on the cross-section for cases 6 and 7. In case 6 the wall was 10cm thick and in case 7 was 14cm thick. In the figure, one can observe higher thermal gradients in the cross-section for case 6 than case 7. The mechanical resistance of the steel profile is maybe more affected in case 7.

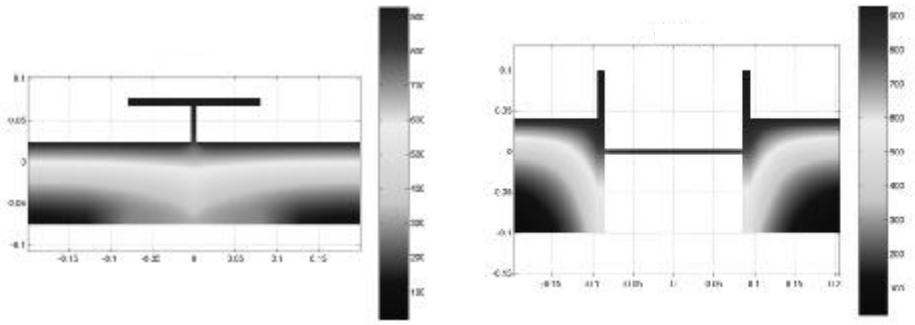

a) b)

Figure 5 – Isothermals in the cross-section a) case 6 b) case 7

3.3. Evolution of temperatures in the middle height section of the steel columns

The temperatures in the experimental tests were measured in 6 points on 5 sections of the steel column (fig. 1). The temperatures in the middle height section of the columns were compared with the ones obtained in numerical simulations for 60min (figs. 6 to 9).

In the case of the web parallel to the wall surface, the temperature in the flange not exposed to the fire (thermocouple 6), is smaller in the case of the walls of smaller thicknesses (figs. 6a and 8a). For the HEA160 the difference is nearly 400ºC for the ST calculations and 300ºC for the experimental tests (fig. 6a) while for the HEA200 the difference is nearly 300ºC for the ST calculations and 150ºC for the experimental tests (fig. 8a).

In the face of the web exposed to the fire, the temperatures are higher for the thin than for the thick walls (thermocouple 3), presenting a difference of almost 5000ºC in the ST simulations and 200ºC in the experimental tests (fig. 8b).

In the case of the web perpendicular to the wall surface, the temperature in the exposed flange (thermocouple 5) is higher in the case of the thin wall than in the thicker wall (figs. 7 a and 9a). For HEA160 the difference is approximately 100ºC both in the ST simulations and in the experimental tests (fig. 7a). For HEA200 the difference is 300ºC in both analyses (fig. 9a).

Curiously in the flange not exposed the temperatures are higher for the thick wall (thermocouple 6). For HEA160 the difference is 200ºC in the experimental test and 150ºC in the ST simulation (fig. 7b) and for HEA200 the difference is almost 200ºC in both analyses (fig. 9b).

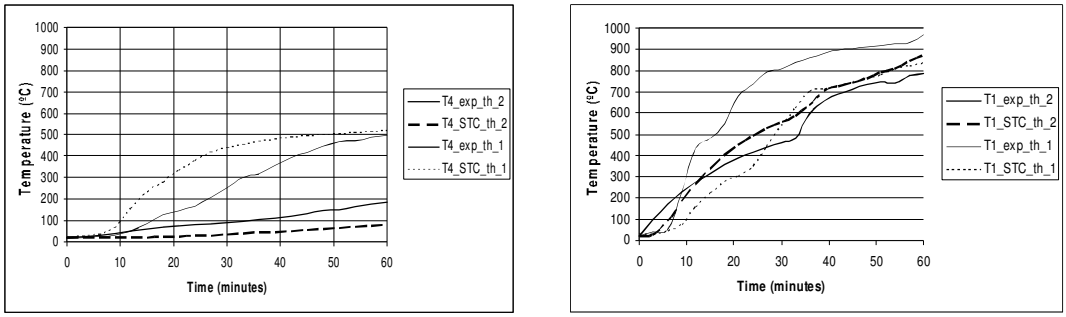

(a) (b)

Figure 6– Temperatures vs time for HEA160 with the web parallel to the wall (cases 1 and 5); a) thermocouple T4 ; b) thermocouple T1

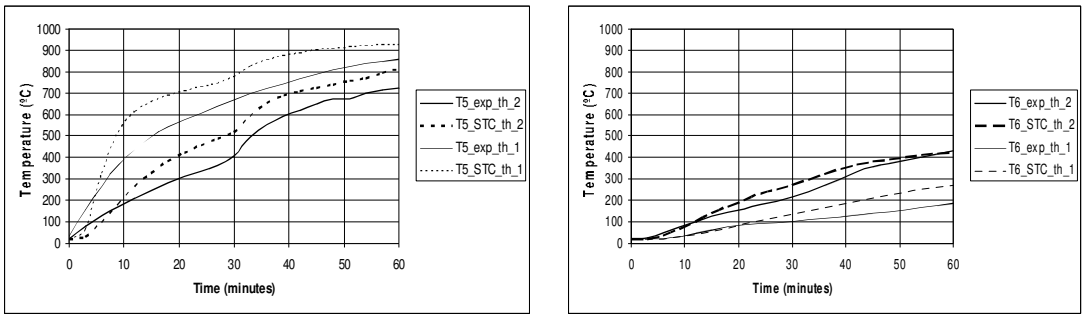

(a) (b)

Figure 7 – Temperatures vs time for HEA 160 with the web perpendicular to the wall (cases 2 and 6); a) thermocouple T5 ; b) thermocouple T6

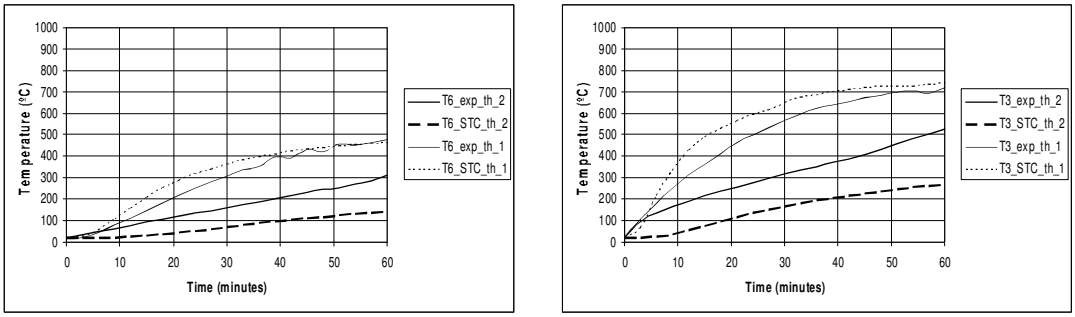

(a) (b)

Figure 8 – Temperatures vs time for HEA 200 with the web parallel to the wall (cases 3 and 7); a) thermocouple T6 ; b) thermocouple T3

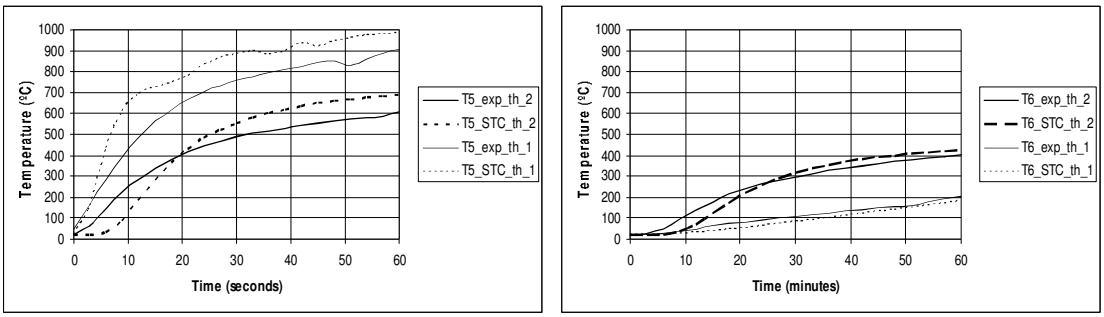

(a) (b)

Figure 9 – Temperatures vs time for HEA 200 with the web perpendicular do the wall (cases 4 and 8); a) thermocouple T5 ; b) thermocouple T6

4. CONCLUSIONS

For cases with web parallel to the wall surface it was concluded that the thicker wall plays a very important role in reducing the temperatures on the unexposed half of the flange and also in the web.

While for cases with the web perpendicular to the wall surface a quite interesting result was observed, in the unexposed face of the flange the temperatures were slight higher on the thicker wall. On the contrary on the exposed flange the temperatures were much higher for the thinner walls.

AKNOWLEDGMENTS

The authors gratefully acknowledge to CBCA, Brazil, FCT - MCTES, PRECERAM S.A., METALOCARDOSO S.A. and A. COSTA CABRAL S.A., Portugal, for their support.

REFERENCES

[1.] Eurocode 3, *EN 1993-1-2, Design of Steel Structures, Part 1.2: General Rules - Structural Fire Design*, European Community (EC), Brussels, Belgium, 2004.

[2.] Anderberg, Y.; *TCD 5.0 - User's Manual*, Fire Safety Design, Lund, 1997.

[3.] Correia, A. M, Rodrigues, J. P. C, Silva, V. P.; *Studies on the fire behaviour of steel columns embedded on walls*, 11th International Conference on Fire Science and Engineering - Interflam, London. 2007.

[4.] Eurocode 2, *EN 1992-1-2, Design of Concrete Structures, Part 1.2: General Rules - Structural Fire Design*, European Community (EC), Brussels, Belgium, 2004.

[5.] Eurocode 1, *EN 1991-1-2, Basis of Design and Actions on Structures, Part 1-2: Actions on Structures - Actions on Structures Exposed to Fire*, European Community (EC), Brussels, Belgium, 2002.

[6.] Silva, V. P., Correia, A. M, Rodrigues, J. P. C., *Simulation on fire behaviour of steel columns embedded on walls*, XXXIII Jornadas Sudamericanas de Ingenieria Estructural, Maio 2008, Santiago, Chile.

NUMERICAL SIMULATION OF STEEL COLUMNS IN FIRE

Luís T. Carvalho [a], João Paulo C. Rodrigues [a], Miguel C. Gonçalves [b] & A. Moura Correia [a]

[a] Faculty of Sciences and Technology, University of Coimbra, Portugal

[b] University of Porto, Faculty of Engineering, Porto, Portugal

INTRODUCTION

The fire resistance of steel columns has been studied for years. A lot of numerical and experimental tests have been performed on single steel columns without thermal restraint. However this does not represent the real behaviour of a steel column in fire. Fire resistance is influenced by thermal restraint forces that are developed in a column when inserted in a building .

In order to clarify the phenomena an experimental program on the fire resistance of steel columns with restrained thermal elongation was carried out in the University of Coimbra. The experimental tests were simulated using the finite element program SAFIR developed by Jean Marc-Franssen, in the University of Liège, in Belgium.

The results of several experimental tests are compared with numerical simulations and several conclusions on the behaviour of steel columns in fire are outlined [1].

1. BASES OF CALCULATION OF SAFIR

The design of steel columns in fire can be assessed by means of experimental tests, simplified and advanced calculation methods. The first two are normally devoted to single elements while the third to the entire structure. There are already several advanced calculation models available to calculate structures in fire. SAFIR is one of those programs that perform thermal and the mechanical non-linear analysis of building elements in fire.

The process of calculation of SAFIR consists of two steps, a thermal and a structural analysis. The thermal analysis allows readings of the distribution of temperature in the section exposed to the fire. The mechanical analysis determines displacements and stresses (axial forces and bending moments) in the section. For each element can be defined a different material since they are known its thermal and mechanical properties at high temperatures.

1.1 The thermal analysis

The heat transfer by conduction is described in SAFIR by the Fourier equation that is calculated according to the standard finite element [2]. In this calculation procedure the following hypotheses are considered:

- The materials are isotropic, not submitted to movements, not compressible and have no mechanical dissipation;
- No contact thermal resistance exists in the interface between adjacent materials

The local equation describing conduction in solid materials follows the equation:

$$K\left(\frac{\partial^2 T}{\partial x^2}+\frac{\partial^2 T}{\partial y^2}+\frac{\partial^2 T}{\partial z^2}\right)+Q-C\rho\frac{\partial T}{\partial t}=0 \tag{1}$$

where:

K = thermal conductivity, W/m.K
T = temperature, K
x, y, z = coordinates, m
Q = internally generated heat, W/m^3
C = specific heat, J/kg.K
ρ = specific mass density, kg/m^3
t =time, s

The classical shape functions, N, are used in the formulation.

If in equation (1) the temperature is replaced by the approximation $T = N_i T$ and then multiplied by a weighting function and integrated on the volume of the element the equation becomes:

$$\int_{element} k\{\nabla N_i\}\langle\nabla N_j\rangle dv T_i + \int_{element} C\rho N_i N_j dv\dot{T}_i + \int_{element} Q N_j dv = \int_{boundary} N_j q_n dS \tag{2}$$

Where ∇ means $\langle\partial/\partial_x;\partial/\partial_y;\partial/\partial_z\rangle$ and q_n is the heat flux at the boundary of the element.

Finally, when the contributions from all the elements are summed, the matrix (equation 3) is obtained, describing the equilibrium of heat fluxes in the structure at any given instant of time:

$$[K]\{T\}+[C]\{\dot{T}\}=\{g\} \tag{3}$$

where:

$[K]$ = matrix of conductivity
$[C]$ = matrix of capacity
$\{\dot{T}\}$ = vector of the temperatures at nodes
$\{g\}$ = vector of heat exchanges at boundaries

The fact that the thermal properties are temperature dependent is taken into account in equation 3 that expresses the thermal equilibrium at a given time.

1.2 The mechanical analysis

The bases of mechanical analysis of structures that experience large displacements is the incremental form of the principal of virtual work. If a total co-rotational configuration is used it is given by equation 4 in which the forces applied on the surface of the structure have not been considered:

$$\int_V \left(\overline{D}_{ijkl}d\overline{E}_{kl}\delta\overline{E}_{ij}+S_{ij}\delta d\overline{E}_{ij}\right)dV=\int_V\left(d\bar{f}_i\delta\bar{u}_i+\bar{f}_i\delta d\bar{u}_i\right)dV \tag{4}$$

where:

$V = \overline{V}$ = the undeformed volume of the element

S_{ij} = tensor of the second Pialo-Kirchoff stress

$\overline{D}_{ijkl} = D_{ijkl}$ = tensor defining the incremental constitutive law of the material

$\delta\overline{E}_{ij}$ = tensor of the Green virtual field of displacement

$\bar{f}_i$ = volume forces

$\delta\bar{u}_i$ = virtual field of displacements from the deformed position of the element

In order to solve this equation in a displacement based finite element formulation we obtain the matrix equation that governs the iteration from one position to the next position of equilibrium:

$$\int_v B^T DBdVdp + \int_v S^T \delta ledVdp = (K_u + K_s)dp = f^{ext} - f^{\text{int}} \tag{5}$$

where:

B = matrix that contains not only spatial derivatives of the shape functions but also the nodal displacements

K_u = comprises the linear elastic and the geometric stiffness matrices

K_s = is the stress generated stiffness matrix

f^{ext} = nodal forces energetically equivalent to the applied forces

f^{int} = nodal forces obtained from integration of the internal stresses

2. EXPERIMENTAL TESTS

In the experimental tests, a new set-up for fire resistance of columns with restrained thermal elongation was developed and used by the Faculty of Sciences and Technology of University of Coimbra (fig. 1).

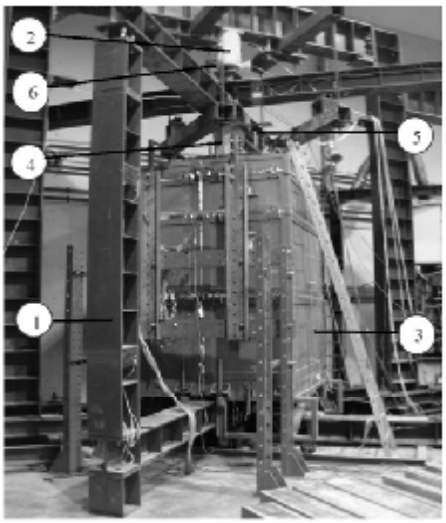

Figure 1. Test set-up for fire resistance tests on building columns

This system comprises a restraining frame of variable stiffness (1) with the function of simulating the stiffness of the surrounding structure to the column in fire.

The columns were subjected to a constant compressive load of 70% of the design value of buckling resistance of the column at room temperature. This load was controlled by a load cell of 1MN located on the head of the hydraulic jack (6). This load simulated the serviceability load of the column when part of a real structure. The load was applied by the hydraulic jack (2) controlled by a servo hydraulic system.

The thermal action was applied by a modular electric furnace (3) that could closely follow the ISO 834 fire curve.

The restraining forces generated in the column due to heating were measured by a load cell of 3 MN located into a steel piston (4). This piston was placed between the testing column and the restraining frame (1).

The axial displacements and rotations on the top and base of the column were also measured by displacement transducers (5) orthogonally arranged in three different points, forming a deformation plane.

In the experimental programme tests were carried out on steel and composite steel and concrete columns with cross-sections of HEA160 and HEA200 with stiffness ratios of 3, 13, 39, 68 kN/mm.

3. NUMERICAL SIMULATIONS

The conditions of the experimental tests were reproduced in SAFIR as most rigorous as possible. The 3m column tested was discretized in 14 beam elements with variable lengths, between 100 mm and 280 mm. In the upper part of the column a piston was placed to measure the restraining forces simulated by a solid cylinder of steel measuring 565 mm in length and 300mm in diameter.

The beams and columns of the restraining frame HEB300 that were used to simulate the stiffness of the surrounding structure of the column, were discretized in 60 beam elements with lengths that varied between 375 and 0935mm.

The temperatures considered in the numeric simulations were the ones registered in the steel of the columns in the experimental tests, although the furnace temperature followed the curve ISO 834. In the cross-section it was considered a uniform distribution of temperatures, since the gradient of temperatures for these sections was very small.

The applied axial loads to the columns were the ones in table 1.

Table 1 – Initial loads

HEA 160	HEA 200
640 kN	1025 kN

The mechanical and thermal properties of the materials are the ones presented in EC1 and EC3 parts 1.2.

Comparison of results

Figure 2 presents the evolution of the restraining forces related to the initial load in function of the mean temperature of the steel of the column. In this figure it can be observed that some difference of values exists, between the experimental tests and the numeric simulations, although the global development of the curves is similar.

In a global analysis, it can be observed that the HEA 200 section suffers a smaller increment of the restraining forces in relation to the HEA 160 section. However the critical temperature in both sections is nearly the same in the tests and the numerical simulations, around 400ºC.

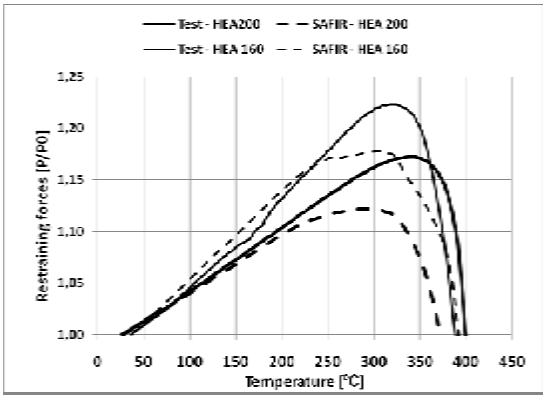

Figure 2 – Restraining forces in function of the mean temperature of the steel

Figure 3 presents the increment of vertical displacements of the columns in function of the mean temperature of the columns.

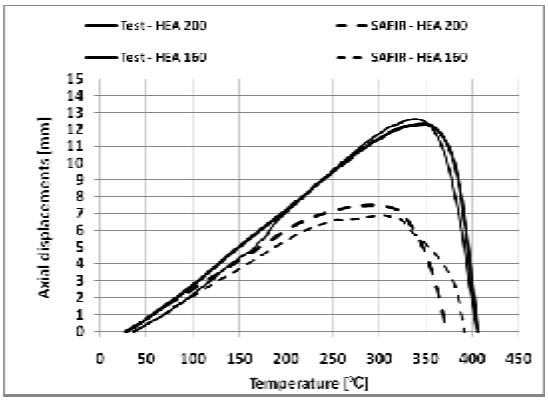

Figure 3 – Axial displacements in function of the mean temperature of the steel

In figure 3 some discrepancy can be observed between the results of the numerical simulations and the results of the experimental tests, although the results of the simulations are very close to each other as well as the results of the tests. For the case of the HEA 160 section, the maximum axial displacement was of 12.63 mm in the tests and 6.87 mm in the numerical simulations. For the case of the HEA 200 section, the maximum axial displacements were 12.35 mm for the test and 7.52 mm for the numerical simulation. A difference in average of 5.30 mm between the numerical simulations and the experimental tests is observed.

The rotations in the top of the column between the tests and the numerical simulations were also compared. In figure 4 the development of the rotations is presented in function of the mean temperature of the steel.

In figure 4 it can be verified that the rotations suffered similar developments in the tests and in the numerical simulations, with values of order of greatness slightly different, mainly in later phases of the tests. Values obtained in tests were of maximum rotations of 117 x 10-5 rad for the HEA160 sections and 66 x 10-5 for the HEA 200 sections. In the numerical simulations, the maximum rotation was of 16 x 10-5 rad for the HEA160 sections and 5 x 10-5 rad for the HEA 200 sections.

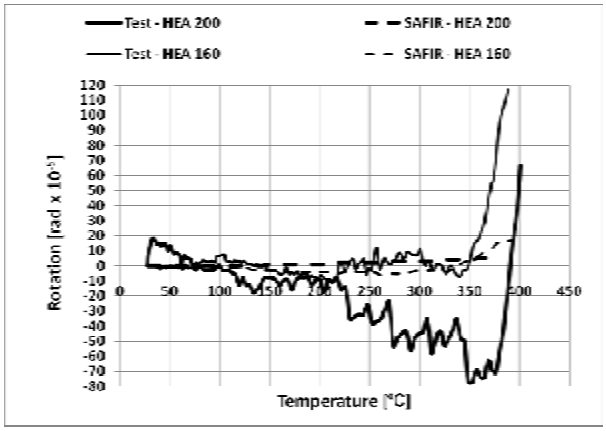

Figure 4 – Rotations in the top of the column in function of the mean temperature of the steel

The values obtained for the rotations of the two cross-sections demonstrate that the superior central node has smaller rotational stiffness in the tests than in the numerical simulation.

4. CONCLUSIONS

The numerical simulations using the program SAFIR described the experimental tests quite well. The differences observed in the restraining forces and in the axial displacements possibly results from the model used and the assumptions made in the numerical simulations for the real test conditions. Some of the differences could be due to the fact that the model cannot correctly foresee the axial and rotational stiffness of the ends of the column.

To sum up, it should be highlighted that in these experiments, there were a large number of factors that could disturb the results. The difference of results obtained between the numeric simulations and the experimental tests can be more or less significant. Factors such as the deviations of straightness of the elements and measurement errors of the sensors are not possible to simulate numerically.

REFERENCES

[1] Carvalho, M. C., *Numerical modelling of steel columns in fire*, MSc Thesis, Faculty of Sciences and Technology of University of Coimbra, 2008.
[2] Franssen, J.-M.; *SAFIR: A thermal/structural program for modelling structures under Fire*, Engineering Journal, third quarter 2005, pp 143-158.
[3] EN 1992-1-2, *"Eurocode 2: Design of Concrete Structures – Part1-2: General Rules - Structural Fire Design"*, European Committee for Standardization, English version, Brussels, Belgium, December 2004.

UNPROTECTED STEEL IN MULTI-STOREY CAR PARKS

15 min Fire Resistance of Unprotected Steel and Composite Members in a Multi-Storey Car Park System

Prof. Peter Schaumann, Thomas Kirsch

Leibniz University Hannover, Institute for Steel Construction, Hannover, Germany

INTRODUCTION

Visible steel structures are aesthetically appealing and cost effective. These advantages can often not be used because steel constructions must be protected for reasons of the structural fire safety. Due to numerous examinations no fire resistance of the support structure is required in Germany for open car parks. For the reason of high ventilation and low fire load densities even the low fire resistance of unprotected steel is adequate.

Fig. 1: Open multi-storey car park (©GOLDBECK)

Thus, unprotected steel is used by a number of providers of multi-storey car parks in Germany during the last decade (Fig. 1). In some European countries, for example the Czech Republic, the fire resistance level R15 for open car parks is required. The objective of the investigation presented in this paper is to check whether the steel or the composite construction fulfils this requirement. For that purpose the authors calculated the fire resistance time of several steel columns and composite beams applying different structural fire design methods according to the Eurocodes [1, 2, 3].

1 FIRE RESISTANCE REQUIREMENTS IN EUROPEAN OPEN CAR PARKS

A survey of the fire resistance requirements in open car parks in Europe is provided in [4]. It becomes obvious that there is a wide scatter of fire resistance times required in different countries. For example in France there is no differentiation made between open and closed car parks or between car parks above or below ground. So the required fire resistance class is R90 in general. If advanced performance based design methods are applied the requirements to steel members may be reduced. In Finland R60 is required. Other countries for example Great Britain and the Czech Republic accept a shorter fire resistance time of 15 min (R15) for car parks above ground with sufficient ventilation openings (cf. Table G1, [5]).

The use of unprotected steel columns and composite beams in German open car parks is applicable because the building regulations do not require any fire resistance. These boundary conditions have been the reason that in Germany the steel/composite construction has become the standard construction method for open car parks. The company GOLDBECK provided the structural data of its system GOBACAR for the investigations dealt with in this paper. These constructions are designed for room temperature conditions according to the European steel

and composite design codes. The question was whether these unprotected steel members are able to withstand ISO standard fire exposure for short duration of 15 min.

2 CALCULATION METHODS

2.1 Simple Calculation Method

According to the Eurocodes there are two possible simplified assessment methods to calculate the fire resistance of steel and composite members. The first method is based on the critical temperature. The second method bases on the load bearing capacity at elevated temperatures. Due to possible stability problems especially for columns the second method was used for this investigation. For the steel columns the method of EC3 part 4.2.3.5 [2] and for the composite beams the method of EC4 annex E [3] was used, respectively.

The temperature of the members was calculated by a formula of Eurocode 3 part 4.2.5.1 [2] using heat transfer conditions according to EC1 part 3.1 [1]. As some input parameters are temperature dependent, the calculation has to be carried out incrementally.

Schaumann developed an approximation that allows an explicit algebraic formulation of the heating curves. These formulae are very helpful because they decrease the computing time compared to the incremental method. The limitation of the area of validity has to be considered (cf. Table 1).

Table 1: Approximation of temperature increase in an unprotected steel section

$\theta_{a,t} = \frac{c_1 \cdot c_2 + c_3 \cdot t^{c_4}}{c_2 + t^{c_4}}$		
$c_1 = \theta_0 = 20°C$	$c_3 = \frac{9875}{0.486 + 1.89 \cdot \ln\left(k_{sh} \frac{A_m}{V}\right)}$	
$c_2 = 11890 \cdot \left(k_{sh} \frac{A_m}{V}\right)^{-1.12}$	$c_4 = 1.253 + 0.071 \cdot \ln\left(k_{sh} \frac{A_m}{V}\right)$	
$\left(A_m/V\right)$ [m^{-1}]	Area exposed to fire divided by volume	Min: 25 m^{-1} Max: 300 m^{-1}
t [min]	Time	Max: 30 min
$\Theta_{a,t}$ [°C]	Steel temperature	Max: 700°C

2.2 Advanced Calculation Method

The more sophisticated and presumably more exact way to achieve the fire resistance time for steel and composite members is the advanced calculation method. At the Institute for Steel Construction the software BoFire is used for this task in most cases. BoFire is a finite-element software based on work done by Schaumann [6] in 1984. It allows simulating the load bearing behaviour of two dimensional bars and frames of steel, concrete and composite constructions. Therefore BoFire is a "Level-3"-method concerning EC3 [2] and EC4 [3]. In 2001 the software was modified by Upmeyer [7] to implement actual material properties concerning the Eurocodes and to give a possibility to use design fires instead of the ISO standard fire.

3 CALCULATION OF FIRE RESISTANCE OF COMPOSITE BEAMS

The study included two different composite beams and twelve columns belonging to the GOBACAR system. The members of the construction system and the applied loads were taken out of the static calculation for a completed car park in Dresden. The two beams consist of a steel section and a concrete slab with a thickness of 103 mm and an effective width of 2500 mm. According to Fig. 2 the first section comprises a hot rolled beam (IPE400a) while the second comprises a welded beam. The slab is connected to the steel section by headed

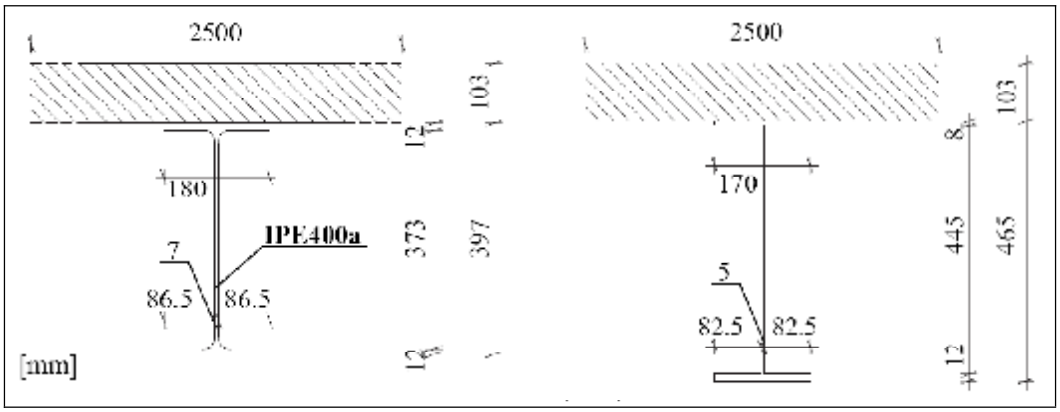

Fig. 2: Dimensions of composite beam with IPE400a profile (left) and welded profile (right)

studs. The materials of both composite beams are equal. Steel grade S355J2G3 and concrete grade C35/45 are used. The headed studs have a maximum tensile strength of 450 N/mm².
According to the load, the assumption of the characteristic dead load is obligatory. The live load is normally multiplied by the combination factor Ψ_2 in case of fire. For traffic areas a value of Ψ_2=0.3 is taken for this in general. Alternatively a more realistic approach of applying the characteristic values of the live load limited to the parking bay area was conducted. In this approach live loads on the lane between the slots were not taken into account. The resulting bending moments are nearly identical. For the further investigation the bending moment calculated by the realistic approach was used. This led to a total design moment of 315 kNm for the hot rolled composite beam (IPE400a) and due to less self weight 311 kNm for the welded one. For the reason that the assembly of the car park is symmetric, the beams can be used for most parts of a storey. Only a few beams in the ramp area are shorter and for that reason not relevant. The load on the beams is also practically equal for each storey. So it was possible to calculate just one beam exemplarily for all beams in the car park.

Fig. 3: Time dependent plastic moment capacity of composite beam with hot rolled section IPE400a

As described before, the temperature was calculated using the incremental method according to EC3 part 4.2.5.1 [2]. The new explicit formulae for calculation of the steel temperature were also used and verified. As the

next step the procedure concerning EC4 annex E [3] was used. So the cross sectional area of any part was multiplied by the yield stress decreased by the reduction factor for steel members $k_{y,\Theta}$ concerning Table 3.2 of EC4 [3]. In this way a resulting force was found for the web and both flanges. By calculating the dependent compressive force of the concrete slab and the inner lever arm, the plastic bending moment was found for every increment. That way the exact time when the plastic moment decreased to a value less than the applied moment of 315 kNm was determined to 15 min and 20 sec (cf. Fig. 3). The plastic moment at 15 min is 328 kNm. So the fire resistance class R15 is reached by the composite beam with the IPE400a section.

Because the flanges and the web of the welded profile are thinner than the parts of the IPE400a profile, the heating of the member is faster. This leads to a fire resistance time of only 14 min and 5 sec. Because of this result advanced calculation methods were applied.

The thermal material properties, the heat transfer coefficient α=25 W/m²K and the emissivity coefficient ε_r=0.8 were taken from the Eurocodes. The configuration factor Φ was set to 1.0 according to EC1 [1]. The plastic moment capacity after 15 min calculated by BoFire is 251 kNm. This is less than the needed plastic moment of 311 kNm and even less than the plastic moment of 272 kNm calculated by the simple calculation method of EC4 [3]. Reason for the difference is a difference in the steel temperatures. The shadow factor k_{sh} taken into account in the simplified calculation method causes lower steel temperatures than the heat transfer assuming a configuration factor Φ = 1.0 in the advanced calculation method. This conflicts with EC4-1-2 cl.4.1(3) which reads: "Tabulated data and simple calculation models should give conservative results compared to relevant tests or advanced calculation models." The shadow factor k_{sh} has been established to consider the fact that not every part of the open section is equally and directly exposed to the fire. Concerning advanced calculation methods, there is a possibility to reduce the heat flux into the member by reducing the configuration factor Φ, but there is no default value given in the Eurocodes for this purpose. Improvement may be based on experimentally checked configuration factors $\Phi < 1.0$. For the time being the fire resistance time calculated by advanced calculation methods is less than calculated by the simple method in this case.

4 CALCULATION OF FIRE RESISTANCE OF STEEL COLUMNS

In contrast to the beams there are differences in the load and thus in the cross section of the columns for the different storeys. In higher car parks the columns of the ground storey need to have a higher load bearing capacity. There are also four different types of columns in any storey. For this reason at least twelve types of columns were analysed including car parks with 2, 4 and 6 storeys. The most interesting four columns are shown in Table 2.

Table 2. Column types for different positions and loads

Number of storeys	Position of column	Normal force [kN]		Bending moment[kNm]		Profile
		at 20°C	in case of fire	at 20°C	in case of fire	
2	Edge column	311	202	9	6	HE-140A
	Internal column	614	399	7	5	HE-180A
6	Edge column	932	606	9	6	HE-220A
	Internal column	1841	1197	7	5	HE-280A

The columns with highest load utilisation ratios are the internal columns while the columns exposed to the maximum bending moment are the edge columns. The two other types of columns are located in the ramp area and there number is lower.

The buckling length of all columns for calculation at 20°C is 2.7 m. This is equal to the height of every storey. In case of fire the static system changes for the ground storey to 0.7 times of the length at 20°C. This leads to a buckling length of 1.89 m.
The constant temperature field of the columns was calculated by the simple method of EC3 [2]. The calculation of the fire resistance was carried out by comparing the load bearing capacity to the applied load using the calculation method of EC3 part 4.2.3.5. The method implies the lateral and the lateral torsional buckling by decreasing the resistance against normal forces. The temperature dependent load capacity was determined for every timestep. So in Table 3 the time is given at which the load capacity becomes less than the applied load. This time is defined as the fire resistance time.

Table 3. Calculated fire resistance time and required profiles (R15) for different column types

Number of storeys	Position of column	Used profile	Calculated fire resistance time	Required profile (R15)	Calculated fire resistance time
2	Edge column	HE-140A	10:01	HE-200A	15:50
	Internal column	HE-180A	11:15	HE-220A	15:00
6	Edge column	HE-220A	12:33	HE-260A	15:45
	Internal column	HE-280A	13:03	HE-320A	15:53

The fire resistance time for all actual used profiles is less than 15 min. This is caused by the high load utilisation factor of nearly 1.0 calculated at 20°C. The advanced calculation by BoFire leads to a shorter fire resistance time than the calculation by the simple method of EC3 [2]. This is caused by the use of the shadow factor k_{sh}, again.
The minimum required profile to reach the aim of R15 is also given in Table 3. For all columns there are profiles needed which are minimum two classes bigger then the already used. This leads to the assumption that it is cheaper to use fire protection materials instead of increasing the size of the steel columns. However, it is possible to use unprotected steel columns for car parks if the fire resistance class R15 is required.

5 CONCLUSIONS

The calculation of the fire resistance time by the simple and advanced calculation methods showed that the more sophisticated method leads to a more conservative solution in this case. This is presumably caused by the shadow factor k_{sh}. This factor is not applicable to advanced calculation methods. The average decrease of the steel temperatures caused by the shadow factor is determined to 95% for the columns (k_{sh}=0.85) and 93% for the composite beams (k_{sh}=0.7). It is obvious that a calculation with advanced methods can not compensate this reduction of temperatures unless taking into account this shadow effect. So the calculated fire resistance time was not increased for the analysed members.
The exact calculation of the fire resistance time of the analysed members by simple calculation methods according to the Eurocodes showed that it is possible to meet the fire resistance class of R15 for composite and steel members. To reach this aim it is necessary that the steel part of the members has either a minimum thickness or a maximum load utilisation factor. It is shown that the investigated hot rolled IPE beam can be used without any fire protection for car parks with a required fire resistance class of R15. In contrast the welded beam with thinner web and flanges is not reaching the required fire resistance class. Concerning the columns the load utilisation factor at 20°C is very high for economic reasons and the fire resistance time is less than 15 min. The class R15 can be reached by using profiles with an increased cross sectional area (overdesign).

6 SUMMARY AND ACKNOWLEDGEMENT

The standard construction method for multi storey car parks in Germany is the steel and composite construction. This is caused by the fact that no structural fire resistance is required according to the building regulations for open car parks. In some other European countries, for example the Czech Republic, a fire resistance class of R15 is obligatory. This leads to the question whether the steel structure of German car park systems withstands this short fire exposure. So the fire resistance time of two composite beams and twelve steel columns was calculated in this investigation.

The calculation of the steel temperature was conducted by the incremental simple method of Eurocode 3 and by an approximated explicit formulation. It has become obvious that the approximated formulae are adequate to calculate the steel temperature in its application range.

Because the required fire resistance class was not reached in any case, the advanced calculation method BoFire was applied. The fire resistance time calculated by the advanced calculation method was found to be more conservative than calculated by the simple method in this case. Reason for this is the shadow factor k_{sh} in the simplified calculation method. An adequate reduction of the heat transfer is not regulated for practical use when advanced calculation methods are applied. So the calculated fire resistance was not increased for the analysed members.

The calculation of the fire resistance time by simple calculation methods according to the Eurocodes showed that it is possible to gain a fire resistance time of 15 min for composite and steel members. One of the investigated composite beams reached the class R15, while the second failed for the reason of a thinner web and flanges.

The load utilisation factor of the analysed columns at 20°C is very high for economic reasons. Thus the fire resistance time was determined to less than 15 min. It is also shown that it is possible to reach the class R15 by increasing the cross sectional area of the columns (overdesign).

This investigation was initiated by the German company GOLDBECK. The authors would like to acknowledge the company for the support in this research.

REFERENCES

[1] Eurocode 1: Actions on structures – Part 1-2: General actions – Actions on structures exposed to fire; German version EN 1991-1-2:2002; Beuth Verlag, Berlin 2002

[2] Eurocode 3: Design of steel structures – Part 1-2: General rules – Structural fire design; German version EN 1993-1-2:2005 + AC:2005; Beuth Verlag, Berlin, 2006

[3] Eurocode 4: Design of composite steel and concrete structures – Part 1-2: General rules – Structural fire design; German version EN 1994-1-2:2005; Beuth Verlag, Berlin, 2006

[4] Innovation in Steel, Parking Structures around the World; International Iron and Steel Institute (IISI), Bruxelles, 2001

[5] CSN 73 0804; Pozarni bezpecnost staveb – Vyrobni objekty; Fire Protection of buildings – Industrial buildings, Cesky normalizacni institut, Praha, 2002

[6] Schaumann, P.: Zur Berechnung stählerner Bauteile und Rahmentragwerke unter Brandbeanspruchung, Technisch-wissenschaftliche Mitteilungen Nr. 84-4, Institut für konstruktiven Ingenieurbau, Ruhr-Universität Bochum, Dissertation, Bochum, 1984

[7] Upmeyer, J.: Nachweis der Brandsicherheit von kammerbetonierten Verbundbauteilen über Grenzbrandlasten, Schriftenreihe Heft 19, Institut für Stahlbau, Universität Hannover, Dissertation, Hannover, 2001, Shaker Verlag

STEEL BEAM-COLUMN UNDER THERMAL GRADIENT

Combined axial-bending capacity of steel double-T cross-sections subjected to non-uniform temperature distribution

C. Tsalikis [a], E. Koltsakis [b], C.C. Baniotopoulos [c]

[a,b,c] Aristotle University of Thessaloniki, Institute of Steel Structures, Thessaloniki, Greece

1 INTRODUCTION

Beam-column is a term which is used to describe a structural member which is simultaneously subjected to an axial compressive force and a bending moment [1]. This type of element is commonly met in steel frame buildings. A beam in such buildings tries to expand due to thermal loading that is induced to it, but the restraints prevent this expansion and as a result, a compressive force develops on the member, in addition to the bending moment in place due to the gravity load. Similarly, a possible expansion of a beam can cause additional moments to the column of the structure, apart from the axial force already imposed to it. Contemporary provisions of the Eurocodes assume a uniformly distributed temperature over the steel members for the estimation of their capacity [2]. Such a hypothesis, for the members that are located on the borders of the fire room, may lead to disproportional results in relation to the true situation. This paper investigates the way that a thermal gradient on a cross-section of a steel beam-column member affects its mechanical strength.

2 STATE OF THE ART

Wang et al. examined the limiting temperatures for elements of frames and found that the presence of thermal gradients and other types of temperature profiles cause significant alterations of the respective results [3]. It was noticed that the non-uniformity of the temperature profiles affect the limiting temperatures depending on the type of the profile, the load ratio and the slenderness of the columns. As the slenderness increases, the limiting temperature goes down. In addition, Wang et al. observed the presence of high bending moments because of the thermal gradient, but refrained from investigating the behaviour of the axial-load moment-capacity envelope in such a situation.

Garlock and Quiel made one more step towards the study of the influence of thermal gradients on beam-columns under several load cases [4]. Neglecting global buckling, local buckling and residual stresses, they loaded the steel members up to their plastic limit and they came up with two forms of normalized axial load – moment capacity envelopes depending on the reference axis of the cross-section. Both forms of graphs point out the alteration of the conventional capacity envelope in the case of a non-uniform temperature over the entire depth of the section. The first one assumes the plastic neutral axis as reference for the estimation of the axial load and bending moment capacity, whilst the second one is based on the centre of gravity being the reference axis. This assumption generates additional bending moment because of the eccentric induction of the axial load, which will result in a more or less conservative capacity envelope depending on the type of external loading and on the slope of the thermal gradient.

The current study poses again the same question of load capacity but deals with it from a different point of view: starting from the assumption of Bernoulli for the strains and combining it with precise material models attempts to estimate capacity envelopes and compare them with those of the Eurocodes. This approach sets forth new questions to further investigations.

3 DESCRIPTION OF THE PROBLEM

As starting point for the formulation within the context of the present work, the planarity of the cross section was assumed in order to remain inside the framework of a beam theory. As known, according to the hypothesis of Bernoulli and Navier, during deflection, the cross-section remains

plane and normal to the deflected centroidal axis [5]; any transverse normal stresses are negligible. Other phenomena, such as creep deformation, thermal elongation, geometric non-linearities and residual stresses are not to be accounted for as the present work is to focus on the strength at a cross section level: introduction of the influence these may have on the bending and axial capacity of the beam-column would exceed the limits of the current study.

The cross-sections that were studied are double T cross-sections and the field of temperatures introduced to them was taken linear over the weak axis (i.e. the *z*-axis according to the Eurocode notation). This means that at the bottom of the lower flange there is the lowest temperature which rises up linearly and reaches its maximum value at the highest part of the top flange. The upper flange is the one assumed to face the internal part of the building and therefore absorbing the maximum temperatures. As no thermal analysis has been made, the assumption of the linear distribution of the temperature is merely a working assumption made in order to obtain an assessment of the phenomenon: the divergence from the real situation is not the issue of the current paper. The later is difficult to estimate as it depends to a number of uncertain factors as the rate of heat release, the position of the plume, the thicknesses of the flanges and the web and, generally, the thermal conditions inside the examined room.

In a cross-section under thermal gradient the relationship describing the material depends on the position of a certain point in the temperature field. For the determination of the beam-column resistance under a specified elevated temperature, EC3-Part 1.2, which addresses the structural fire design for steel elements, proposes the use of the ambient temperature stress-strain relationship with some additional reduction factors [2]. These reduction factors affect the yield strength, the modulus of elasticity and the proportionality limit of the material and they are inversely proportional to the increase of the temperature, as shown in *Fig. 2*. This relationship of EC3-1.2, may be used to determine the resistances to tension, compression, moment or shear. For this investigation, apart from the use of the formulae that are proposed by EC3 without taking into account the strain-hardening, another stress-strain relationship is formulated by the authors which is based on the combination of two other publications. Burgess et al. studied the behaviour of steel beam in fire with the use of a constitutive model based on a Ramberg-Osgood type of equation [6], [7]. The formula, which had been adopted, represents the stress-strain relationship as given in *Eq. (1)* and the parameters, that depend on the temperature, were obtained from test data [7], [8]:

$$\varepsilon_{(T)} = \frac{\sigma_{(T)}}{A_{(T)}} + 0.01\left(\frac{\sigma_{(T)}}{B_{(T)}}\right)^{n_T} \tag{1}$$

where ε is the strain, σ is the stress and A(T), B(T) and n(T) are the parameters which depend on the temperature

In order to attain similarity between the two material descriptions, the Ramberg-Osgood equation was inverted using Mostaghel's method [9]. According to this method, equation (1) was divided into two parts: the first part consists of the elastic strains and the second one of the plastic strains. Following a first order approximation for the plastic dominated region, Mostaghel et al. came up with a stress-strain relationship that describes both the elastic and the plastic region with negligible errors. By substituting the parameters that Burgess et al. proposed into the new stress-strain relationship, a new formula was created which provides the stress as a function of both the strain and the temperature as following:

$$\varepsilon = f(\sigma, T) \rightarrow \sigma = f(\varepsilon, T) \tag{2}$$

This formula is created for the verification and the comparison of the material model proposed by the Eurocode (*Fig. 3)*.

The core of the procedure used in the present work was to compute (through integration over the cross section) internal forces corresponding to a set of assumed strain and temperature fields that span the possible operational conditions expected for a structural element to face. Knowing the temperature and the strain in every point of the section, the next step is to calculate the stress at

every single point using either the relationship that Eurocode proposes or the inversed Ramberg-Osgood formula (*Fig. 1(b), 1(c)).* As mentioned, these relationships change their parameters (yield strength, modulus of elasticity and proportional limit of the material) in relation to the temperature (*Fig. 3).* This procedure will reveal the true stresses that develop at every single point of the cross-section. It has to be mentioned that due to the fact that stress depends on both the strain and the temperature, which is a function of the position of a point, the stress field will be neither uniform nor linear type but a complex higher-order field, as shown in *Fig. 1(d).*

After the calculation of the stress field, the internal forces are obtained by means of the evaluation of integrals: first, the axial force is computed as the integral of the stress field over the area of the cross-section:

$$N = \int_A \sigma_x dA \tag{3}$$

where σ_x is the stress at each point and A is the total area of the section.

For the estimation of the bending moment that is carried by the section, the stresses that cause the above axial force should be subtracted from the general stress field in order for the stresses that create the bending moment to be revealed. Specifically, the normalized stress σ_o which is responsible for the axial force derives from the following expression *Eq. (4)*:

$$\sigma_o = \frac{N}{A} \tag{4}$$

where N is the axial force as described in *Eq. (3)* and A is the total area of the section.

Subtracting the uniform stress σ_o from σ_x, the new stress field σ_M is obtained (*Fig. 1(f)).* The integration of the stress σ_M multiplied by the distance from the "zero stress" axis over the whole area of the section will give us the bending moment, as seen in *Eq. (5)*:

$$M = \int_A (\sigma_y - \sigma_o) z_{ZSA} dA \tag{5}$$

where Z_{ZSA} is the distance of a point from the "zero stress" axis (i.e. the points which have σ_M=0) .

The traditional neutral axis is where the strains are zeroed and, in our model, it is applied by the user in order to represent every possible combination of external loading, as described above. On the other hand, the "zero stress" axis is where the σ_M reaches zero. At that point, the integration of the positive stresses over the area that are distributed equals the integration of the negative ones. Apparently, the distribution of σ_M(z) is not linear, as in that case the ZSA will always be located at the centre of the cross-section. At this point, it is necessary to mention that there are strong indications that the stress field that we are getting from the above analysis cannot be described only with the first-order moment, but higher-order moments are needed: this line of investigation is not within the scope of the present study but a goal for further investigation.

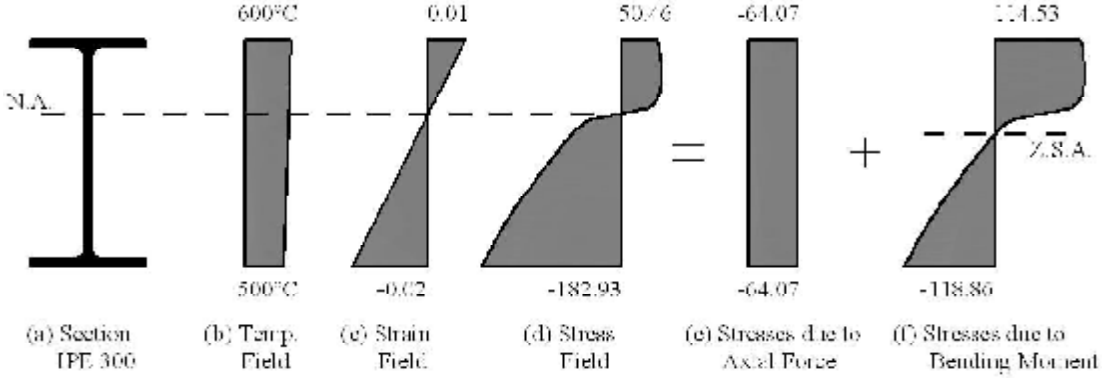

Fig. 1. Temperature, Strain and Stresses fields through the depth of an IPE300 cross-section

4 IMPLEMENTATION AND CONCLUSIONS

4.1 Implementation

All the above theoretical approach was modelled in a code using the program CAST3M. CAST3M is a computer code for structural analysis using the finite elements method. The cross-sections that were modelled are IPE300, HEA300 and IPE200. Each section was discretized using a suitable mesh for the most precise solution to be achieved. As far as the temperature is concerned, SCI's technical report proposes the practical rates of heating to be 5^{o}C/min for well insulated sections and 20^{o}C/min for unprotected sections [10]. Taking this for granted, the temperatures, which are applied on the top and bottom edge of the sections, obtained various values from 300^{o}C to 700^{o}C, to represent an unprotected structural member in fire between the 15^{th} and the 35^{th} minute. The distribution of the temperature field onto the cross-section was made as described above. For the strain field, an effective strain limit of 2% was adopted for determining the strength at elevated temperatures [10]. This means that the values at the extreme fibres of the cross-section fluctuate from -0.02 to 0.02.

4.2 Results and conclusions

The stress-strain relationship that the Eurocode proposes for elevated temperatures is depicted in (*Fig. 2*). In *Fig. 3* one can see the differences between the EC and the Ramberg-Osgood approach. In particular, the EC produces higher values for the modulus of elasticity for the elastic region than the R-O equation. This fact changes as the cross-section enters the plastic region where the R-O modulus of elasticity shows a more prominent hardening, a fact that makes the R-O seem more optimistic, especially, when the temperatures are not the highest that may develop during a fire.
Each point in the N-M plane of Figs.4-6 corresponds to a pair of strains imposed to the upper / lower fibre of the cross section. The step used for the coverage of the strain domain is constant; therefore the increase of the density of the images of strain points in the N-M space represents a reduction of the stiffness of the cross section due to partial plastification. Using the EC relationship for the estimation of the axial load-bending moment capacity, it was found that the capacity envelope that EC 3 (*Part 1.1 – cl.(6.36))* proposes may be conservative or non-conservative in relation to the real situation [11]. As being described in the example that *Fig. 4* shows, the thermal gradient alters the capacity of the cross-section. Each point on this figure represents the normalized N-M value and derives from the combination of a distribution of strains and a thermal gradient. The normalization of N-M values was made for the (constant) mean value of the temperature field. EC envelopes illustrate the capacities of the beam-column elements, assuming uniformly distributed temperatures [11]. On the one hand, in the region where the accumulation of the points falls outside the safety envelopes, EC appears conservative, whilst in the opposite situation, the EC approach appears to be optimistic. Similarly, in *Fig. 5* these discrepancy regions become greater. Therefore, as the slope of the thermal gradient increases, so does the discrepancy between the EC capacity envelopes and the true ones.
Furthermore, the alteration of the N-M values, as the slope of the thermal gradient rises, is clearly shown in *Fig. 6.* In *Fig. 7,* the evaluation of the stress field was made according to R-O's formula. The N-M images of the two approaches are quite similar, apart from the difference the density increase in the edges of the strain span, a fact easily attributable to the difference of the two stress-strain relationships. This observation is, also obvious at *Fig. 8* and *Fig. 9.* The temperatures of these last figures represent a possible fire history scenario. The alteration of the region of points shows the way that the growth of the fire affects the capacity of the cross-section.
As conclusion, it can be said that:
- the region of safe operation of the cross section presents under that presence of thermal gradient shows a differentiation in shape that is not accounted for by the present regulatory framework;
- extensive parametric research is needed in order to obtain N-M interaction safety regions for the commonly used structural steel cross sections;

- the absence of a distinct hardening form of the stress-strain curve at elevated temperatures requires, to the authors opinion, a reconsideration of the concept of allowable stress so as to obtain the same safety margin with the low temperatures range.

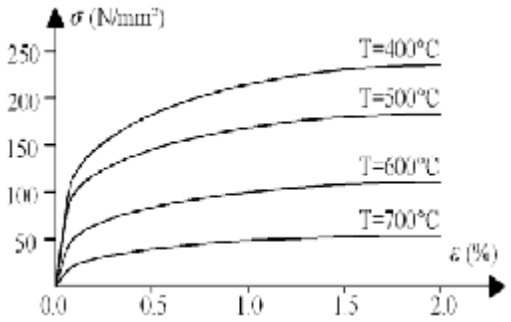

Fig. 2. Stress-strain relationship at elevated temperatures according to EC3

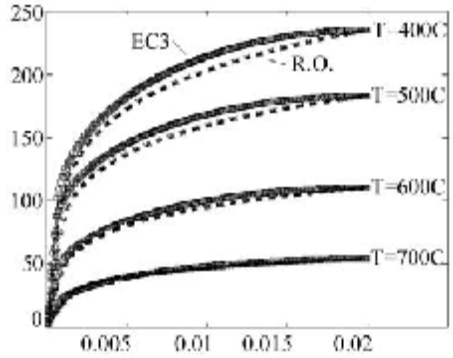

Fig. 3. Stress-strain relationships at elevated temperatures (EC3 + Ramberg-Osgood)

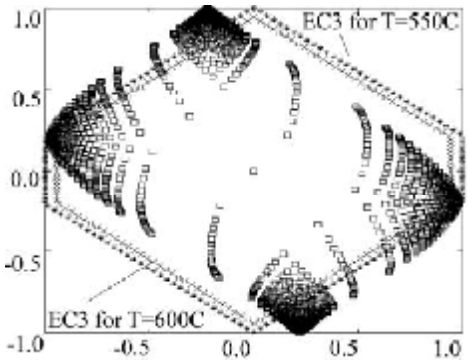

Fig. 4. Normalized M-N capacity for non-uniform temperature (Tmax=600C/Tmin=500C) and EC3 capacity envelopes (T=550 → External / T=600C → Internal)

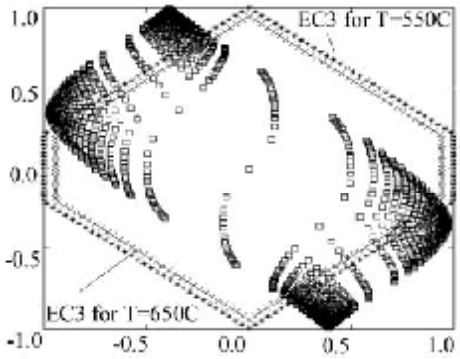

Fig. 5. Normalized M-N capacity for non-uniform temperature (Tmax=650C/Tmin=450C) and EC3 capacity envelopes (T=550 → External / T=650C → Internal)

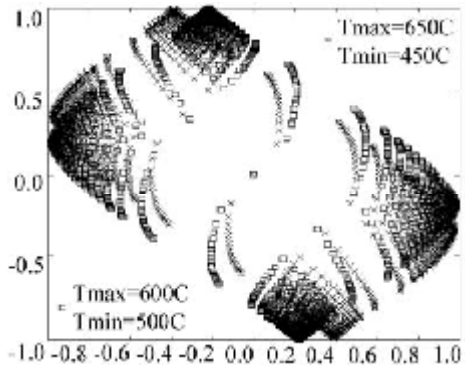

Fig. 6. Normalized M-N capacities for non-uniform temperatures using EC3 stress-strain relationship

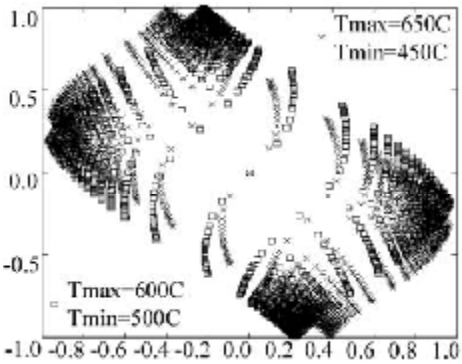

Fig. 7. Normalized M-N capacities for non-uniform temperatures using Ramberg-Osgood stress-strain relationship

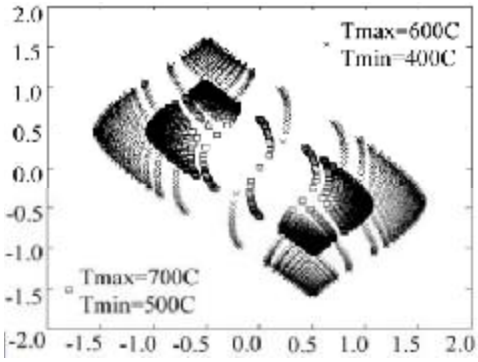

Fig. 8. Normalized M-N capacities for non-uniform temperatures using EC3 stress-strain relationship

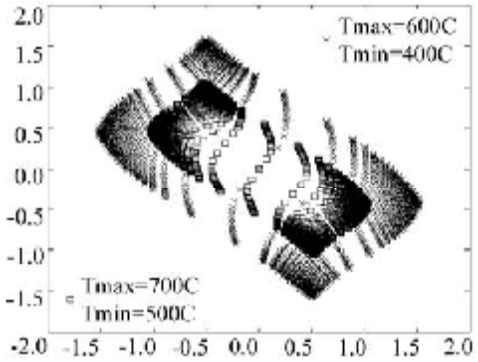

Fig. 9. Normalized M-N capacities for non-uniform temperatures using Ramberg-Osgood stress-strain relationship

REFERENCES

[1] W.F. Chen, T. Atsuta, Theory of beam-columns, *J. Ross publishing,* 2008

[2] Eurocode 3: Design of steel structures, Part 1.2: General Rules – Structural Fire Design, *European Committee for Standardisation,* Brussels 2003

[3] Y.C. Wang, T. Lennon & D.B. Moore, The Behaviour of Steel Frames Subject to Fire, *J. Construct. Steel Research 35,* p. 291-322, 1995

[4] M. E.M. Garlock, S.E. Quiel, Combined axial load and moment capacity of fire-exposed beam-columns with thermal gradients, *Fourth International Workshop "Structures in Fire",* Aveiro, Portugal, 2006

[5] Z.P. Bazant, L. Cedolin, Stability of Structures: Elastic, Inelastic, Fracture and Damage Theories, *Dover Publications,* 2003

[6] I.W. Burgess, J. El Rimawi & R.J. Plank, Studies of the Behaviour of Steel Beams in Fire, *J. Construct. Steel Research 19,* p. 285-312, 1991

[7] C.G. Bailey, I.W. Burgess & R.J. Plank, Analyses of the Effects of Cooling and Fire Spread on Steel-framed Buildings, *Fire Safety Journal 26,* p. 273-293, 1996

[8] B.R.Kirby & R.R. Preston, High Temperature Properties of Hot-rolled Structural Steels For Use in Fire Engineering Design Studies, *Fire Safety Journal 13,* p.27-37, 1988

[9] N. Mostaghel, R.A. Byrd, Inversion of Ramberg-Osgood equation and description of hysteresis loops, *International Journal of Non-Linear Mechanics 37,* p.1319-1335, 2002

[10] R.M. Lawson, G.M. Newman, Structural Fire Design to EC3&EC4, and comparison with BS 5950, *Technical Report – SCI publication 159,* 1996

[11] Eurocode 3: Design of Steel Structures, Part 1-1: General rules and rules for buildings, *European Committee for Standardisation,* Brussels 2005

BEHAVIOUR OF SCREWED SHEAR SHEETING CONNECTION IN FIRE

Wei Lu, Pentti Mäkeläinen [a], Jyri Outinen [b]

[a] Helsinki University of Technology, Department of Structural Engineering and Building Technology, Espoo, Finland

[b] Rautaruukki Oyj, Ruukki Construction, Vantaa, Finland

INTRODUCTION

Corrugated steel sheets are normally attached to the underlying purlins or more commonly straight to the steel trusses by self-drilling or self-tapping screws. The behavior of sheeting connections in fire conditions is important because of the maximum compression force during thermal expansion and maximum tension force in catenary action exerted to the screw connectors at supports [1]. In this paper, the performance of screwed connections between a thinner plate and a thicker plate are investigated to simulate the structural application of connecting the roof sheeting to underneath truss members. The investigations are carried out via both single lap shear tests and Finite Element (FE) modeling both at room temperature and at elevated temperature. The aims of this study are (1) to understand the failure mechanism of the screwed connection and (2) to get the load-displacement curves so that they can be used in the further research.

1 SINGLE LAP SHEAR TEST

Fig. 1 shows the standard testing set-up according to ECCS recommendations [2]. However, due to the limitation of dimensions of the furnace available, the dimensions of the specimens are reduced accordingly (*Fig. 2*). Two kinds of tests have been carried out: one is to validate the testing results of specimens with Reduced Dimensions (RD) with Standard Dimensions (SD); and the other is to do the tests for a group of temperatures, i.e. 20 °C, 200 °C, 400 °C and 600 °C. Since the displacement of the specimen inside furnace is recorded as the plate end displacement, measurement setting (dotted lines in *Fig. 1*) has been removed in the SD test.

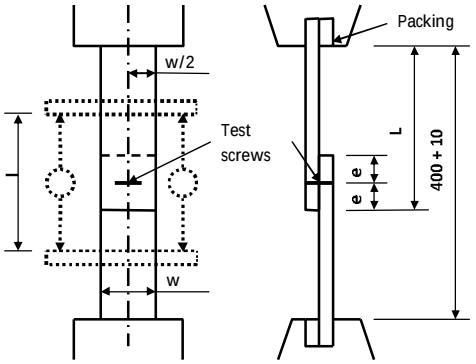

Fig. 1. Standard testing set-up

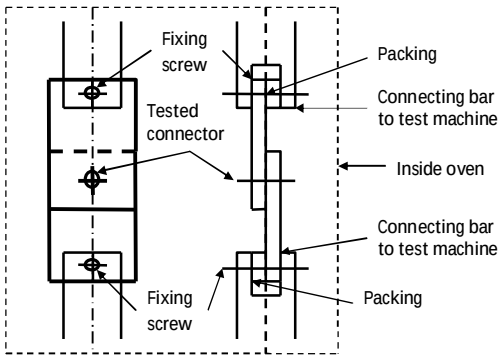

Fig. 2. Testing set-up in this research

In the room temperature tests, the rate of loading in the initial stage of testing shall not exceed 1 kN/min. Until the ultimate load is reached the rate of straining shall not exceed 1 mm/min [2]. The displacement control is used. At elevated temperatures, the tests are carried out in two steps. Firstly, the temperature is raised to a given temperature. Then the loading is applied to the specimen with the rate of 0.1 to 0.3% per minute. According to [2], the maximum load is reached in a deformation of 3 mm in order to avoid the extra deformations in the connection. However, in fire case the large deformation is an alternative mechanism to avoid the failure of the structure. Thus, the tests have been stopped when the displacement of 20 mm is reached at room temperature and 15 mm at elevated temperature. The maximum load is recorded as the one in this range of deformation.

The deformation histories for SD specimens at room temperature are shown in *Fig. 3*. It can be seen that the deformation of connection starts from the progressively curling or tilting of thinner plate because of the eccentricity of single lap shear joint (a). Then the slipping in the thinner plate is observed when the slipping is out of the cover of screw. The slipping is due to the local yielding of material when the bearing of screw fastener against thinner plate (b). Because of the large local strain, the cracking appeared in the thinner plate when the ultimate strength of material is reached. The tearing of thinner plate continues and in the later stage the base plate of screw cut into the thinner plates (c). The same deformation histories for RD specimens have been observed and the final failure mode is shown in (d).

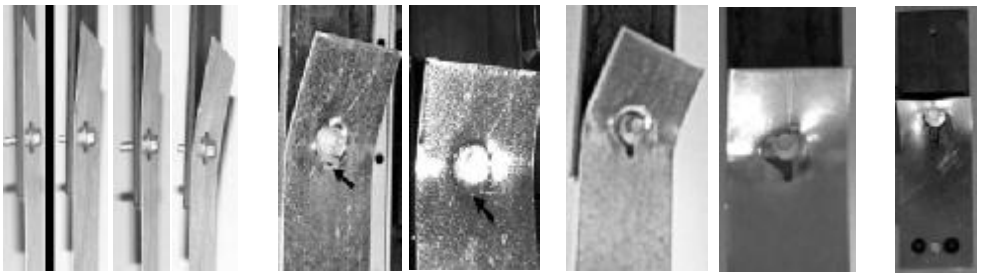

Fig. 3. Deformation histories of SD specimen (a), (b), (c), failure mode of RD specimen (d)

In order to show the feasibility of testing results with RD specimens, a load-deflection curve is taken out respectively for SD and RD specimens as shown in *Fig. 4* (a). According to 7 points (0-6) marked on the curves, it can be seen that the deformation histories of two types of specimens are the same due to the same shapes of two curves. The maximum loads of the connections (point 5) are at about the same level. However, due to the displacement of SD specimen has been measured at the end of the plate instead of around the connection area, the RD specimens are more stiff than SD ones. The load-displacement curves for other RD and SD testing specimens are shown in *Fig. 4* (b).

Due to the limitation of the testing furnace, the deformation histories of specimen at elevated temperatures cannot be observed. Only the final failure modes of the specimens are shown in *Fig. 5*. Two failure modes have been observed: bearing and tearing failure of thinner plate below at 200 °C (a) and shearing failure of screw connector at 400 °C (b) and 600 °C (similar mode to 400 °C). The main factor that determines the final failure mode in the connection might be the relative material strength involved in the connections. At room temperature, the material strength of thinner plate is lower than that of screw connector. Thus the failure mode is Mode 1 failure. When the temperature is above 400 °C, the material properties for screw

connector might drop dramatically because the ways of increasing of material strength to be used as screws (for instance heat treatment).

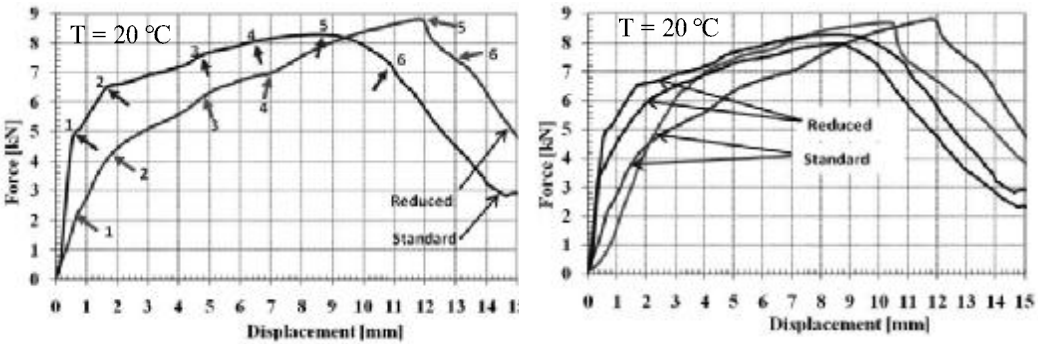

(a) Key points on load-displacement curves (b) Testing curves for other specimens

Fig. 4. Load-displacement curves of SD and RD specimens

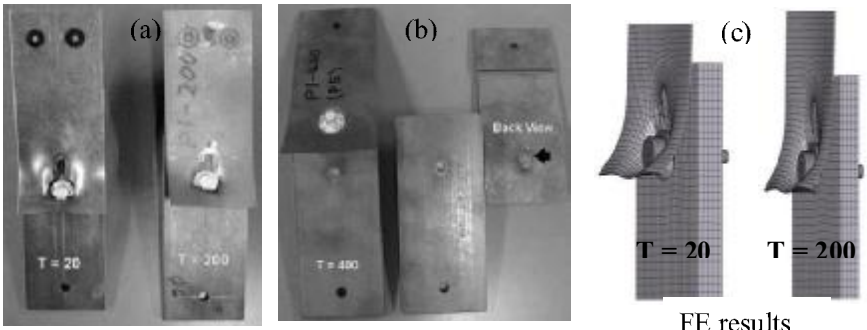

Testing results FE results

Fig. 5. Failure modes of testing results and FE results

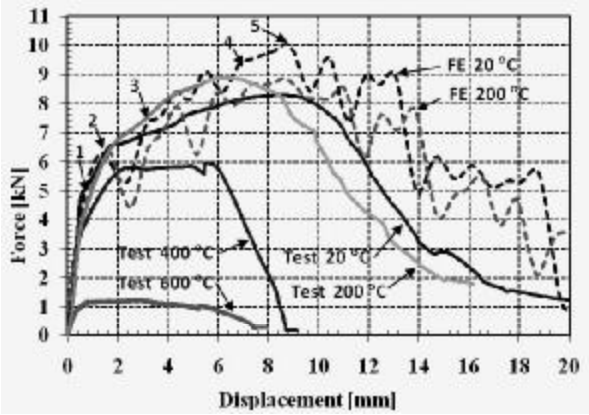

Fig. 6. Load-displacement curves from tests and from FE modelling

The load-displacement curves from tests are shown in *Fig. 6.* When comparing load-displacement curves at 20 °C to that at 200 °C, it can be seen that up to point 2 these two curves are very close because both strength and modulus of elasticity are not much reduced at

200 °C. Then load-deformation curves at 200 °C are higher than those of at 20 °C but with reduced ductility. The stiffness and maximum load at 400 °C and 600 °C are lower than those at room temperature because of the reduction of strength and modulus of elasticity of materials at elevated temperatures. The ductility has been reduced as well due to the brittle failure mode of screw connectors when comparing to the bearing tearing failure of thinner plate at 20 °C and 200 °C respectively.

2 FINITE ELEMENT MODELLING

Fig.7 shows the structural assembly of the single lap shear screw connection and connection details. Thinner sheet with thickness 0.8 mm simulates the steel sheeting in roofing system. The thicker sheet (10 mm) represents the top chord (structural hollow section) of the roof truss to which the sheeting is connected. The lengths of the two sheets are 150 mm, respectively. One screw connector ϕ 5.5 mm x 26 mm with head diameter 11 mm is used to connect two sheets. The main function of screw thread is to prevent the screw from being moved along its axial direction, thus only three threads are modelled in order to improve the computational efficiency. The steel washer with diameter 15 mm is used between the screw connector and thinner sheet. The distances of centre of the screw connector to the sheet edges are both transversely and longitudinally 30 mm. Commercial FE software, ABAQUS/Explicit, is used as an analysis tool. Three dimensional eight nodes solid elements with reduced integration point (C3D8R) are chosen for modelling the thicker sheet, the thinner sheet, the screw, the screw thread and the washer. The description of mesh details, the loading steps and boundary conditions are presented in reference [3].

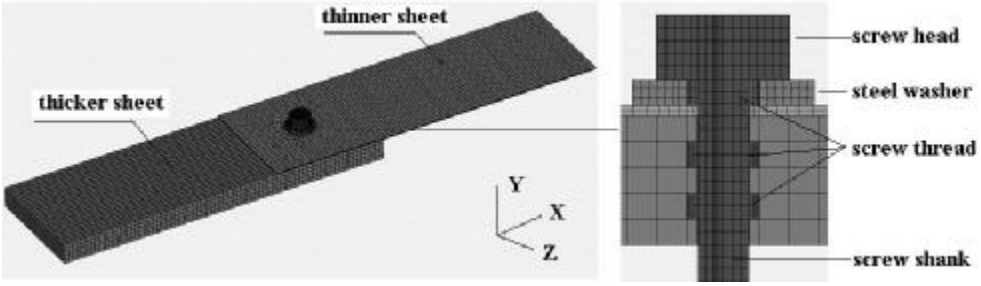

Fig. 7. Structural modelling of single lap shear screw connection and connector details

In order to simulate the real behaviour of material, true-stress and true-strain curves are used. Due to the high local strain in the thinner sheet in vicinity of screw connector, the progressive damage and failure of material are included in the analysis. From our trail simulations, it is assumed that the damage initiation starts when the equivalent plastic strain is 0.45 and the material failure is reached when the equivalent plastic strain is 0.5. The damaged elements are not removed from the analysis. The reduction factors for the yield strength and modulus of elasticity follow the values defined in the main text of EN 1993-1-2 [4].

Researches [5] have revealed that failures normally do not take place in the screw connector itself. So the following assumptions are made in FE analysis: the screw connector has the higher strength and rigidity than other materials in the connection assembly. Therefore, the screw connector and washer have the linear elastic material properties with the same values of yield strength and modulus of elasticity as those of steel sheet at 20 °C. However, from our testing, the failure of screw occurred at 400 °C and 600 °C. Thus, the material model of screw

connectors needs to be modified in order to further apply the FE modelling. Therefore, in the following sections, only results at 20 °C and 200 °C are compared.

3 VERIFICATION OF FE MODEL

Fig. 5 shows that at 20 °C and 200 °C the failure modes from FE analysis is the same as those from testing results. Similar to 7 points in *Fig.4*, the load-displacement curves from FE analysis at 20 °C and 200 °C can be divided also by 6 points up to maximum load (*Fig.6*). It can be concluded that FE model simulates the deformation history very well.
Table 1 shows the comparisons of the maximum load from tests and from FE analysis. It can be seen that at 20 °C, the FE results are about 20% higher than testing results. At 200 °C, due to the differences of real material properties and model used in FE modelling, the maximum load values are the same but the ductility from FE analysis is larger than that from tests.

Table 1. Comparisons of maximum load and corresponding deformation from FE analysis to those from tests

	Test		FE Analysis		Comparisons
	MaxLoad [kN]	Deformation [mm]	MaxLoad [kN]	Deformation [mm]	MaxLoad (FE/Test)
20 °C	8.5	9.1	10.0	8.7	1.17
200 °C	8.8	6.1	8.8	8.6	1.00

4 ANALYSIS OF FAILURE MECHANISM

The verified model has been used to understand the failure mechanism of connection at 20 °C and 200 °C. According to the 5 points in *Fig. 6*, the following mechanisms at 20 °C are illustrated in *Fig.8*. (1) The yielding of thinner plate due to the bearing of screw connector starts early, for instance, it has been observed at the deformation of 0.6 mm and initial slip happened due to material yielding (Point 1). (2) Then the local buckling of thinner plate around screw connector has been observed at 1.2 mm (Point 2). However, in order to show it clearly, the deformation of 3.0 mm has been chosen. At the same time the thinner plate tilts due to the eccentricity of single lap shear connection. (3) At point 3 (deformation of 3.6 mm or better to show with 4.2 mm), the buckling of the thinner plate has been observed. (4) With the continuation of buckling, bending stresses appeared at the edge of thinner plate (ex. deformation of 7.2 mm). At point 4, the thinner plate slips out of washer. (5) When the maximum load is reached (point 5), the material failure occurred. This can be seen from the reduction of bending effects at deformation of 8.4 mm. (6) At deformation of 15 mm, it has been shown clearly the tearing of the thinner plate and the washer's cutting into the thinner plate. The locations of maximum stresses have been transferred due to the tensioning of thinner plate. The failure mechanism at 200 °C is similar to that described at 20 °C. The differences are as follows: (1) yielding of material occurred earlier (2) the maximum load is lower. These differences are due to the reduction of strength at elevated temperatures.

5 SUMMARY AND ACKNOWLEDGMENT

The test results have shown that (1) It is reasonable to use the specimens with reduced dimensions. (2) The failure modes of connections at room temperature is bearing and tearing failures of thinner plates. The maximum load is reached when the first tearing appeared in the thinner plate. (3) Two failure modes are observed at elevated temperatures: Mode 1 is the bearing and tearing failure of thinner plate at 200 °C; Mode 2 is the shearing failure of screw connectors at temperature equal or higher than 400 °C. (4) Mode 2 is unfavourable mode

because of connector's brittle failure. This failure mode can be avoided when using such as shot-nailed connections. (5) The 6 points can be used to describe the load-displacement curves of connections at temperatures of 20 °C and 200 °C.

With the testing results, it has been shown that FE modelling can predict the behaviour of connection well at 20 °C and 200 °C. The verified FE model has been used to understand the failure mechanism of the screwed connection at 20 °C and 200 °C.

The Finnish company Rautaruukki Oyj financially supported this research. Mr. Reijo Lindgren in CSC Finland provided many helps in using ABAQUS Commercial software when creating the connection models.

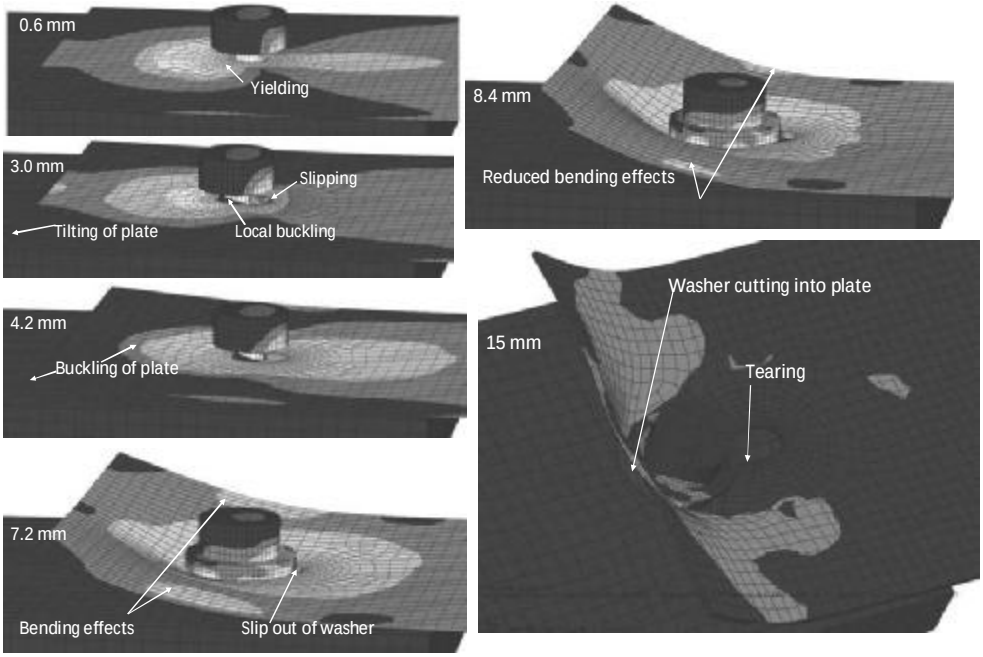

Fig. 8. Failure mechanism at 20 °C according to FE analysis

REFERENCES

[1] Lu, W., Mäkeläinen, P. and Outinen, J., Numerical Simulation of Catenary Action in Cold-Formed Steel Sheeting in Fire. Proceedings of 5th International Conference on Thin-Walled Structures: Recent Innovations and Developments, *Edited by M. Mahendran*, Gold Coast, Australia, June 18-20, pp. 713-720, 2008.

[2] ECCS-TC7.10, The Testing of Connections with Mechanical Fasteners in Steel Sheeting and Sections, *ECCS Publication 124*, 2008.

[3] Lu, W., Mäkeläinen, P. and Outinen, J., Single Shear Screw Connections in Steel Sheeting in Fire – Finite Element Modeling. Proceedings of 5th European Conference on Steel and Composite Structures, Graz, Austria, September 3-5, pp.1031-1036, 2008.

[4] EN 1993-1-2, Eurocode 3: Design of steel structures, Part 1.2: General rules – structural fire design, 2005.

[5] Sokol Z., Wald F., Structural integrity of corrugated sheets exposed to fire. Steel - a new and traditional material for building, *edited by Dubina and Ungureanu, Taylor & Francis Group, London, 561-566*, 2006.

UNPROTECTED BI-AXIALLY LOADED STEEL COLUMNS UNDER FIRE CONDITIONS

Yao Yao[a], *Tan Kang Hai[b]

[a]ExxonMobil Upstream Research Company, Houston, Texas, USA

[b]Nanyang Technological University, School of Civil and Environmental Engineering, Singapore

(*corresponding author)

INTRODUCTION

Up till now, there has been limited research work conducted on bi-axially loaded steel columns under fire conditions. Under normal ambient temperature, the load-bearing capacity of steel columns is governed by the interaction of strength and stability considerations, which gives rise to Rankine method. The authors extended this method to predict the fire resistance of steel columns subjected to bi-axial loading under standard fire curve. Basically, the authors developed an interaction equation based on column failure surface to account for the effects of axial load and bending moments in two directions. Predictions from the proposed approach were benchmarked against a well-established finite element program SAFIR for steel columns under standard fire conditions. The same approach is then extended to include natural fire curves. To model a compartment fire with different geometries, thermal characteristics of boundary walls, different fire loads and ventilation factors, a zone fire modelling program Ozone was used. Coupling Ozone to SAFIR, the failure times of steel columns in a compartment fire were predicted. These numerical predictions were compared with those from the proposed approach and reasonable agreement was obtained.

1 EXTENDED RANKINE METHOD FOR BI-AXIALLY LOADED STEEL COLUMNS UNDER FIRE CONDITIONS

In the European and the American codes, the design of steel columns exposed to fire is generally based on the national and international code recommendations. In buildings, due to initial imperfection, most of the columns are bi-axially and eccentrically loaded. It is necessary to develop a rational design method for structural engineers to calculate the fire resistance of such columns under realistic fire conditions, herein referred to as natural fire curves. For columns subjected to biaxial load and elevated temperature conditions, the traditional Rankine formula can be modified to:

$$\frac{1}{P_R(T)} = \frac{1}{P_{Rx}(T)} + \frac{1}{P_{Ry}(T)} - \frac{1}{P_{Ro}(T)} \tag{1}$$

where $P_R(T)$ is an approximate value of ultimate load in biaxial bending with eccentricities e_x and e_y; $P_{Ry}(T)$ is the ultimate load at temperature T when only eccentricity e_x is present (e_y = 0); $P_{Rx}(T)$ is the ultimate load at temperature T when only eccentricity e_y is present (e_x = 0); $P_{Ro}(T)$ is the ultimate load at temperature T for concentrically loaded column;

Incorporating the effect of load eccentricity, a plastic load reduction factor u_p is defined:

$$P_p(T) = u_p P_p(T) \tag{2}$$

To consider the effect of initial crookedness, residual stress and thermal gradient, the elastic critical load reduction factor u_e is defined as follows:

$$P_e(T) = u_e P_e(T) \tag{3}$$

From Eqs. (1) to (3), the biaxial bending formula based on Rankine method can be derived:

$$\frac{1}{P_R(T)}=\frac{u_{px}P_p(T)+u_{ex}P_e(T)}{u_{px}u_{ex}P_p(T)P_e(T)}+\frac{u_{py}P_p(T)+u_{ey}P_e(T)}{u_{py}u_{ey}P_p(T)P_e(T)}-\frac{P_p(T)+P_e(T)}{P_p(T)P_e(T)} \tag{4}$$

where u_{px} and u_{py} are the plastic load reduction factor of major and minor axis, respectively; u_{ex} and u_{ey} are the elastic critical load reduction factor of major and minor axis, respectively. For convenience, this equation can be transformed to:

$$\frac{1}{P_R(T)}=\alpha_p\frac{1}{P_p(T)}+\alpha_e\frac{1}{P_e(T)} \tag{5}$$

where $\alpha_p=1+1/u_{px}+1/u_{py}$ and $\alpha_e=1+1/u_{ex}+1/u_{ey}$, which considers the effect of bi-axial bending based on Rankine approach.

The values of u_p for I- or H-sections were proposed by Horne (1979):

1) For I-sections or H-sections bending about the major axis,

$$u_p=\frac{1}{5}\left(\sqrt{(eA/S)^2+10}-eA/S\right) \text{ for } eA/S\geq 4.5;\ u_p=\left(1+\frac{eA/S}{1.125}\right)^{-1} \text{ for } eA/S\leq 4.5 \tag{6}$$

2) For I-sections or H-sections bending about the minor axis,

$$\begin{aligned} u_p&=\sqrt{(eA/S)^2+2}-eA/S \text{ for } eA/S\geq\sqrt{4.5};\\ u_p&=\frac{1}{2.25}\left(\sqrt{(eA/S)^2+2.25^2}-eA/S\right) \text{ for } eA/S\leq\sqrt{4.5}\end{aligned} \tag{7}$$

where S is the plastic modulus of column sections.

The elastic critical load reduction factor u_e can be found from the following equation (Gere and Timoshenko, 1991):

$$1=\frac{e_{equ}}{\Delta_f}\left(\sec(\frac{\pi}{2}\sqrt{u_e})-1\right)+\frac{a_{equ}/\Delta_f}{1-u_{er}} \tag{8}$$

where e_{equ} and a_{equ} are the equivalent load eccentricity and equivalent initial crookedness, respectively; Δ_f is the control deflection or the allowable deflection and is taken as L/C; C is a parameter related to fire conditions and is a function of $\frac{eA}{S}$; for biaxial bending, the maximum value of $func(e_xA/S_x)$ and $func(e_yA/S_y)$ is used.

Based on Eq. (8), the following equation is recommended to calculate u_e:

$$u_e=\left(\frac{2}{\pi}\arccos(1/(\frac{L_e}{eC}+1))\right)^2 \tag{9}$$

where for ISO 834 fire curve: $C=76.1\times\frac{eA}{S}$ if $\frac{eA}{S}\leq 1$; $C=0.24\left(\frac{eA}{S}\right)^2-6.14\frac{eA}{S}+82$ if $\frac{eA}{S}>1$, obtained by curve fitting the column test results (Tang et al. 2001) and $0<u_e\leq 1$.

For natural fire conditions, the authors propose the following formula for C:

$$C_{natural}=0.7{v_f}^{0.5}Q_f^{0.25}C \tag{10}$$

Due to the lack of experimental data for column tests under natural fire conditions, Eq. (10) is obtained from least-squares regression analysis by curve fitting zone modeling program Ozone and finite element program SAFIR predictions to a large group of steel columns under different natural fire conditions.

It is expedient to formulate the method in terms of the buckling coefficient $N(T)$, which can be obtained as a ratio of Rankine load $P_R(T)$ (taken as the applied load P at the critical temperature) to the plastic collapse load $P_p(T)$:

$$N(T) = P_R(T) / P_p(T) = P / P_p(T) \tag{11}$$

Thus, a simple expression for $N(T)$ can be obtained:

$$N(T) = 1/(1 + \Lambda(T)^2) \tag{12}$$

where $\Lambda(T)$ is the normalized slenderness ratio of columns defined by the following equation:

$$\Lambda(T) = \sqrt{\alpha_e P_p(T) / \alpha_p P_e(T)} \tag{13}$$

It is convenient to express $P_p(T)$ and $P_e(T)$ in terms of their respective values at ambient temperature $P_p(20)$ and $P_e(20)$: where $P_p(T) = \phi_p(T) P_p(20)$; $P_e(T) = \phi_e(T) P_e(20)$. Thus:

$$\Lambda^2(T) = [\phi_p(T) / \phi_e(T)] \cdot \Lambda^2(20) \tag{14}$$

Since

$$N(T) = N(20) / \phi_p(T),\ N(20) = \phi_p(T) / 1 + \frac{\phi_p(T)}{\phi_e(T)} \cdot \Lambda^2(20) \tag{15}$$

where $N(20)$ is the modified buckling coefficient at ambient temperature (T = 20°C) and $\Lambda(20)$ is the modified normalized slenderness ratio.

In Eq. (15), the terms ϕ_p and ϕ_e are the respective load reduction factors of plastic collapse load and elastic critical load, accounting for the material deterioration at elevated temperatures. Thus, $\phi_p(T) = P_p(T) / P_p(20)$ and $\phi_e(T) = P_e(T) / P_e(20)$. For steel columns, the plastic collapse load $P_p(T)$ is equivalent to its squashing load $f_y(T)A$, where $f_y(T)$ is the effective yield strength of steel at temperature T, and A is the cross-sectional area. The term $f_y(T)$ can be expressed in terms of its initial value at ambient temperature $f_y(20)$ by $f_y(T) = k_y(T) f_y(20)$, where $k_y(T)$ is the reduction factor for effective yield strength of steel at temperature T. This research adopts the EC3 material model for the values of reduction factors for strength $k_y(T)$ (Euro code 3: Part 1.2, 2003). There is no reduction in strength for steel less than 400°C, but beyond which it reduces rapidly. At 1200°C, steel ultimately loses all its strength and $k_y(T)$ is practically 0. Apparently, the following relationship can be established between $\phi_p(T)$ and $k_y(T)$:

$$\phi_p(T) = f_y(T)A / f_y(20)A = k_y(T) \tag{16}$$

On the other hand, the elastic critical load $P_e(T)$ is equal to the Euler buckling load:

$$P_e(T) = \pi^2 E_s(T) I / L_e^2 \tag{17}$$

where $E_s(T)$ is the elastic modulus of steel at temperature T; I is the second moment of area of the cross-section about its neutral axis; L_e is the effective column length taking account of different support conditions.

Once again, the term $E_s(T)$ can be expressed in terms of its value at ambient temperature $E_s(20)$ by $E_s(T) = k_E(T) E_s(20)$, where $k_E(T)$ is the reduction factor for elastic modulus of steel at temperature T. The value of $k_E(T)$ starts to reduce at a temperature of 100°C and eventually reaches 0 at 1200°C. It can be shown that:

$$\phi_e(T) = k_E(T) \tag{18}$$

Thus, the column failure load at ambient temperature $N(20)$ can be defined:

$$N(20) = k_y(T) / (1 + \frac{k_y(T)}{k_E(T)} \cdot \Lambda^2(20)) \tag{19}$$

2. DISCUSSIONS OF RESULTS FROM PROPOSED APPROACH & SAFIR

Generally, the reduction factors ϕ_p and ϕ_e are functions of the steel temperature T. Thus, $N(20)$ can be expressed as a function of steel temperature and column slenderness $\Lambda(20)$. For a given column, the magnitude of $N(20)$ and $\Lambda(20)$ can be estimated by performing simple structural analysis at ambient temperature. Thus, the column failure temperature can be determined graphically or by a trial-and-error method. Due to the scarcity of test data for columns subjected to biaxial loading, the proposed method was verified by SAFIR program. Fig. 1 shows the prediction of Rankine method for a group of steel columns (slenderness ratio from 22 to 271, load ratio from 10% to 80%, cross section from HE100A to HE500B, load eccentricity from (25mm, 25mm) to (100mm, 100mm)) subject to bi-axial bending under ISO 834 fire conditions. The results are compared with SAFIR predictions. It is found that the prediction of Rankine method is conservative and consistent. It is also found that the Rankine method can only be applied for steel columns with a slenderness ratio smaller than 200;, with higher slenderness ratio, the proposed method will give unsafe predictions compared with SAFIR. This is partly due to the increasing importance of secondary effect with increasing column slenderness ratio.

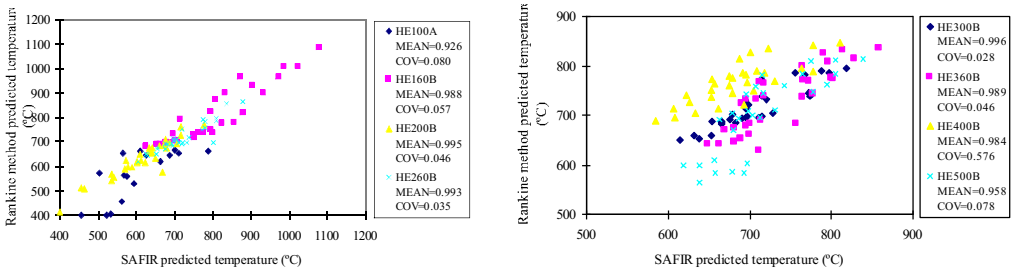

Fig. 1. Predictions of failure temperature for bi-axial loaded steel columns under standard fire conditions

After determining the column failure temperatures, Eq. (20) can be used to calculate the failure times of columns under standard fire conditions; this information can also be obtained from the New Zealand steel element design guide (NZS3404 1997):

$$t = (-4.7 + 0.0263T_R + \frac{1.67T_R}{A_m / V}) \tag{20}$$

where T_R is the temperature predicted from Rankine method; A_m is the exposed surface area of member per unit length; V is the volume of member per unit length.
Eq. (20) is valid in the temperature range of 500°C to 850°C, and has a limit for the size of the steel section factor, with the A_m / V value between 15 and 275 m^{-1}.

3. COMPARTMENT FIRE MODELLING

Up till now, there is limited research work conducted on natural fire conditions. It is useful to extend the proposed Rankine method for biaxially-loaded steel columns subjected to natural fire conditions. Fire modelling is required which takes account of actual fire load, ventilation conditions and thermal characteristics of compartment walls. In the absence of available test results for columns subjected to natural fire conditions, the authors used zone fire modelling program Ozone and finite element program SAFIR as benchmark tests as a basis of comparison with predictions from proposed approach based on Rankine. There are three

phases in the fire resistance calculations, viz. fire modelling, heat transfer and structural analysis. The benchmark tests consist of fire modelling using Ozone software. Through heat transfer process, the predicted thermal field is input into SAFIR to determine the mechanical responses of steel columns subject to elevated temperature. For heat transfer analysis, the authors proposed a simplified empirical formula (Eq. (10)), which incorporates heat transfer analysis directly into Rankine formula. The authors proposed Eq. (21) to predict the failure times of columns under natural fire conditions, considering the effects of fire load, ventilation factor and thermal properties of boundary walls. A compartment fire can basically be characterized by these three parameters. Similar to Eq. (10), Eq. (21) is obtained from least-squares regression analysis by curve fitting Ozone and SAFIR predictions to a large group of steel columns under different natural fire conditions.

$$t_{natural} = 0.9 Q_f^{-0.1} v_f^{-0.25} \Gamma \times t \qquad (21)$$

where Q_f =the fire load (MJ/m^2); v_f = the ventilation factor; $\Gamma = \sqrt{\dfrac{(v_f/0.04)}{(b/1160)}}$; $v_f = A_v\sqrt{H_v}/A_t$ (m$^{1/2}$); H_v = $(A_1H_1+A_2H_2+...)/A_v$; A_v = $A_1+A_2+...$; $b = \sqrt{c\rho\lambda}$ (J/m^{2}s$^{1/2}$K); A_v is the area of vertical openings (m^2); A_1, A_2…are the respective area of opening 1, 2… (m^2); H_v is the weighted average height of vertical openings (m); H_1, H_2…are the respective height of opening 1, 2… (m); A_t is the total area of enclosure, i.e., walls, ceiling and floor, including openings (m^2); c is the specific heat capacity of enclosure (J/kg K); ρ is the density of enclosure (kg/m^3); λ is the thermal conductivity of enclosure (W/m K), and t is obtained from Eq. (20) for standard fire condition. The predictions of the proposed method are compared and validated with numerical predictions from SAFIR and Ozone. The geometry, ventilation size and thermal characteristics of boundary walls of a fire compartment are given in Table 1.

Table 1. Geometrical and thermal conditions of the analyzed fire compartment

Compartment Length L_1	5.0 m
Compartment Width L_2	5.0 m
Compartment Height H_c	3.0 m
Ventilation Opening Height H_v	2.0 m
Ventilation Opening Width B_v	0.778, 1.556, 3.111, 4.667 m
Enclosing Boundary	Walls, ceiling and floor all of heavy concrete Density ρ 2300 kg/m^3 Specific Heat c 1230 J/kg K Thermal Conductivity λ 1.3 W/mK Thickness 0.200 m

A large pool of steel columns has been investigated. The columns have different slenderness ratios (from 22 to 271), load levels (from 10% to 80%), load eccentricities in both axes (from (25 mm, 25 mm) to (100 mm, 100 mm)). In addition, the compartment is subjected to a range of fire loads Q_f from 200 MJ/m^2 to 1200 MJ/m^2 and different ventilation factors v_f from 0.02 to 0.12. Predicted failure temperatures from the proposed approach (vertical axis) and SAFIR coupled with Ozone (horizontal axis) are given in Fig. 2a. Only the case of v_f=0.08 is presented in this paper. It shows that the Rankine approach is able to provide accurate and safe predictions of critical temperatures of steel columns under different heating conditions.

Based on Eq. (21), the failure times can be obtained. This information is useful for assessing the adequacy of evacuation of occupants in a fire compartment. From Fig. 2b, the proposed approach is conservative compared to SAFIR predictions but should not be applied to rooms with a ventilation factor less than 0.02, in which case, the method will give ultra-conservative predictions compared with numerical predictions using SAFIR (with Ozone). This is partly due to inaccuracy of zone modeling predictions within this range.

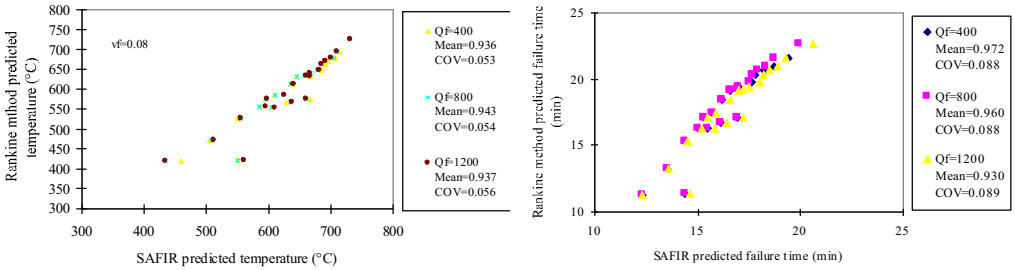

Fig. 2. Comparison of bi-axial loaded steel columns failure temperature and time under different heating conditions predicted by the proposed method and SAFIR (with Ozone modelling) (for the case of v_f=0.08)

4 CONCLUSIONS

A theoretical model based on Rankine method is proposed to predict the fire resistance of bi-axially-loaded steel columns under both standard and natural fire conditions. A large pool of columns with different slenderness ratios, load levels, eccentricities, cross sectional areas, and material strengths has been analyzed with Ozone and finite element program SAFIR. Comparisons of predictions between the proposed method and SAFIR (with fire curves predicted by Ozone) are performed. The results show that the proposed method can be safely applied for most fire curves and for different thermal boundary conditions.

5 ACKNOWLEDGMENT

The authors would like to acknowledge funding support from the ministry of education, Singapore, for research project titled “failure modes and ultimate strength of tubular joints under elevated temperatures” with account number arc 2/07.

REFERENCES

[1] Euro code 3 (2003). “Design of Steel Structures”. Part 1.1& Part 1.2 London: British Standard Institution.
[2] Gere, J.M. and Timoshenko, S.P. (2000). “Mechanics of Materials” 5th Ed. Chapman & Hall, London.
[3] Horne, M.R. (1979). “Plastic Theory of Structures”, Oxford: Pergamon Press Ltd.
[4] SNZ (1997), Steel Structures Standard NZS 3404: Part 1 & Part 2 1997, Standards, New Zealand Wellington.
[5] Tang, C. Y., Tan, K. H. and Ting, S. K. (2001). “Basis and Application of a Simple Interaction Formula for Steel Columns under Fire Conditions,” J. of Struct. Engrg., ASCE, 127, 1214 –1220.

COMPUTER PROGRAM FOR FIRE CHECK OF CONCRETE MEMBERS

Radek Štefan, Jaroslav Procházka

Czech Technical University in Prague, Faculty of Civil Engineering, Department of Concrete and Masonry Structures, Prague, Czech Republic

INTRODUCTION

Structural fire resistance is one of the most important requirements that have to be fulfilled by a structural design. Concrete has excellent fire resistance properties, but that does not mean that concrete and reinforced concrete (RC) structures are not adversely affected by a fire or high temperatures. According to the European Standard EN 1992-1-2 [1], if a mechanical resistance in the case of a fire is required, RC structures shall be designed and constructed in such a way that they maintain their load bearing function during the required time in fire exposure.

For a fire design of RC structures, a member analysis is usually sufficient. For the verification of members under fire conditions, tabulated data, simplified calculation methods or advanced (general) calculation methods are suitable. The member analysis by means of the tabulated data given in EN 1992-1-2 [1] is very simple, but it can be very conservative. Another objection that might be raised against the design using the tabulated data is that these data are valid for specific types of members and only for a standard fire exposure. Also, the tabulated method can't be used for a fire design of members with a protective layer (insulation).

For more realistic member analysis, simplified or advanced calculation methods may be used, provided that a temperature distribution through the cross section is known. Temperatures in RC members exposed to fire may be determinate from tests or calculations. As a simplification, the temperature profiles given in the Annex A of EN 1992-1-2 [1] may be used, but these profiles are valid only for members (slabs, beams and columns) exposed to the standard fire and the profiles can't be used for members with a protective layer.

In this paper, the computer program FRCB500 (**F**ire **R**esistance of **C**oncrete **B**eams – **500**°C Isotherm Method) for fire check of RC beams is described. A temperature distribution through a cross section to-be-checked is calculated by means of the finite elements method (FEM) using the material models suggested by EN 1992-1-2 [1]. A design resistance in the fire situation is determined by means of the 500°C isotherm method given in the Annex B.1 of EN 1992-1-2 [1]. The program may be used in a conjunction with both standard and parametric fires (see EN 1991-1-2 [2]) and it is possible to enter cross sections with a protective layer.

The program FRCB500 is developed in the MATLAB environment. It is a non stand-alone application (that means the program FRCB500 can't run without MATLAB), but presently, a stand-along version will be developed. The source files (so-called M-files) of the application FRCB500 are available in the Department of Concrete and Masonry Structures, Faculty of Civil Engineering CTU in Prague. Together with the program FRCB500, the application for fire check of RC slabs (FRCS500) was developed. Stand alone versions of the programs FRCB500 and FRCS500 will be available via the CTU web pages.

1 TEMPERATURE ANALYSIS

Before a fire resistance check can be performed, it is necessary to determine temperatures in the cross section to-be-checked. The dialog window "FRCB500 – Temperature Analysis" is shown in the *Fig. 1*. A user can define dimensions of a beam, properties of concrete, a thickness and properties of insulation (if the cross section is considered insulated), a design fire scenario, a fire exposure (two- three- or four-sided) and a time in fire exposure.

By means of the window "FRCB500 – Temperature Analysis", the temperature-time curve or the temperature profile can be displayed and the temperature in a point given by coordinates (x, y) can be calculated.

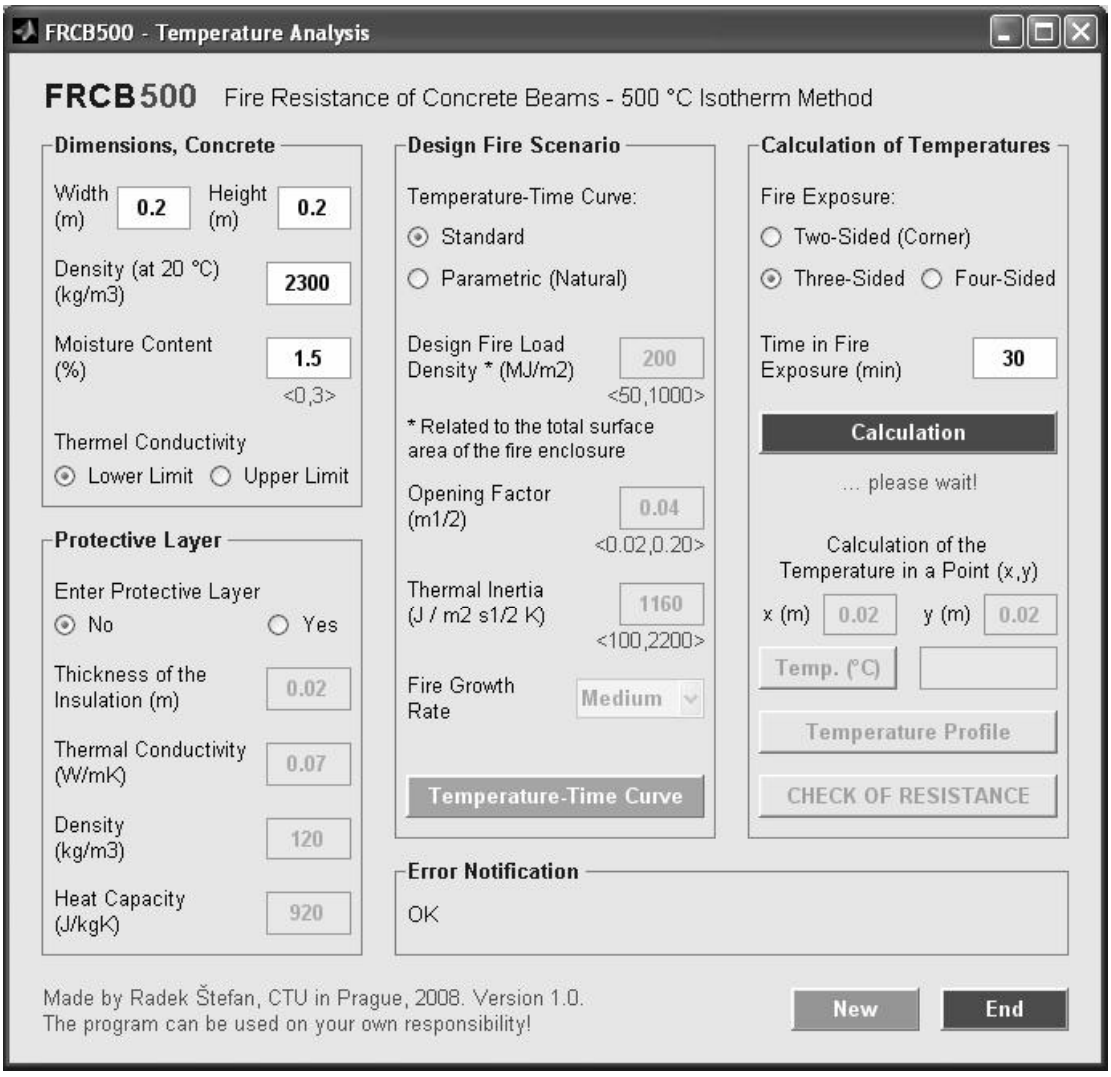

Fig. 1 Dialog window "FRCB500 – Temperature Analysis"

1.1 Dimensions, Concrete

The beam to-be-checked is given by a width, b (m), and a height, h (m), of the beam's cross-section.

Concrete is defined by a density at 20 °C, $\rho(20)$ (kg·m^{-3}), by a moisture content, u (% of concrete weight), and by a thermal conductivity, λ_c (W·m^{-1}·K^{-1}). The thermal conductivity is defined by means of the lower or upper limit suggested by EN 1992-1-2 [1]. A variation of a density with a temperature and a variation of a heat capacity (specific heat) with a temperature and with a moisture content is described in EN 1992-1-2 [1].

1.2 Protective Layer

If the cross section is considered insulated, the protective layer is given by a thickness of the insulation, d_{iz} (m), and by constant values of a thermal conductivity, λ_{iz} (W·m^{-1}·K^{-1}), a density, ρ_{iz} (kg·m^{-3}), and by a heat capacity (specific heat), $c_{p,iz}$ (J·kg^{-1}·K^{-1}). The protective layer is considered on all sides of the cross section that are exposed on fire.

1.3 Design Fire Scenario

A fire exposure is represented by the standard temperature-time curve (ISO 834) or alternatively by the parametric temperature-time curve given by a design fire load density, $q_{t,d}$ (MJ·m^{-3}), related to the total surface area of the fire enclosure, by an opening factor, O (m$^{1/2}$), by a thermal inertia, b (J·m^{-2}·s$^{1/2}$·K^{-1}), and by a fire road rate, according to EN 1991-1-2 [2].
Using the push button "Temperature-Time Curve", the design fire scenario is displayed (*Fig. 2a, b*).

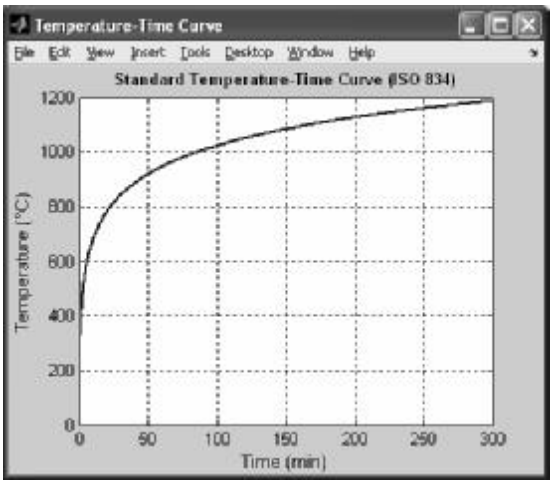

Fig. 2a Window with the standard temperature-time curve

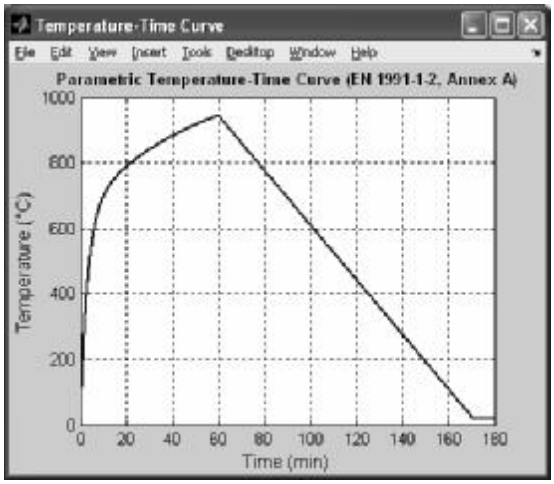

Fig. 2b Window with the parametric temperature-time curve

1.4 Calculation of Temperatures

At first, it is necessary to define a fire exposure (two-sided, three-sided or four-sided exposed cross section) and a time in fire exposure, t (min).
The temperature distribution through the cross section to-be-checked is calculated by means of the finite elements method (time approximation is based on the finite difference method).
The problem is solved as a one-dimensional heat transfer (finite element's dimension 10 mm). At first, it is calculated with respect to x, after that with respect to y. The temperature in a point (x, y) is given in *Eq. (1)*,

$$\theta(\mathrm{x},\mathrm{y}) = \theta(\mathrm{x}) + \theta(\mathrm{y}) - \frac{\theta(\mathrm{x})\cdot\theta(\mathrm{y})}{\theta(0)}, \qquad (1)$$

where θ(x,y) the temperature in the point (x,y),
θ(x) the temperature in the depth x of the "slab" with the width b (+insulation),
θ(y) the temperature in the depth y of the "slab" with the width h (+ insulation),
θ(0) the surface temperature.

The approximation given in *Eq. (1)* is explained in *Fig. 3*. The temperature distribution through the cross section is determined without taking into account steel bars. The reinforcement temperature is assumed to coincide with the concrete temperature in the same point.
Using the push button "Calculation" (see *Fig. 1*), the temperature analysis is started. After calculation, the temperature profile (or temperature field, see *Fig. 4a, b*) can be displayed and the temperature in the point given by coordinates (x, y) can be calculated. Also, using the push button "CHECK OF RESISTANCE", the window "FRCB500 – Check of Resistance" (see *Fig. 6*) is displayed.
As shown in *Fig. 5*, the temperature profiles provided by the program FRCB500 (for the standard fire) are in agreement with the temperature profiles given by EN 1992-1-2 [1].

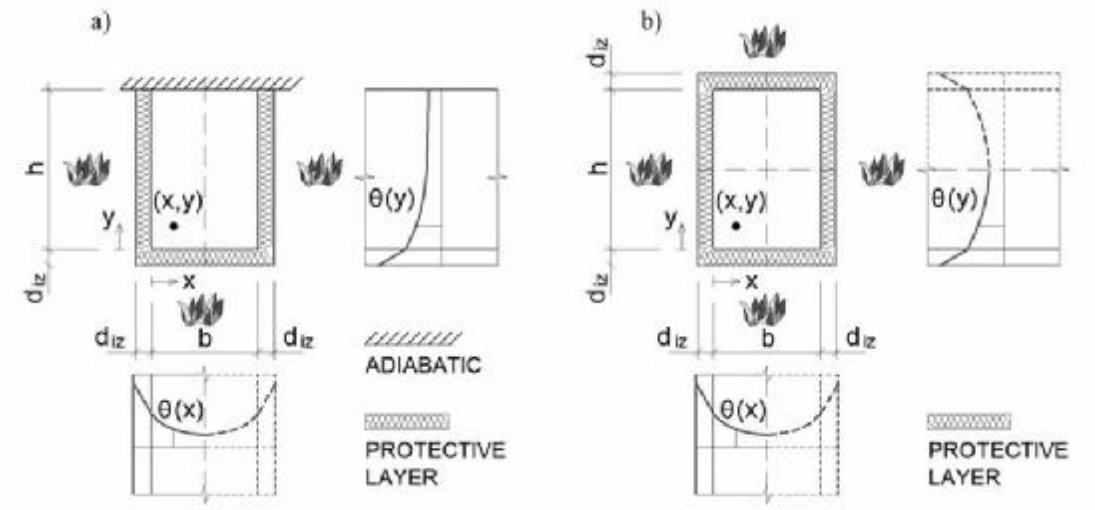

Fig. 3 Temperature analysis: a) three-sided exposed beam, b) four-sided exposed beam

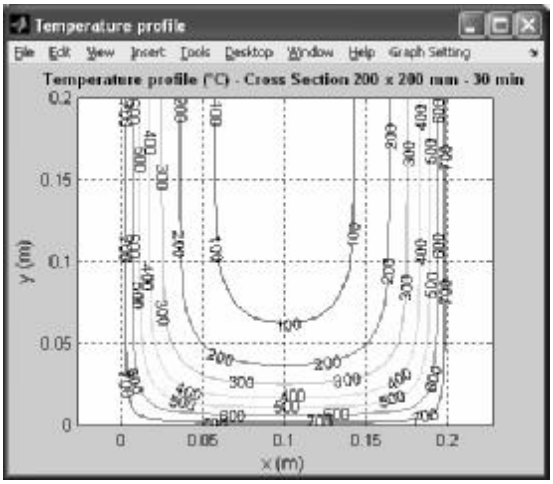

Fig. 4a Temperature profile

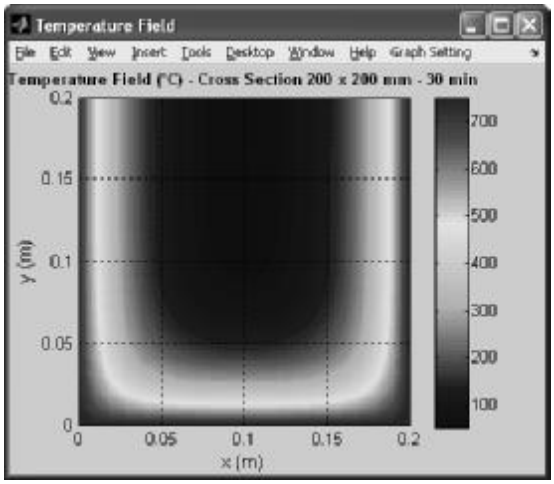

Fig. 4b Temperature field

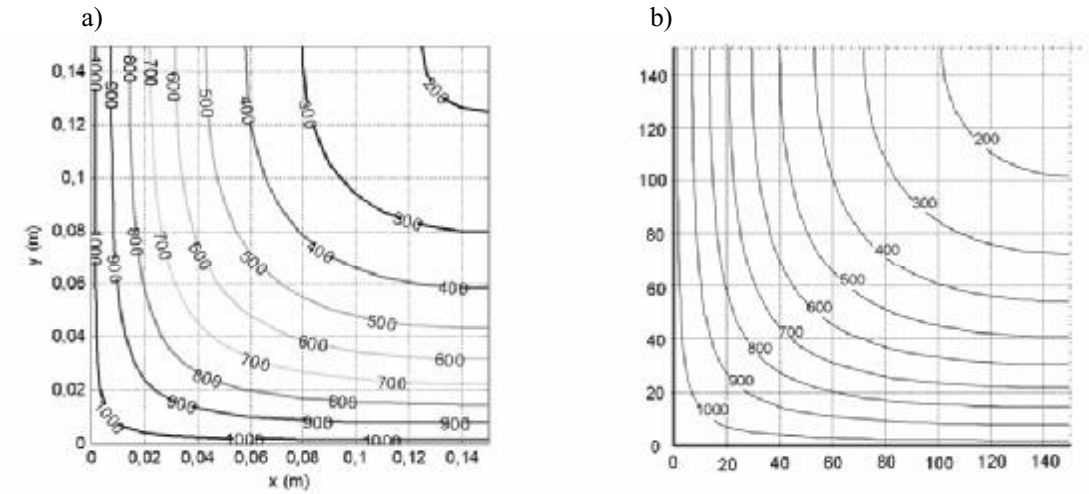

Fig. 5 Comparison of the temperature profiles for the cross section 300 x 300 mm, t = 120 min, a) FRCB500, b) EN 1992-1-2 [1]

2 CHECK OF RESISTANCE

It is possible to check only three- or four-sided exposed cross sections. Also, the requirements on a minimum width of the cross-section as a function of a fire resistance (for the standard fire exposure) or a fire load density (for the parametric fire exposure) have to be fulfilled. The dialog window "FRCB500 – Check of Resistance" is shown in the *Fig. 6*.

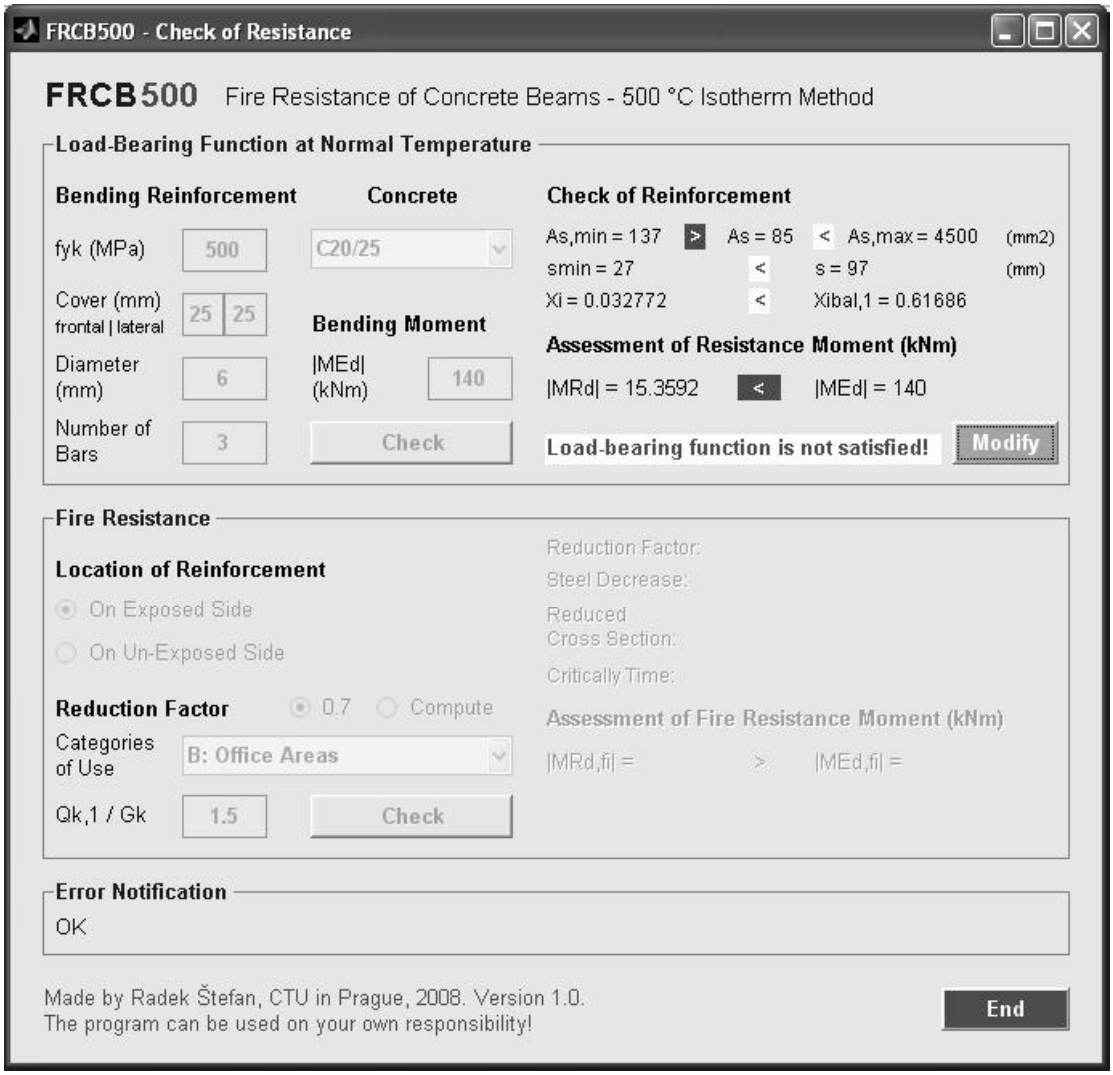

Fig. 6 Dialog window "FRCB500 – Check of Resistance"

2.1 Load-bearing Function at Normal Temperature

At first, an assessment of the load-bearing function at normal temperature is determined. The beam to-be-checked (see *Fig. 7*) is defined by a bending reinforcement (characteristic yield strength, f_{yk} (MPa), frontal cover, c_1 (mm), lateral cover, c_2 (mm), bar diameter, ϕ (mm), number of bars, n), by a concrete class, and by a design value of an applied internal bending moment (absolute value), $|M_{Ed}|$ (kNm). The assessment consists of verification of detailing rules and comparing the design bending moment with the moment of resistance, according to EN 1992-1-1 [3]. Outputs are displayed on the right part of the window.

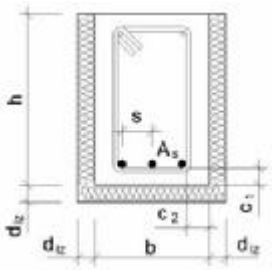

Fig. 7 Beam

2.2 Fire Resistance

The beam can be checked at fire situation, if all requirements at normal temperature are fulfilled. A design effect of actions for the fire situation (bending moment $M_{Ed,fi}$) is determined using a reduction factor η_{fi}. The reduction factor is computed using the equation (2.5) given in EN 1992-1-2 [1]. Alternatively, a value $\eta_{fi} = 0{,}7$ may be used.
The moment of resistance $M_{Rd,fi}$ is calculate using the 500°C isotherm method. The method is based on the hypothesis that a concrete at a temperature more than 500 °C is neglected in the calculation of the load-bearing capacity. Concrete at a temperature below 500 °C is assumed to retain its full strength. The strength of the reinforcement is reduced with the temperature according to EN 1992-1-2 [1]. For the standard fire exposure, the fire check is performed at the time t in the fire exposure. For the parametric fire exposure (if $t > t_{max}$), the fire check is performed at the time t_{max} (see *Fig. 2b*, t_{max} = 60 min) and than repeatedly in the interval 60 seconds, until the time t (or until the fire resistance is not satisfied). Outputs are displayed on the right part of the window (see *Fig. 8*).

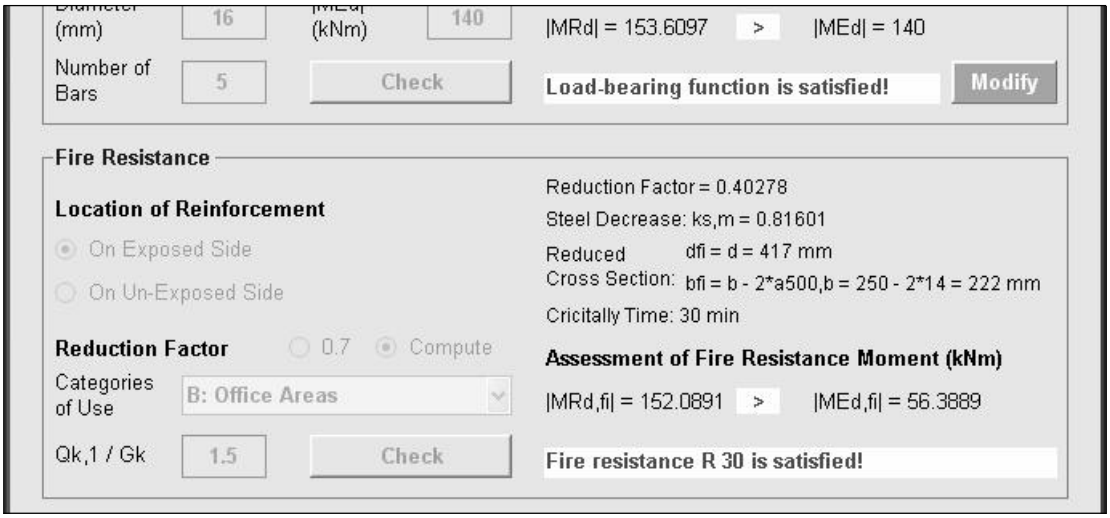

Fig. 8 Check of fire resistance

SUMMARY

Member analysis using the 500°C isotherm method is one of the methods suggested by EN 1992-1-2 for a verification of structural fire resistance of concrete members. The calculation method can be used provided that a temperature distribution through a cross section is known.
In this paper, the computer program FRCB500 for fire check of RC beams was described. A temperature distribution through the cross section to-be-checked is calculated by means of the finite elements method using the material models suggested by EN 1992-1-2 [1]. The program may be used in a conjunction with both standard and parametric fires. A design resistance in the fire situation is determined by means of the 500°C isotherm method given in EN 1992-1-2 [1].

This work was supposed by project MSM 6840770001.

REFERENCES

[1] Eurocode 2: Design of concrete structures – Part 1-2: General rules – Structural fire design (EN 1992-1-2). CEN, Brussels, 2004.

[2] Eurocode 1: Actions on structures – Part 1-2: General actions – Actions on structures exposed to fire (EN 1991-1-2). CEN, Brussels, 2002.

[3] Eurocode 2: Design of concrete structures – Part 1-1: General rules and rules for buildings (EN 1992-1-1). CEN, Brussels, 2004.

CONNECTIONS OF TRAPEZOIDAL SHEETS AT ELEVATED TEMPARATURE

Petra Kallerová, Zdeněk Sokol, František Wald

Czech Technical University in Prague, Department of Steel and Timber Structures, Prague, Czech Republic

INTRODUCTION

The behaviour of steel structure under fire situation differs from the behaviour under ambient temperature. The mechanical properties and the thermal expansion are changing with increasing temperature. Especially the yield stress and the modulus of elasticity have significant influence on the bearing capacity of steel members. This is significant especially for thin-walled elements. The corrugated sheet is able to transfer the bending moments at the early phase of the fire. The thermal expansion of steel leads to extension of the sheet and results in increased deflection. At this stage the bolted connection is loaded by forces induced by thermal expansion. At higher temperatures the bending moment resistance is reduced and major part of the load is transferred by tension membrane. At this moment the resistance and stiffness of the bolted connection has significant influence on the sheet behaviour. The connections transfer the membrane force to the supports. The performance of the connection is important also at the cooling phase of the fire.

The resistance of the connection is expressively influenced by the change of the mechanical properties of corrugated sheet. The increase of the temperature leads to the decrease of the yield stress and the modulus of elasticity of thin-walled cold formed steel members. The decrease of these mechanical properties leads to the reduction of the load bearing capacity of the structure. However, the ultimate strength is slightly increased for higher temperatures. The maximum strength is reached at 250 °C and the original value is obtained at about 350 °C. Additional increase of the temperature leads to decrease of the bearing capacity. For temperatures higher than 400 °C the yield stress on the force-deformation diagram is not visible. Buckling of the thin walled elements is influenced by reduced value of modulus of elasticity.

1 DESCRIPTION OF EXPERIMENT AND TESTED SPECIMENS

1.1. Experiments with screwed connections

It the laboratory of Faculty of Civil Engineering of Czech Technical University in Prague there were carried out two sets of tests with screwed connections under ambient and elevated temperatures. Within these experiments the mechanical properties of screwed connections at steady state conditions were determined. The steady state tests (SST) are faster and simpler in comparison with the transient state tests. The SST can be used for the prediction of behaviour under fire situation when the temperature is changing in time [1]. The experiments were focused on stiffness, resistance, deformation capacity and collapse mode of the connections during fire.

By this time, four sets of experiments were performed. In the year 2005 two sets of tests were carried out [2]. The set A was with screws E-VS BOHR 5-5.5x38 and sealed washer ø 19 mm, in the set B the same screws were used and the sealed washer was replaced by steel

washer with diameter 29 mm. The thickness of trapezoidal sheet for sets A and B was 0.75 mm. The next two sets of experiments were carried out in 2007 [3]. The tested screwed connections were made by self-drilling screws from carbon steel with marking SD8-H15-5.5x25 (set C and set D). Test specimens were cut out from the trapezoidal sheet with nominal thickness 0.75 mm. In the set of tests C the trapezoidal sheets with measured thickness 0.75 mm, width 75 mm and length 500 mm were tested. The specimens for the set of tests D were from measured sheet thickness 0.80 mm, width 50 mm and length 350 mm. The values of material properties of used trapezoidal sheet were obtained by material experiments. For measured sheet thickness 0.75 mm was the yield stress 338 MPa and ultimate strength 428 MPa, for measured sheet thickness 0.80 mm these values reached 327 MPa for the yield stress and 426 MPa for the ultimate strength.

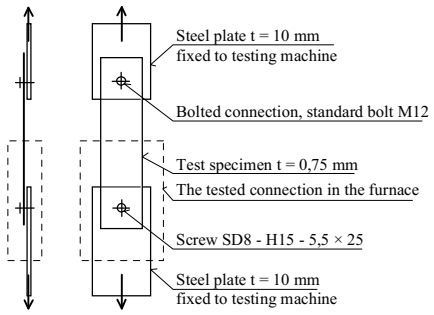

Fig. 1. The test set up

Fig. 2. The electric furnace for tests in 2007

In each sets of tests there were made experiments with two specimens for ambient temperature 20 °C and for constant elevated temperatures 200 °C, 400 °C, 500 °C, 600 °C and 700 °C. The steel sheets with thickness 10 mm simulated the bearing roof structure and they were anchored into grips of the testing machine, see Fig. 1. Due to these thicker sheets the force from testing machine to the specimens was transferred. The tested screwed joints were situated in the middle in the electrical furnace. The specimens tested in 2006 were heated in electric furnace with internal diameter 150 mm and height 300 mm. The temperatures of the connection were measured by thermocouple attached to steel sheet close to the bolt.

1 min 10 s *2 min 15 s* *4 min 15 s* *4 min 45 s*

Fig. 3. The deformation of the connection

The experiments from 2007 were carried out in a smaller furnace with one opening and internal dimensions 50x130x125 mm, see Fig. 2. The thermocouple for measuring the temperature of connection was located in a hole drilled in the screw head. The air

temperatures in the furnaces and the temperatures of the tested connections were measured by one thermocouple. The electrical furnace had one opening which was filled with glass with high temperature protection. During the fire tests there was the possibility to see the behaviour and the deformation of the tested connections. In the course of the experiments the photo documentation in interval 5 seconds was provided. On Fig. 3 you can see four photos which were taken during one of the tests. The edges of the specimens were marked at the spacing 5 mm for displacement measurement. The constant rate of movement was established.

1.2. Experiment with the trapezoidal sheet and its catenary action

In 2007 in the laboratory of PAVUS in Veselí nad Lužnicí there was provided one fire experiment for check of the catenary effect of the thin-walled trapezoidal sheet. The specimen for fire experiment was from the trapezoidal sheet with sheet thickness 0.75 mm and the height of the waves was 55 mm. This sheet was put above the furnace with diesel burners. The specimen was fastened by self-drilling screws SD8-H15-5,5x25 to the bearing steel frame which was made from HEB200 profiles. The inner dimension of this frame was 800 x 3000 mm. In each lower wave of trapezoidal sheet two self-drilling screws were used. The frame was protected by the thermal insulation against the effect of the high temperatures.

Four rectangular iron plates with thickness 30 mm, dimensions 450 x 580 mm and weight 60 kg each were used as the mechanical load. The total load on the tested specimen was 240 kg which corresponds to 1 kN/m^2. The iron plates were uniformly distributed on the trapezoidal sheet. The distance between the load and the edge of the specimen was 300 mm and the distance from each other was 200 mm. On Fig. 4 there is a view of the tested specimen before the fire experiment. There can be seen the trapezoidal sheet, the mechanical load, the bearing frame and the thermal insulation of the whole specimen.

Fig. 4 The tested specimen before fire experiment

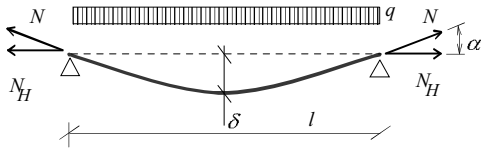

Fig. 5 The catenary action on simply supported beam

The thermocouples and a vertical deflectometer in the half of the span of the simple beam were located directly on the sheet. The thermocouples were placed in the midspan and in the quarter of the span of the trapezoidal sheet, three on the screws and three near the screws on the sheet. Two thermocouples were used for measuring the gas temperature in the furnace; they were placed at the distance of 350 mm from the upper surface of the upper wave of the sheet.

2 RESULTS OF EXPERIMENTS

2.1. Experiments with screwed connections

The resistance of the connection with sealed washer (set A) was limited by bearing resistance of the thin sheet. The sealant washer does not have any influence on the behaviour because the sealant burns at higher temperatures. The stiffness of the connection with steel washers (set B) was much higher and the resistance was almost doubled compared to the previous set. The thin sheet was deformed and accumulated in front of the washer which was accompanied by creation of two shear zones on both sides of the washer, see Fig. 6. This failure mode is characterized by deformation capacity larger than 30 mm. However, at temperatures higher than 500°C shear failure of the bolt was observed, see Fig. 7.

Fig. 6. The collapse mode of connection from the set B, temperature 200°C

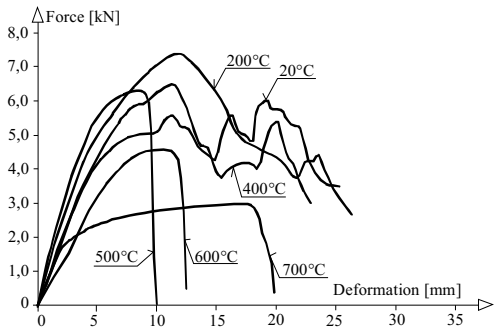

Fig. 7. The force-displacement diagrams of the screwed connections from the set B

On Fig. 8 there is the force-deformation diagram of the connections from set D and the collapse mode for connection from set C is on Fig. 9. For all specimens with the measured thickness of sheet 0.75 mm the failure in bearing was reached which occurred by tearing of trapezoidal sheet. Two modes of failure were observed for the sheet thickness 0.80 mm. For the temperatures from 20°C to 600°C the failure of sheet in bearing occurred, whereas for the temperature 700°C the mode of failure was the shear failure of the screw.

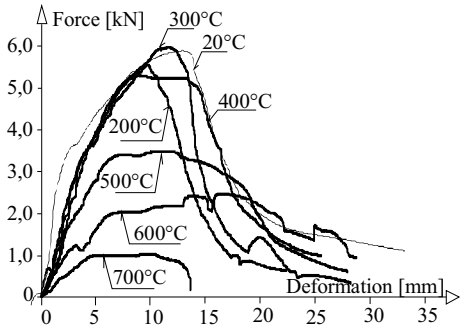

Fig. 8 The force-displacement diagrams of the screwed connection from the set D

Fig. 9 The collapse mode of the connection from set C, temperature 200°C

In the initial phase of loading the elastic behaviour can be seen. Then the force was increasing until the maximum bearing capacity was achieved and the tearing of sheet occurred. In the next phase of force-deformation diagram the decrease of force can be noticed. Due to

accumulation of deformed sheet in front of the screw the increase and subsequent decrease of force can be seen on the diagram. The deformation capacities of connections were high. Due to the dimensions limits of the electrical furnace all the experiments were terminated before their ultimate failure, but after the exhaustion of the residual bearing capacity.

The results of these experiments show how the temperature increase leads to decrease of the bearing capacity of the connections. For the temperature 550°C is the bearing capacity of the connection reduced approximately to half of the bearing capacity under ambient temperature and for the temperature 700°C the bearing capacity is less than 20% from the bearing capacity under the ambient temperature. The reduction of 45% for temperature 500°C and 90% for 700°C is used for calculations of connections with bolts and nuts. The experiments confirm the higher reduction of the resistance of the self-drilling screws in bearing in the initial phase of heating (up to temperature 550°C) and smaller reduction for higher temperatures. These two things mentioned above lead to unfavourable brittle failure of connection in shear [4]. Temperatures lower than 500°C don't have significant influence on the initial stiffness of the connection. The deformation capacity for higher temperatures is reduced by failure of the screw in shear. This mode of failure occurred only for screwed connection with the sheet thickness 0.80 mm and temperature 700°C.

2.2. Experiment of the trapezoidal sheet and its catenary action

The fire load was modelled by multilinear fire curve which simulated fire load used for the fire tests in Cardington. The usage of the similar fire curves is helpful for subsequent comparison of the results from different fire experiments. The maximum measured gas temperature in the furnace was 1096°C. This value was reached in the 55.minute, the total length of fire experiment was 2 hours. The temperature of the trapezoidal sheet above the support was 447°C and this temperature is about 58% lower than temperature of the trapezoidal sheet in the midspan (1084°C), see Fig. 10. In case of unprotected load bearing structure the temperature would be higher.

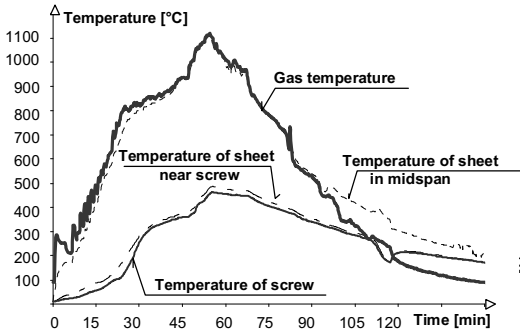

Fig. 10 The measured temperature on the specimen

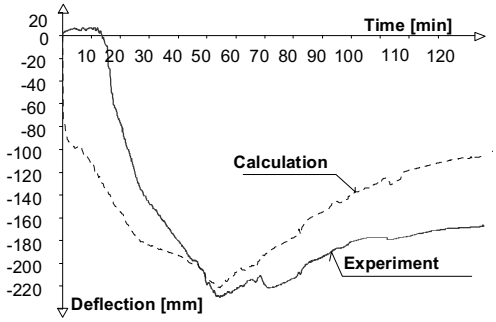

Fig. 11 The vertical deformations in midspan of trapezoidal sheet

The behaviour of trapezoidal sheet during fire experiment was quite the same as the behaviour of simple beam on which the elongation is restrained. At the beginning of the fire test the temperatures are low and the trapezoidal sheet isn't deflecting by the influence of the temperature. The sheet is elongating in its plane and the screws in supports are loaded in shear. As the temperature increases, the extension as a result of the thermal expansion of material occurs and the yield stress and the modulus of elasticity decrease. As a result of these effects the deflection is increased. By increase of the deflection and decrease of bending

stiffness there is a change of tensile forces in the supports and the sheet starts to behave like a tensile membrane. This effect is known as catenary action. On Fig. 5 there is a scheme of catenary action on simply supported beam.

The collapse of structure depends on the bearing capacity of the connections and on the ability of the load bearing structure to carry the tensile forces. On Fig. 11 there is a comparison of the deflection as a function of time for the values calculated by equations and those obtained during the experiment. The comparison of maximum deflections and the times where the deflection are obtained are in a good agreement. The maximum measured deflection of trapezoidal sheet was 229 mm, the calculated vertical deformation was 222 mm.

3 SUMMARY AND ACKNOWLEDGMENT

Resistance of the connection in relation to temperature is shown on Fig. 12. Resistance is reduced at higher temperatures; the reduction is small at temperatures up to 400°C but significant at temperatures higher than 500 °C. The diameter of the washer or of the screw head has significant influence on the resistance. The resistance of screwed connection from set A is approximately 40 % lower than resistance of the screwed connection from set D. When the connection from set B is used the resistance is similar to connection from set C. Shear failure of the screw may lead to low deformation capacity at temperature higher than 500 °C. These experiments will be used for development of design model of the connections at high temperatures.

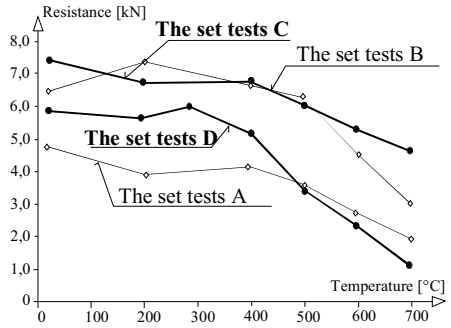

Fig. 12. The resistance of the connections

By the experiment with trapezoidal sheet supported like a simple beam the catenary action was confirmed. High fire resistance of the trapezoidal sheet which depends on suitable design of screwed connection to bearing structure was also confirmed.

This outcome has been achieved with the financial support of the Ministry of Education, Youth and Sports, project no. 1M0579.

REFERENCES

[1] Outinen J., Mechanical properties of structural steels at high temperatures and after cooling down, *Espoo*, 2007.

[2] Sokol, Z., Design of Corrugated Sheets Exposed to Fire, Progress in Steel, *Composite and Aluminium Structures*, 2006.

[3] Kallerová, P., Experiments with bolted connections – experiments at normal and elevated temperatures, *research report CTU in Prague*, 2007.

[4] Wald, F. et al., Calculation of the fire resistance of structures, CTU in Prague, 2005.

STRUCTURAL ANALYSIS OF STEEL STRUCTURES UNDER FIRE LOADING

Chiara Crosti, Luisa Giuliani, Konstantinos Gkoumas, Franco Bontempi
University of Rome "La Sapienza", School of Engineering, Rome, Italy

INTRODUCTION

This paper builds on assumptions and findings from a second paper presented at the same conference [1], and focuses on the structural analysis of steel structures under fire loading. The use of analysis with thermo-plastic materials and with geometric nonlinearities and the modelling of the fire action using parametric curves, allow the faithful evaluation of the effective behaviour of steel structures subject to fire. In this context, once these two basic aspects are clarified, they are applied in steel structures under fire loading. For these structures the collapse can be quantified when they are subject to localized fire, modelled using a parametric curve. The evaluation of the structural collapse is very tricky and depends from many aspects; in particular, in a Performance Based approach for buildings subject to fire, it is important to consider the global vision of the structure itself. The prescriptions derived by the exploitation of the Fire Safety Engineering, come as an aid to the above.

1 CONSIDERATIONS ON THE PERFORMANCE BASED APPROACH

The European Standard [2] classifies the fire action as an accidental action, intended as an action occurring after an accident. In the above sense, the design of a structure subject to fire must highlight the capacity of the structural system in achieving the objective of safety related to different performance levels. The designer is called to make a responsible choice of the performance to assign. This liberty of decision allows finding the more effective solution, one that avoids useless operations, which is the case of when following a prescriptive approach.
It is common, when assessing the performance of a structure subject to fire, to define a conventional collapse connected to the typology of structural elements and to the function that each element must perform.
It is important though to highlight that the performance based approach is not easy and immediate as is the case of a prescriptive approach. In fact, the latter approach involves the understanding of the safety levels and the accomplishment of a precise prescription and in this sense it seems to be easy to apply. On the contrary, the performance based approach requires specific knowledge from the designer. Moreover, another important difference between these two kinds of approaches is that the prescriptive one divides the situations in "checked" or "not checked", while the performance one allows to graduate the consequence on the structure and to the persons, in function of accepted risk levels.
A step very important to guarantee a determinate level of safety is to verify that the resistance of the structure under fire loading is higher than the fire severity (fire resistance > fire severity). In the particular case of steel beams, it is possible to define the conventional collapse when, the maximum vertical displacement of one node of the element, becomes equal to L/20, where L is the length of the beam. The temperature and the time of fire exposition corresponding to this displacement are defined as the critical temperature and time for the considered element.

2 STRUCTURAL ANALYSIS OF STEEL STRUCTURES UNDER FIRE

In this paragraph the structural behaviour of two steel structures is investigated. The structures under inquiry, although both in steel, characterised by distinctive features due to their different construction and complexity, the first one being a simple frame structure, while the second a somewhat more complex structure in truss.
Objective of the analyses is, in a first place, to highlight some of the peculiar effects arising from the fire loading, and to some extend, provide a starting point for the characterisation of the collapse resistance of the structures. The performed analyses (implemented in commercial FEM codes) account for the material and geometry nonlinearities, thus being able to accurately describe the actual behaviour of the structure.
In both cases, some aspects of the process are common. In order to assess the safety of these structures in case of fire, for the specific case, the performance level that does not contemplate collapse for all the duration of fire has to be guaranteed. As a consequence, in order to evaluate the fire resistance, a check is done by modelling the fire action using the nominal standard curve (ISO834) provided by [2]. This curve has been applied only to the elements directly involved to the fire action. Thus, the (localized) fire interests a limited area of the whole structure, in which, the release of heat, remains concentrated in the area itself.

2.1 Structural analysis of a single storey steel framed open deck car park under fire

The structure under inquiry is a single storey steel framed open deck car park. The facility shown in *Fig. 1*, is 32 meters long, 15 meters wide and has a maximum height of 3 meters. The deck consists in three rows of primary beams supporting seven rows of secondary beams, while the vertical elements are contemplated by appropriate steel braces.

Fig. 1. Picture of the steel framed car parking under inquiry

The FEM of the structure (modelled in STRAND® [3]) can be seen in *Fig. 2*.

Fig. 2. Finite element model of the structure

Due to the simplicity in the configuration of the structure and of its particular utility, a comprehensive risk analysis has not been performed, thus being the fire scenarios identified during a process of preliminary risk analysis. For the sake of brevity, only one fire scenario is briefly presented (refer to [4] for further analyses), the one involving three vehicles eventually catching fire in the proximity of the intermediary of the primary beams, in the area delimited by the four external secondary beam rows (*Fig. 3*), with two columns influenced by the fire.

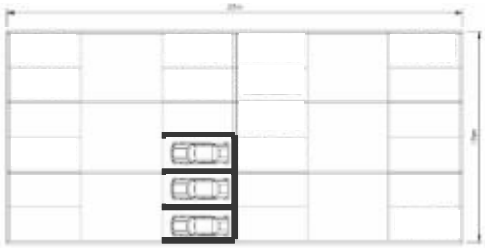

Fig. 3. Deformed configuration of the structure

The vertical displacements in time of a node at the middle of the beam in correspondence to the central column is shown in *Fig. 4*. As can be seen various phases can be identified. In a first phase, the terminal excursion leads to the uplifting of the node. This terminates at about 600 sec. after the fire ignition, with the column abruptly failing due to buckling in two distinct time points. Part of the displacement has to be attributed to the thermal bowing effect (see for example [5]) resulting from differential thermal expansion over the cross-section of the non-uniformly heated supported beam.

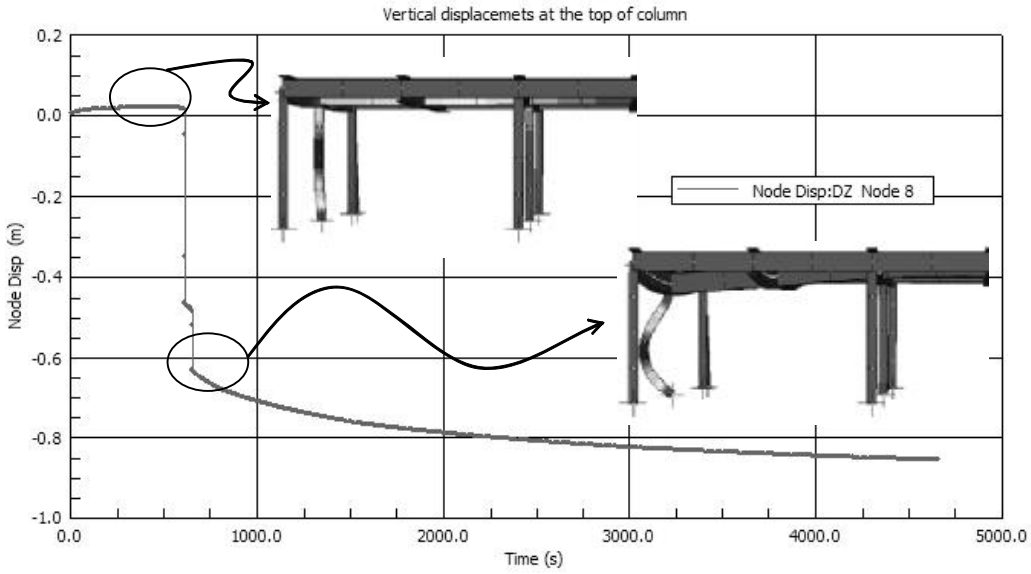

Fig. 4. Vertical displacements of a node of the column and corresponding deformed shape

The column continues to sag, leading to the final configuration of *Fig. 5*, where the inner column is also deformed.
For the sake of brevity, at this point, no further considerations are made on the front of the collapse resistance of the structure.

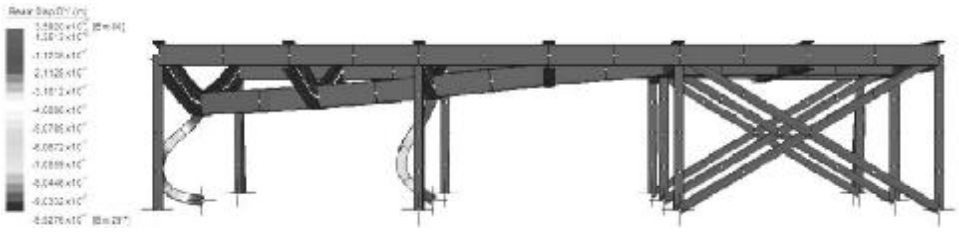

Fig. 5. Deformed configuration of the structure

2.2 Structural analysis of an industrial facility under fire

The structure under inquiry is an industrial facility in steel, used for the storage and maintenance of helicopters, therefore it presents with an elevated fire risk. The facility is 64.64 meters long, 32.85 meters wide and has a maximum height of 12.9 meters as shown in *Fig. 6.*

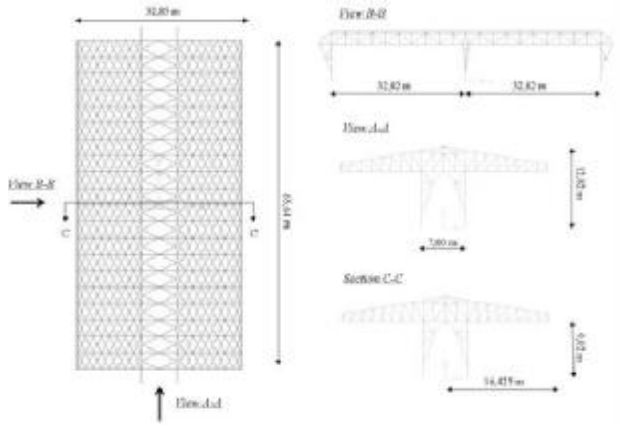

Fig. 6. Geometry of the facility

This facility presents a relatively complex geometry. The structure is isolated, it presents symmetry both in the x and in the y direction and it has a truss covering. There are six vertical elements, composed by a block of concrete at the end of these, start steel elements, those composes the column.

Some initial considerations are necessary on the front of the structural dependability of the facility [6], in terms of collapse resistance [7]. If a structure is redundant, then there are many alternative load paths, large deformations can develop without a loss of its load bearing capacity, and structural failure must be accounted for in a different way. This phenomenon creates sufficient reserve capacity to allow most of such structures to survive fires with little structural damage. For the above reason, it is important to make some considerations about the facets of structural collapse. It is possible to verify that the collapse of a single metal bar, although of a certain significance, doesn't compromise the global behaviour of the whole structure. Therefore, the local collapse of a single (or a limited number) of the covering bars has to be dealt with differently compared to the collapse (or loss of resistance) of the vertical elements (columns) which do not offer redundancy in this building. The collapse can be evaluated as a function of the global behaviour of the whole structure, assigning particular importance to the more resistant elements, and after that, to the columns.

To evaluate the fire resistance of this structure, three fire scenarios are considered, as indicated in [1]. For the sake of brevity, only the 1st scenario is presented, in which fire is concentrated in the central zone of building, involving also the central columns. However, similar considerations can be made for the 3rd scenario, considering the nodes of the extreme columns subject to fire (presented in [8]), while results referring to the 2nd scenario are omitted since this scenario doesn't involve the columns, therefore, it doesn't lead to structural collapse. FEM analyses are performed on the ADINA® [9] commercial code, and involve a large engagement in terms of time and memory on the computer: for example, for the specific model with 1205 nodes, corresponding to 7230 degrees of freedom, the analysis lasts five hours with a normal processor. Particular attention is given also to the static scheme of this structure, composed by a reticular covering and it is so very redundant, as shown in *Fig. 7*.

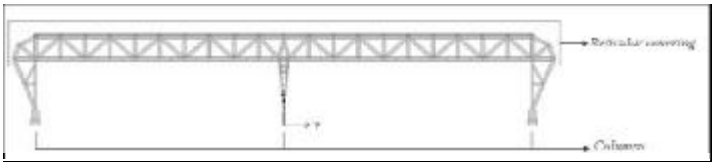

Fig. 7. Identification of the structural elements of the building, view B-B

The trend of the node displacement corresponding to the column affected by the fire is reported referring to the 1st scenario (*Fig. 8*). For this scenario, the trend of one node of the central column is evaluated.

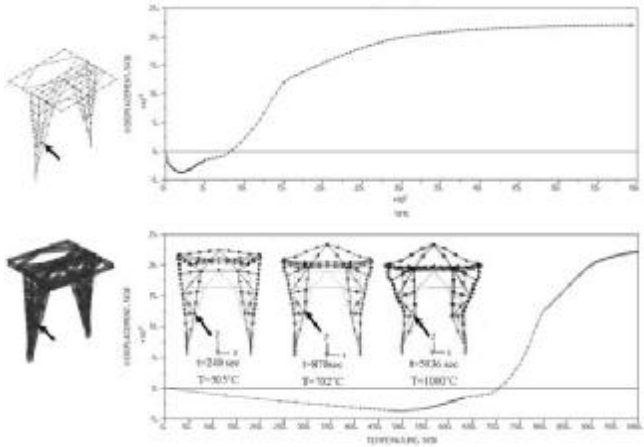

Fig. 8. Displacements of a node of the column along the x axis

For this trend a point of discontinuity seems easily to single out. In fact, after 800 seconds, which corresponds to a temperature of approximately 700°C, the trend of displacements of the x axis of the node goes through negative values, for the effect of temperature that initially produces large thermal expansion, to positive values.
This passage is due to loss of stiffness and resistance produced by the elevated temperature, in this way the element starts to skid towards the weakest direction. From what said, it is not possible to suggest that after 13 minutes the structure collapses, but it is reasonable to think that over this time limit, the column suffers a modification of stiffness and resistance that, in a Performance Based approach, highlights the possibility that the safety of the structure cannot be guaranteed.

In *Fig. 9* and *Fig. 10* the initial and deformed configurations along the x and y axis are shown, with reference to this scenario.

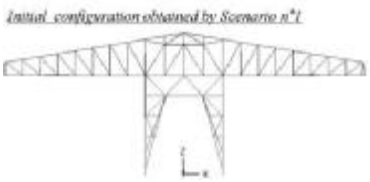

Fig. 9. Initial configuration, view A-A

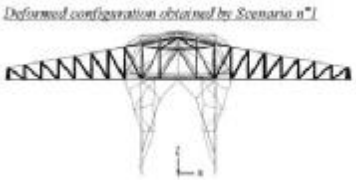

Fig. 10. Deformed configuration, view A-A

From these considerations it is possible to conclude that for the scenarios involving the columns, after 800 seconds, which correspond to a temperature of 700°C, the structure shows an abrupt change in stiffness, and therefore, this temperature represents a critical state that can make this structure less safe regarding to its stability.

3 CONCLUSIONS

In this paper, some initial thoughts about the performance of two distinctive structures under fire loading are presented. To this aim, the application of nonlinear analysis on the thermo-mechanic behaviour of materials and on the structures as a whole, together with the appropriate fire modelling in pragmatic scenarios, consents to demonstrate and verify the performance of the structure in terms of resistance to fire during the design phase.
The effective behaviour of steel structures subject to fire is rather complex, and therefore, their evaluation must to be assessed considering the global behaviour of the structure, considering also that the definition of collapse of a structure is connected to many aspects.

REFERENCES

[1] Gkoumas, K., Crosti, C., Giuliani, L., Bontempi, F. Definition and selection of design fire scenarios. Book Proceedings: Applications of Structural Fire Engineering, Prague 19-20 February 2009.

[2] Eurocode 3 - Design of steel structures, Part 1.2: Structural fire design, Commission of the European Communities, Brussels, 1993.

[3] STRAND®, www.strand7.com

[4] Crosti, C., Bontempi, F., Benchmarching/Betatesting di codici di calcolo utilizzabili per l'analisi strutturale in caso di incendio (in Italian), available online on 01/2009 at http://dx.medra.org/10.3267/HE2008

[5] Cooke, G.M.E., Morgan, P.B.E., Thermal bowing in fire and how it affects building design, BRE Information Paper 21/88, Building Research Establishment, 1988.

[6] Bontempi, F., Giuliani, L., Gkoumas, K., Handling the exceptions: dependability of systems and structural robustness, in Recent Developments in Structural Engineering, Mechanics and Computation, Alphose Zingoni (Ed.), Millpress, Rotterdam, 2007.

[7] Starossek, U., Wolff, M., Design of collapse resistant structures, Workshop on robustness of structures (JCSS and IABSE), November 28-29, 2005.

[8] Crosti C., Bontempi F., Safety performance evaluation of steel structure under fire action by means of nonlinear analysis, in Proceedings of the CST2008 & ECT2008 Conferences, Athens, 2-5 September 2008.

[9] ADINA®, www.adina.com

CONNECTION TEMPARATURES DURING THE FIRE TEST IN MOKRSKO

Jiří Chlouba, František Wald

Czech Technical University in Prague, Department of Steel and Timber Structures, Czech Republic

INTRODUCTION

The fire test in Mokrsko was focussed mainly to the overall behaviour of the structure and the connection temperatures, both of which may not be observed on the separate elements. Except for the three types of flooring systems, six wall structures with mineral wool were tested.

The fire experiment was conducted in Mokrsko in Central Bohemia, Czech Republic, 50 km south from Prague 18 September 2008, see [1]. The new building was made in front of the Czech technical University in Prague educational centre Joseph gallery, see www.uef-josef.eu. The experiment follows the seven large fire tests in Cardington laboratory on steel frame from 1998 – 2003, see [2]. During the experiment were used the knowledge learned during the Ostrava fire test, see [3] and [4] as well. The structure was designed by the design office EXCON a.s. Prague with cooperation of the all parties involved into the structural parts delivery. The fire design of the structure was prepared at Czech Technical University in Prague, The University of Sheffield and Slovak Technical University in Bratislava. The behaviour of slender castellated beams and beams with the corrugated web were simulated including the concrete slab and the connection behaviour at the elevated temperature by the VULCAN programme.

Fig. 1 Experimental building

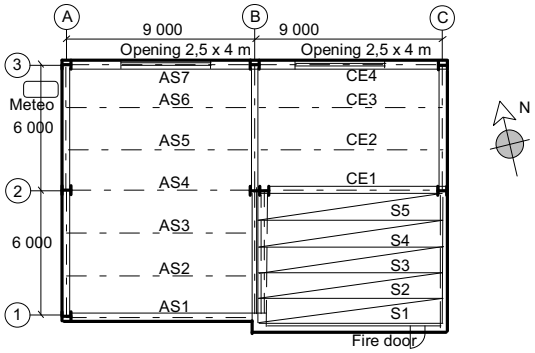

Fig. 2 Plan view of the structure

1 EXPERIMENTAL STRUCTURE

The structure represents one floor of the administrative building of size 18 x 12 m, see Fig. 1 and Fig. 2. The composite slab on the castellated beams was designed with a span 9 to 12 m and on beams with corrugated webs with a span 9 to 6 m. The deck was a simple trapezoidal composite slab of thickness 60 mm with the height over the rib 120 mm with sheeting CF46 (Cofraplus 0.75 mm) and concrete of measured cubic strength 34 N/mm^3 in 28 days reinforced by a smooth mesh ø 5 mm 100/100 mm, with strength 500 MPa and coverage 20 mm. The prefabricated panels Spiroll of height 320 mm with hollow core openings formed a span 9 m. The panels were supported by concrete wall and primary hollow beam from the welded double IPE 400 section. The height of the castellated beams with sinusoid openings

Angelina, design by ArcelorMittal, made of IPE 270 section from steel S235 was 395 mm. The beams with corrugated webs, design by Kovové profily s.r.o., have flanges 220 x 15 mm and web 2.5 mm thick with height 500 mm steel S320. The edge beams were from sections IPE 400 steel S235. The fire protected columns were prepared from HEB 180 sections. The horizontal stiffness of the frame was reached by concrete walls with 250 mm thickness made of concrete C30/37 and two cross braces of L 80x80x8. The beam to beam and beam to column connections were designed as header plate, plate 10 mm with four bolts M16 class 8.8. The improved fire resistance was reached by encasing two bolts in the concrete of the slab.

Two walls were composed from cladding, linear trays, mineral wool and external corrugated sheets. In two 6 m spans was compared the system with the internal grid and horizontal sheeting and with vertical sheeting without the internal grid. Two other walls were made of sandwich panels of thickness 150 mm filled with mineral wool. In front of the concrete wall was a brick wall made of plaster blocks. The fire protection of columns, primary and edge beams as well as bracings was designed for R60 by board protection 2 x 15 mm Promatect H.

2 MECHANICAL AND FIRE LOAD

Mechanical load was designed to comply with regular administrative building. The dead load of tested structure reached 2.6 kN/m^2. The variable load 3.0 kN/m^2 was simulated by 78 sand bags with road metal. The weight of the bags varied from 793 kg to 1087 kg. They were coupled on pallets by three to reach an average weight 900 kg, see Fig. 3. The applied load represented the characteristic value of the variable action at elevated temperature 3.0 kN/m^2 and the characteristic value of flooring and partitions 1.0 kN/m^2.

Fig. 3 Position of mechanical load

Fig. 4 Distribution of fire load

The 15 m^3 unwrought wooden cribs 50 × 50 mm of length 1 m of softwood dried to moisture till 12% represented the fire load. The cribs were placed into 50 piles, see Fig. 4. Each pile consisted of 12 rows with 10 cribs, which means 35.5 kg/m^2 of timber and simulates the fire load 620 MJ/m^2. The design characteristic fire load of administrative building is calculated as 420 MJ/m^2. The simultaneous ignition of piles was reached by their connection by the steel thin-walled channels filled by a mineral wool and penetrated by paraffin. The channels were located on the second layer of cribs and connected three/four piles together. The fire test starts by reaching the gas temperature 50 °C. The openings of height 2.54 m and total length 8.00 m with parapet 1 m ventilated the compartment. To allow a smooth development of fire no glazing was installed.

Fig. 5 Thermocouples for gas and steel temperatures

Fig. 6 Thermocouples on beam to column connection

3 MEASUREMENTS

The gas temperature in the fire compartment was measured by 14 jacketed 3 mm thermocouples located 0.5 m below the ceiling in the level of the beams lower flanges, see Fig. 5. Two thermocouples were placed in the openings. The temperature profile along the compartment height was measured between the window and in the back of the fire compartment below the secondary beam. For measuring the temperature of the structure 2 mm jacketed thermocouples were used. In the composite slab were designed 12 thermocouples, on beams 11, in bolted connections 37, see Fig. 6, in the hollow core panels 6, in concrete wall 16, in external cladding 24, in the fire protected internal column 7, and on the external column 24. On the West linear scaffold a meteorological station was installed to record the external temperature and the wind direction and its speed. The behaviour was documented by photographs, video and thermo imaging records.

3.1 Temperatures

The prediction of the gas temperatures by the parametric fire curve and by the zone model expected conservatively in 60 min of the fire the temperature 1057 °C, see Fig. 7. Under the composite slab with castellated beams was measured in 60 min the temperature 935°C. At the beginning of the fire the highest gas temperatures were reached in the front of the fire compartment and during the full developed fire in the back of the fire compartment. The East and West part of the compartment showed different temperature development. In the Eastern part of the fire compartment with the concrete wall reached in 21 min temperature 810°C, in 30 min temperature 935°C, and in 58 min temperature 855°C. In the Western part of the fire compartment the developed gas temperature was very similar to the nominal standard fire curve [5]. The temperatures in both parts of the fire compartment were different due to the different walls and a small change in the wind direction during the test.

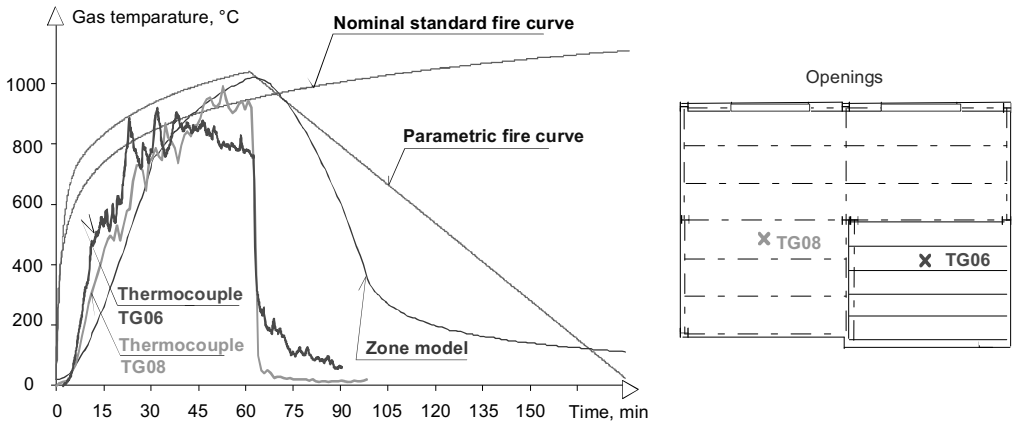

Fig. 7 Comparison of predicted and measured gas temperatures

3.2 Response of the structure

The lower flange at the midspan of the unprotected castellated beam AS4 reached in 23 min 487 °C with deformation 135 mm, see Fig. 8 and 9. In 34 min of the fire were the temperature 790 °C and the deflection 378 mm. The failure of the slab occurred in 62 min of the test in the cooling phase of the fire with the measured temperature of the beam's lower flange at the mid span 895 °C. The damage of the ceiling started in the Southeast corner. The slab lost the resistance in compression in 62 min of the experiment. The edge beam buckled on its developed free length. Due to the spalling of the top of the concrete column the anchors lost the tensile resistance. The bolted connection of the primary box girder was exposed to torsion, which leads its lost of its bolt shear resistance.

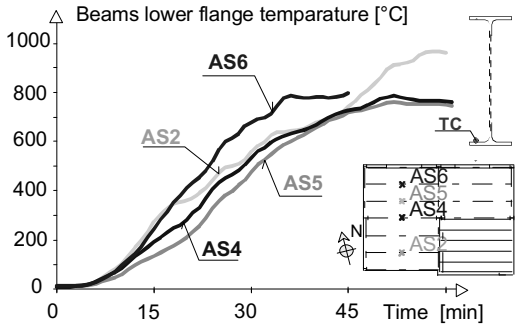

Fig. 8 Temperatures of the lower flanges of cellular beams

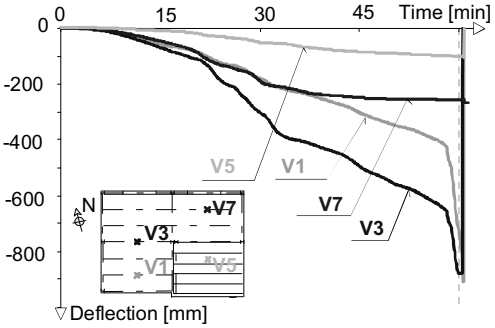

Fig. 9 Deflection of the ceiling

3.3 Connection temperatures

One of the goals of this experiment was to examine connections with higher fire resistance, which is reached by encasing them in the concrete slab. The maximal temperature of the lower part of the beam to column joint was 520°C, whereas the upper encased part reached 157°C. The highest temperature of the lower flange of the beam in the midspan was 932°C. In the case of beam to beam connection, the temperatures differences were similar; the lower part of the joint reached the maximal temperature 410°C, the upper encased part 198°C, whilst the lower flange at the beam's midspan 881°C. The connections end plate plastically

deformed before the collapse of the slab, see Fig. 10. On Fig. 11 there is presented temperature in the connection of castellated beam AS4 to column and Fig. 12 shows temperatures of the connection of castellated beam AS5 to primary beam.

a) b) c)

Fig. 10 a) Deflections of the structure in 58 min, b) the beam to column connection after the test, c) the deformation of the end plate of the beam to beam connection

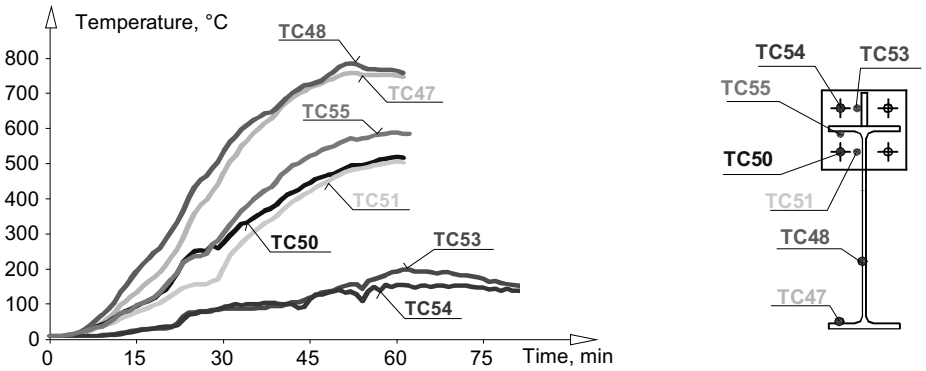

Fig.11 Temperatures in the beam to column connection of the castellated beam AS4

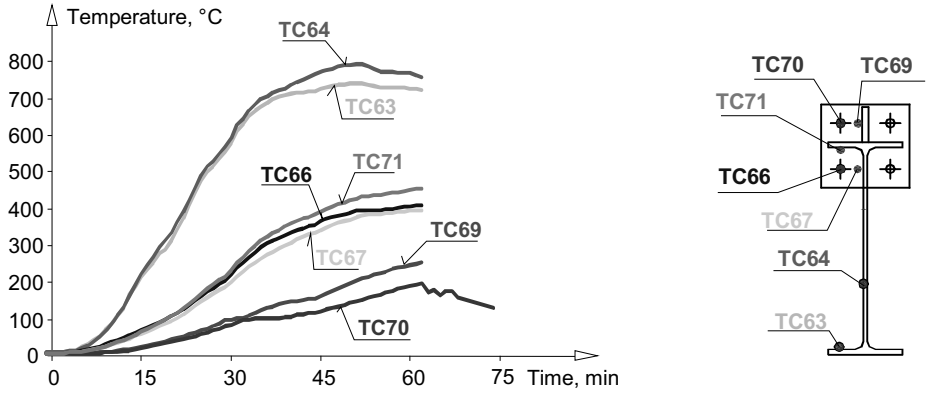

Fig.12 Temperatures in the beam to beam connection of the castellated primary beam AS5

To predict the temperature in the connection, which is partially encased into the concrete slab, the program SAFIR, see [6], was selected. The 3D model of the joint is shown on Fig. 13. The fire was modelled by program Ozone 2.2, see [7]. The predicted temperatures in the connection can be seen on Fig. 14.

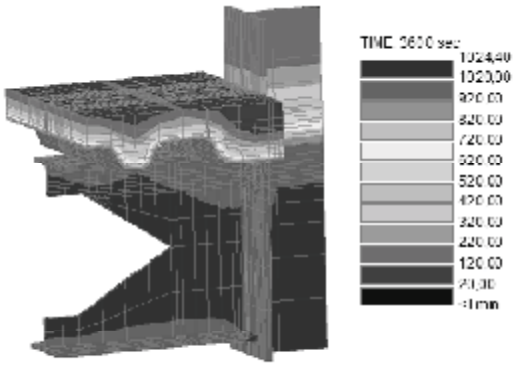

Fig. 13 Simulation of temperatures of the beam to column connection in 60 min

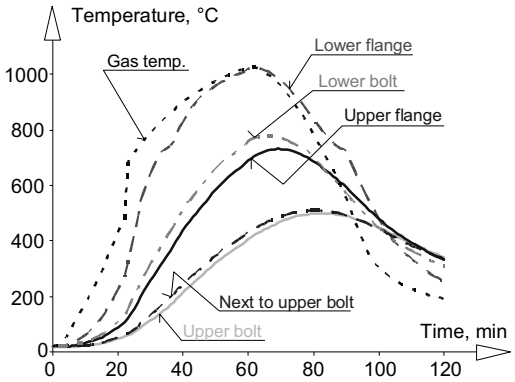

Fig. 14 Predicted temperatures in the connection

4 SUMMARY

The fire test shows the differences between the behaviour of the element and of the structure exposed to high temperatures during fire. The collapse of the composite slab was reached.

The maximum temperature of the lower bolt in the beam to column connection reached 56% of the temperature in the lower flange in the beam midspan, the upper encased bolt 17% of the midspan maximum in the flange. In case of beam to beam connection, the temperature in the lower unprotected bolt was 46% of the maximal temperature in the beam's flange in the midspan, whilst the upper protected bolt 22% of the same maximal temperature.

5 AKNOWLEDGEMENT

This work was supported by grant Fire improved joints No. OC 190 and by the research centre of Ministry of education, youth and sports CIDEAS No. 1M0579.

REFERENCES

[1] Kallerová P. a Wald F., Požární zkouška na experimentálním objektu v Mokrsku, *ČVUT v Praze*, srpen 2008, ISBN 978-80-01-04146-8.
[2] Wald F., Simões da Silva L., Moore D.B., Lennon T., Chladná M., Santiago A., Beneš M. and Borges L., Experimental behaviour of a steel structure under natural fire, *Fire Safety Journal 2006*,Volume 41, Issue 7, pp. 509-522.
[3] Kallerová P. and Wald F., Ostrava fire test, *Czech Technical University in Prague*, CIDEAS report No. 3-2-2-4/2, p.18, www.cideas.cz.
[4] Chlouba J., Wald F., Sokol Z., Temperature of connections during fire on steel framed building, *International Journal of Steel Structures*, accepted for printing.
[5] EN 1991-1-2: 2002. Eurocode 1: Basis of design and actions on structures – Part 2-2: Actions on structures – Actions on structures exposed to fire, *CEN, Brussels*.
[6] Franssen J.M., Kodur V.K.R., Mason J., User's Manual for SAFIR 2004: A Computer Program for Analysis of Structures Subjected to Fire, *University of Liège*, 2005.
[7] Ozone V2, *University of Liège*, URL: http://www.argenco.ulg.ac.be/logiciel.php.